Universitat Autònoma de Barcelona

# Electronic Tongues for food and security applications

**Andreu González Calabuig**


# Electronic Tongues for food and security applications

Andreu González Calabuig

Doctoral Thesis

Doctoral Studies in Chemistry

Director: Dr. Manel del Valle Zafra

Departament de Química

Facultat de ciències

2018

# Declaration

Thesis submitted to aspire for the doctoral degree

Andreu González Calabuig

Director's approval:

Dr. Manel del Valle Zafra, Professor of Analytical Chemistry

Bellaterra (Cerdanyola del Vallès), April 2018

# Funding acknowledgement

This present thesis has been carried out in the laboratories of the Grup de Sensors i Biosensors of the Department de Química in the Universitat Autònoma de Barcelona, with the the financial support of the Ministry of Economy and Innovation (MINECO) project “Electronic tongue fingerprinting: aplicaciones en el campo alimentario y de seguridad” (MCINN, CTQ2013-41577-P) and the ICREA program.

Grup de Sensors i Biosensors

Unitat de Química Analítica

Departament de Química

Universitat Autònoma de Barcelona

Edifici Cn 08193, Bellatera

The research produced during this thesis has produced the following publications:

- Xavier Cetó, Andreu González-Calabuig, Nora Crespo, Sandra Pérez, Josefina Capdevila, Anna Puig-Pujol, Manel del Valle. *Instrumental measurements of wine sensory descriptors using a voltammetric electronic tongue*. Sensors and Actuators, B: Chemical 207 (PB), pp. 1053-1059.( February 2015).
- Xavier Cetó, Andreu González-Calabuig, Josefina Capdevila, Anna Puig-Pujol, Manel del Valle. *Electronic tongues to assess wine sensory descriptors*. Talanta 162, pp. 218-224. (December 2014).
- Núria Serrano, Andreu González-Calabuig, Manel del Valle. *Crown ether-modified electrodes for the simultaneous stripping voltammetric determination of Cd(II), Pb(II) and Cu(II)*. Talanta 138, pp. 130-137. (June 2015).
- Andreu González-Calabuig, David Guerrero, Núria Serrano, Manel del Valle. *Simultaneous voltammetric determination of heavy metals by use of crown ether-modified electrodes and chemometrics*. Electroanalysis 28 (4), pp. 663-670.( April 2016).
- Xavier Cetó, Andreu González-Calabuig, Manel del Valle. *Electronic tongue for nitro and peroxide explosive sensing*. Talanta 153, pp. 340-346. (June 2016).
- Xavier Cetó, Andreu González-Calabuig, Manel del Valle. *Use of a biolectronic tongue for the monitoring of the photodegradation of phenolic compounds*. Electroanalysis 27 (1), pp. 225-233. (January 2015).
- Andreu González-Calabuig, Manel del Valle. *Voltammetric electronic tongue to identify Brett character in wines. On-site quantification of its ethylphenol metabolites*. Talanta 179 , pp. 70-74. (March 2018).

# Summary

## Summary

This thesis memory is focused on the continuation of the electronic tongue line of investigation in the Sensors and Biosensors Group in the Department of Chemistry of Universistat Autònoma de Barcelona. This line has been heavily focused on the application of the group know-how in electrochemical sensor development to design several sensors arrays to be applied following electronic tongue principles in different analytical scenarios. The electronic tongue principles are the new paradigm in the sensor field, where a large number of sensors with low selectivity are used in conjunction with chemometric data processing tools.

The electrochemical data was acquired using voltammetry in its different variants: cyclic voltammetry and differential pulse voltammetry. Statistical treatment was performed to extract and select the relevant chemical information from the data samples; the main methods employed were Principal Component analysis and Lineal Determinant Analysis for qualitative studies and Partial Least Squares and Artificial Neural Networks for quantitative studies.

The applications described in this thesis memory are comprised in 3 different fields: homeland security, environmental monitoring and beverage field.

In the field of homeland security an Electronic Tongue system coupled with chemometric tools was used to identify and quantify the explosive compounds such as: TNT, Tetryl, HMX, RDX, PETN and TATP. Also a quantification study with ternary mixtures of TNT, Tetryl and TATP was performed.

The Electronic Tongues developed in the field of environmental monitoring have 2 disctinct branches. The first one is the detection of heavy metals in water, in this case two applications where developed to simultaneously detect cadmium, lead and copper or cadmium, lead and mercury. The second application is the quantification of ternary mixtures of persistent phenolic pollutants such as: cresol, m-cresol and guaiacol in wastewaters

In the beverage field the works presented focus in the detection of the *Brett* defect in wines, caused by the presence of certain volatile phenols, and the classification and prediction of designation of origin and sensory panel scores in red and white wines.

## Resum

En la present tesi doctoral s'aprofundeix en l'estudi de les llengües electròniques i el seu desenvolupament com a línia d'investigació del grup de Sensors i Biosensors de la Universitat Autònoma de Barcelona. Aquesta línea d'investigació posa el focus en l'aplicació dels coneixements del grup d'investigació en desenvolupament de sensors electroquímics per a desenvolupar matrius de sensors per al seu ús en aplicacions del tipus Llengua Electrònica en diferents camps. La llengua electrònica es considera un nou paradigma en el món dels sensors ja que millora el resultats analítics mitjançant el tractament amb eines quimio mètriques.

Les dades electroquímiques van ser obtingudes mitjançant la tècnica de voltamperometria en les diferents variants: cíclica i diferencial de polsos. El tractament estadístic es va utilitzar per a extreure i seleccionar la informació química rellevant de les dades originals; els mètodes utilitzats van ser l'Anàlisi de Components Principals i l'Anàlisi Discriminant Lineal per estudis qualitatius i la Regressió de Mínims Quadrats Parcials i les Xarxes Neuronals Artificials per estudis quantitatius.

Les aplicacions descrites en el present manuscrit estan classificades en tres camps diferenciats: seguretat, seguiment mediambiental i sector del vi.

En el primer camp, la seguretat, les Llengües Electròniques conjuntament amb les eines quimio mètriques s'han utilitzat per a la quantificació de components com: TNT, Tetryl, HMX, RDX, PETN i TATP. A l'apartat quantitatiu es determinaren mescles ternàries de TNT, Tetryl y TATP.

Les Llengües Electròniques desenvolupades en el camp mediambiental es divideixen en dos camps. La primera va ser desenvolupada per a la detecció de metalls pesants en aigua on es van desenvolupar dues aplicacions per detectar simultàniament cadmi, plom i coure o cadmi, plom i mercuri. La segona aplicació és la quantificació de mescles ternàries de contaminants persistents tals com: cresol, m-cresol i guaiacol en mostres d'aigua residual.

En el camp alimentari es presenten dos treballs: la detecció de defectes tipus *Brett* en vi, causats per la presència de fenols volàtils i la classificació i predicció de la denominació d'origen i la nota de tast de vins negres i blancs de Catalunya.

## Resumen

En la presente tesis doctoral se ahonda en el estudio de las lenguas electrónicas y su desarrollo en la línea de investigación del grupo de Sensores y Biosensores de la Universidad Autónoma de Barcelona. Esta línea de investigación se focaliza en la aplicación de los conocimientos del grupo de investigación en desarrollo de sensores electroquímicos para desarrollar matrices de sensores para su empleo en aplicaciones tipo lengua electrónica en diferentes campos. Las lenguas electrónicas se consideran un nuevo paradigma en el mundo de los sensores ya que mejora los resultados analíticos mediante el tratamiento con herramientas quimio métricas.

Los datos electroquímicos fueron obtenidos mediante la técnica de voltametría en sus diferentes variantes: cíclica y diferencial de pulsos. El tratamiento estadístico se utilizó para extraer y seleccionar la información química relevante de los datos originales; principalmente los métodos utilizados fueron el Análisis de Componentes Principales y el Análisis Discriminante Lineal para estudios cualitativos y la Regresión de Mínimos Cuadrados Parciales y las Redes Neuronales para los estudios cuantitativos.

Las aplicaciones descritas en el presente manuscrito están clasificadas en tres campos diferenciados: seguridad, monitorización medioambiental y sector del vino.

En el primer campo, el de la seguridad, las Lenguas Electrónicas conjuntamente con las herramientas quimio métricas se utilizaron para la cuantificación de componentes como: TNT, Tetryl, HMX, RDX, PETN y TATP. En el apartado cuantitativo se determinaron mezclas ternarias de TNT, Tetryl y TATP.

Las Lenguas Electrónicas desarrolladas en el campo medioambiental se dividieron en dos campos. La primera fue desarrollada para la detección de metales pesados en agua en el que se desarrollaron dos aplicaciones para detectar simultáneamente cadmio, plomo y cobre o cadmio, plomo y mercurio. La segunda aplicación es la cuantificación de mezclas ternarias de contaminantes persistentes tales como: cresol, m-cresol y guaiacol en muestras de agua residuales.

En el campo alimentario se presentan dos trabajos: la detección de defectos tipos *Brett* en vino, causados por la presencia de fenoles volátiles y la clasificación y predicción de la denominación de origen y la nota de cata para vinos tintos y blancos de la región de Cataluña.

# Abbreviations

| | |
|---|---|
| **§** | Section |
| **ABA** | 4-aminobenzoic acid |
| **ANNs** | Artificial Neural Networks |
| **AU** | Auxiliary Electrode |
| **BR** | Bayesian Regulation |
| **CB** | Carboxybenzo |
| **CE** | Counter electrode |
| **CI** | Causal Index |
| **CV** | Cyclic Voltammetry |
| **CVA** | Canonical Variate Analysis |
| **DA** | Discriminant Analysis |
| **DF** | Discriminant Functions |
| **DFT** | Discrete Fourier Transform |
| **DOs** | Designation of origin |
| **DPV** | Differential Pulse Voltammetry |
| **DWT** | Discrete Wavelet Transform |
| **EE** | Electronic eye |
| **EN** | Electronic Nose |
| **ET** | Electronic Tongue |
| $\mathbf{E_w}$ | Potential at work electrode |
| $f_c$ | Comparison factor |
| **FFT** | Fast Fourier Transform |
| **FP** | False positive |

| | |
|---|---|
| **FN** | False negative |
| **GA** | Genetic Algorithms |
| **GC** | Gas Chromatography |
| **GEC** | Graphite epoxy composite electrode |
| **GSB** | Grup de Sensors i Biosensors |
| **I** | Intensity Current |
| **$I_{ce}$** | Current Intensity at Counter electrode |
| **$I_{we}$** | Current Intensity at Work electrode |
| **ICP** | Inductive coupled Plasma |
| **ICS** | International Chemometrics Society |
| **IUPAC** | International Union of Pure and Applied Chemistry |
| **k-NN** | k Nearest Neighbors |
| **LDA** | Linear Discriminant Analysis |
| ***Logsig*** | Log Sigmoid transfer function |
| **LV** | Linear Voltammetry |
| **LVs** | Latent Variables |
| **MES** | 2-(N-morpholino)-ethanesulfonic acid |
| **MLR** | Multiple Linear Regression |
| **MS** | Mass Spectrometry |
| **NP** | Nanoparticles |
| **n PLS** | N way Partial Least Squares |
| **PARAFAC** | Paralel Factor Analysis |
| **PC** | Principal Component |

| | |
|---|---|
| **PCA** | Principal Component Analysis |
| **PCR** | Principal Component Regression |
| **PLS** | Partial Least Squares |
| **PVC** | Polyvinyl chloride |
| ***Purelin*** | Linear transfer fuction |
| ***r*** | *Correlation coefficient* |
| **$R^2$** | *Determination coefficient* |
| **RE** | Reference electrode |
| **RSS** | Residual sum of squares |
| ***Satlins*** | Symmetric suturing linear transfer function |
| **S/N** | Signal to Noise ratio |
| **Sulfo-NHS** | N-hydroxysulfosuccinimide |
| **SWV** | Square Wave Voltammetry |
| ***Tansig*** | Hyperbolic tangent sigmoid transfer function |
| **TF** | Transfer Functions |
| **TP** | True positive |
| **TN** | True negative |
| **V** | Potential |
| **WE** | Work electrode |

# Table of Contents

# 1. Introduction

# 1. Introduction

## 1.1. Electronic Tongue approach

### 1.1.1. Biologic taste

Traditionally, biology has explained the mammals taste sense, hence human taste, as a number of specific taste receptors grouped in a sensory organ, the tongue. The receptors for the traditional flavors, salty, sweet, sour and bitter, are so called taste buds and they are believed to be grouped in the tongue according to Figure 1.1. As general rule taste buds in the tip of the tongue are selective to sweet flavors, at the sides for sour, on top for salty and the ones at the back of the tongue are bitter selective. From some time ago, some studies indicate that a fifth flavor exist, the *umami*, supposedly the corresponding receptors have a high sensitivity for L-glutamate and 5'-ribonulceotides and are distributed evenly on the tongue surface [1].

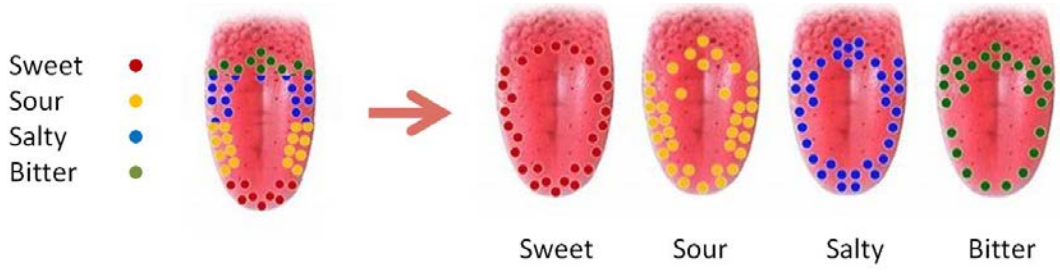


**Figure 1.1.** Classical taste distribution *versus* real taste distribution.

The exact mechanism at work when a specific molecule stimulates the taste buds is still not known but a necessary condition for the stimulation/detection is the solubility in water of the molecule [2]. The receptors in the taste buds are formed by a combination of support and receptor cells, the receptor cells have structures named *microvili*; such structures maximize the contact surface and contain the specific receptor units for the different flavors [3]. The reported bibliography has demonstrated the presence of different proteins in the receptors depending on the tongue zone [4].

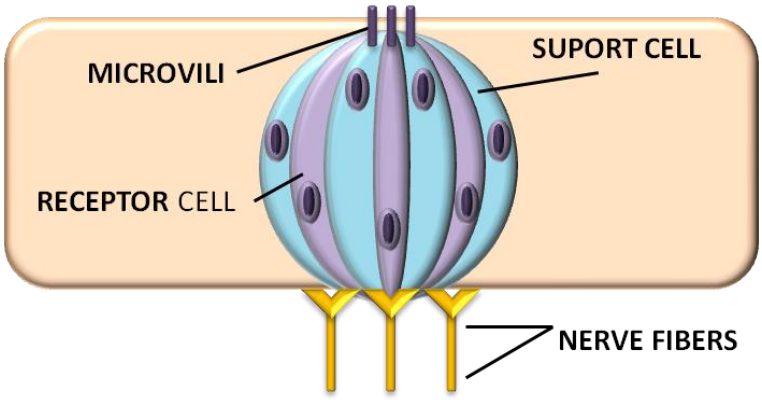


**Figure 1.2.** Schematic view of Taste bud receptors.

Molecules that evoke a specific flavor are named *sapides,* from the Latin word *sapere*, flavor. Particulars flavors are produced by the detection of the *saporific* units in the cell receptors, the cell produces an electric signal that is transmitted by the nervous system to the brain where the neuron networks identifies patterns previously memorized.

Taste and smell senses work on a coordinate manner to identify the maximum number of substances but the number of taste buds can change from person to person and the higher the number of buds the higher the sensitivity to the distinct flavors.

However, recent studies have shown that these receptors are not entirely specific towards one flavor but have a different sensitivity towards all the different flavors; it is this cross-response the main characteristic that the electronic tongue approach wants to mimic.

## 1.1.2. Electronic tongue, the concept

In the last decades, the use of informatics in the daily life has been on the rise thanks to the miniaturization and the increase of computational capabilities of computers. Chemistry field is no exception, in the particular case of analytical chemistry where the main focus is the obtention of the maximum amount of information in the minimum time possible. This fact and

the difficulty of developing sensors selective towards specific compounds, which are able to operate in every media without any matrix effect, have propitiated the apparition of new approaches to the problems that analytical chemistry faces.

Systems combining physical sensors and mathematical treatments are often called biomimetic systems and draw inspiration from natural world. In the field of Analytical Chemistry, the main biomimetic systems [5] take after three mammal senses: smell, taste and sight. Therefore, authors have reported electronic noses (EN), electronics eyes (EE) and electronic tongues (ET) [6][7], other fields more connected to engineering/architecture fields have described electronic skin approaches; one can say there are also other bioinspired sensing systems developed observing senses from other animals, as it would be the Radar or the Sonar. The biomimetic systems, in opposition of classical methods, are based on the combination of low selective and/or cross-responsive sensors to obtain rich and complementary analytical information.

The concept of ET was proposed by Vlasov in the late 90s' to describe an array of sensors whose signal is treated with mathematical procedures [8]; since then the number of publications applications have only increased, as it can be seen in Figure 1.3 in blue, demonstrating the potential of the ET approach has. However the main applications of ETs make use of more common chemometric techniques, such as partial least squares, but the group of sensors and biosensors of the Universitat Autònoma de Barcelona has traditionally focused in the use of Artificial Neural Networks as the main method to process and model the data, in figure 1.3 in red can be seen the number of papers with ET plus artificial neural networks as keywords.

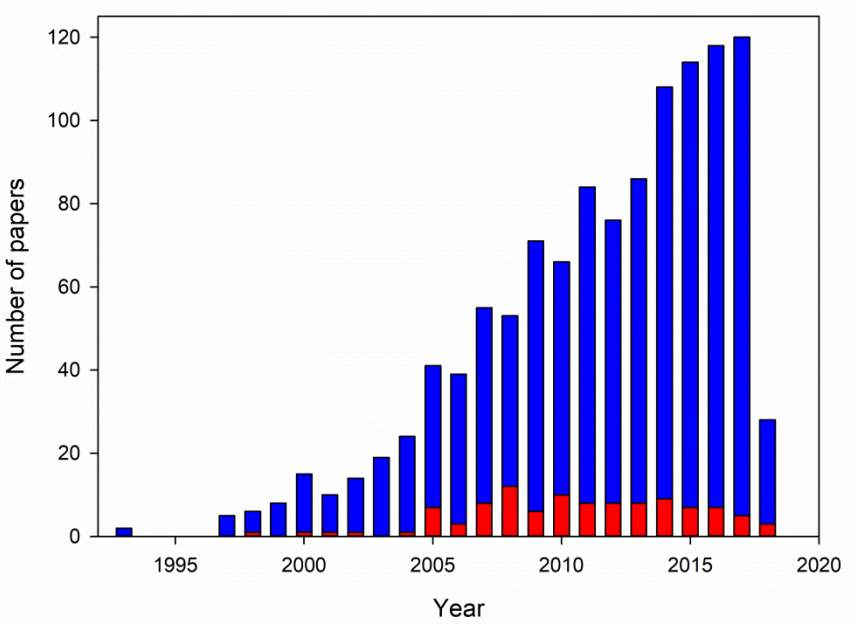


**Figure 1.3.** Year *versus* number of publications containing the keyword electronic tongue (blue) and electronic tongue plus artificial neural networks (red) from Scopus database.

On the whole, an ET by definition is comprised of the following sub-units:

- An array of sensors that have low selectivity and cross-response towards the desired compounds in the sample.
- A chemometric tool able to model and interpret the data according to the specific application.

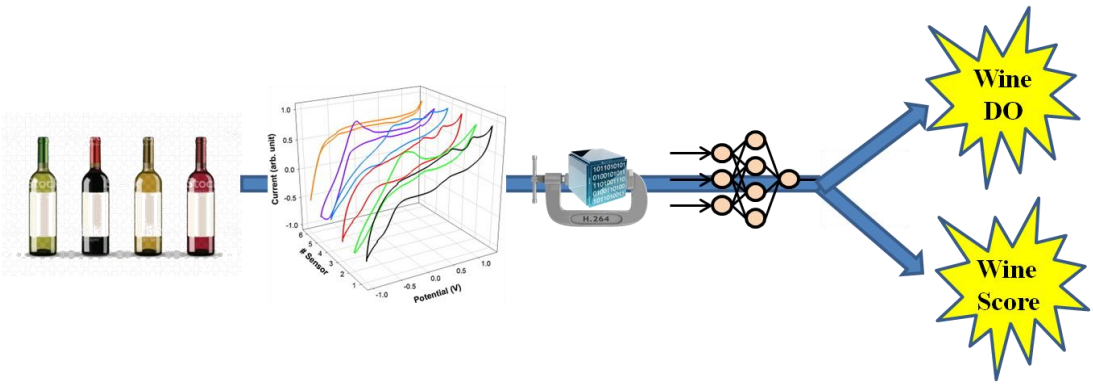


**Figure 1.4.** Scheme of the ETs tongue prediction process in the specific case of use of voltammetric sensors and applied in the wine field.

Another important point is that even though the electronic tongue was conceived with unspecific sensors in mind in the last years some authors have incorporated some measure of

selectivity in the electrodes that form the array, through the use of enzymes [9], molecular imprinted polymers [10] or other selective elements, with this approach it is possibilited to perform an enhanced discrimination of compounds within a group analysis.

### 1.1.3. Single electrode vs Electrode array

The general definition of a sensor is the following: a device or element capable to convert external stimulus into a signal, usually an electric one. The International Union of Pure and Applied Chemistry (IUPAC) define a chemical sensor as the device that transforms chemical information, ranging from the concentration of a specific sample component to total composition analysis, into a useful signal [11]. In the analytical field the sensor has to be able to selectively transform selectively chemical, physical or biological information into a quantifiable signal.

Chemical sensors are composed of two basic units: the receptor and the transducer (Figure 1.5). Firstly, the receptor transforms the chemical information into a form of energy which may be measured by the transducer, the primary signal, while also providing selectivity to the sensor. Afterwards, the transducer transforms the energy generated by the receptor into a useful analytical signal, the secondary signal, generally an electric one.

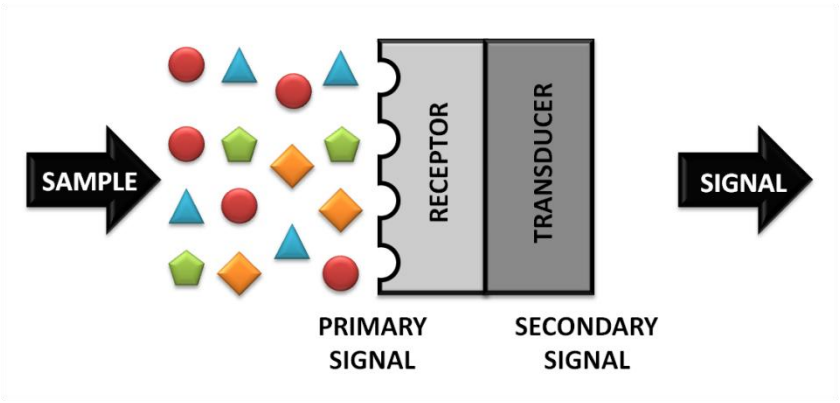


**Figure 1.5.** Scheme of the chemical sensor and the transduction process

Moreover, sensors should ideally have certain special features as they have to be selective to a determinate stimulus, sturdy and capable of producing real time information, among other important characteristics.

Receptors can be classified based on the different principles on which they operate: physical sensors (where no chemical reaction takes place; .e.g. based on the measurement of absorbance, refraction index or conductivity), chemical sensors (in which a chemical reaction

with participation of the analyte gives rise to the analytical signal) and biochemical sensors (based on different biochemical processes as the source of the signal, like immunosensors or enzymatic biosensors).

As previously commented the ideal sensor should have certain characteristics that we look for in a good sensor. Next parameters are used to evaluate sensor performance characteristics: selectivity, sensitivity, resolution, signal to noise ratio (S/N), response time, linearity, reversibility and absence of hysteresis. The former parameters are the commonly used characteristics to define a sensor performance; however, there are others that would be desirable depending on the final application such as a long lifetime of the sensor, a wide lineal range, low-cost or high portability among other advantages.

As previously explained, our sensor should resemble the characteristics of an ideal sensor; however, this is not always feasible. To tackle down this problem, sensors are designed to work under specific conditions and in certain kind of samples. Therefore, in controlled situations the signal of the sensor becomes independent of the others components present in the sample matrix, so it is not necessary that only responds to a particular analyte.

Even when it is not possible to fix such conditions for our sensor, there are various procedures to still carry out the measurement. The classical solutions focus on the elimination or masking the interfering species through pre-treatment steps; nevertheless, this goes against the principles of sensors that intend to merge all the steps of the analytic process, moreover, increasing also analysis time, money cost and requiring trained personnel.

To overcome such limitations in the past years a new trend has arisen as an alternative to the classical treatments, that is, the use of an array of sensors instead of using a single sensor [12]. With this methodology it is possible to obtain more information of the chemical system and bypass the problems found with classical approaches.

Therefore, in this manner, unspecific sensors, that still present adequate reproducibility, can be joined in an array and used for multicomponent analysis, through the building of a multivariate calibration model and the processing of the signals. Henceforth, the complexity of the problem can be displaced from the chemistry field onto the data processing and signal treatment field.

The different arrays of sensors can be classified depending of the kind on sensors comprising the matrix [12].

- **Matrix of redundant sensors:** when the matrix is composed of the same kind of sensors the signal is replicated, this increases the sturdiness and precision of the method. Also, it gives us a tool to detect abnormalities in the functioning of the sensors or the chemical system.

- **Matrix of specific sensors:** it is based in the combination of different kinds of selective sensors, each one selective towards the different species, which allows a simultaneous multicomponent determination. This method allows a reduction in the time and cost of the analysis.

- **Matrix of unspecific sensors:** in this case the matrix is composed of unspecific sensors with low selectivity that present a cross-response with differentiate sensitivity towards a certain number of analytes. This allows the simultaneous determination of the species present in a complex sample with the use of processing tools to correct the interferences that occurs between them. Hence, this strategy gives us a powerful tool to extract information of our system, which in addition allows us to obtain information that is related to a perception like the smell or the taste senses. This variant is the one that inspired biomimetic systems such as the electronic tongues (ETs).

## 1.2. Electroanalytical techniques

The field of electroanalytical chemistry is based on the electric properties of a dissolution containing the analyte or analytes of interest within an electrochemical cell [13], the change in these properties is directly or indirectly related to the analyte concentration.

These techniques have some advantages that classic analytical methodologies struggle to achieve. The ability to discriminate among different metal oxidation states (i.e. $M^{+}/M^{2+}$) instead of providing the total amount of the metal, the easy miniaturization of the equipment required to perform the measurements allowing the on-field analysis or the relative low cost of the instrumental involved are some of the characteristics that make electroanalytical methods an attractive alternative to more established methods such as ICP-MS or GC-MS. However, present several downsides such as the drift in the measurements, higher limits of detection or less robust methods caused by fouling of the electrode surface.

### 1.2.1. Voltammetry

Voltammetry is a group of electroanalytical methods where the analyte information is obtained from the measured current intensity at different electrical potentials when a polarization is created at the working electrode. The recorded current is generated from the

electronic transfer that takes place on the electrode surface between the electrode and the compounds in the dissolution when the potential is applied; depending of the applied potential the species are oxidized or reduced.

These group of techniques work with a minimal consumption of analyte at the working electrode and in practice are considered non-destructive techniques. Voltammetry allows the possibility of oxidation and reduction of the analytes making it a versatile tool; also depending on the specific voltammetric technique the reversibility of redox processes can be studied.

## 1.2.2. Electrochemical cell

The electrochemical cell employed to apply the potential in the measurements is composed by 3 different electrodes: one or more working electrodes (WE), one reference electrode (RE) and an auxiliary also called counter electrode (CE). This cell configuration, called 3-electrode cell, is necessary to apply the desired potential and at the same time measure the current intensity (Figure 1.6). In a three electrode cell potential and current measurements are separated into a RE and a CE loop. The potential of the working electrode is measured with respect to the reference electrode. The input of the RE has a high-impedance forcing all current to flow through the counter electrode. The function of the working electrode or electrodes is to be the platform where the electrochemical reaction takes place, the auxiliary electrode acts as a counter electrode to close the circuit and the reference electrode ensures a correct polarization of the working electrodes.

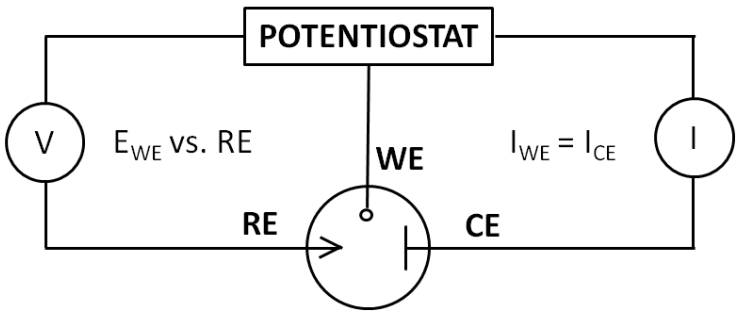


**Figure 1.6.** Scheme of a three-electrode electrochemical cell configuration.

## 1.2.3. Voltammetric excitation signals

Voltammetric techniques differ in the way the excitation signal is applied, the polarization potential (V), generating a characteristic response in the recorded signal, the measured current (I). The different excitation signals gave name to the different voltammetric techniques:

- **Linear sweep:** It is the classical excitation signal in voltammetry (Figure 1.7A), the potential applied to the cell increases linearly as a function of time. It gives name to Linear Voltammetry (LV).
- **Differential pulse:** It is a variation of the linear sweep where a pulse is applied while the potential increases linearly as a function of time (Figure 1.7B). The current is measured before and after the pulse. It gives name to Differential Pulse Voltammetry (DPV).
- **Square wave:** In this variation of the excitement signal the pulse applied changes in a stair shape, superimposing a square wave with the linear sweep (Figure 1.7C). As before the current is measured before and after the potential change. It gives name to Square Wave Voltammetry (SWV).
- **Triangular:** The excitation signal presents a triangular shape (Figure 1.7D) where the potential is cycled between two values, first increasing linearly to the maximum value and then decreasing with the same slope to the starting value. This process can be repeated as many times as desired and gives name to the Cyclic Voltammetry (CV).

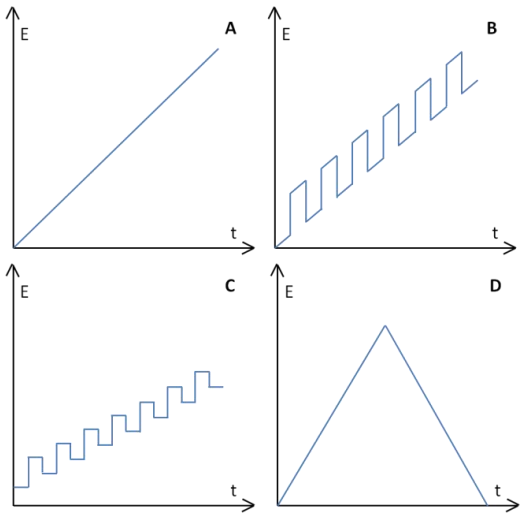


**Figure 1.7.** Scheme of the different excitement signals usually employed in voltammetry. (**A**) Lineal sweep, (**B**) Pulse voltammetry, (**C**) Square wave voltammetry and (**D**) Cyclic voltammetry.

The previously mentioned excitement signals can be fine tuned to obtain the desired excitation signal for the desired application. The main excitement signals share some parameters such as step potential (V) and scan rate ($V \cdot s^{-1}$), other parameters like pulse frequency (Hz) and amplitude (V) are only tunable for SWV and DPV [14].

All in all, voltammetry is far from the capabilities of more established methods such chromatography or mass spectrometry, but its instrumental allows for quick on-field analysis for screening purposes of a wide variety of substance for a relatively low price.

## 1.3. Data processing and Chemometric analysis

A common problem that arises when electrochemical arrays are employed is the high complexity and dimensionality of the generated data, in the particular case of voltammetric systems this means obtaining a tensor composed by intensities x electrodes x samples. The traditional multi-variate statistical methods are insufficient to deal with this huge amount of raw data, in this context chemometrics proves to be the solution. The advanced and complex multilinear methods are required to extract and process the relevant information contained in the original data.

In 1975, the International Chemometrics Society (ICS) defined chemometrics as “the chemistry discipline that uses mathematical and statistical methods to design or select tailor-made methods and experiments, to provide maximum chemical information by means of data analysis”. Such discipline comprises a wide variety of methods that can be applied to chemical data, among the tools one can mention optimization of experimental parameters, design of experiments and pattern recognition are among the most important.

In the recent years chemometrics has found its place among research and industry; chemometrics are widely used in many different areas and some of those applications have been robust enough to be transferred to the industry, an example of this is the NIR on-line applications for quality control.

The main chemometric methods focus either on qualitative analysis (Principal Component Analysis, Linear Discriminant analysis or Support Vector Machines) or quantitative analysis (Partial least Squares, Multiple linear regression or n-Way partial least squares) with some exceptions that can perform both types of analysis (Artificial Neural Networks). The works presented in this thesis memory will be focused in the later.

Finally, in the following sections the necessary preprocessing steps to use the certain chemometric methods and the employed chemometric techniques will be explained.

### 1.3.1. Compression

The advances in hardware have made possible an exponential increase in the computational power of the computers, however the amount of data (currents x sensors x samples) obtained with the voltammetric electronic tongue systems still makes it difficult to build and train a model without somehow reduce the huge dimensionality of the generated data.

There are some approaches to overcome such limitations; the most employed being the compression of the original data before the construction of the predictive model. The compression of the data has two main objectives; on one hand it reduces the data complexity while preserving the meaningful information on the other allows a faster training time of the model and a considerable increase in the generalization (predictive) capabilities of the model [15][16].

In the work comprised within this thesis cyclic voltammetry (CV) and differential pulse voltammetry (DPV) were the main voltammetric techniques employed, in the case of CV a previous step named *unfolding* is needed prior to the data compression. In the unfolding step the cyclic voltammograms are converted into a 2 dimension matrix, as is shown in Figure 1.8 followed by the desired chemometric multivariate methods, lineal or not, such as partial least squares (PLS) or artificial neural networks (ANNs).

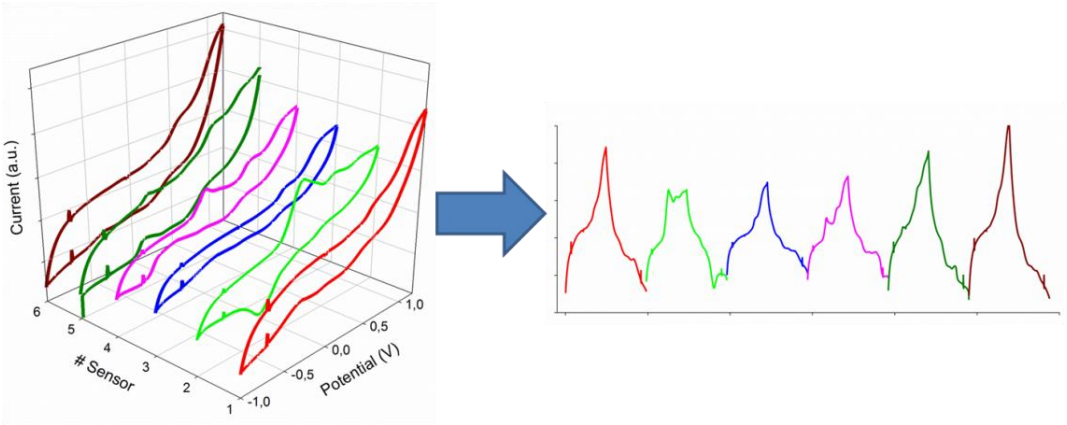


**Figure 1.8.** 3D voltammograms to unfolded voltamograms>

As commented before there are a wide variety of compression methods described in the bibliography such as: feature selection [17], sliced window integral method [18], principal component analysis (PCA) [19][20], Legendre's polynomials [21], *kernel* functions [22], Fast

Fourier Transform (FFT) [9] or Discrete Wavelet Transform (DWT) [23]. The methods employed in the thesis are extensively described within thesis in the 3.X section.

Nevertheless, it is noteworthy to mention that exist methods able to deal with high dimensional data without the need of compression pre-treatments, such methods are PARAFAC models or n partial least squares regression (n-PLS) [24]. However, as mentioned previously in this section these methods are highly complex and require a more refined and sophisticated architecture design that limits its possibilities. In many cases much simpler methods can achieve similar results with the adequate pre-treatments [25].

## 1.3.2. Qualitative Analysis

The qualitative analysis is one of the most extended and it is commonly used to group and discriminate samples. The models are build using powerful chemomentric tools; Principal component Analysis [26], Linear Discriminant analysis [27] or Partial Least Squares coupled with Discriminant Analysis [28] are some of more common employed methods but there are others like Supported Vector Machines [29] or Independent Components Analysis [30].

### 1.3.2.1. Principal Component Analysis (PCA)

Principal Component analysis is one of the more common methods employed to reorganize the data and uncover certain class patterns, it consists in a mathematical re-arrangement of the multivariate original data where the main criterion is the maximization of the sample variability as depicted in Figure 1.9.

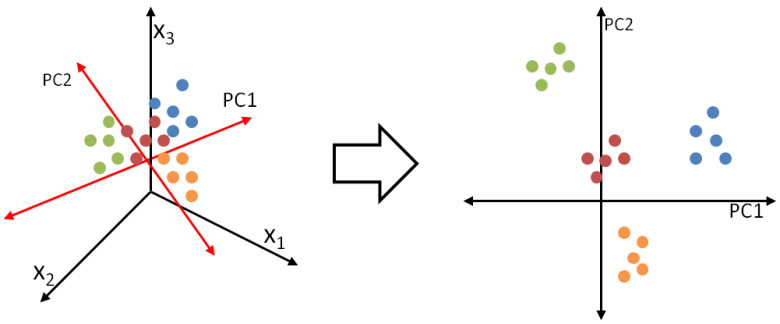


**Figure 1.9.** Scheme of the data transformation trough PCA

The famous iris flower set will be used as an example to depict how PCA works [31], Figure 1.10 plots the 4 variables (sepal length, sepal width, petal length, petal width) to evaluate class separation.

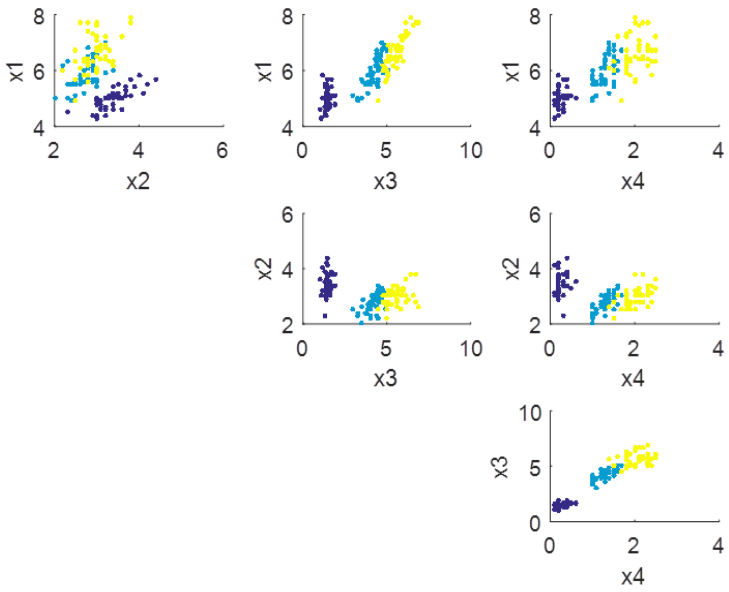


**Figure1.10.** Plotting the variables vs. each ()other allows us to differentiate the possible classes, in this case 3 classes (blue, teal and yellow).

The mathematical procedure begins with an adjusted data matrix, X, which consists of *n* observations (rows) on *p* variables (columns). The adjustment is made by subtracting the variable's mean from each value. That is, the mean of each variable is subtracted from all of that variable's values. This adjustment is made since PCA deals with the covariances among the original variables. New variables are constructed as weighted averages of the original variables. These new variables are called the factors, latent variables, or principal components (PCs). Their specific values on a specific row are referred to as the factor scores, the component scores, or simply the scores. The matrix of scores will be referred to as the matrix Z. The basic equation of PCA is, in matrix notation, given by equation 1.1 in matrix notation are detailed for each factor in equation 1.2.

$$U'X \qquad \textbf{Equation 1.1}$$

$$z_{ij} \quad w_{1i}x_{1j} + w_{2i}x_{2j} + \cdots + w_{pi}x_{pj} \qquad \textbf{Equation 1.2}$$

The PCs are a weighted average of the original variables. The weight matrix, W, is constructed so that the variance of PC1, Var(PC1), is maximized. Also, so that Var(PC2) is maximized and that the correlation between PC1 and PC2 is zero. The remaining PC's are calculated so that their variances are maximized while maintaining the covariance equal zero

constraint. The matrix of weights, W, is calculated from the variance-covariance matrix, S. This matrix is calculated using the equation 1.3.

$$s_{ij} = \frac{\sum_{k=1}^{n}(x_{ik}-\bar{x}_i)(x_{jk}-\bar{x}_j)}{n-1} \qquad \textbf{Equation 1.3}$$

The singular value decomposition of S provides the solution to the PCA problem. This can be defined as U'SU=L, where L is a diagonal matrix of the eigenvalues of S, and U is the matrix of eigenvectors of S. Finally, W is calculated from L and U, using equation 1.4.

$$W = UL^{-1/2} \qquad \textbf{Equation 1.4}$$

The newly projected coordinates are arranged in a decreasing amount of sample variability, so usually the authors plot only the scores of the first 2 PCs unless the accumulated variance of the first 2 PCs is less than 90 %. The coordinates obtained with the projection are called *scores (Zij)* and the weights of the different variables in the new PCs are called *loads (Wij)* [26].

There are different ways of interpreting the different information provided by the PCA the more usual is the scores plot in 2D or 3D (Figure 11.A and X.B) but the loadings plot (Figure 12.A) and a combination of the former two called a *biplot* (Figure 12.B) is also used depending on the authors or the applications.

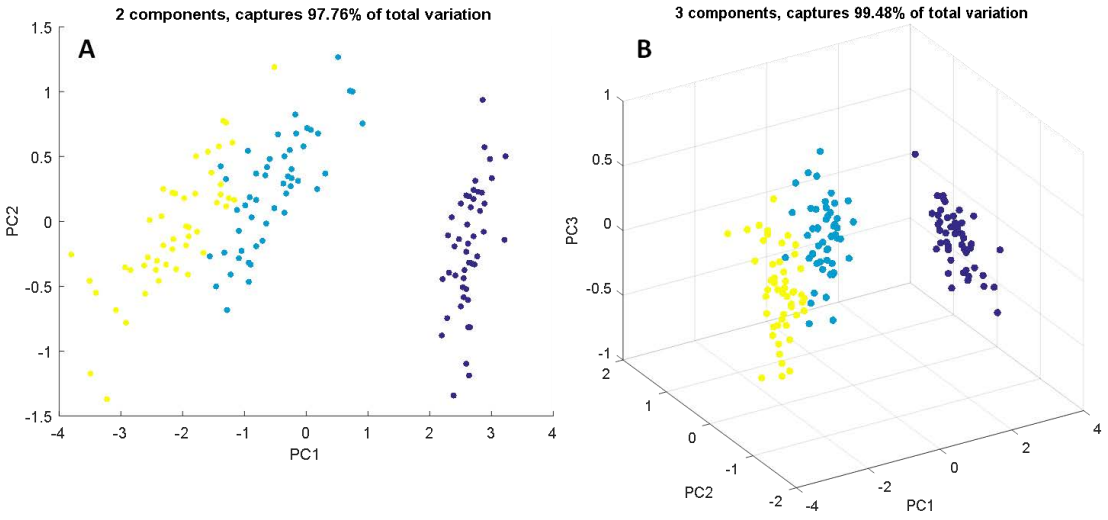


**Figure 1.11.** (A) Scores plot of the first 2 PCs for the iris data set and (B) Scores plot of the first 3 PCs for the iris data set.

The similar compositions samples will group in clusters while the distance between the different clusters will provide information of the interclass similarities. In the case of the *loadings* plot the different variables are plotted for the desired PCs, the plot provides information of the influence of a certain variable in a certain PC, therefore variables that appear closer to the center have a smaller impact that those that appear at larger distances. In the case of the *biplot* scores and loadings are simultaneously plotted, this variant is useful when the original samples have a relatively small number of variables.

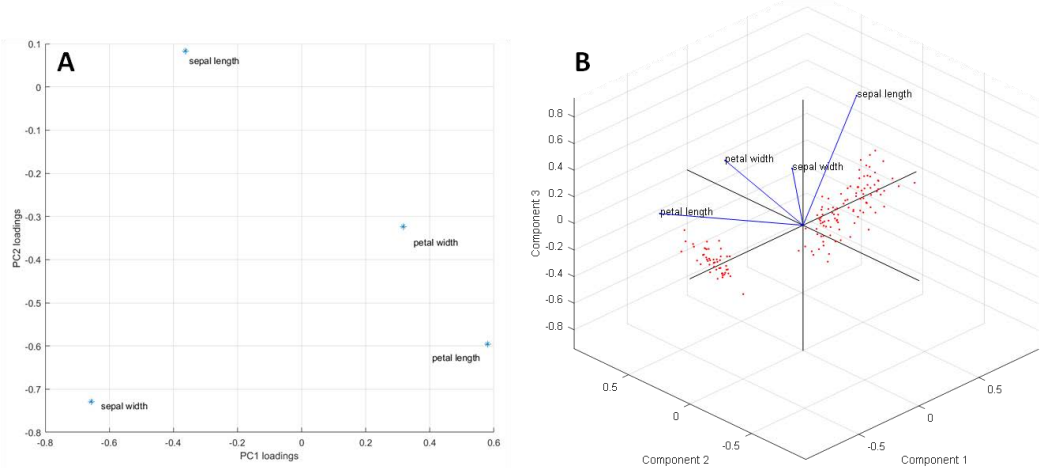


**Figure 1.12**. (A) Loadings plot of the first 2 PCs for the iris data set and (B) Biplot of the first 3 PCs for the iris data set.

Despite all the advantages that PCA provides it necessary to remember that this method does not classify the different samples it simply provides a new arrangement in another set of

coordinates; hence, it is necessary to couple PCA with a classifier such as k nearest neighbors (k-NN) or artificial neural networks (ANNs) among others [32].

### 1.3.2.2. Linear Discriminant Analysis

Linear discriminant analysis (LDA) is a method that projects the original data in a new axis, named discriminant functions (DFs), but unlike PCA, LDA is a supervised method. LDA searches for a combination of variables that provide maximum variability between the samples told to form a class; the selected variables are linearly combined to build the new DFs coordinates, Figure 1.13. Also in contrast with the PCA in LDA the number of DFs obtained is equal to *k*-1, where *k* is the number of classes, and moreover as LDA can act as a classifier [33].

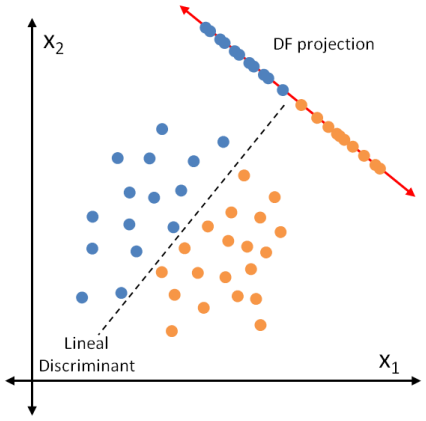


**Figure 1.13.** Scheme of LDA projection

The original LDA is based in the Bayes formula and depending of the function used to define the boundaries can be linear or quadratic. However, LDA was designed to be used in 2 class situations, methods related to LDA or that expand the number of classes that can treat are often named LDA. These methods such as Fischer discriminant analysis or canonical variate analysis (CVA) appear in preprogrammed software, i.e. Solo Eigenvector® or R language, under the name of LDA but strictly are not LDA as it was originally described.

### 1.3.2.3. Partial least squares and Discriminant analysis (PLS-DA)

PLS-DA is a special case of PLS, it is employed when that target matrix is binary [34]. It has some similarities with PCA, where the original data is projected into new coordinates and with LDA as it is a supervised method. As in PLS (section 1.3.3.2), the data are projected in the directions that maximize the predictive capabilities of the model and the obtained scores are used as predictors.

### 1.3.3. Quantitative Analysis

The possible methods for qualitative analysis are divided depending on how the regression is performed; the methods are divided among linear and non-linear. In the linear methods the data set is modeled after a lineal function, usually by means of partial least squares. In the case of non-linear regressions the model is built after a function that combines non-linearly parameters of the model and the independent variables through successive iterations.

Briefly, the linear methods comprises multiple linear regression (MLR) [35], principal component regression (PCR) [36], partial least squares (PLS) [37] and N-way partial least squares (nPLS) [38]. Among the non-linear methods artificial neural networks (ANN) [39][40] stand out. The more employed methods are going to be described in the following sections.

#### 1.3.3.1. Multiple linear regression (MLR)

MLR is a classic regression method that linearly combines a certain number of predictors (dependent variables, y) that correlate with one response (independent variable, x) as it is depicted in Figure 1.14 [41]. This independent variable is traditionally the concentration of the targeted species, as commented before one of the limitations of the classic regression methods is the incapacity of predict more than 1 species with the same model, a limitation that share with PLS-1 but can be overcome coupling PCA treatment with a MLR (Principal Component Regression (PCR)). Therefore if more than one species is involved it is necessary to build a model for each of the considered species.

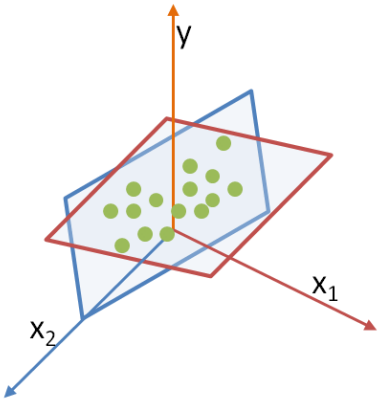


**Figure 1.14.** Scheme of the MLR regression

### 1.3.3.2. Partial Least Squares (PLS)

Partial least square regression is a method that combines PCA and multiple regression characteristics. In this case instead of search for the maximum variance in the samples as the PCR does it focuses on the maximum predictive performance. The maximum predictive performance is achieved through the simultaneous modeling of sensor responses (X) and target concentrations (Y), the treatment allows to calculate the latent variables (LVs) [38]. LVs are similar to the PC's in the PCA but represent new variables that correlate in a linear fashion with the desired targets, Figure 1.15.

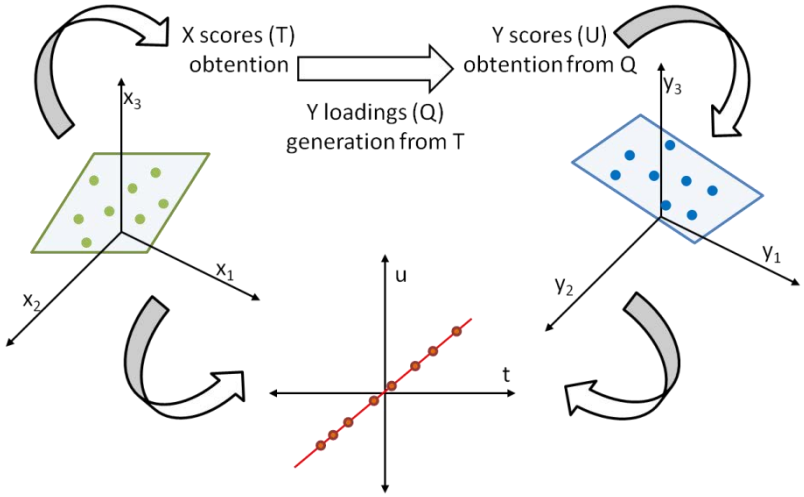


**Figure 1.15.** Scheme of the PLS model creation. X and Y are simultaneously decomposed maximizing the covariance between responses and targets.

The data and target matrix are decomposed simultaneously in a sum of *n* factors as it is shown in equation 1.5 and 1.6, in that equation T and U correspond to the Loadings matrixes of X and Y respectively.

$$X = TP^T + E = \sum_{i=1}^{n} t_i p_i^T + E \qquad \textbf{Equation 1.5}$$

$$Y = UQ^T + F = \sum_{i=1}^{n} u_i q_i^T + F \qquad \textbf{Equation 1.6}$$

The decomposition of the matrix is not independent as it occurs in PCA but it is performed simultaneously through an internal relation between X and Y scores as is shown in equation 1.7, where the circumflex indicates the estimated value and $b_a$ is the regression coefficient for each component.

$$\hat{}_a \quad b_a t_a \qquad \textbf{Equation 1.7}$$

The Y matrix is calculated using the ûa relation, where B is the regression coefficients ba and F the residual matrix of Y.

$$Y \quad TBQ^T + F \qquad \textbf{Equation 1.8}$$

The PLS methods are differentiated by the number of predicted variables, in the case of PLS-1 the response is only formed by 1 variable and in the case of more target variables, the number of variables is added at the end, i.e. in PLS-2 the response is a 2xn matrix.

Once the matrix of coefficients is built the desired properties are predicted using equation 1.9, where xi stands as the predictors vector, $y_i$ as the predicted properties and $b^T_0$ the vector that allows the prediction without the need of decomposing the sample in scores and loadings.

$$y_i^T \quad b_0^T + x_i^T B \qquad \textbf{Equation 1.10}$$

PLS methods are widely employed in the chemometric field due its simple optimization, the treatment reduces the original data dimensionalty as only a certain number of LVs are employed in the final model, only the number of LVs has to be optimized to achieve the lowest error possible, Figure 1.16.

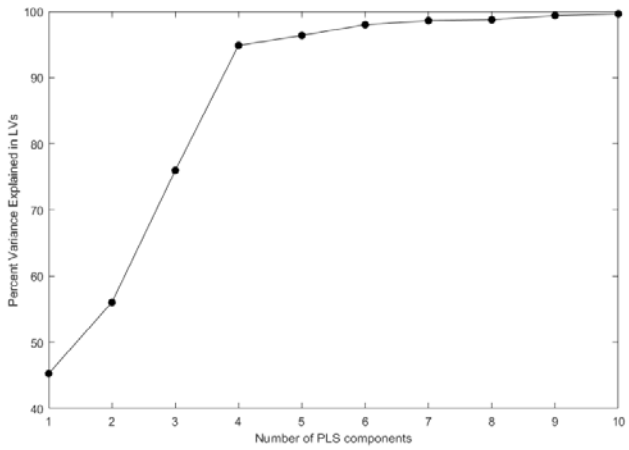


**Figure 1.16.** Cumulative variance *versus* the number of Latent variables employed

### 1.3.3.3. Multiple Partial Least Squares (nPLS)

Multiple Partial least square is an extension of the standard PLS method designed to be used in cases where the data has more than 1 dimension [42]. This tensorial method allows the treatment of the original data without the need of pretreatments to reduce the dimensionality, i.e. unfolding the voltammograms, thus avoiding discontinuities in the data, i.e. the joining ends of the voltammograms, distorting the modeling step [43].

The main difference with the PLS is the dimension of the loadings matrix, in the case of n-PLS the loadings matrix is a 2D matrix. Therefore, the scores and loading for both signal and targets are adjusted simultaneously to build the final predictive model. As in PLS the scores are adjusted to maximize the covariance of the predictors. The multiway treatment allows n-PLS surpass the 1-way methods due to the higher flexibility, second order advantages, in building the predictive models [44]. However, the high complexity of the model and the pre-supposition of data linearity are its main drawbacks.

### 1.3.3.4. Artificial Neural Networks (ANNs)

Originally, ANNs were built with the idea of mimicking the biological learning processes that take place in the mammal brain [45]. Therefore, ANNs are bio-inspired mathematical models and since its emergence in the field of chemometrics [40] have been employed in numerous qualitative and quantitative applications in multivariate analysis [46]. These methods do not have an explicit algebraic model but are built from independent logic units called *perceptrons*, these basic units are interconnected and process the information through the modification of the interconnection weights between units [47].

A difference that sets ANNs apart from the previously mentioned methods is their modelling flexibility; ANNs can use linear and non-linear functions but also can combine both to achieve the maximum performance. This flexibility in the modelling give ANNs an extra edge when the data is obtained from sensors with non-linear responses, i.e. voltammetric sensors, allowing the construction of models with relatively high complexity allowing to outperform the lineal models, i.e. PLS. However, this high complexity has some disadvantages such as the time required to optimize as it is very difficult to predict the optimal architecture (combination of the ANN parameters), the more common method is by *trial-and-error* [48]. Also as previously commented in 1.3.1 voltammetry sensors have a high dimensionality therefore the data has to be pre-processed to reduce its dimensionality before building the ANN model.

## 1.3.3.4.1. Neuron *versus* Perceptron

As commented, ANNs are biomimetic systems. The basic processing unit of an ANN is called *perceptron*, which is an approximation to the biological neuron, the cell in the nervous system (Figure 1.16.A). The *perceptron* is a decision-making unit with several input connections ($x_n$) and a single output ($a_k$) every input has a determined weigh ($W_i$) and sometimes a bias (b) is applied, if the sum of the weighted inputs surpasses a certain threshold ($T_{ki}$) the perceptron is activated and produces an output signal, the mathematical equivalent is shown in equation 1.11.

$$y_{k=\sum_{i=1}^{n} W_i X_i + b}$$ **Equation 1.11**

Afterwards, the perceptron output signal is modulated by a transfer function (*f*), the analogy of a neuron vs. A perceptron is sketched on Figure 1.17.B.

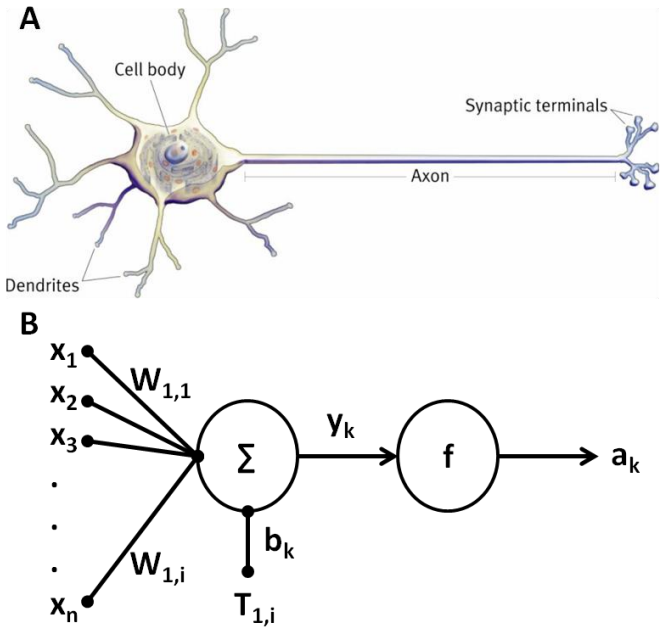


**Figure 1.17.** Scheme of neuron (A) versus perceptron (B)

As in the biologic systems single units (neurons) have little computational power so they are arranged in networks, i.e. the brain, to increase the learning capabilities. Imitating these networks the *perceptrons* are organized in different layers, each layer is a grouping of

*perceptrons* that share the same inputs. Layers of perceptrons give name to the more employed architectures of ANN in chemometrics: the Multilayered ANNs.

## 1.3.3.4.2. Multilayered ANN

A single perceptron is a limited data processing unit; to increase the modelling capabilities is necessary to group sets of associated perceptrons. This can be done in two different ways: first giving the perceptrons neighbours to form a layer of units which share inputs from the environment; secondly by introducing further layers, each taking as their input, the output from the previous layer. In this way, the network of perceptrons used for numerical models is known as the multilayered ANN. It is important to note that the all the perceptrons and layers are built with the connections with the other in the same direction, for this reason the multilayered ANNs with this configuration are named unidirectional networks or *feed-forward* networks, Figure 1.18.

The layers are differentiated by their function and are divided in three types:

-**Input Layer:** It is the first layer and its function it to transmit the information towards the network. The number of neurons in input layer depends on the data dimensionality. The layer does not modify the data it just distributes it to the next layer.

- **Hidden Layers:** Usually formed by a single layer. It is formed by a variable number of perceptrons between 1 and 12 and it is where the processing of the information takes place.

- **Output Layer:** This layer receives the processed signals from the hidden layer and provides information on the targets.

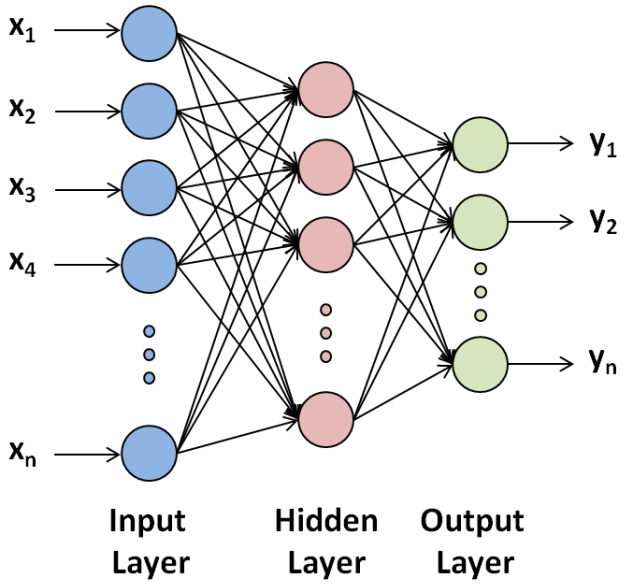


**Figure 1.18.** Scheme a multilayered ANN.

As in the single perceptron case the ANNs weights need to be optimized through an iterative process to obtain the best combination to predict the targets. Additionally the data is transmitted from layer to layer by means of transfer functions (TFs) that also need to be selected to maximize performance, the more employed TFs are depicted in Figure 1.19.

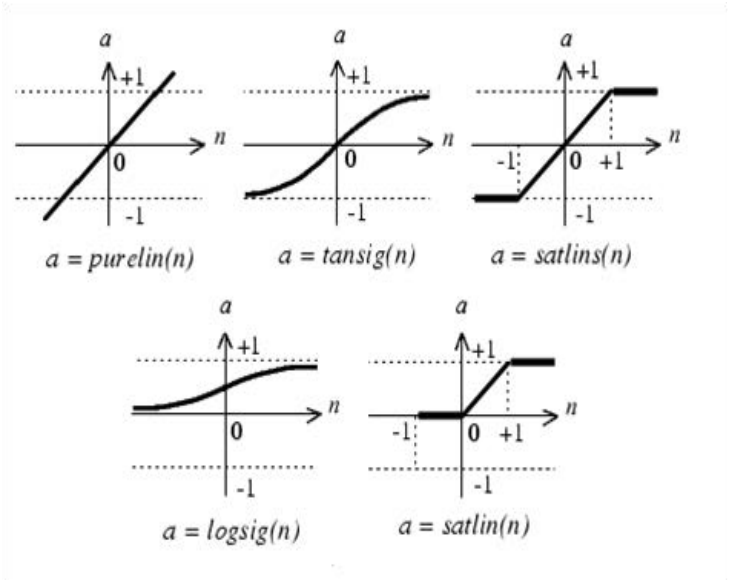


**Figure 1.19**. Some of the more common Transfer Functions employed in ANNS architectures.

## 1.3.3.4.3. Learning process

In the process of building an ANN model, either using a single perceptron or a multilayered network, the learning or training step is a key step that presents more complexity than the previously mentioned methods. The key process during the training step is the adjustment of the weights of the connexions between neurons; the weights are adjusted through an iterative process until the ANN model is able to predict the outputs within a certain error.

The training process is absolutely necessary due to the random values that are assigned to each of the weights when the ANN model is initiated. As commented, the process is based on successive iteration each one adjusting the weights in such a way that the error in the output is minimized [49]. This iteration process is based in the comparation of the desired outputs with the values generated by the model. As it is expected the iterative process is exponentially more complex in the case of layered networks rather than single perceptrons, the main reason is that in a unidirectional flow networks, such is the case in all the models employed in this thesis compendium, the weight adjustment a layer modify the values of the weights in the next layer. The more common strategy used to minimize the errors are the back-propagation algorithms.

Therefore, the error is calculated as the semi-sum of the squared difference between the theoretical output ($S_{nj}$) and the predicted output ($a_{nj}$) for each sensor ($n$) and standard ($j$), equation 1.12. Then, the error is used modify the values of the weights in order to minimize its value, each cycle in the iteration process in known as an epoch.

$$\boldsymbol{Ep} \quad \frac{1}{2}\sum_{j}^{n}(\boldsymbol{s_{nj}} - \boldsymbol{a_{nj}})^2 \qquad \textbf{Equation 1.12}$$

Tthe weight modification can be done in different ways, the two more employed algorithms being the gradient descent retro-propagation [50] and the Levenberg-Marquard algorithm [51]. The first is based in the modification of the output layer weights and then the adjustment of the weights in the previous layers, the so called Delta rule depicted in equation 1.13, and the second is based on the simultaneous adjustment of the weights by means of advanced mathematical optimizations achieving faster and more efficient epochs.

Delta rule is one of the more employed gradient descent learning rule to update the weights of the inputs for ANNs, equation 1.13, where $\alpha$ is the learning rate, $g(x)$ is the neuron's activation function, $t_j$ is the target output, $h_j$ is the weighed sum of the neurons inputs, $y_j$ is the actual input and $x_i$ is the $i$th input.

$$\Delta w_{ji} \quad \alpha(t_j - y_j)g'(h_j)x_i \qquad \textbf{Equation 1.13}$$

However, ANN are powerful modellers but the whole process of adjusting the weights, if its incorrectly done, can lead to one of the major disadvantages of these kinds of models: the overfitting of the predictive model, commonly known as just overfitting. The overfitting a model takes places when the model has adjusted the different parameters, forcing the model to achieve very small errors, in such a way that has lost the generalization ability and the prediction of samples that not belong to the group employed in training are incorrectly predicted or predicted with a big error in the case of quantitative cases. In Figure 1.20 is illustrated an example of a good model vs. an overfitted model to illustrate graphically the situation that takes place in when a model is overfitted. This fact highlights the importance of the external validation models when ANN models are involved as they are prone to overfit.

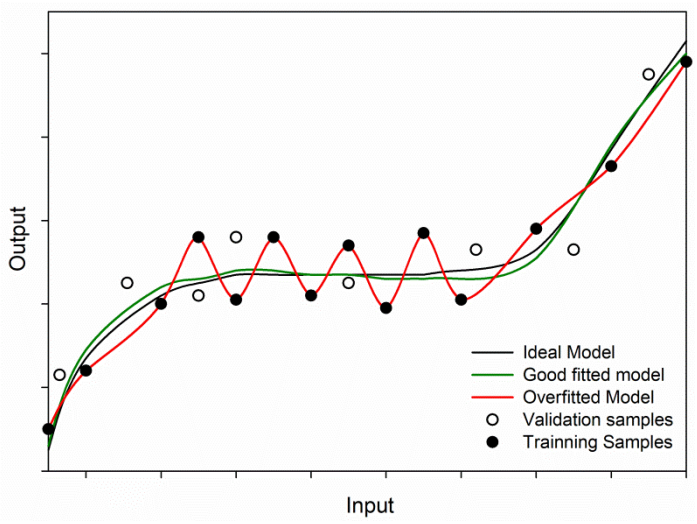


**Figure 1.20.** Simplified view of a good fitted model *versus* an over fitted model.

Nevertheless, overfitting is a big problem but there are some strategies to avoid these situations:

- Early time stop: This strategy consists in the use of a subset of samples used to control the weight adjustment. In this strategy there are 3 subsets of samples employed: a

training set, internal validation set and the external validation set. The error of the training set and the internal validation are simultaneously calculated and the whole process is stopped when the error of the training test is decreasing and at the same time the error in the internal validation set increases surpassing a threshold [52].

- Bayesian Regularization (BR): Its main advantage is that generates the simplest neuronal network that can model the system, avoiding overfitting and normally performing better for external validation samples. The algorithm not only reduces the prediction error but also takes into account the weight importance, minimizing the absolute value and distributing more or less evenly the importance of the inputs. The models obtained using BR avoid overfitting without the need of an internal validation set [53][54].

## 1.4. Areas of application

The applications presented in this thesis are focused in the wine field, environmental monitoring and homeland security. The electronic tongue approach provides of a powerful tool to extract the meaningful information and construct the appropriate predictive models.

The work in the beverage field has followed the lines of work in the sensors and biosensors group, the wine sector. In this field has been developed different ETs able to emulate the functions of a *sommelier*. The ETs built have been designed to identify regions (DOs), type of grape, sensory score and volatile phenolic defects (4-ethylphenol compounds)

In the field of homeland security the work has focused in the development of a voltammetric electronic tongue able to identify and simultaneously determine nitro and peroxide based explosive compounds, two families that represent the majority of compounds employed either in commercial mixtures or in improvised explosive devices.

In environmental monitoring the work has been mainly focus in trace metal detection. A specially modified array with different crown ethers has been built to allow the resolution of ternary mixtures of different metals at the ppb level. Also an enzymatic ET capable of monitoring the persistent phenolic content in wastewater has been developed.

## 1.5. Bibliography


[1] S. Yamaguchi, K. Ninomiya, *J. Nutr.* **2000**, *130*, 921S–926S.

[2] A. L. Huang, X. Chen, M. A. Hoon, J. Chandrashekar, W. Guo, D. Tränkner, N. J. P. Ryba, C. S. Zuker, *Nature* **2006**, *442*, 934.

[3] M. A. Hoon, E. Adler, J. Lindemeier, J. F. Battey, N. J. P. Ryba, C. S. Zuker, *Cell* **1999**, *96*, 541–551.

[4] B. Lindemann, *Nature* **2001**, *413*, 219.

[5] K. Toko, *Biomimetic Sensor Technology*, Cambridge University Press, **2000**.

[6] F. Röck, N. Barsan, U. Weimar, *Chem. Rev.* **2008**, *108*, 705–725.

[7] Y. Tahara, K. Toko, *IEEE Sens. J.* **2013**, *13*, 3001–3011.

[8] Y. Vlasov, A. Legin, *Fresenius. J. Anal. Chem.* **1998**, *361*, 255–260.

[9] X. Cetó, F. Cespedes, M. del Valle, *Talanta* **2012**, *99*, 544–551.

[10] A. Herrera-Chacon, A. González-Calabuig, I. Campos, M. del Valle, *Sensors Actuators B Chem.* **2018**, *258*, 665–671.

[11] H. Adam, G. Stanisław, I. Folke, *Pure Appl. Chem* **1991**, *63*, 1250–1274.

[12] M. del Valle, M. del Valle, *Electroanalysis* **2010**, 1539–1555.

[13] D. A. Skoog, F. J. Holler, S. R. Crouch, *Principles of Instrumental Analysis*, Cengage Learning , **2017**.

[14] A. J. Bard, L. R. Faulkner, J. Leddy, C. G. Zoski, *Electrochemical Methods: Fundamentals and Applications*, Wiley New York, **1980**.

[15] J. M. Palacios-Santander, L. M. Cubillana-Aguilera, M. Cocchi, A. Ulrici, I. Naranjo-Rodríguez, R. Seeber, J. L. H.-H. de Cisneros, *Chemom. Intell. Lab. Syst.* **2008**, *91*, 110–120.

[16] L. Moreno-Barón, R. Cartas, A. Merkoçi, S. Alegret, J. M. Gutiérrez, L. Leija, P. R. Hernandez, R. Muñoz, M. del Valle, *Anal. Lett.* **2005**, *38*, 2189–2206.

[17] X. Cetó, F. Céspedes, M. I. Pividori, J. M. Gutiérrez, M. del Valle, *Analyst* **2012**, *137*, 349–356.

[18] X. Cetó, F. Céspedes, M. del Valle, *Electroanalysis* **2013**, *25*, 68–76.

[19] R. M. de Carvalho, C. Mello, L. T. Kubota, *Anal. Chim. Acta* **2000**, *420*, 109–121.

[20] X. Cetó, C. Saint, C. W. K. Chow, N. H. Voelcker, B. Prieto-Simón, *Sensors Actuators B Chem.* **2017**, *247*, 70–77.

[21] M. B. and W. E. van der L. Jo Simons, *Analyst* **1995**, *120*, 1009–1012.

[22] R. Gutierrez-Osuna, H. T. Nagle, *IEEE Trans. Syst. Man, Cybern. Part B* **1999**, *29*, 626–632.

[23] L. Moreno-Barón, R. Cartas, A. Merkoçi, S. Alegret, M. del Valle, L. Leija, P. R. Hernandez, R. Muñoz, *Sensors Actuators B Chem.* **2006**, *113*, 487–499.

[24] R. Bro, *Crit. Rev. Anal. Chem.* **2006**, *36*, 279–293.

[25] D. Ebrahimi, E. Chow, J. J. Gooding, D. B. Hibbert, *Analyst* **2008**, *133*, 1090–1096.

[26] I. Jolliffe, in *Encycl. Stat. Behav. Sci.*, John Wiley & Sons, Ltd, **2005**.

[27] G. McLachlan, *Discriminant Analysis and Statistical Pattern Recognition*, John Wiley & Sons, **2004**.

[28] M. Barker, W. Rayens, *J. Chemom.* **2003**, *17*, 166–173.

[29] M. M. Adankon, M. Cheriet, in *Encycl. Biometrics*, Springer, **2009**, pp. 1303–1308.

[30] A. Hyvärinen, J. Karhunen, E. Oja, *Independent Component Analysis*, John Wiley & Sons, **2004**.

[31] R. A. Fisher, *Ann. Hum. Genet.* **1936**, *7*, 179–188.

[32] S. B. Kotsiantis, I. Zaharakis, P. Pintelas, *Emerg. Artif. Intell. Appl. Comput. Eng.* **2007**, *160*, 3–24.

[33] R. A. Johnson, D. W. Wichern, *Applied Multivariate Statistical Analysis*, Prentice-Hall New Jersey, **2014**.

[34] V. Vinzi, W. W. Chin, J. Henseler, H. Wang, **2010**.

[35] G. Grégoire, *Eur. Astron. Soc. Publ. Ser.* **2014**, *66*, 45–72.

[36] I. T. Jolliffe, *Appl. Stat.* **1982**, 300–303.

[37] H. Wold, *Encycl. Stat. Sci.* **1985**.

[38] H. Abdi, *Wiley Interdiscip. Rev. Comput. Stat.* **2010**, *2*, 97–106.

[39] J. A. Anderson, *An Introduction to Neural Networks*, MIT Press, **1995**.

[40] R. Lippmann, *IEEE Assp Mag.* **1987**, *4*, 4–22.

[41] H. Martens, P. Geladi, in *Encycl. Stat. Sci.*, John Wiley & Sons, Inc., **2004**.

[42] R. Bro, *J. Chemom.* **1996**, *10*, 47–61.

[43] N. K. M. Faber, J. Ferré, R. Boqué, J. H. Kalivas, *Chemom. Intell. Lab. Syst.* **2002**, *63*, 107–116.

[44] V. Gómez, M. P. Callao, *Anal. Chim. Acta* **2008**, *627*, 169–183.

[45] F. Rosenblatt, *Psychol. Rev.* **1958**, *65*, 386.

[46] J. R. M. Smits, W. J. Melssen, L. M. C. Buydens, G. Kateman, *Chemom. Intell. Lab. Syst.* **1994**, *22*, 165–189.

[47] F. Despagne, D. L. Massart, *Analyst* **1998**, *123*, 157R–178R.

[48] D. R. Hush, B. G. Horne, *IEEE Signal Process. Mag.* **1993**, *10*, 8–39.

[49] A. P. Plumb, R. C. Rowe, P. York, M. Brown, *Eur. J. Pharm. Sci.* **2005**, *25*, 395–405.

[50] H. B. Demuth, M. H. Beale, O. De Jess, M. T. Hagan, *Neural Network Design*, Martin Hagan, **2014**.

[51] M. T. Hagan, M. B. Menhaj, *IEEE Trans. Neural Networks* **1994**, *5*, 989–993.

[52] H. Demuth, M. Beale, **1992**.

[53] D. J. C. MacKay, *Neural Comput.* **1992**, *4*, 415–447.

[54] F. D. Foresee, M. T. Hagan, in *Neural Networks, 1997., Int. Conf.*, IEEE, **1997**, pp. 1930–1935.

# Objectives

## 2. Objectives

In the presented doctoral thesis were developed a variety of voltammetric electronic tongues a wide range of applications such as the food field, specifically the wine industry, environment monitoring and the explosive detection. The data obtained using the sensor array was processed employing chemometrics, mainly using artificial neural networks and partial least squares regression for quantification purposes and principal component analysis and discriminant analysis for qualitative purposes.

The specific objectives of this thesis were divided in three sections:

**1.** Beverage field:
   **1.1.** To develop a suitable electronic tongue for its application in the wine field, with special focus in the subjective properties such as the sensory score.
   **1.2.** To develop an electronic tongue for the identification and quantification of the volatile 4-ethylphenols causing of the *Brett* trait in wines.

**2.** Environmental monitoring:
   **2.1.** To develop an electronic tongue for the simultaneous detection of heavy metals such as Cu(II), Zn(II), Pb(II) and Cd(II).
   **2.2.** To develop an electronic tongue for monitoring the presence of persistent phenolic pollutants in wastewater.

**3.** Homeland security:

**3.1.** To develop an electronic tongue capable of the identification of the most used explosive compounds, nitro and peroxo containing compounds, and the quantification of ternary mixtures of 2,4,6-trinitrotoluene, pentaerythritol tetranitrateand and triacetone triperoxide.

# Experimental

# 3. Experimental

## 3.1. Sensor construction

The applications that will be described in detail in §4 have been developed using graphite epoxy composite based sensors (GEC); these sensors have been used for a long time in the group of Sensors and Biosensors (GSB) of the *Universitat Autònoma de Barcelona* [1]. Composite materials are a mix of two materials that have different properties of the original products. In the case of the composite material employed, the epoxy resin provides a matrix where the graphite particle will be allocated; the new material is a robust conductive material that can have its surface easily regenerated with a light polishing with sandpaper.

The electrodes can be built in different shapes but in this work all the electrodes employed had a cylindrical shape. The construction process is detailed in Figure 3.1 and is comprised of the following steps:

**1.** A copper disc of 5mm of diameter is cut and then cleaned of oxide with a diluted HCl solution. Next, the copper disk is soldered to an electrical connector.

**2.** The connector with the soldered copper disc is encased into a 20mm PVC tube. The tube has a 6 mm internal diameter. Once the connector is in place a cavity of 4mm depth remains to be filled with the composite paste.

**3.** The graphite epoxy composite is prepared using the epoxy resin commercial kit (Epotek H77, part A and B) and graphite (particle size 50 µm) in a 20:3 ratio, the ratio can change slightly depending on the modifiers and catalysts employed. The mixture is stirred until the complete homogenization, usually 45-50 min. In this step there is the possibility of include a 2% of modifiers to obtain an electrode with catalytic properties. Once the mixture is prepared the cavity is filled and the electrode is cured in the oven during 2-3 days at 80 ºC until the resin has hardened. If the modifier is a biologic compound, such as an enzyme, the temperature employed is lowered to 45ºC and kept in the oven for an entire week.

**4.** The final step is to polish the surface using sandpaper with decreasing grain size and finaly polishing it with alumina paper. The final electrodes have a geometric area of 28 $mm^2$.

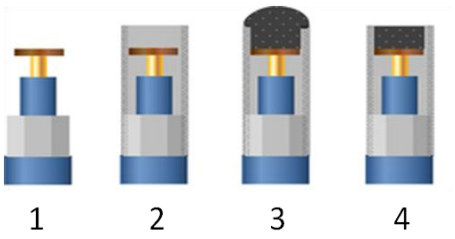


**Figure 3.1.** Scheme of the different steps in the building of the electrode

Additionally, metallic electrodes were prepared in the same configuration. The metallic electrodes were constructed with metal wires of the corresponding metal electrode, the wires were soldered to the electrical connector and encased in resin epoxy, finally as in the composite electrodes were polished. Table 3.1 details the different electrodes employed in the applications developed during this doctoral thesis.

**Table 3.1**. List of electrodes employed during these doctoral thesis.

| Electrode | Applications |
|---|---|
| GEC electrode | [2][3] |
| 1Ø mm Pt | [2][3][4] |
| 1Ø mm Au | [2][3][4] |
| 1Ø mm GEC | [4] |
| CB-15-crown-5-GEC | [5][6] |
| CB-18-crown-6-GEC | [5][6] |
| Co Phthalocyanine | [2][3][7] |
| Cu NPs GEC | [7][8] |
| Pt NPs GEC | [2][3] |
| Tyrosinase-GEC | [8] |
| Tyrossinase/laccase-GEC | [8] |
| $WO_3$ NPs GEC | [7] |
| $Bi_2O_3$ NPs GEC | [7] |
| Polypyrrole GEC | [7] |

## 3.2. Sensor modification

In certain applications the surface of the graphite-epoxy composite has been modified to fine tune the selectivity through the covalent binding of different selective crown ethers. The immobilization of the crown ethers was performed covalently though carbodiimide coupling [5][6]. The specific steps for the modification of the GEC are described below:

- Diazonium salt electrochemical grafting: The in situ generation of the aryl diazonium was performed by adding $5 \cdot 10^{-3}$ equivalents of sodium nitrite to an aqueous acidic solution (1 M HCl) of 4-aminobenzoic acid (ABA). These solutions were mixed during 30 min in an ice bath, prior to the electrochemical grafting process [9] conducted by scanning the potential at 0.2 $V \cdot s \cdot M^{-1}$ from 0 V to -1 V for 100 cycles. Afterwards, the newly functionalized electrodes were thoroughly rinsed with Milli-Q water and methanol to remove any physisorbed compounds that could remain onto the surface.

-Covalent immobilization of crown ethers via carbodiimide coupling: The carboxyl groups of the electrografted diazonium salt were activated by incubating the functionalized electrodes in a 26 mM *N*-(3-dimethylaminopropyl)-*N'*-ethyl-carbodiimide hydrochloride (EDC) and 35 mM N-hydroxysulfosuccinimide (sulfo-NHS) solution in 100 mM 2-(N-morpholino)-ethanesulfonic acid (MES) buffer (pH 4.5) for 1 h. In order to conjugate the carboxy-functionalized electrode with the carboxy-modified ligand, a lysine spacer was intercalated between the anchoring point and the crown ether, by using the two amino functionalities to form amido bonds[5]. The surface activated groups reacted overnight with the α-amine group of the lysine. Prior to cross linking with EDC/sulfo-NHS, 2.9 mg of 4-carboxybenzo-18-crown-6 or 4-carboxybenzo-15-crown-5 were incubated with 100 µL 5 mM lysine in 0.1 M MES buffer for 3 h.

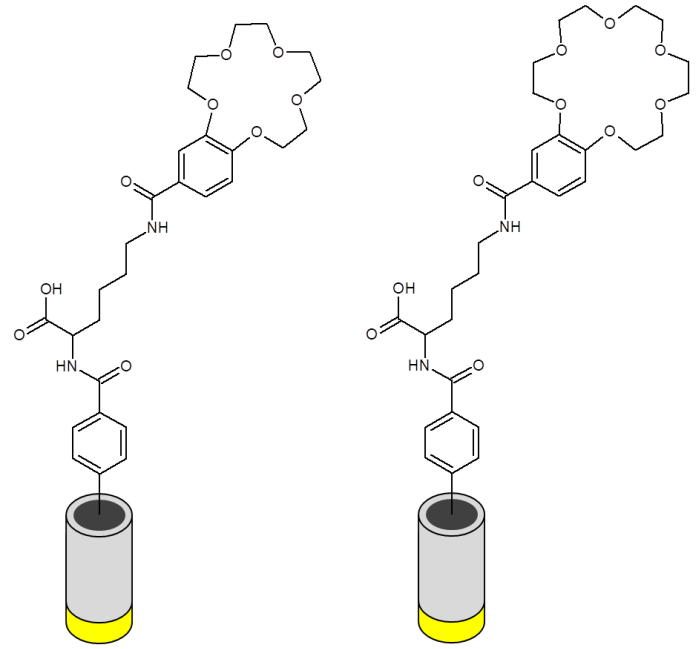


**Figure 3.2.** Ilustration that show the CB-15-crown-5-GEC and CB-18-crown-6-GEC electrodes modified through electrochemical grafting.

The electrochemical response using 2 mM ferrocyanide/ferricyanide as redox probe in 100 mM phosphate buffer (pH 7.4) was investigated at each functionalization step using cyclic voltammetry (CV) leading voltammograms that confirm the modifications occurring on the electrode surface. This procedure has been thoroughly tested achieving high repeatable and reproducible results [5].

## 3.3. Experimental Design

One of the most important decisions that can affect the performance of a model is the training set of samples, ANN need a large set of samples that are employed to train the model. This fact is one of the major disadvantages of ANN as it requires different set of samples to train, test and validate the model. Therefore, to construct a model that has good predictive capabilities and is robust enough to predict unknown samples the experimental design is a key factor.

The first step for experimental design is to determine the experimental domain, range of concentrations for each analyte. The range of concentrations is not necessary the same for each compound. Once the concentration range is determined the next step is to chose the experimental design, the works presented in this thesis uses the full factorial ($3^3$) and a modification of a full factorial ($3^3$) both traditionally employed in the GSB [10]. The modified model consists of a factorial design with a 45 degree rotation in each axis, figure 3.3.B.

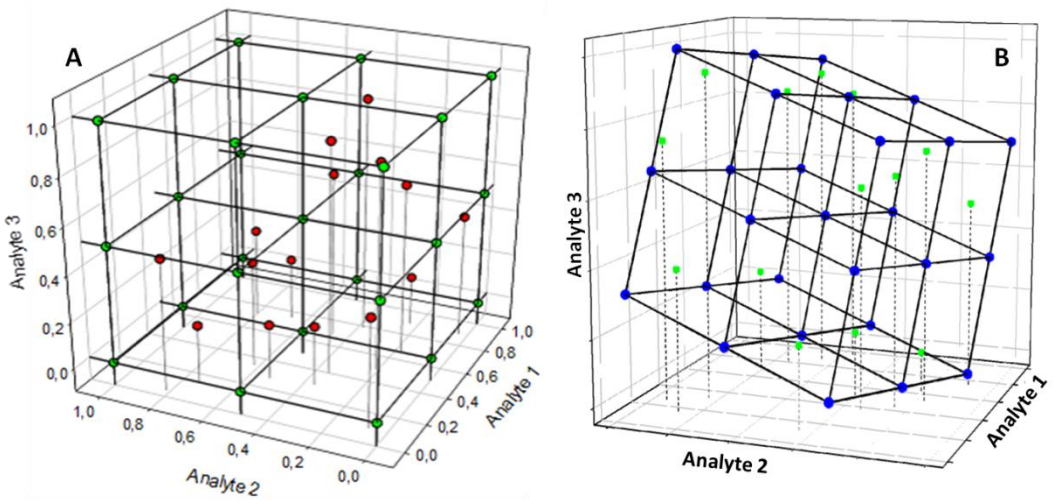


**Figure 3.3.** (A) 3^3 factorial design and (B) 3^3 modified factorial design

Once the experimental domain and the samples required to build the model are defined the next step is to generate the test subset. The test subset is employed to evaluate the predictive capabilities of the model, the number of samples in the test subset can vary but a common proportion is 25-30% of the number of samples employed as train set. As their function is to evaluate the goodness of the model the samples in this set are generated randomly along the experimental design.

## 3.4. Measurement procedure

The technique employed in the works presented in this thesis compendium has been voltammetry; the variants used were cyclic voltammetry and differential pulse voltammetry and it theoretical base is explained in §1.2.1. The cell employed during the experiment was composed by the working electrodes and a Ag/AgCl combined electrode with auxiliary Pt (Crison 5261,Barcelona, Spain).

The main employed technique has been cyclic voltammetry. In the case of the explosive determination the potential was cycled between -1.0V and +0.9V vs Ag/AgCl pseudo reference electrode, with a scan rate of 100mV s-1 and a step potential of 9mV [4]. In the case of wine samples the potential was cycled between −1.0V and +1.3V vs. Ag/AgCl with a step potential of 9 mV and a scan rate of 100 mV s−1 [2][3]. For the phenol samples a complete voltammogram was recorded for each sample by cycling the potential between -0.4V and +0.8V vs. Ag/AgCl with a step potential of 9 mV and a scan rate of 100 mV s-1 [8]. In the case of Brett compounds detection the potential was cycled between -1.1V and +1.2V vs. Ag/AgCl with a step potential of 9 mV and a scan rate of 100 mV $s^{-1}$ [7].

However, in the case of metal determination the technique employed was differential pulse adsortive voltammetry with the following conditions: -1.4V as the applied accumulation voltage with stirring during a $t_d$ of 300s and followed by a rest stage of 10s at the same applied potential, the determinations were done by scanning potential from -1.4 to -0.2 V (+0.7V in the case of mixtures containing Hg(II)) using a step potential of 4mV and pulse amplitude of 50 mV [6][5].

In all the cases whre the samples were prepared a buffer solution was employed, buffers employed in the different applications are detailed in table 3.2.

**Table 3.2**: The following table details the composition of the different buffers employed in the works presented in this thesis memory.

| Buffer | Composition | Ph | Article |
|---|---|---|---|
| Artificial Wastewater | 3.8 mM $(NH_4)_2SO_4$ + 8.3 mM $MgSO_4$ + 0.66 mM $MnSO_4$ + 0.03 mM of $FeSO_4$ | - | [1] |
| Phosphate Buffer | 100 mM $H_2PO_4^-$/ $HPO_4^{2-}$ + 100 mM KCl | 6.5 | [1] |
| Acetate buffer | 100 mM $CH_3COOH$/ $CH_3COO^-$ | 4.5 | [2, 3] |
| Acetonitrile/Phosphate buffer | 50 mM $H_2PO_4^-$/ $HPO_4^{2-}$ + 50 mM KCl | 6.5 | [4] |
| Cleaning Buffer | 50 mM KCl | 10 | [4, 5] |
| Ferro/Ferryciannyde Buffer | 2 mM $[Fe(CN)_6]^{4-}$/$[Fe(CN)_6]^{3-}$ + 100 mM $H_2PO_4^-$/ $HPO_4^{2-}$ | 7.4 | [2, 4-7] |

In order to eliminate any remaining impurities from the electrode, an electrochemical cleaning stage was considered between measurements. This stage was performed by applying a conditioning potential ($E_{cond}$) for a duration after each measurement, in a cell containing fresh buffer solution.

The measurements were performed using an Autolab PGSTAT20 (Ecochemie, Netherlands) potentiostat in a multichannel configuration and the software employed to record the measurements was GPES Multichannel 4.7.

**Figure 3.4.** 6-channel AUTOLAB PGSTAT20 employed with GPES Multichannel 4.7

## 3.5. Array selection

After more than 20 years of research, in the sensors and biosensors field, Sensors and Biosensors group has developed a wide catalogue of composite sensors (§3.1). However, the number of sensors used in certain applications is limited by the hardware available; in our case the number of sensors is limited to 6 as we the equipment used in all works comprised in this thesis memory is a 6-channel Autolab PGSTAT20. Therefore the next issue is the selection of a relevant and non-redundant 6 sensor array.

As explained in §1.3.2.1 Principal Component Analysis is a tool that allow the maximization in the variance of a set of samples, this makes PCA an ideal tool to detect (dis)similarities and redundancies between electrodes. PCA enables us to evaluate the similarities between sensors with the objective of select the best combination of sensors, which is an array where its sensors display a high degree of complementarity. Therefore, instead of using the global response of the array to perform the PCA each sensor sample data is considered an individual

sample, in this manner the number of samples is multiplied by the number of sensors. When performing the PCA the main focus is to select those electrodes that appear in opposite coordinates when plotting the scores plot of the first principal compounds, as can be observed Figure 3.5 the scores plot is divided in the four quadrants ( +/+, +/-, -/+ and -/- ) and the selected electrodes are those that appear in each quadrant. This approach is specially useful when each sensor provides multiple values and the traditional loadings plot is difficult to interpret due the high amount of original variables.

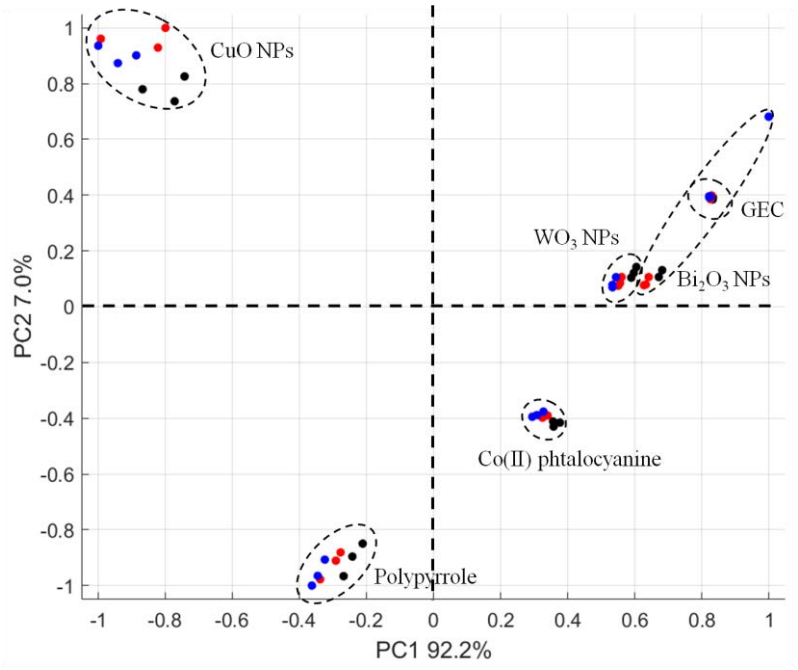


**Figure 3.5.** Score plot for the first 2 PCs for a set of electrodes, The red, green and blue are the different compounds considered

## 3.6. Model construction

In order to predict the different variables from the Electroanalytical measurements it is necessary the use of chemometric techniques to build an effective predictive model. Mainly the model consists in a mathematical construct that taking into account the electrochemical responses of the array (the predictors) is able to predict the desired variables.

The model will be built in three differentiates steps: data pretreatment, optimization of the model and model validation. The first step is focused on the data dimensionality reduction and/or noise elimination; the complexity of this step will depend on the chemometric method chosen, even though some methods do not specifically require a pretreatment step it has been proven that some treatments improve the quality of the original data [11][12]. The second

step is the selection of the chemometric method, PLS or ANNs, and its optimization. Finally, the optimized model will be evaluated comparing the predicted values versus the real values of an independent sample set (cross validation).

In the next sections are the detailed the procedures used in the different steps of the model construction.

### 3.6.1. Data preprocessing

The main disadvantage when ETs are involves is the high dimensionality of the obtained data. This high dimensionality can affect negatively the predictive capabilities of the model and lead to an over fitting situation or to a local minimum in the model. Therefore, a preliminary step is required, in this step the data is usually treated to avoid baseline problems and then compressed to reduce and extract the meaningful information. There are many options to correct the base line in the different samples and different methods to compress the data, the following sections will detail the different methods from simpler ones to more complex.

### 3.6.2. Data pretreatment

When different sensors are involved in the array response certain precautions have to be taken into account. First of all, the weights of the different sensors have to be of equal importance. The main measures to ensure that are data centering, normalization, standardization and autoscalation:

- **Data centering**: It relates the data with the arithmetic mean in a way that all the data has an arithmetic mean of 0 ($\bar{x}$=0).

$$= \quad - \bar{} = \quad - \frac{1}{n}\sum_{=1}^{n} \qquad \textbf{Equation 3.1}$$

- **Standardization**: It equals the dispersion of the different sensor data in a way that all the data has a standard deviation of 1 (s=1).

$$x_i = \frac{x_i}{\sqrt{s_i}} = \frac{x_i}{\sqrt{\frac{1}{n-1}-\sum_{i=1}^{n}(x_i-\bar{x})^2}} \qquad \textbf{Equation 3.2}$$

- **Autoscale**: this operation combines the two previous ones, data centering and standardization. The data is centered at 0 and the standard deviation is 1 ($\bar{x}$=0 and s=1).

$$x = \frac{x_i - \bar{x}}{\sqrt{s_i}}$$ **Equation 3.3**

- **Normalization**: It scales the data between a certain range of values, the more common are from 0 to 1 (Equation 3.4) or -1 to 1 (Equation 3.5), so all the sensors have the same variation range and scale.

$$x_i = \left(\frac{x_i - min(x)}{max(x) - min\,(x)}\right)$$ **Equation 3.4**

$$x_i = 2 \cdot \left(\frac{x_i - min(x)}{max(x) - min\,(x)}\right) - 1$$ **Equation 3.5**

### 3.6.2.1. Feature selection

This method is the simplest one, the input data is reduced though the manual selection of the data points considered relevant. This method may seem crude but with an experienced user doing the selection of the different data points the resulting model will be able to predict within an acceptable margin the problem samples. An early example of this method of selection of input data was used in the Sensors and Biosensors group to build a predictive model to predict the polyphenol concentration [13][14]. Nevertheless, this method has been abandoned in favor of more efficient and automatized methods which take into account the whole range of data available.

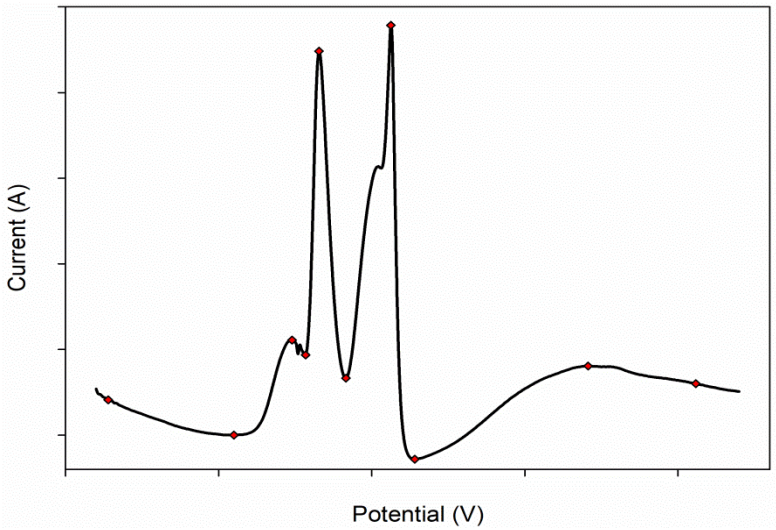


**Figure 3.6.** Example of input selection: in red the manually selected points.

Feature selection methods have been improved with the use of statistical treatments and algorithms to select the optimal inputs, one of the most used are the Causal Index (CI) and Genetic Algorithms (GA) [15][16][17].

In this thesis CI has been used to select and reduce the amount of inputs feed to the artificial neural networks models by taking into account the overall weight contribution of each the input and then removing the less significant, this process is repeated until the number of inputs is low enough that causes a degradation in the model predictive performance. n. The CI is calculated as the sum of the product of all "pathways" between each input to each output, Equation 3.6 has been used to determine the contribution of each input, where e there are h hidden neurons, $W_{kj}$ are the connection weights from hidden neuron j to output k, $W_{ji}$ are the connection weights between input i to hidden neuron j.

$$CI = \sum_{j=1}^{h} W_{kj} \, x \, W_{ji} \qquad \textbf{Equation 3.6}$$

The CI numerical results are relative as they indicate the magnitude and sign of a change in an output when a particular input is changed. Their advantage is that they do not depend on a particular input vector, but on the connection weight set that represents all the training input vectors. This is also one of their limitations, as a local situation may be overlooked in the global representation. Examining the CI for each output as a function of the inputs' number reveals the direction and the magnitude of the relationship of the inputs on the particular output.

In the case of GA, the selection procedure is performed in a much different way. The original inputs (genes) to be feed to the model are arranged in N binary string (chromosomes), and then these chromosomes are subjected to "reproduction", "mutation" and "crossover".

The "reproduction" step means that the good chromosomes (those that have good predictive results) are passed to the next iterations unchanged, the "mutation" operation consist in generation of new chromosomes though the random change, usually limited to 1 gene, and the "crossover" step where each chromosome competes with its neighbor. The losers are discarded whereas the winners are crossed and placed in the next generation. The competitors always consist of a mutated and crossed chromosome respectively. An example of the process is schematized in Figure 3.7.

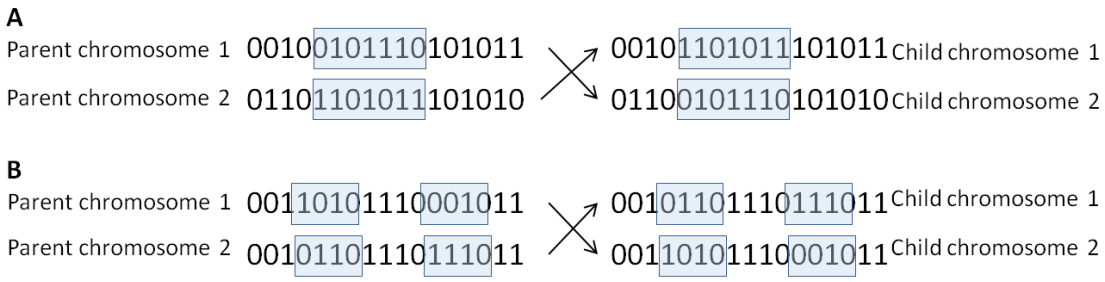


**Figure 3.7.** Crossover scheme, (A) cross-over type 1 and (B) cross-over type 2.

However, these strategies require a considerable amount of training time and computational power than simple compression methods, such as Fast Fourier Transform or Discrete Wavelet Transform, as they are based in the convergence of the optimal input sets though a relatively long iterative procedure.

### 3.6.2.2. Polynomial fitting

The next simpler option is the fitting of the voltammogram using a polynomial function of n grade, such as exponential, Gaussian, wave functions (sine or cosine), etc [18]. The obtained function coefficients will be used to build the predictive models as inputs.

The fitting of the voltammograms are usually performed though the resolution of the Legendre polynomials (Equation 3.7) employing the standard power series method, if the folling conditions are meets: $|x| < 1$, n is an integer and the series for this solution terminates (i.e. it is a polynomial). These solutions form a polynomial sequence of orthogonal polynomials called the Legendre polynomials. Each Legendre polynomial $P_n(x)$ is an nth-degree polynomial. These polynomials can be expressed with Rodrigues simplified formula, (Equation 3.8).

$$P_n(x) = \frac{1}{2^n n!}\frac{d^n}{dx^n}[(x^2-1)^n] \qquad \textbf{Equation 3.7}$$

$$P_n(x) = \frac{1}{2^n}\sum_{k=0}^{n}\binom{n}{k}^2 (x-1)^{n-k}(x-1)^k \qquad \textbf{Equation 3.8}$$

### 3.6.2.3. Sliced windowed integral

One of the more effective and simple procedures is the sliced windowed integral. The basis for this method is to use the area under the curve instead of the current that can be considered an average of the current values considered [19]. In the method the

voltammogram is divided in sections (*k*), as can be seen in Figure 3.8, and the area under the curve of each section is calculated.

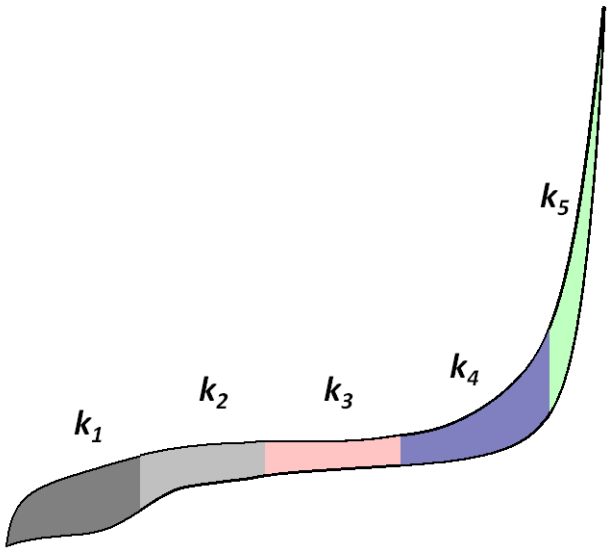


**Figure 3.8.** Scheme for a sliced windowed integral pre processment with k=5

Its high effectivity can be correlated to the classical voltammetric methodologies where the peaks are identified and its height or area is used to build the different calibration curves.

As it happens with other methods the number of sections in which the voltammogram is divided is the key parameter in this method. If the number of sections is too small the information obtained is not going to be representative of the voltammogram, at larger *k* the fidelity and reproducibility of the original signal is better at an expense of the compression level. A compromise between compression and fidelity of the original signal must be achieved, the optimal number is difficult to know beforehand and a combination of previous knowledge and optimization of the number of sections is required to find the optimal *k*.

### 3.6.2.4. Principal component analysis

Another tool available to perform the dimensionality reduction and the feature extraction is the Principal Components Analysis (PCA). PCA is mainly used as a preliminary explorative method, explained in detail in § 1.3.2.1, but can be used to reduce the data dimensionality and in some cases can improve the signal to noise ratio.

The PCA calculates new orthogonal directions that maximize the variability of the samples; the new coordinates are calculated in a variability gradient such as the first new coordinate (1 PCs) contain the higher variance. In this fashion a sample that usually has between 200 and

450 points per voltammogram can be compressed up to 5-10 PCs. The fact that the first coefficients contain the more relevant information (higher variability between samples) allows us to use PCA as a compression method simply discarding the last PCs.

The number of coefficients (PCs) used as inputs will depend of the nature of the data always reaching a compromise between compression ratio and preserved information. In this case the reconstruction of the signal is impossible but the cumulative variance of the PCs can be used as a guideline to select the number of inputs.

#### 3.6.2.5. Fast Fourier Transform

Discrete Fourier Transform (DFT) is widely used in different digital signal processing applications but it is the Fast Fourier Transform (FFT) algorithm variant that is more commonly employed. FFT algorithm is highly efficiency and when large datasets are involved its use can represent a reduction of the computational time of 1-2 magnitude orders. The Fourier transform decomposes the original signal using a pair of cosine and sine functions at different frequencies; the frequency contribution to the original signal is determined by a calculated coefficient. In this fashion a number of coefficients equal to the original signal are obtained, each point corresponds to an associated frequency band for a specific section of the original signal.

In a similar fashion as PCA the first coefficients contain the more relevant information and it is possible achieve a high degree of compression, while relevant information is preserved, selecting the first coefficients and discarding the rest. Additionally this method can be used as a filter to eliminate the high frequency noise present in the measurement [20]. Another advantage of FFT method is the possibility of signal reconstruction using the inverse Fourier transform, which enables the evaluation of compression step (§1.4.1.8).

#### 3.6.2.6. Discrete Wavelet Transform

Discrete Wavelet Transform (DWT) is a preprocessing technique that offshoots from Fourier transform, it was first developed in the late 80s [21]. The main difference between the Fourier and Wavelet transform is that the former one projects the signal using sinusoidal functions while Wavelet uses wavelet mother functions and is able to obtain both the frequency and the location of the relevant information. This last characteristic has made DWT a widely employed tool in chemical analysis especially in noise cancellation, signal filtering, baseline corrections or resolution of overlapping peaks [22].

Wavelet transform uses a set of functions to decompose the original signal; this set of functions is obtained from a mother wavelet function through a series of translations and dilations [21]. The *Daubechies* family is the more employed in DWT applications but different mother functions can be used with the same effectiveness; Figure 3.9 shows the more employed mother functions.

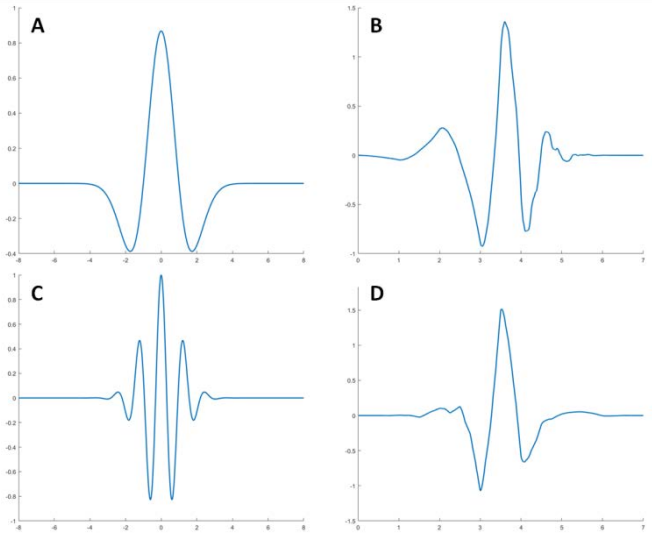


**Figure 3.9.** Some of the more employed wavelets. (A) Mexican hat wavelet, (B) Daubechies 4 wavelet, (C) Morlet wavelet and (D) Symlet 4 wavelet.

The procedure to decompose the signal and obtain the coefficients is the Mallat's tree algorithm. Figure 3.10 shows the workflow of Mallat's algorithm applied upon a signal of length M decomposing it in orthogonal subspaces of M/2 length on every compression cycle [21]. In this fashion, this step can be repeated k times to increase the compression level. However, the compression degree comes at a cost as the reconstruction grade will be degraded in each cycle of compression a certain amount.

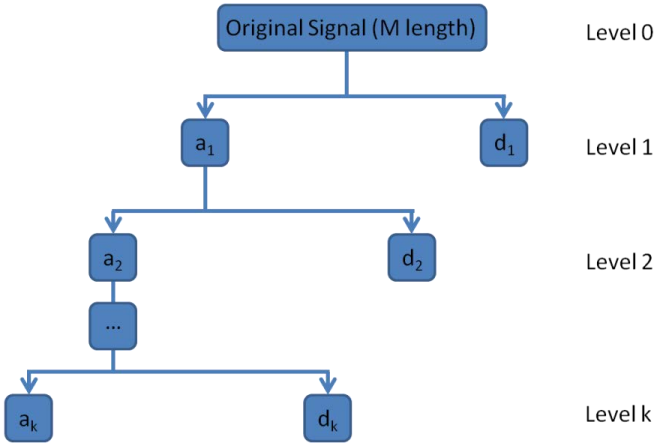


**Figure 3.10.** Depiction of Mallat's decomposition scheme.

As happened with FFT, wavelet transform presents the advantage of combining the compression with a noise filtering effect. On the whole, DWT is a versatile tool that allows compression, feature extraction and noise filtering in the same preprocessing step with the additional advantage of being able to reconstruct the compressed signal to evaluate the compression degree.

### 3.6.3. Reconstruction degree evaluation

Finally, the goodness of the compression method needs to be evaluated; in the cases that the compression can be undone, FFT and DWT, the reconstruction rate is calculated. The reconstructed parameter allows us to select an optimal level of compression where the compression allows the conservation of the meaningful information while reducing the overall complexity of the departure information. In Figure 3.11 can be seen different reconstructed signals and the degradation in the reconstructed signal at higher compression rates.

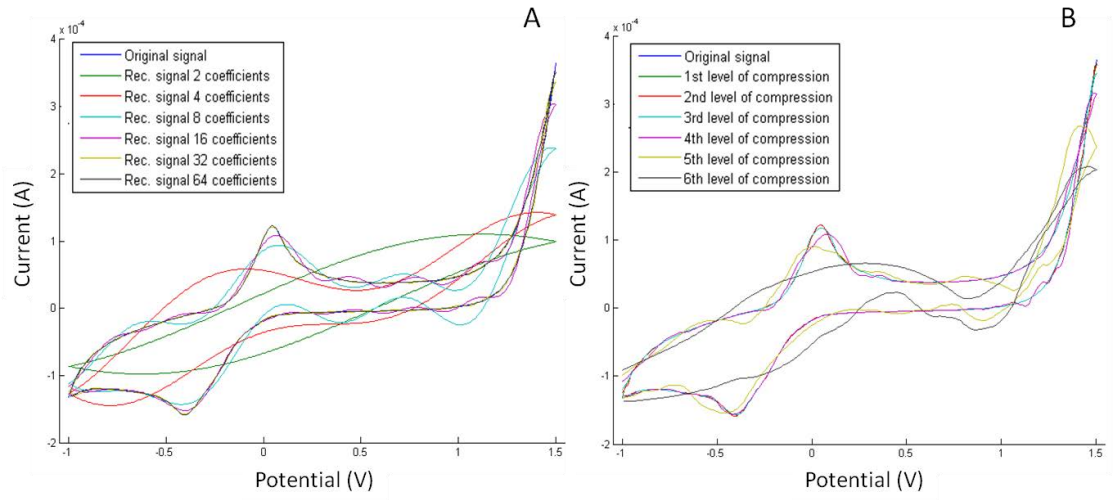


**Figure 3.11.** (**A**) Original signal vs Reconstructed signal with different levels of compression with FFT. (**B**) Original signal *vs* Reconstructed signal with different levels of compression with DWT.

Reconstruction degree was calculated using 2 parameters: the determination coefficient ($R^2$) between the original data (A) the reconstructed data (B) and the $f_c$ parameter that consider the area under the voltamograms when the original and the reconstructed voltammograms are superimposed [12].

The parameters are calculated with the unfolded voltammograms; figure 3.12, without taking into account the potential where the currents are measured. The first parameter, $R^2$, corresponds to the linear correlation between the original data and the reconstructed data. The second parameter, $f_c$, is defined by the rate between the intersected area, A parameter in equation 3.8, and the area under the original and reconstructed voltammograms, B parameter in equation 3.8.

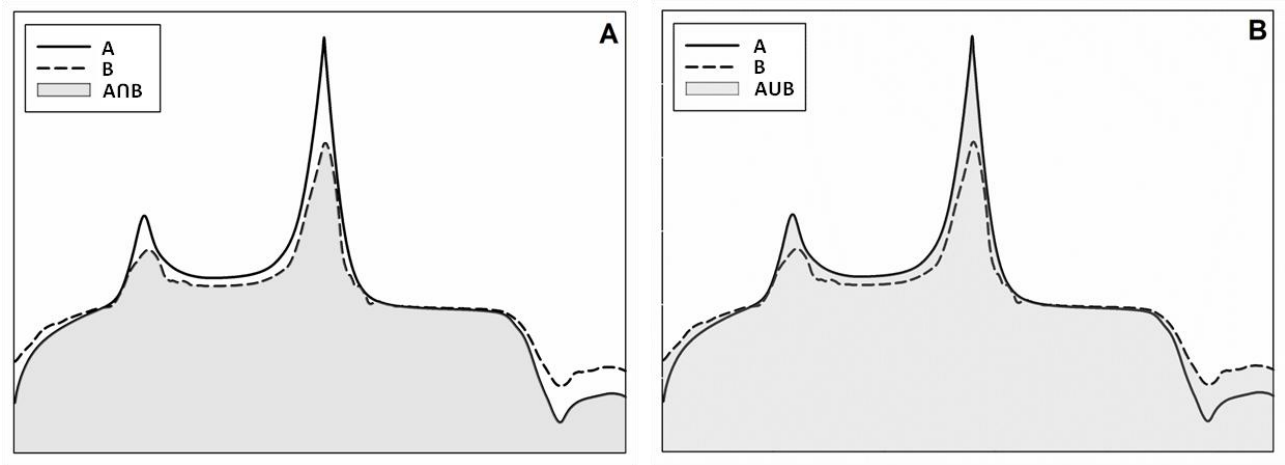


**Figure 3.12.** Scheme of the *f*c, in (A) A∩B and (B) AUB

$$f_c = \frac{A \cap B}{A \cup B} = \frac{\sum_{i=1}^{M} (max\langle a_i, b_i \rangle - |a_i - b_i|)}{\sum_{i=1}^{M} (min\langle a_i, b_i \rangle - |a_i - b_i|)}$$ **Equaction 3.8**

Both parameters give a result between 0 and 1, being 1 a perfect match between voltammograms and 0 the maximum difference between voltammograms. The $f_c$ parameter evaluates the similarity between the voltammograms in a similar fashion of $R^2$ but it is more sensitive to small changes.

### 3.6.4. Construction and Validation

Once the data set is clearly defined by the variables or coefficients that will be used as inputs in the model, the next step is the modelitzation of the target variables/outputs. The first step is to determine the type of information that we want to predict, depending on the information to be predicted the model will be qualitative (for classification and differentiation purposes) or quantitative (to quantify of the different compounds present in a sample). The type of application to be developed will influence the chemometric tool to be employed in the predictive model.

Therefore, in both cases the first step is the division of the experimental data in two subsets prior to the model construction. The first subset will contain approximately the 66% of the

experimental data points and will be used to model the output variables; this subset is commonly named the train subset. The second subset, containing the 33% of the data, will be used to validate the goodness of the model, henceforth is named the test subset. This last set is not used in the modeling of the data; it is exclusively used to validate the predictive capabilities of the different models interpolating the signals of this subset of samples.

The evaluation of the goodness of the model is performed with through the correlation of the predicted values *versus* expected values. A good correlation with the expected values means that the model has achieved configuration able to predict the samples within the training subset limits. On the other hand, a bad correlation means that the model is not able to correctly describe independent samples within the limits of the training subset, this can be due to the lack of relation between the analytical signal and the variables of interest or due to an overfitting situation (§ 1.3.3.4.3), unable to predict samples that are not those of the training subset.

However, it is common to employ a third subset of samples, named validation subset, is used to act as a failsafe in case of overfitting and to stop the training procedure before reaching a compromised situation. Nonetheless, in the case of ANNs the use of a validation set is not necessary if the Bayesian Regulation algorithm is employed in the training procedure (§1.3.3.4.3) as it's designed specifically to avoid overfitting situations [23].

In the following sections the main methods for both qualitative and quantitative modeling tools employed in the works presented in this thesis memory will be described. Also the employed modeling strategies in the validation procedures will be explained in detail.

## 3.7. Qualitative Analysis

The qualitative analysis has been performed using 2 methods: principal component analysis (PCA) and linear discriminant analysis (LDA). PCA and LDA are closely related as both methods look for the best linear combinations that explain the variation in the data set [24]. However, the difference between the 2 methods is in the learning step; while the PCA is an unsupervised method, on itself do not classify the different samples and requires an additional tool to perform any kind of classification, which helps to recognize hidden patterns in the data; LDA is a supervised method meaning that there is a modeling step previous to the classification, the LDA seeks to build a model that explain the variance between sample classes while the PCA seeks variance between all the samples.

This classification between models is based in how the data is handled to obtain the modeling functions. In one hand the supervised methods require a training subset plus the desired variable values of this subset, the model is build taking into account the parameters that will correctly model the desired variables and then is validated by an independent subset of data (test subset). On the other hand, the unsupervised methods only the input data is considered, the samples are not divided in different subsets and the class labels are not provided. The unsupervised models present only a different visualization of all the samples, a new point of view that maximizes the similarities and differences between samples, for this reason PCA is often employed as a visualization tool to visualize sample clusters and can not be considered a pattern recognition method by itself.

### 3.7.1. Principal Components Analysis (PCA)

Principal component analysis (PCA) is a mathematical procedure where the data, a set of *j* observations with *n* dependent variables, is orthogonally transformed to obtain a new set of n variables linearly independent named Principal Components (PCs) [25]. Therefore, the original information contained in the n variables is contained in a new set of variables, the PCs, with new coordinates named scores, Figure 1.9.

As stated in the previous paragraph the orthogonal transformation does not imply a reduction in the number of variables but only a change in the coordinates system. However the new variables are generated in a way that contain the maximum amount of variability in a descendent gradient, i.e. the first PC (PC1) is the direction that explain best the variability of the data set (maximum variance), PC2 is orthogonal to PC1 and contains the second maximum variance, and so on.

Once the PCs are obtained the new coordinates for the data set are obtained as the sum of the original data multiplied by the corresponding PC coefficient. This new values are known as scores and each samples has 1 score per PCs, resulting in matrix of n scores and j observations same dimensions as the original data set.

PCA allows us to select the first PC, usually the first 5-10, to explain the variability of the sample set, reducing the n variables (usually 250 in the case of voltammetric data) to a few coefficients. This capacity to explain the variability in a reduced number of variables is what makes PCA a method used to reduce the data dimensionality, especially in Statistics, allowing the evaluation of the variability sources and quantify their contributions. Finally, it has to be

noted that PCA is sensible to the scale of the variables and they need to be normalized to avoid distortions in the analysis.

### 3.7.2. Linear Discriminant Analysis (LDA)

Linear discriminant analysis (LDA) is a supervised classification method based on the Bayes' theorem. In LDA the model is formed by *k*-1 lineal discriminant functions, where *k* is equal to the number of classes and also will be the number of possible axis/dimensions, based in the lineal combination of predictive variables; the criteria to chose the linear combinations is to maximize the discrimination between classes[26].

Therefore, the new axes instead of being based in the maximum variation in the response matrix (like PCA) in LDA are based in the maximum discrimination between sample groups (classes), Figure 1.12. In this way the samples are classified taking into account the distance between sample and the class centroid, being the Mahalanobis distance one of the more employed.

Mahalanobis distance is used to determine the similarity of a certain sample with the different class clusters, the main difference with Euclidian distance is that it takes into account the covariance between variables [27]. Therefore, it corrects the problems that arise with different variable scale and correlation between variables, in this sense Mahalanobis distance is the equivalent to the use of variance for univariate measurements, taking into account the different variables in each direction and the variable covariance.

As in all methods described the functions are generated from a train subset with known information about sample class and it is evaluated with an independent subset (test) with unknown classes. Additionally, LDA can be combined with feature selection mechanisms such as the step inclusion methods [26], these methods are extremely useful to select the relevant variables and discard the ones that not contribute and diminish the possible predictive distortions. Therefore from an extensive variable collection, some of which predictively relevant but most of them useless, a reduced subset of inputs can be selected to optimize the classification task.

The variable selection is based in statistical criteria such as Wilk's Lambda (Λ) or Mahalanobis distance [26][28]. Wilk's lambda is used in discriminant analysis as a separation measure between the centroid of the different classes and used to select the variables used in the model; the inclusion of certain variable depends on by how well each independent variable contributes to the model. The scale ranges from 0 to 1, where 0 means total discrimination

and 1 means no discrimination. Each independent variable is tested by putting it into the model and then taking it out generating a Λ statistic. The significance of the change in Λ is measured with an F test; if the F value is greater than the critical value, the variable is kept in the model. In the same way Mahalanobis distance is used to optimize the classification, a big value in the distance indicates a good separation between class clusters.

Wilk's lambda is defined as measure of the percent variance relation in dependent variables (class) not explained by differences in the independent variable; it relates the intra-class inertia and the total inertia and restricted to a value ranging from 0 to 1, if only a small portion of the inertia is not explained by the group separation then there exists a good separation and the average of the class is significantly distinct. A value of zero means that there is a good separation between class clusters [26][28].

## 3.8. Quantitative Analysis

In the case of numerical variables the model will simultaneously model the target variables to predict the sample quantitative information. The main difference is the possibility of building multiresponse models, to predict simultaneously different variables (a target matrix) as opposed to qualitative cases (a target vector). Many methods of qualitative analysis exist, linear or non-linear, such as multiple linear regression (MLR), principal component regression (PCR), partial least squares (PLS), n partial least squares (nPLS) or artificial neural networks (ANN) but this section will be focused in artificial neural networks (ANN) and partial least square (PLS).

The classification of the different methods is based in the way the regression analysis is performed. In the case of non linear methods the data set is modeled through function that combined in a non-linear fashion the different model parameters and the data variables in an iterative process. In the linear methodologies the fitting consist in a linear regression, usually the least squares approach.

The group of sensors and biosensor has a wide experience using ANNs thus it is the default method employed to address the different work scenarios, also PLS was employed for comparison purposes as it is the standard chemometrics method [29]. However, ANNs is the one of the more complex methods and requires a more time consuming optimization step than the more classical linear methods [30].

### 3.8.1. Partial Least Squares (PLS)

Partial least square regression is a method that combines PCA and multiple regression characteristics. PLS is focused on the maximum predictive performance. This maximization of the predictive performance is achieved through the simultaneous modeling of sensor responses and target variables; the treatment transforms the original variables into a new set of variables (LVs) that maximize the prediction rate [31]. Latent variables are similar to the PCs in PCA but represent new set of variables that correlate in a linear fashion with the desired target variable(s).

The PLS methods can be used to predict more than one variable, i.e. in the case of PLS the response is a single variable, while in the case of multiple target variables the term PLS-*n* is frequently employed, i.e. in PLS-2 the response matrix will have a 2 x *n* being n the number of samples. This methods is widely employed in the chemometric field due its relatively simple optimization, only the number of LVs has to be optimized, and its short training times. The main parameter that has to be taken into account when a PLS model is optimized is the number of latent variables employed in the linear regression, as it was explained in § 1.3.3.2 the number of LVs is equal to the number of points in the original sample. Therefore, the number of LVs is chosen according to the cumulative variance (Figure 1.15) and the root mean square error (RMSE) that the model yields when the predicted values are compared with the real ones.

### 3.8.2 Artificial Neural Networks (ANN)

Artificial neural networks (ANNs) are mathematical models inspired by the functioning of the animal nervous system (in particular the brain) that are used as a tool for chemometric multivariate analysis. ANNs work imitating the biological learning task, i.e. requiring a training process where the weights of those connections are adjusted, and build a model that will allow the prediction of the desired parameters. Its complexity allows a high versatility, great performance and its significant likeness to human pattern recognition mechanisms. However, the complexity of ANN models (connections weights and biases, transfer functions, etc) is also one of the major disadvantages as the network architecture or topology is crucial to achieve the desired results [32]. Therefore, the architecture parameters have to be optimized either with previous knowledge of the data or more commonly through systematic evaluation of the different architectures [33].

The first limitation that appears when using voltammetric data is dimensionality of the input data, ANNs require to be feed with monodimensional data and in the case of

voltammetric arrays the data present a high dimensionality (current intensities x sensors x samples). Therefore, a previous treatment is required to reduce the dimensionality of the data.

The standard treatment to reduce the dimensionality in the case of voltammetric data is the unfolding of the voltammograms from a 3D matrix (tensor) to a 2D matrix, then the data of each sensor is catenated, Figure 1.8. In this fashion, each unfolded voltammogram is combined in a single vector. However, this procedure can generate discontinuities that can distort the data and hinder the modeling step.

Also it has to be taken into account that to obtain a good predictive capabilities and a model able to generalize in a reasonable time the number of inputs per sample has to be limited, as explained in § 1.3.3.4.3. Limiting the number of inputs per sample, employing the strategies described in § 3.2.6.1, the training time is reduced and the possibilities of overfitting the model in the training step are considerably reduced.

Once the set of inputs is reduced and before the obtention of the final model its architecture needs to be optimized. As explained, the different inner parameters (number of hidden layers neurons, training algorithms, transfer functions, etc) are selected though trial-and-error.

All predictive models in this thesis memory were built using a single hidden layer as the obtained results were quite satisfactory. However, the number of hidden layers can be increased if the case has a high complexity. Once the number of hidden layers is fixed then the number of neurons in this hidden layer has to be optimized, the number of neurons was optimized between 1 and 12. The number of neurons in the input layer is determined by the nature of the input data (number of coefficients or number of data points) and the neurons in the output layer depend on the modeled variables.

Mathematically, each output represents just a specific linear combination with specific weights from each preceding perceptron, though passage from layer to layer is also modulated by the transfers function used. Those are used to limit the neuron output and generally came from the interpretation we give to the said output. It is common to use sigmoidal transfer functions in the hidden layer, like the log-sigmoidal (logsig) and the tan-sigmoidal (tansig), or lineal ones like purelin, satlin or satlins (Figure 1.19).

The type of ANN was chosen according previous experiences of the group of sensors and biosensors, the chosen ANN models where feed-forwards models with a back-propagation learning algorithm (Bayesian Regulation) or the use of a single hidden layer Additionally, the

inner parameters such as learning rate (α=0.01), momentum (β=0.4), and max error (0.03) were also fixed according to our experience on the topic [34].

## 3.9. Validation methods

Once the model architecture is defined and the model is built it is necessary an evaluation of its predictive capabilities. The standard procedure in qualitative and quantitative models consists in the comparison between the predicted values and the expected real values for an independent subset of samples.

### 3.9.1 Data Subset selection

The first step to build the model and its posterior validation is to define the train and test subsets. The first set will be used to train the model, to train the model contain the response matrix (*x*) and the target matrix (*y*) are feed to the model; in other words the model inner parameters will change to be able to predict the train *y* matrix from *x*. The second set will be used to evaluate the goodness of the model and its predictive capabilities by comparing the values obtained from the model when *x* is provided with the real target values (cross validation).

The key factor in validation is the type of subset division chosen to evaluate the model. Therefore, there are different validation methods that can be used such as Leave-one out, K-fold, Montecarlo, Bootstrapping or Jack-knife all with slightly different ways of dividing and/or substitute the data samples [35][36]. However, the methodologies more employed used in ETs approaches are the ones detailed as it follows:

- The **train/test division** is the most employed method, it consist in a division of the total data set from 60:40 to 80:20 rates between train and test subsets. This method is especially useful when the work case is obtained through experimental design, the train samples will be described by the design while the test samples will be randomly distributed inside the experimental domain, if that is not the case the samples are distributed randomly between train and test subset.
- In **Leave-X-out** or **K-fold** method the data set is randomly divided in *k* subsets, always taking into account the different sample type proportion and maintaining it in the different folds (*k*). Therefore, one of the generated subsets is employed as a test set while the others are used as a train set, this process is repeated *k* times for each subset in a manner that ensures that all the subsets are treated once as a test set. Finally, the results for each fold are grouped and averaged to obtain the final model predictor

matrix. The main advantage of this method is that ensures that all the samples are taken into account in the train (*k*-1 times) and validation process (*k* times) [37].

- A variation of the previous method is the **Leave-one-out** method, in this case *k*=1 and is extensively used. Each sample is individually used as the test set and the process is repeated for each sample. In this fashion, the sample is classified using the rest of the samples as the train set, the models obtained using this cross validation strategy usually yield slightly over optimistic results.
- The **repeated random subsampling** validation was suggested as an alternative when the previously described methods did not yield acceptable results [38]. In this case the test data set is comprised of randomly chosen samples, the number of samples in the test set can vary from 1 sample to a group of samples [39]; the main advantage of this method is that avoids the dependence of train/test subdivisions as the subsampling cycle is repeated *k* times, the prediction error is calculated averaging the different results in each cycle. Therefore, this method allows the estimation of prediction confidence intervals [40].

## 3.10. Evaluation of the model

The evaluation of the predictive model will depend on the modeled variable; the models can be divided in qualitative models (classifiers) and quantitative models.

### 3.10.1. Qualitative models

Qualitative models are models built to classify the unknown samples in different categories. The main tools and parameters employed to evaluate qualitative models are confusion matrixes, success rate, sensitivity and specificity [41].

- The first tool to evaluate the predictive capabilities is the confusion matrix of the test subset, Table 3.3. The confusion matrix is a tool that allows a quick visualization of the predictive capabilities, it is formed by a square matrix where rows correspond to the number of cases in each class while columns show the number of samples assigned to that specific class, and correct samples can be easily revised as they will appear in the diagonal.

**Table 3.3.**Example of a confusion matrix for a binary system

| | | Predicted | |
|---|---|---|---|
| | | Positive | Negative |
| Expected | Positive | True Positive (TP) | False Negative (FN) |
| | Negative | False Positive (FP) | True Negative (TN) |

- The success rate is defined by the number of correctly classified samples divided by the number of samples in a certain class. Equation 3.9. It shows only the number of correctly classified samples, true positives (TP), but it does not take into account the misclassified samples, false positive (FP), and the relative size of each class.

$$\frac{\sum_{i=1}^{n} TP_i}{\sum_{i=1}^{n} TP_i + FP_i} \qquad \textbf{Equation 3.9}$$

- The sensitivity, also called true positive rate, measures the proportion of positives that are correctly identified, Equation 3.10. It shows the capabilities of the built model to classify as positive samples only the real positive ones.

$$\frac{1}{n} \sum_{i=1}^{n} \frac{TP_i}{TP_i + FN_i} \qquad \textbf{Equation 3.10}$$

- The specificity, also called the true negative rate, measures the proportion of negatives that are correctly identified, Equation 3.11. It measures the capabilities of the built model to only classify real negative samples as negative.

$$\frac{1}{n} \sum_{i=1}^{n} \frac{TN_i}{TN_i + FP_i} \qquad \textbf{Equation 3.11}$$

- The Pearson chi square test is used to provide a measure of the goodness of fit. It is calculated from the respective confusion matrix with a 95% confidence level, the coefficient of contingency is also calculated to describe numerically the ability of the constructed model [42].

### 3.10.2. Quantitative models

The evaluation of qualitative models is handled mainly with 2 different methods as the predicted response is numeric. The first one is the construction of comparison graphs of predicted concentration values *versus* expected concentration values and its correlation analysis; the second is based on the root mean square error (RMSE) or the normalized root mean square error (NRMSE). In the evaluation of the different constructed models both methods are employed.

- A linear regression is obtained from the predicted vs. expected plots for the *j* analaytes considered. The values of the slope (m), the intersect (b) and the correlation coefficient (r) are calculated. Comparing the the 3 parameters values with their ideal values (1, 0 and 1respectively) as an indicator of the model goodness. To facilitate the evaluation of the model the sum of the difference between each value and the ideal value has been calculated as it is shown in Equations 3.11 and 3.12.

$$X = \sum_j |1 - X_j| \qquad \textbf{Equation 3.11}$$

$$b = \sum_j |b_j| \qquad \textbf{Equation 3.12}$$

  In the case of correlation the values of Δr and Δm the values range from 0 to j, being 0 when the fitting is perfect and increasing up to j when the model degrades. The range of Δb will depend of the measure units being 0 the ideal value to achieve.

- Root mean square error is a measure that compares one by one the values of the data points of the predicted values and the original ones, Equation 3.13. For each point the error is calculated with the difference between the real value ($c_i$) and the predicted value ($\hat{c}_i$), the quadratic sum of those differences is divided by the number of points (n) minus 1 and the square root is calculated to obtain the correct units. In case of the total RMSE the number of analytes (*k*) must be considered as there will be *n* data points per analyte [43].

$$RMSE = \sqrt{\frac{\sum_{ij}(c_{ij} - \hat{c}_{ij})^2}{k \cdot n - 1}} \qquad \textbf{Equation 3.13}$$

The advantage of RMSE is that represents the average distance respect the fitted line in the same units, it provides an easy interpretable parameter in terms of measure. Therefore, the lower the value of RMSE the better is the fitting and the predictive capabilities of the model. An alternative to RMSE is the normalized root mean square error (NRMSE). NRMSE is obtained dividing the obtained RMSE by the concentration range of their respective analyte, Equation 3.14, the obtained parameter will range from 0 to 1 and will provide of the error for each analyte (*j*=1) or the global NRMSE (j>1).

$$\mathrm{NRMSE} = \frac{1}{\mathrm{j}} \sum_{\mathrm{j}} \frac{\mathrm{RMSE_i}}{\mathrm{c_{i,max} - c_{i,min}}} \qquad \textbf{Equation 3.14}$$

The advantatge NRMSE has over RSME is that allows for an easier interpretation in the global error, especially when the analytes involved have different concentration ranges. In this fashion, the problem is easily solved though a simple normalization of the RMSE values and changing an absolute error measure to a relative error.

## 3.11. Software

All the measurements and recollection of data was performed with GPES 4.7 and GPES Multichannel 4.7 (Autolab, Ecochimie, Netherlands). Chemometric methods and mathematical treatments were done with MATLAB (2016b) and the Neural Network Toolbox and Statistics Toolbox built in packages. The analysis and representation of the results was performed with Sigmaplot (Systat Software Inc, California, USA).

## 3.12. Bibliography


[1] F. Céspedes, E. Martinez-Fabregas, S. Alegret, *TrAC Trends Anal. Chem.* **1996**, *15*, 296–304.

[2] X. Cetó, A. González-Calabuig, J. Capdevila, A. Puig-Pujol, M. del Valle, *Sensors Actuators B Chem.* **2015**, *207*, 1053–1059.

[3] X. Cetó, A. González-Calabuig, N. Crespo, S. Pérez, J. Capdevila, A. Puig-Pujol, M. del Valle, *Talanta* **2017**, *162*, 218–224.

[4] A. González-Calabuig, X. Cetó, M. del Valle, *Talanta* **2016**, *153*, 340–346.

[5] N. Serrano, A. González-Calabuig, M. del Valle, *Talanta* **2015**, *138*, 130–137.

[6] A. González-Calabuig, D. Guerrero, N. Serrano, M. del Valle, *Electroanalysis* **2016**, *28*, 663–670.

[7] A. González-Calabuig, M. del Valle, *Talanta* **2018**, *179*, 70–74.

[8] X. Cetó, A. González-Calabuig, M. del Valle, *Electroanalysis* **2015**, *27*, 225–233.

[9] D. Belanger, J. Pinson, *Chem. Soc. Rev.* **2011**, *40*, 3995–4048.

[10] A. Mimendia, Desenvolupament I Aplicació de Llengues Electròniques per Anàlisi Ambiental, Universitat Autònoma de Barcelona, **2011**.

[11] L. Moreno-Barón, R. Cartas, A. Merkoçi, S. Alegret, J. M. Gutiérrez, L. Leija, P. R. Hernandez, R. Muñoz, M. del Valle, *Anal. Lett.* **2005**, *38*, 2189–2206.

[12] L. Moreno-Barón, R. Cartas, A. Merkoçi, S. Alegret, M. del Valle, L. Leija, P. R. Hernandez, R. Muñoz, *Sensors Actuators B Chem.* **2006**, *113*, 487–499.

[13] A. Gutés, F. Céspedes, S. Alegret, M. Del Valle, *Biosens. Bioelectron.* **2005**, *20*, 1668–1673.

[14] A. Gutés, A. B. Ibanez, F. Céspedes, S. Alegret, M. del Valle, *Anal. Bioanal. Chem.* **2005**, *382*, 471–476.

[15] Z. Boger, *Anal. Chim. Acta* **2003**, *490*, 31–40.

[16] J.-M. Vesin, R. Grüter, *Signal Processing* **1999**, *78*, 321–327.

[17] E. Richards, C. Bessant, S. Saini, *Chemom. Intell. Lab. Syst.* **2002**, *61*, 35–49.

[18] V. Pravdová, M. Pravda, G. G. Guilbault, *Anal. Lett.* **2002**, *35*, 2389–2419.

[19] X. Cetó, F. Céspedes, M. del Valle, *Microchim. Acta* **2013**, *180*, 319–330.

[20] D. E. Smith, *Anal. Chem.* **1976**, *48*, 517A–526a.

[21] S. G. Mallat, *IEEE Trans. Pattern Anal. Mach. Intell.* **1989**, *11*, 674–693.

[22] X.-G. Shao, A. K.-M. Leung, F.-T. Chau, *Acc. Chem. Res.* **2003**, *36*, 276–283.

[23] F. Burden, D. Winkler, in *Artif. Neural Networks*, Springer, **2008**, pp. 23–42.

[24] R. O. Duda, P. E. Hart, D. G. Stork, *Pattern Classification*, John Wiley & Sons, **2012**.

[25] I. Jolliffe, in *Encycl. Stat. Behav. Sci.*, John Wiley & Sons, Ltd, **2005**.

[26] R. A. Johnson, D. W. Wichern, *Applied Multivariate Statistical Analysis*, Prentice-Hall New Jersey, **2014**.

[27] B. F. J. Manly, J. A. N. Alberto, *Multivariate Statistical Methods: A Primer*, CRC Press, **2016**.

[28] D. J. Hand, *Wiley Ser. Probab. Math. Stat. Chichester Wiley, 1981* **1981**.

[29] H. Wold, *Encycl. Stat. Sci.* **1985**.

[30] I. A. Basheer, M. Hajmeer, *J. Microbiol. Methods* **2000**, *43*, 3–31.

[31] E. Richards, C. Bessant, S. Saini, *Electroanalysis* **2002**, *14*, 1533–1542.

[32] J. R. M. Smits, W. J. Melssen, L. M. C. Buydens, G. Kateman, *Chemom. Intell. Lab. Syst.* **1994**, *22*, 165–189.

[33] F. Despagne, D. L. Massart, *Analyst* **1998**, *123*, 157R–178R.

[34] M. del Valle, *Compr. Anal. Chem.* **2007**, *49*, 721–753.

[35] M. R. Chernick, W. González-Manteiga, R. M. Crujeiras, E. B. Barrios, in *Int. Encycl. Stat. Sci.*, Springer, **2011**, pp. 169–174.

[36] R. G. Miller, *Biometrika* **1974**, *61*, 1–15.

[37] P. Refaeilzadeh, L. Tang, H. Liu, in *Encycl. Database Syst.*, Springer, **2009**, pp. 532–538.

[38] L. Kanal, B. Chandrasekaran, *Pattern Recognit.* **1971**, *3*, 225–234.

[39] S. D. Peddada, **1993**.

[40] A. M. Molinaro, R. Simon, R. M. Pfeiffer, *Bioinformatics* **2005**, *21*, 3301–3307.

[41] M. Sokolova, G. Lapalme, *Inf. Process. Manag.* **2009**, *45*, 427–437.

[42] J. N. K. Rao, A. J. Scott, *J. Am. Stat. Assoc.* **1981**, *76*, 221–230.

[43] D. Wallach, B. Goffinet, *Ecol. Modell.* **1989**, *44*, 299–306.

# Results and Discussion

# 4. Results and Discusion

This chapter will be organized in three different Topic sections, each one explaining the results obtained in each field of work:

- Enviromental monitoring

**Article 1**: Use of a bioelectronic tongue for the monitoring of the photodegradation of phenolic compounds. X. Cetó, A. González-Calabuig, M. del Valle, Electroanalysis, 2015, *27*, 225–233.

**Article2:** Simultaneous Voltammetric Determination of Heavy Metals by Use of Crown Ether-modified Electrodes and Chemometrics. A. González-Calabuig, D. Guerrero, N. Serrano, M. del Valle, Electroanalysis 2016, 28, 663–670.

**Article 3:** Crown ether-modified electrodes for the simultaneous stripping voltammetric determination of Cd (II), Pb (II) and Cu (II). N. Serrano, A. González-Calabuig, M. del Valle, Talanta 2015, 138, 130–137.

- Beverage field

**Article 4:** Instrumental measurement of wine sensory descriptors using a voltammetric electronic tongue. X. Cetó, A. González-Calabuig, J. Capdevila, A. Puig-Pujol, M. del Valle, Sensors Actuators B Chem. 2015, 207, 1053–1059.

**Article 5:** Electronic tongues to assess wine sensory descriptors. X. Cetó, A. González-Calabuig, N. Crespo, S. Pérez, J. Capdevila, A. Puig-Pujol, M. del Valle, Talanta 2017, 162, 218–224.

**Article 6:** Voltammetric electronic tongue to identify Brett character in wines. On-site quantification of its ethylphenol metabolites. A. González-Calabuig, M. del Valle, Talanta, 2018, *179*, 70–74.

- Homeland Security

**Article 7:** Electronic tongue for nitro and peroxide explosive sensing. A. González-Calabuig, X. Cetó, M. del Valle, Talanta 2016, 153, 340–346.

# Article 1:

**Use of a bioelectronic tongue for the monitoring of the photodegradation of phenolic compounds**

Xavier Cetó, Andreu González-Calabuig, and Manel del Valle

*Electroanalysis,* 2015*,* 27, 225–233

The application of a voltammetric bioelectronic tongue for the simultaneous monitoring of catechol, m-cresol and guaiacol in wastewater is reported. Voltammetric responses obtained from an array of bulk modified sensors, containing enzymes such as tyrosinase and laccase, were combined with chemometric tools such as ANNs for building the quantitative prediction model. To this end, the chemometric model was first built employing a factorial design, validated employing an external test set of samples, and afterwards applied to the monitoring of the mineralization of the three phenol pollutants during a photo-Fenton advanced oxidation process.

As already stated, prior to using the BioET as a monitorization tool for the photodegradation process of the phenolic compounds photodegradation process, a response model was built. To this aim, a total set of 41 phenolic ternary mixtures, with concentrations ranged from 0 to 80 mg $L^{-1}$ for each compound, were first analyzed and used to build and validate the ANN model; so that afterwards, it may be used for the simultaneous monitoring of the compounds under scrutiny during its mineralization.

### 4.1.1 BioET Array Response

In first instance, voltammetric responses for each of the electrodes towards individual compounds should also be checked. That is, to ensure that enough differentiated signals were observed for the different electrodes, generating rich data that might be a useful departure point for the multivariate calibration model.

To this aim, under the described conditions in Section 3.4, individual stock solutions of catechol, m-cresol and guaiacol were analyzed and their voltammograms inspected (Figure 4.1). Basically, two processes could be observed there: the oxidation of the corresponding phenol to its quinone form, and the reduction of the quinone to the phenolic form, as previously reported [1]. Besides, clearly differentiated curves are obtained for each of the considered compounds and for each electrode, the desirable condition for an ET study.

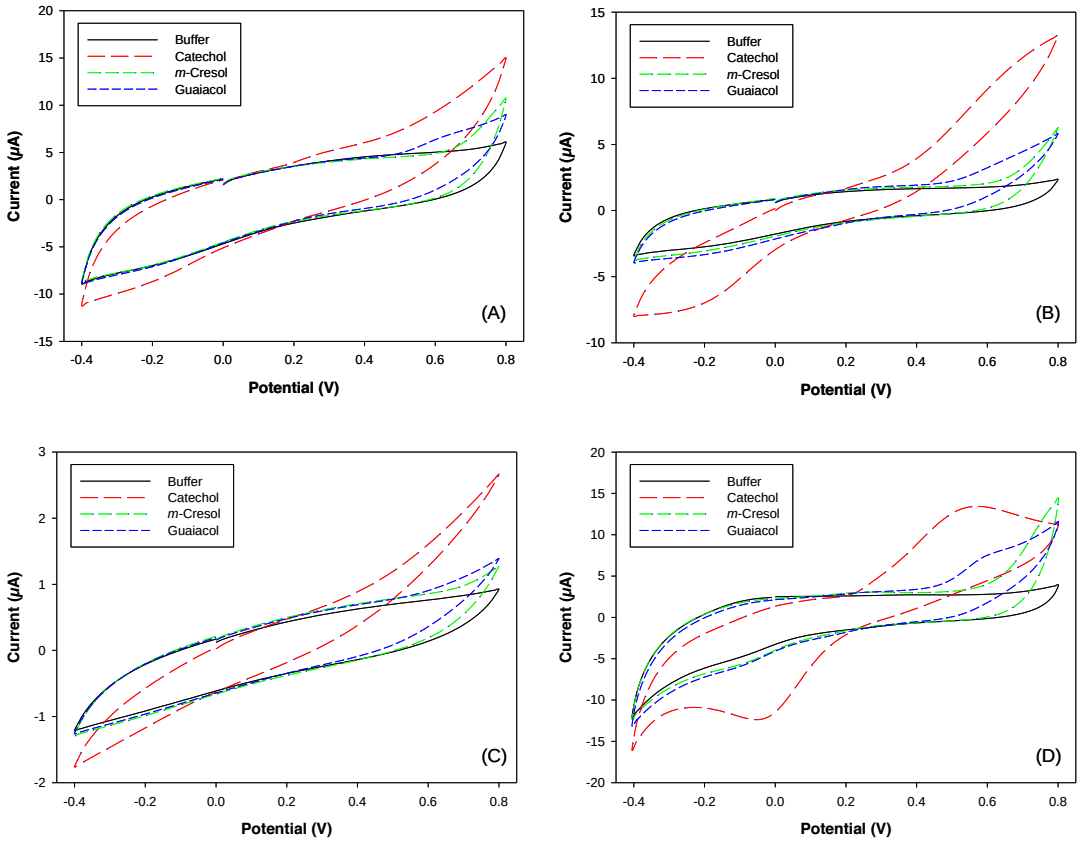


**Figure 4.1.** Example of the different voltammograms obtained with (A) graphite–epoxy sensor, (B) tyrosinase modified biosensor, (C) tyrosinase+laccase modified biosensor and (D) Cu nanoparticle modified electrodes for buffer and stock solutions of each of the three phenolic compounds considered (23 $mg \cdot mL^{-1}$).

In addition, the benefits derived from the incorporation of the enzymatic biosensors may also be noticed, for which higher currents were obtained, especially in the reduction region close to 0 V where obtained net current is clearly enlarged; a situation more patent for catechol and m-cresol, which do not show any response with the bare electrode in that region. Similarly, some catalytic effect can also be observed for the sensor modified with copper nanoparticles, a fact somehow explained given both tyrosinase and laccase are copper containing redox enzymes.

Therefore, once it was confirmed that differentiated behavior was observed by the BioET array towards the different compounds under study, the next step was to proceed with the building of the ANN model.

### 4.1.2 Building of the ANN Model

Under the conditions previously described, the training and testing sets of samples were measured employing the multielectrode array, obtaining a complete voltammogram for each of the (bio)sensors, and each sample. However, the large dimensionality of the data generated hinders their treatment; especially if ANNs are to be used. Therefore, raw voltammetric responses were compressed down to 32 coefficients by means of FFT, which allowed for a compression of the original information up to 88.1%. The next step was the building and optimization of the ANN model. For this, the ANN model was first trained employing data from the training subset, and its performance evaluated employing the samples from the testing subset; this allowed to characterize the accuracy of the quantification model and to detect any overfitting situation due to the use of unbiased data.

After a systematic evaluation of different topologies, from a total number of 90 different configurations, the final architecture of the ANN model had 128 neurons (4 sensors x 32 FFT coefficients) in the input layer, 5 neurons and *logsig* transfer function in the hidden layer and 3 neurons and *tansig* transfer function in the output layer, providing simultaneously the concentration of the three phenolic compounds considered.

Subsequently, comparison graphs of predicted vs. expected concentrations, both for training and testing subsets, for each of the compounds were then built to check the prediction ability of the obtained ANN model (Figure 4.2). It may be seen that a satisfactory trend is obtained, with regression lines almost indistinguishable from the theoretical ones (slope=1, intercept=0), this condition especially significant for the external test set.

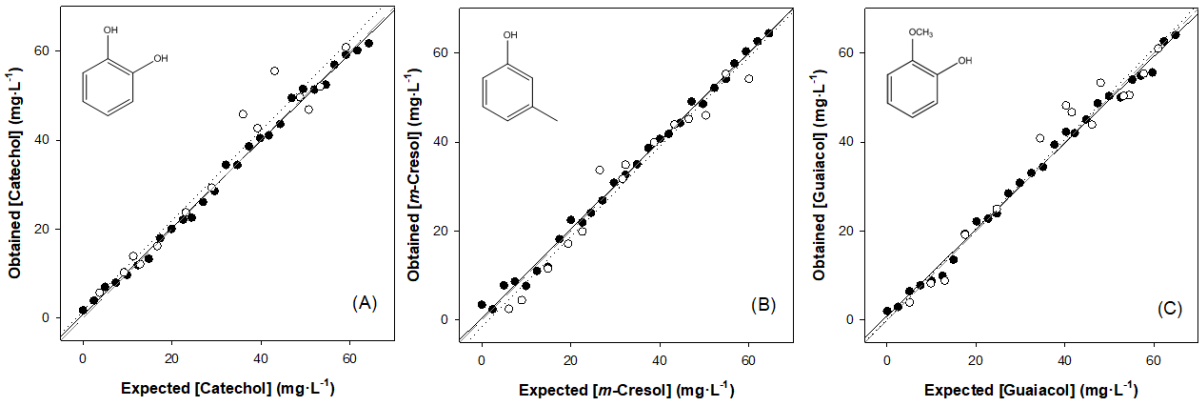


**Figure 4.2.** Modelling ability of the optimized FFT-ANN. Sets adjustments of obtained vs. expected concentrations for (A) catechol, (B) *m-cres*ol and (C) guaiacol, both for training (●, solid line) and testing subsets (○, dotted line). Dashed line corresponds to theoretical diagonal line.

## 4.1.3 Accuracy and Precision of the ANN Model

After optimization and selection of the ANN architecture, next step was to evaluate its performance and accuracy employing the data from the testing subset. That is, to determine whether or not the concentrations estimated by the ANN model statistically differ from the nominal concentrations, when presenting new samples to it. To this aim, regression statistics were evaluated in two different manners, using t and F distribution based tests [2]. Firstly, regression parameters of the comparison graphs were calculated (Table 4.1), and as deduced from the graphs, a satisfactory linear trend is observed for all the cases, with regression lines almost indistinguishable from the theoretical ones. But, as usual in data modeling, with an improved behavior for the training subset due to the lower dispersion attained. However, since the external testing subset data is not employed at all for the modeling, its goodness of fit is a more correct indicator of the accomplished modeling performance. Nevertheless, the results obtained for both subsets are close to the ideal comparison values (slope 1, intercept 0 and correlation coefficient 1), being these values included in the confidence intervals.

**Table 4.1.** Results of the fitted regression lines for the comparison between obtained vs. expected values, both for the training and testing subsets of samples and the three considered species (intervals calculated at the 95% confidence level).

| | | | ***Training subset*** | | |
|---|---|---|---|---|---|
| *Compound* | *r* | *Slope* | *Intercept* | *RMSE* | *Total RMSE* |
| Catechol | 0.998 | 0.979±0.028 | 0.76±1.05 | 0.025 | |
| *m*-Cresol | 0.997 | 0.995±0.030 | 0.50±1.12 | 0.029 | 1.50 |
| Guaiacol | 0.997 | 0.972±0.031 | 0.90±1.19 | 0.023 | |
| | | | ***Testing subset*** | | |
| *Compound* | *r* | *Slope* | *Intercept* | *RMSE* | *Total RMSE* |
| Catechol | 0.975 | 1.017±0.146 | 1.54±5.23 | 4.80 | |
| *m*-Cresol | 0.981 | 1.012±0.127 | -1.46±4.63 | 3.63 | 4.20 |
| Guaiacol | 0.979 | 1.012±0.134 | 0.17±5.43 | 4.09 | |

RMSE: Root Mean Square Error; Intercept and RMSE values are expressed in $mg \cdot L^{-1}$

Additionally, joint confidence intervals were calculated and plotted according to advanced linear regression methodology [2][3]. The usage of this plot constitutes a rapid visualization tool to detect if there are or not differences between two compared methods, judging simultaneously the goodness of slope and intercept. Thus, taking into account the uncertainties in both axes to calculate the estimated covariance matrix based on an F distribution. Hence, we examined whether the theoretical comparison point (1,0) was included in the elliptical region of the joint confidence intervals of slope and intercept for plots shown in Figure 4.2. As can be observed in Figure 4.3, the point (1,0) is included in the confidence intervals for the three species, both for the training and testing subsets; thus confirming that statistically, there are no significant differences for the BioET predicted values and the real ones. Again, it can be seen how results obtained for the training subset are more precise, but with remarkable satisfactory accuracy for both subsets; being all of them close to the ideal point (1,0). The fact that bigger confidence intervals are obtained for the external test subset can be explained by two simple facts. On one side, this data is not employed at all during the building of the model, then being a true test of its generalization ability. On the other side, the number of samples in the testing subset is lower, and consequently, the tabulated values of t and F are higher, which implies higher confidence intervals.

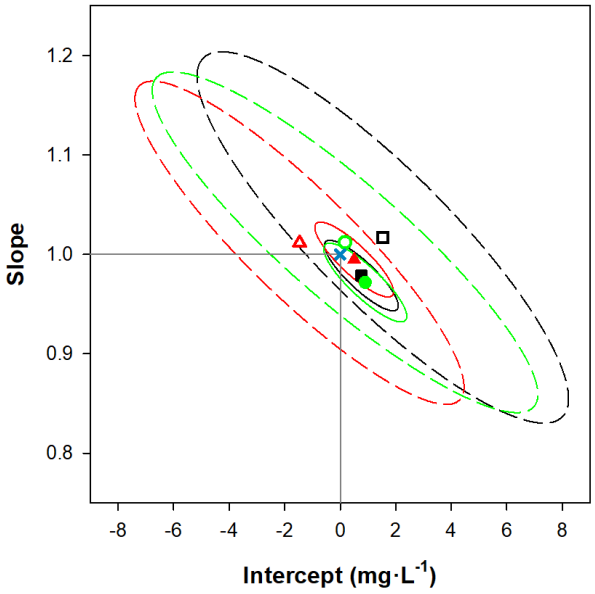


**Figure 4.3.** Joint confidence intervals for the three species: (●) catechol, (▲) *m-cresol* and (■) guaiacol, both for training (filled symbols, solid lines) and testing (empty symbols, dashed lines) subsets. Also ideal point (1,0) is plotted (x); intervals calculated at the 95% confidence level.

Lastly, as an additional verification of the proposed approach, a Student's paired samples t test for the external test subset was performed. Obtained experimental t values were 1.73, 1.13 and 0.54 for catechol, m-cresol and guaiacol respectively, while the critical tabulated t value with 95% confidence level and 13 degrees of freedom is 2.16. Therefore, from the comparison graphs and these t- test results, it could be again concluded that there are no significant differences between the BioET predicted values and the real ones.

### 4.1.4 Monitoring of Phenolics Mineralization

After building and validating the generated model, the next step was the application of the proposed ET towards the monitoring of the photodegradation process of phenolic compounds mixtures. To this aim, a ternary mixture of catechol, m-cresol and guaiacol (72.8 mg·L$^{-1}$, 69.4 mg·L$^{-1}$ and 65.6 mg·L$^{-1}$, respectively) was prepared in AWW. Then, its photodegradation was carried out. During the process, aliquots of the solution from the photoreactor were removed at specific times from the beginning to up to ca. 200 min, and measured with the BioET with no further pretreatment than its mere dilution 1 : 1 with buffer solution. Recorded voltammetric responses were then preprocessed with FFT, and obtained coefficients were input into the previously built model which allowed the simultaneous

determination of the three compounds. Lastly, actual concentration of each compound in the reactor batch was obtained by multiplying by the proper dilution factor.

An extract of the recorded signals obtained during the photodegradation process is shown in Figure 4.4, where it can be clearly seen how currents decreased monotonously as reaction progressed. Thus, even from the raw voltammetric responses, it would be possible to monitor the mineralization process (and detect its end point). However, in that case, not allowing the resolution of the different phenolic compounds. Besides, the use of the BioET might not be limited to monitor the mineralization process, but also to detect whether or not some residual wastewater must be treated. Thus, requiring in that case the quantification of each of the compounds, to determine if their levels are under the required ones; what will be achieved thanks to the use of the chemometric model.

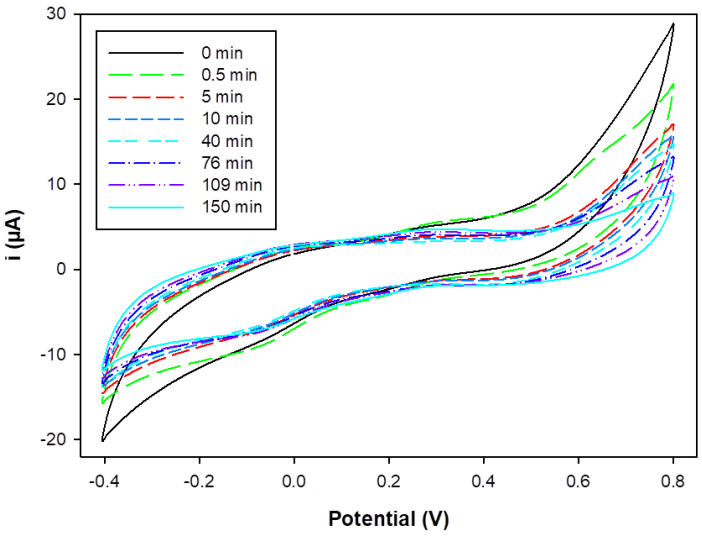


**Figure 4.4.** Voltammetric responses obtained for some samples collected during the photodegradation process with Cu nanoparticle modified sensor, as example

Evolution along time of the photo-Fenton mineralization process is plotted in Figure 4.4. At first sight, it can be seen how the ANN model confirms what was already ex- pected from the voltammetric responses; that is, an exponential decrease in the concentration of each of the compounds. Moreover, the trends observed agree with previous reported results [4], where degradation rate is described by first-order kinetics with respect to phenols concentration.

In this direction, and considering an independent behavior of each phenolic compound (i.e. the compounds not interacting with the others during the degradation) [5], degradation rate for each compound can be described by a pseudo-first order kinetics with respect to its

concentration according to Equation 4.1, where $k_{obs}$ corresponds to the apparent pseudo-first-order rate constant.

$$\ln C = \ln C_0 - k_{obs} t \qquad \textbf{Equation 4.1}$$

Thus, the plotting of the ln of the concentration of each compound vs. time in every experiment leads to a straight line whose slope is $k_{obs}$. Calculated values are summarized in the inset table in Figure 4.5, where also the obtained correlation coefficients for the linearized least squares regression are detailed, corroborating the pseudo-first order kinetics. As an extra validation, it has to be said that these results coincide with those reported in the literature, e.g. [4][6].

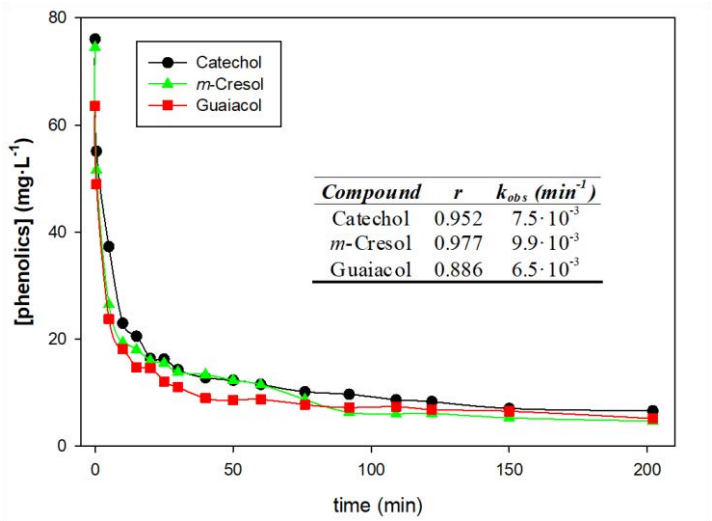


**Figure 4.5.** Photo-Fenton mineralization and its monitoring with the BioET. Representation of the found values for each of the considered species: (●) catechol, (▲) *m-cresol* and (■) guaiacol. Inset table corresponds to the calculated apparent pseudo-first-order rate constants ($k_{obs}$) calculated from the linealizations

Therefore, it has been demonstrated that ETs (i.e. the combination of voltammetric measurements with chemometric tools) are an analytically powerful approach for the speciation of different phenolic compounds in wastewater and the monitoring of its mineralization. This approach is particularly useful since it does not only allow the identification of the presence of the phenolic compounds, but also the individual quantification of the amount present in the mixtures analyzed. Besides, with the same experimental setup, the approach proposed herein might be alternatively applied for the quantification of analogous or different mixtures, even quaternary or more complex mixtures, with a proper retraining set of samples. Lastly, this also represents a viable system with

significant promise for on-field measurements given its simplicity, rapidity and portability; therefore, really suitable for screening analysis

# Article 2:

**Crown ether-modified electrodes for the simultaneous stripping voltammetric determination of Cd(II), Pb(II) and Cu(II)**

Núria Serrano, Andreu González-Calabuig and Manel del Valle

*Talanta,* 2015*,* 138*, 130–137*

This paper describes the immobilization of 4-carboxybenzo-18-crown-6 (CB-18-crown-6) and 4-carboxybenzo-15-crown-5 (CB-15-crown-5) assisted by lysine on aryl diazonium salt monolayers anchored to the surface of graphite–epoxy composite electrodes (GEC), and their use for the simultaneous determination of Cd(II), Pb(II) and Cu(II) by differential pulse anodic stripping voltammetry (DPASV).

The modified electrodes display a good repeatability and reproducibility with detection and quantification limits at levels of mg $L^{-1}$, confirming their suitability for the determination of Cd (II), Pb(II) and Cu(II) ions in environmental samples.

The overlapped nature of the multimetal stripping measurements was resolved by employing the two-sensor array CB-15-crown-5-GEC and CB-18-crown- 6-GEC, since the metal complex selectivity exhibited by the considered ligands could add some discrimination power. For the processing of the voltammograms, Discrete Wavelet Transform and Causal Index were selected as preprocessing tools for data compression coupled with an artificial neural network for the modeling of the obtained responses, allowing the resolution of mixtures of these metals with good prediction of their concentrations

## 4.2.1. GEC characterization

The electrochemical response using 2 mM ferrocyanide/ferricyanide as redox probe in 100 mM phosphate buffer (pH 7.4) was investigated at each functionalization step using cyclic voltammetry (CV). CV measurements were performed in unstirred conditions scanning the potential at 0.1 V $s^{-1}$ from -0.7 to 1 V. Electrografting resulted in a decrease in the current as expected (Figure 4.6). Covalent binding of complexing agents through the α-amine group of the lysine also resulted in lower current peaks compared to bare electrode, as shown in Fig. 3 for CB-18-crown-6-GEC. These observed changes in the voltammograms confirmed the modifications occurring on the electrode surface.

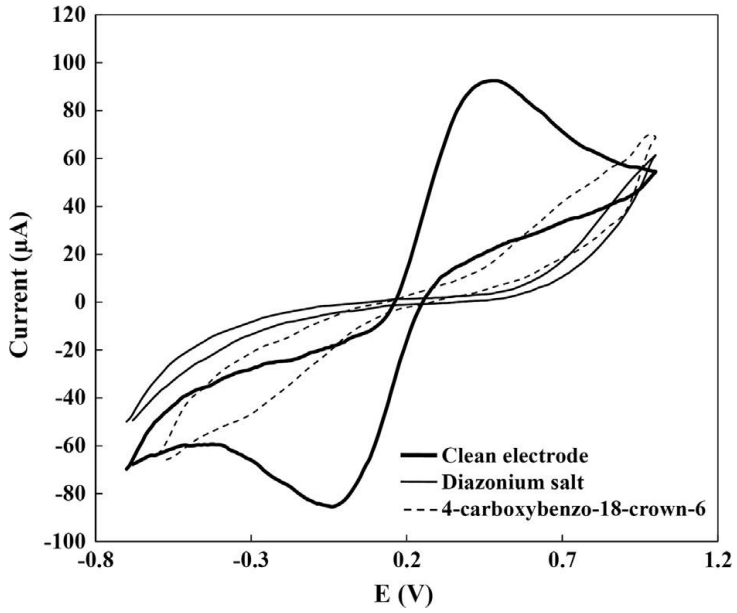


**Figure 4.6.** CVs plots recorded at each electrode functionalization step. Measurements were performed in a 2 mM ferrocyanide/ferricyanide solution in phosphate buffer.

## 4.2.2. Repeatability and reproducibility

The selected Ed, td and tr were firstly optimized to ensure the detection of each metal at each ligand-modified electrode in the selected concentration range; the compromise conditions were for all cases: -1.4 V as the applied accumulation voltage with stirring during a td of 300 s and followed by a rest stage of 10 s at the same applied potential. Three different pH values 4.5, 6.0, and 6.8 were also tested for the simultaneous determination of Cd(II), Pb(II) and Cu(II). At pH values of 6.0 and 6.8 a significant decrease in the peak current of Cu(II) was detected with respect to the obtained at pH 4.5 suggesting some degree of metal hydrolysis. According to this study, an optimal pH value of 4.5 was selected.

Stripping measurements of a 125 mg $L^{-1}$ Cd(II), Pb(II) and Cu(II) solution (mixed solution) by applying the optimized voltammetric conditions were carried out using both ligand-modified electrodes in order to test their repeatability and reproducibility. The reproducibility calculated from three different modified GEC units for each complexing agent within a series of five repetitive yielded RSD of 3.1%, 2.1%, and 2.2% for Cd(II), Pb(II) and Cu(II), respectively for the CB-18-crown-6-GEC and 6.4%, 2.7%, and 3.0% for Cd(II), Pb (II) and Cu(II), respectively for the CB-15-crown-5-GEC. The repeatability estimated using for each complexing agent the same electrode unit for five repetitive measurements produced RSD of 3.1%, 4.3%, and 2.2% for Cd(II), Pb(II) and Cu(II), respectively for the CB-18-crown-6-GEC and 5.2%, 3.3%, and 1.6% for Cd(II), Pb(II) and Cu(II), respectively for the CB-15-crown-5-GEC.

## 4.2.3. Linearity, limit of detection and limit of quantification

First of all, separate calibration of Cd(II), Pb(II) and Cu(II) ions by stripping voltammetry (DPASV) was carried out on each CB-18-crown-6-GEC and CB-15-crown-5-GEC respectively. The LOD was calculated as 3 times the standard deviation of the intercept over the slope of the calibration curve of the target ions. LOQ was evaluated by considering 10 times the previous ratio. The lowest value of the linear concentration range was established from the corresponding limit of quantification (LOQ). For LOD and LOQ determinations, 10 different standards of the considered ions were used to build the calibration lines. Figure 4.7 a–c shows, as an example, the evolution of DPASV signals of each metal using the CB-15-crown-5-GEC sensor when the concentration of Cd(II), Pb(II) and Cu(II) respectively increases (CB-18-crown-6-GEC with equivalent behavior). In all cases, well defined stripping peaks without any clear evidence of signal splitting were observed over the considered concentration range. Linear calibration curves were obtained for Cd(II), Pb(II) and Cu(II) up to a maximum concentration level of 191.1, 186.5, and 177.3 µg $L^{-1}$ respectively. The corresponding regression equations and the correlation coefficients for both sensors are shown in Table 4.2.

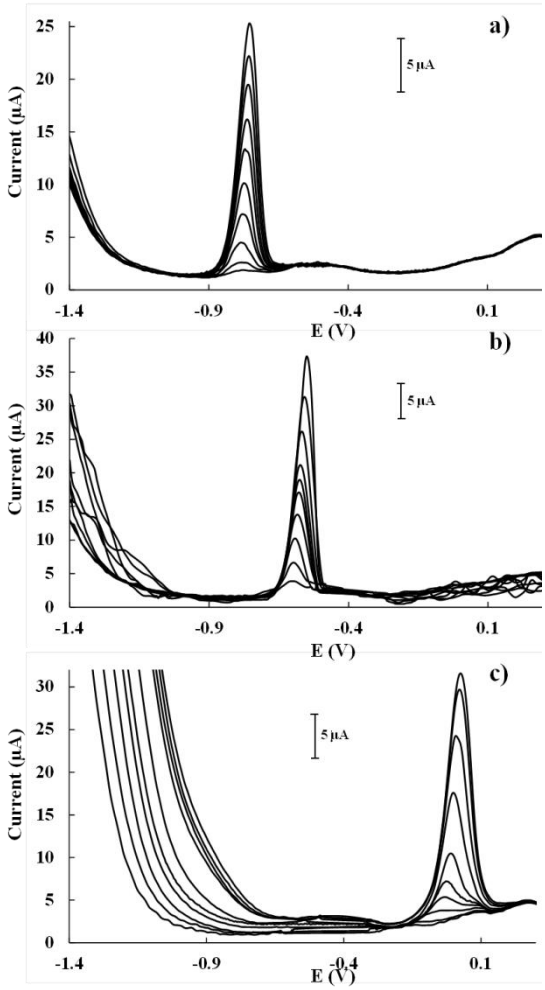

**Figure 4.7.** DPASV measurements of (a) Cd(II), (b) Pb(II), and (c) Cu(II) alone (0–200 μg $L^{-1}$ concentration range) recorded on a CB-15-crown-5-GEC sensor at pH 4.5 using a Ed of -1.40 V during 300 s and tr of 10 s.

**Table 4.2.** Calibration data for the determination of Cd(II), Pb(II) and Cu(II) on CB-18-crown-6-GEC and CB-15-crown-5-GEC at $E_d$ of -1.4 V using a $t_d$ of 120 s at pH 4.5.

| | **Cd (II)** | | **Pb (II)** | | **Cu (II)** | |
|---|---|---|---|---|---|---|
| | **CB-18-crown-6-GEC** | **CB-15-crown-5-GEC** | **CB-18-crown-6-GEC** | **CB-15-crown-5-GEC** | **CB-18-crown-6-GEC** | **CB-15-crown-5-GEC** |
| **Regression**[a] | $y = 0.016\,x - 0.13$ | $y = 0.011\,x - 0.11$ | $y = 0.021\,x + 0.31$ | $y = 0.014\,x - 0.013$ | $y = 0.015\,x - 0.052$ | $y = 0.020\,x - 0.39$ |
| **$R^2$** | 0.999 | 0.998 | 0.999 | 0.999 | 0.999 | 0.999 |
| **Linear range (μg $L^{-1}$)**[b] | 7.9 – 191.1 | 15.7 – 191.1 | 5.0 – 186.5 | 10.9 – 186.5 | 5.1 – 177.3 | 7.7 – 177.3 |
| **LOD (μg $L^{-1}$)** | 2.4 | 4.7 | 1.5 | 3.3 | 1.5 | 2.3 |

[a] *y* is the peak area (a.u.) and *x* the concentration (μg $L^{-1}$).

[b]The lowest value of the linear range was considered from the LOQ.

It must be pointed out that similar voltammetric responses for Pb(II), Cd(II) and Cu(II) were also observed using CB-18-crown-6-GEC sensor at the same experimental conditions. Nevertheless, regarding the sensitivities considered as the value obtained from the slope of the calibration curves, it can be mentioned that: i) using CB-18-crown-6-GEC, Pb (II) was the metal ion showing better sensitivity; and ii) using CB-15-crown-5-GEC, Cu(II) was the most sensitive metal. The LOD of the assay for the three metal ions in both modified electrodes varied from 1.5 to 4.7 μg $L^{-1}$ depending on the metal ion (Table 4.2) and the LOQ ranged from 5.0 to 15.7 μg $L^{-1}$ depending on the metal ion (Table 4.2). For Pb(II) and Cu(II) the obtained results are comparable with the values reported in earlier studies [7][8][9]. In the case of Cd(II) no previous LOD and LOQ data are available in the literature. In comparison with previous results achieved using others solid composite electrodes, e.g., graphite solid composite electrode, solid composite silver electrode, carbon composite solid electrode modified with silica gel… [10], the LODs obtained in this work are similar or even significantly lower

depending on the solid composite electrode considered. Furthermore, lower concentrations ranges and better detection limits could easily be achieved using the proposed method by increasing the deposition time. Therefore the reported calibration data suggest that both CB-18-crown-6-GEC and CB-15-crown-5-GEC sensors could be fully suitable for the determination of Cd(II), Pb(II) and Cu(II) at the ultra-trace level in environmental samples. The second observation is that the use of the two electrodes as an array could add some discrimination power to resolve a multimetal mixture.

### 4.2.4 Metal complex selectivity

Taking into account that the immobilized crown ethers on the GEC surface are used as molecular collectors with ability to selectively coordinate with the metal ions, both the ionic diameter of metal ions and the cavity size/structure of the crown ethers play a crucial role for the complex formation by means of ion–dipole interaction with metal ions. The ability of each considered metal ions for forming the complex with both CB-18-crown-6 and CB-15-crown-5 is displayed in Figure 4.8. Voltammetric peak current responses for equal concentrations ofmetal ion solution (175 μg $L^{-1}$ of Cd(II), Pb(II) and Cu(II)) show that CB-18-crown-6 exhibits the highest selective complex forming ability with Pb(II) followed by Cu(II); on the contrary, CB-15-crown-5 offers the highest interaction with Cu(II) followed by Pb(II). In both considered crown ethers, Cd(II) shows the smallest ion–dipole interaction being CB-15-crown-5 a little bit more selective than CB-18-crown-6. Comparing the ionic diameter of the considered metal ions (1.5 Å for Cu(II), 1.9 Å for Cd(II), and 2.4 Å for Pb(II) ) with the cavity size of both crown ethers (cavity diameter, 1.7-2.2 Å for CB-15-crown-5 and 2.6-3.2 Å for CB-18-crown-6), the described behavior is consistent with studies by Christensen et al. in 1971 who suggested that cation diameter to host cavity size ratios of 0.75-0.90 are favorable for direct ion–crown ether binding [11][12]. Thus, for Pb(II) a ratio of 0.75-0.92 was achieved for CB-18-crown-6 reflecting the size match for that ion. Likewise, ratios of 0.86-1.11 and 0.68-0.88 for CB-15-crown-5 were obtained for Cd(II) and Cu(II), respectively, consistent with the observed selectivities. The hypothesis is, therefore, that the use of the two electrodes as an array will provide higher information to resolve a multimetal mixture than that obtained from a single electrode. Two were the electrodes considered here, given that these are the ligands commercially available. With synthetic approaches, the number of differently modified sensors might be increased at will.

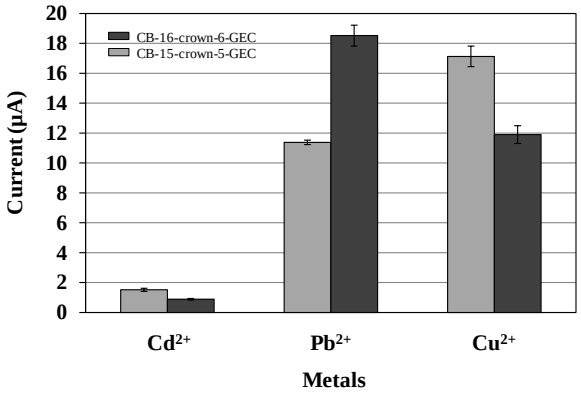


**Figure 4.8.** Differential pulse anodic stripping voltammetric peak current of 175 µg $L^{-1}$ of Cd(II), Pb(II) and Cu(II) using both CB-15-crown-5-GEC and CB-18-crown-6-GEC sensors

## 4.2.5. Multimetal stripping voltammetric measurements

The behavior of the stripping signals of different mixtures of Cd(II), Pb(II) and Cu(II) was studied in the concentration range 1.5-200 µg $L^{-1}$ using both CB-18-crown-6-GEC and CB-15-crown-5-GEC sensors in order to detect possible interactions between metal ions. As an example, a sample of five stripping voltammograms obtained using CB-15-crown-5-GEC (arbitrary concentrations) is displayed in Figure 4.9. As it can be seen, in contrast to the individual signals of metals (Figure 4.7), an overlapping effect and the formation of some intermetallic compounds hinder the direct determination of the mixtures. Comparing both individual and multimetal stripping measurements the potential of the oxidation peak of each considered metal in the complex voltammograms could be assigned at ca. -0.75 V, -0.55 V, and 0.03 V for Cd(II), Pb(II) and Cu(II), respectively. A comparison between the voltammograms provided by both modified sensors displayed no significant differences in metal peak shapes and peak potentials, however different levels of metal interactions were observed in agreement with metal complex selectivity. Thus, for example, in the calibration mixture of 100.7 µg $L^{-1}$ of Cd(II), Pb(II) and Cu(II) the greatest voltammetric peak currents were obtained for Cu(II) and Cd(II) using the CB-15-crown-5-GEC, and for Pb(II) using CB-18-crown-6-GEC (inset in Figure 4.9). In this way, the stripping voltammetric responsewill be different depending on the metal ion concentration in each calibration mixture, the used modified sensor and the metal complex selectivity. For example, in the calibration mixture of 146.5, 116.0, and 24.4 µg $L^{-1}$ of Cd(II), Pb(II) and Cu(II) using the CB-15-crown-5-GEC (Figure 4.9, (D) thin line), the peak current of Cd(II) and Pb(II) increases substantially with respect to the mixture of equal concentration of metal ions (Figure 4.9, (A) thick line), whereas the peak current of Cu(II) decreases considerably. Apart from the initially observed complexity, as the

next step, the sets of voltammograms of heavy metal mixtures obtained from the two-sensor array were postulated to be used to calibrate Cd(II), Pb(II) and Cu(II) using an appropriate ANN model that may consider any non-linearity or overlapping in the determination of the considered metal ions.

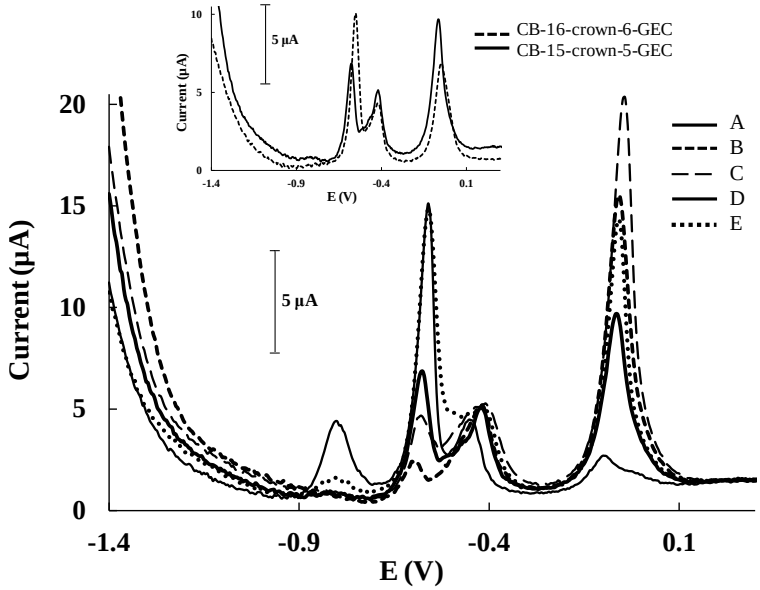


**Figure 4.9.** Some voltammograms generated during the build of the response model recorded at the same conditions as Figure 4.7. Sample composition: (A) 100.7 µg $L^{-1}$ of Cd(II), Pb(II) and Cu(II); (B) 54.9 µg $L^{-1}$ of Cd(II), 85.5 µg $L^{-1}$ of Pb(II) and 177.1 µg $L^{-1}$ of Cu(II); (C) 123.6 µg $L^{-1}$ of Cd(II), 108.4 µg $L^{-1}$ of Pb(II) and 169.4 µg $L^{-1}$ of Cu(II); (D) 146.5 µg $L^{-1}$ of Cd(II), 116.0 µg $L^{-1}$ of Pb(II) and 24.4 µg $L^{-1}$ of Cu(II); (E) 169.4 µg $L^{-1}$ of Cd(II), 123.6 µg $L^{-1}$ of Pb(II) and 93.1 µg $L^{-1}$ of Cu(II). Inset in (b): comparison between the response of both sensors for sample composition (A).

## 4.2.6. Quantification of the metal mixtures

Once the data were compressed by use of Wavelet Transform and Causal Index in this study case, the first step in building the appropriate ANN model is choosing the topology of the neural network to be used. Normally, given the difficulties to predict the optimal settings in advance this is a trial-and-error process, where several parameters (training algorithms, number of hidden layers, transfer functions, etc.) are fine-tuned in order to find the best configuration that optimizes the performance of the model [13].

In consequence, the samples from the training subset were used for building the ANN model, and its accuracy was then evaluated towards samples of the external test subset by employing the built model to predict the concentrations of the metals of those samples

(external validation). Taking into account that the external test subset data is not used at all for the modeling, its goodness of fit is a measure of the completed modeling performance. With the aim of facilitating the verification of the prediction ability of the obtained ANN model, comparison graphs of predicted vs. expected concentrations for the considered compounds were plotted, both for training subset and testing subsets. Once calculated the root mean square error (RMSE) [14][15], the best model will be the one that has the lowest RMSE values and additionally, regression parameters from the comparison graphs are close to the ideal values (i.e. slope and correlation coefficient equal 1, and intercept equal 0).

In our case, the resolution of the Cd(II), Pb(II) and Cu(II) mixtures was attempted using the data from the two voltammetric sensors. To this aim, the set of samples was measured with the two electrodes (CB-15-crown-5-GEC and CB-18-crown-6-GEC) and the obtained voltammetric responses were compressed employing DWT-CI and the different ANN models were optimized. After a systematic study for the fine tuning of the different parameters, the final architecture of the ANN model had 21 neurons in the input layer, 4 neurons and logsig transfer function in the hidden layer and three neurons and tansig transfer function in the output layer, providing the concentrations of the three species considered. Afterwards, comparison graphs of predicted vs. expected concentrations for the considered compounds were built (Figure 4.10). As it can be observed, a satisfactory trend was obtained for all three metal ions with regression lines close to the theoretical ones. In addition, the obtained linear comparison parameters were calculated (Table 4.3) resulting close to the ideal values, with intercepts close to 0 and slopes and correlation coefficients close to 1, meaning that there are no significant differences between the values predicted by the ANN model and those expected and provided by the reference method.

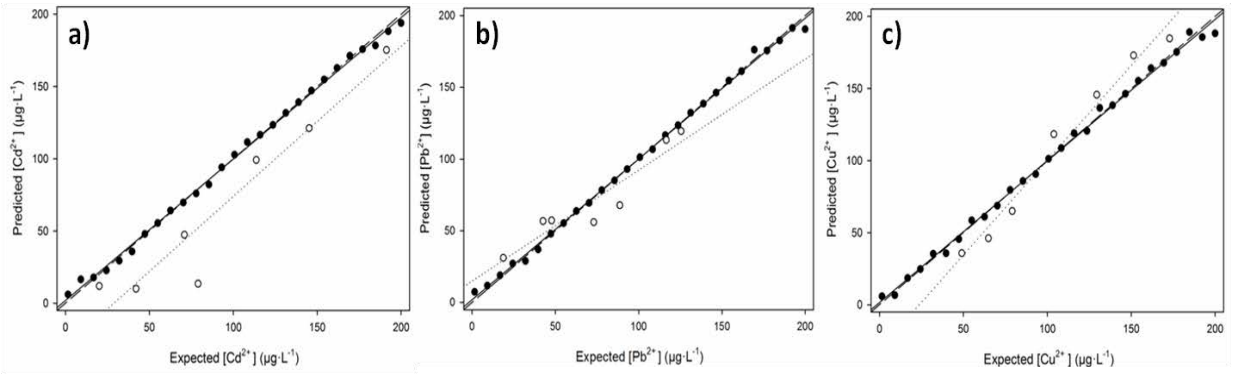


**Figure 4.10.** Modeling ability of the optimized ANN for the two-sensor array. Comparison graphs of obtained vs. expected concentrations for (a) Cd(II), (b) Pb(II) and (c) Cu(II) metals, both for training (●, solid line) and testing subsets (○, dotted line). Dashed line corresponds to theoretical diagonal line (Y¼X).

**Table 4.3.** Results of the fitted regression lines for the comparison between obtained vs. expected values, both for the training and testing subsets of samples and the different metal species (intervals calculated at the 95% confidence level).

| | Metal | Correlation | Slope | Intercept (µg $L^{-1}$) | RMSE (µg $L^{-1}$) | NRMSE (µg $L^{-1}$) | Total RMSE (µg $L^{-1}$) | Total NRMSE (µg $L^{-1}$) |
|---|---|---|---|---|---|---|---|---|
| | Pb(II) | 0.999 | 0.98±0.04 | 1.9±4.3 | 2.91 | 0.015 | | |
| **tr** | Cd(II) | 0.999 | 0.97±0.04 | 1.9±4.3 | 3.02 | 0.015 | 3.17 | 0.016 |
| | Cu(II) | 0.996 | 0.98±0.05 | 1.5±5.5 | 3.66 | 0.018 | | |
| | Pb(II) | 0.942 | 0.77±0.64 | 14.9±52.0 | 14.24 | 0.071 | | |
| **ts** | Cd(II) | 0.957 | 1.04±0.72 | -29.9±49.3 | 34.10 | 0.170 | 22.35 | 0.120 |
| | Cu(II) | 0.989 | 1.31±0.45 | -31.2±52.3 | 17.31 | 0.087 | | |

**tr**: training subset; **ts**: testing subset; **RMSE**: root mean square error; **NRMSE**: normalized root mean square error

# Article 3:

**Simultaneous Voltammetric Determination of Heavy Metals by Use of Crown Ether-modified Electrodes and Chemometrics**

Andreu González-Calabuig, David Guerrero, Núria Serrano and Manel del Valle

*Electroanalysis,* 2016, 28, 663–670

A three-sensor array consisting of a graphite epoxy composite electrode, 4-carboxybenzo-18- crown-6-GEC and 4-carboxybenzo-15-crown-5-GEC was employed for the simultaneous determination of Cd(II), Pb(II) and Hg(II) by differential pulse anodic stripping voltammetry .

This work focus in the determination of Hg(II) with the aim of combining the Hg(II) determination with a simultaneous determination of previously studied metals; secondly, peak current responses confirmed that the sensors showed differentiated response for the three considered metals.

A response model was developed to resolve mixtures of Cd(II), Pb(II) and Hg(II) at the mg $L^{-1}$ level; Discrete Wavelet Transform was selected as preprocessing tool and artificial neural network was used to model the obtained voltammetric responses.

## 4.3.1 Results and Discussion of Pb(II) and Cd(II)

As the most novel part of the present work is the part concerning Hg(II) sensing, this was studied in detail; next, the sensor array was employed for the simultaneous determination of the three considered metals, in an electronic tongue approach, the details for the characterization for the Pb(II) and Cd(II) are detailed in Section 4.2.

## 4.3.2 Calibration Data

Most influential parameters in the ASV voltammetric response for a given metal are the operating parameters, such as deposition potential (Ed), the accumulation potential (td) and pH of the medium. The optimized compromise conditions for the simultaneous determination of Pb(II), Cd(II) and Hg(II) using the three-sensor array were an Ed of -1.4V with stirring during a td of 300 s and followed by a rest period of 10 s at the same applied potential in 0.1 mol $L^{-1}$ acetic acid/acetate buffer pH 4.5.

Once stablished the working conditions, the electrodes of the array (GEC, CB-18-crown-6-GEC and CB-15-crown-5-GEC) were analytically characterized for the determination of Hg(II) given that there are no previous studies in this regard; on the other hand, responses towards Cd(II) and Pb(II) were already studied in the previous article (section 4.2).

First of all, individual calibration of Hg(II) ion by stripping voltammetry (DPASV) was carried out using the three-sensor array. The LOD was calculated as 3 times the standard deviation of the intercept over the slope of the calibration curve of the target ions. LOQ was evaluated by considering 10 times the previous ratio. The lowest value of the linear concentration range was established from the corresponding limit of quantification (LOQ). For LOD and LOQ

determinations, eleven different standards of the considered ion were used to build the calibration lines.

The three sensors evaluated provided a well-defined stripping peak over the considered concentration range. Excellent linear responses of peak currents versus Hg(II) concentrations were obtained for GEC, CB-18-crown-6 GEC and CB-15-crown-5-GEC up to a maximum concentration level of 200 mg $L^{-1}$. The corresponding regression equations and the correlation coefficient for the sensors of the array are shown in Table 4.4.

**Table 4.4.** Calibration data for the determination of Hg(II) on GEC, CB-18-crown-6-GEC and CB-15-crown-5-GEC at $E_d$ of -1.4 V using a $t_d$ of 120 s at pH 4.5.

| | GEC | CB-18-crown-6-GEC | CB-15-crown-5-GEC |
|---|---|---|---|
| **Regression**[a] | y = 0.157 x + 2.88 | y = 0.146 + 3.26 | y = 0.128 + 4.76 |
| **$R^2$** | 0.985 | 0.995 | 0.995 |
| **Linear range (μg $L^{-1}$)**[b] | 37 – 200 | 42 – 200 | 41 – 200 |
| **LOD (μg $L^{-1}$)** | 11 | 13 | 12 |

[a]y is the peak area (μA) and x the concentration (μg $L^{-1}$).

[b]The lowest value of the linear range was considered from the LOQ.

With respect to the sensitivities considered as the value obtained from the slope of the calibration curves, it can be stated that: Hg(II) shows a very similar sensitivity for the three considered sensors suggesting that the three electrodes respond in the same way versus Hg(II). However, comparing the two crown ether-modified sensors it can be observed that their sensitivities are slightly different suggesting that CB-18-crown-6-GEC offers a higher interaction than CB-15-crown-5-GEC with Hg(II). Related to the unmodified GEC it has a sensitivity slightly higher than other sensors, this fact is because the graphite structure where the mercury can be introduced into the own structure of the graphite making it especially sensitive. As shown in Table 4.4, both LOD and LOQ were at the level of $mgL^{-1}$ for all considered sensors. In comparison with previous results achieved at other crown ethermodified electrodes, the LODs provided by CB-18-crown-6-GEC and CB-15-crown-5-GEC sensors were similar than the LOD obtained using a ferrocenoylpolythia crown ether—Nafion-modified glassy carbon electrode [16], and much lower than the LOD achieved using a carbon-paste electrodes modified with

18-crown-6 [17]. It must be point out that in this work an enrichment time of 300 s was selected looking for a compromise between the peak currents and the time of the analysis, nevertheless lower concentrations ranges and better detection limits could easily be achieved using the proposed method by increasing the enrichment time.

Comparing both unmodified GEC and crown ether modified GEC it can be observed that the LOD and LOQ values obtained for both CB-18-crown-6-GEC and CB-15-crown-5-GEC sensors are in the range of those obtained for the unmodified graphite composite electrode. Therefore the reported calibration data suggest that all considered sensors could be fully suitable for the determination of Hg(II) at low $mg \cdot L^{-1}$ level in natural samples. However, until no simultaneous determinations of Hg(II) with other heavy metal ions such as Cd(II) and Pb(II) are performed, it cannot be established which of the considered sensor is the best especially in terms of selectivity for Hg(II) determination.

### 4.3.3 Multimetal Stripping Voltammetric Measurements

Before the application of the three considered sensors as an array for the simultaneous determination of Cd(II), Pb(II) and Hg(II) is import to know if this array can add some discrimination power to resolve the mixture. Therefore, the cross-response of these sensors was examined. Considering that the immobilized crown ethers on the GEC surface are used as molecular collector with ability to selectively coordinate with the metal ions, both the ionic diameter of metal ions and the cavity size of the crown ethers play a crucial role for the complex formation by means of ion-dipole interaction with metal ions.

Although, it is known that both CB-18-crown-6 and CB-15-crown-5 exhibit a cross-response for Cd(II) and Pb(II) [18], it is unknown whether with Hg(II) has this characteristic response. With this aim voltammetric peak current responses for equal concentrations of metal ion solution (175 mg $L^{-1}$ of Cd(II), Pb(II) and Hg(II)) were recorded using the three-sensor array. Figure 4.11 shows that, on the one hand, CB-18-crown-6-GEC and GEC exhibit the highest interaction with Pb(II) and Hg(II) being the iondipole interaction of CB-18-crown-6-GEC with Hg(II) slightly higher than with Pb(II); on the other hand, CB-15-crown-5-GEC offers the highest selective complex forming ability with Hg(II) followed by Cd(II). Although, for the three considered sensors Hg(II) shows a similar interaction, it can be seen that CB-18-crown-6-GEC is a little bit more selective than CB-15-crown-5-GEC. Comparing the ionic diameter of the considered metal ions (1.9 Å for Cd(II), 2.1 Å for Hg(II), and 2.4 Å for Pb(II)) with the cavity size of both crown ethers (cavity diameter, 1.7-2.2 Å for CB-15-crown-5 and 2.6-3.2 Å for CB-18-crown-6), the described behavior is consistent with studies by Christensen et al. in 1971 who

suggested that cation diameter to host cavity size ratios of 0.75-0.90 are favorable for direct ion-crown ether binding [12]. Thus, ratios of 0.66-0.81 and 0.75-0.92 for Hg(II) and Pb(II), respectively, were achieved for CB-18-crown-6 reflecting the size match for those ions. Likewise, a ratio of 0.86-1.11 for CB-15-crown-5 were obtained for Cd(II) consistent with the observed selectivities.

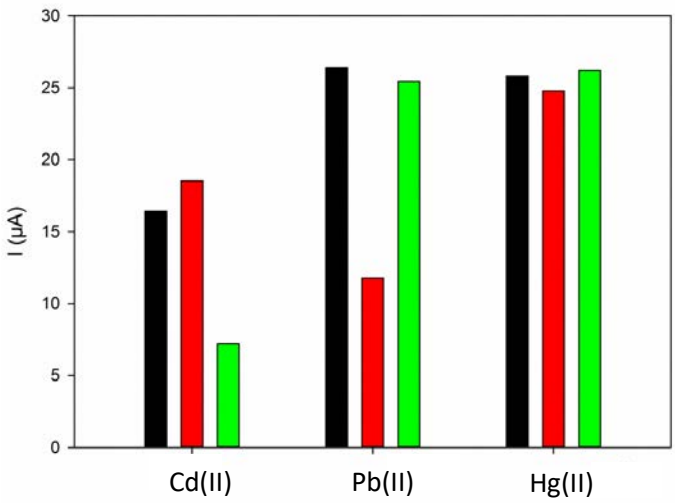


**Figure 4.11.** Differential Pulse anodic stripping voltammetric sensitivity, from peak current of 175 µg L−1 of Cd(II), Pb(II) and Hg(II) using the three-sensor array. Black: graphite epoxy composite electrode (GEC); res: CB-15crown-5-GEC; green: CB-18-crown-6-GEC.

Therefore, from Figure 4.11 it can be evidenced the existence of cross-response between the three metal ions and the considered sensors. In this way, whereas additionally a maximum signal for each metal is obtained for a different electrode, the use of the three-sensor array would provide higher information to resolve the multimetal mixture than that obtained from a single electrode. As an example, a sample of four stripping voltammograms obtained using CB-18-crown-6-GEC (arbitrary concentrations) is displayed in Figure 4.12. Relatively well-defined stripping peaks without any clear evidence of signal splitting or overlapping effect were observed over the considered concentration range. The potential of the oxidation peak of each considered metal in the complex voltammograms was assigned at ca. -0.73 V, -0.48 V, and 0.31 V for Cd(II), Pb(II) and Hg(II) respectively.

A comparison between the voltammograms provided by unmodified GEC and both crown ethers-modified sensors displayed no significant differences in metal peak shapes and peak potentials (at shown concentration levels), however different degree of metal interactions were observed in agreement with metal complex selectivity (inset in Figure 4.12). Thus, the stripping voltammetric response will be different depending on the metal ion concentration in

each calibration mixture, the used sensor and the metal complex selectivity. As the next step, the sets of voltammograms of heavy metal mixtures obtained from the three-sensor array were postulated to be used to calibrate Cd(II), Pb(II) and Hg(II) using an appropriate ANN model that may consider any non-linearity or splitting in the determination of the considered metal ions.

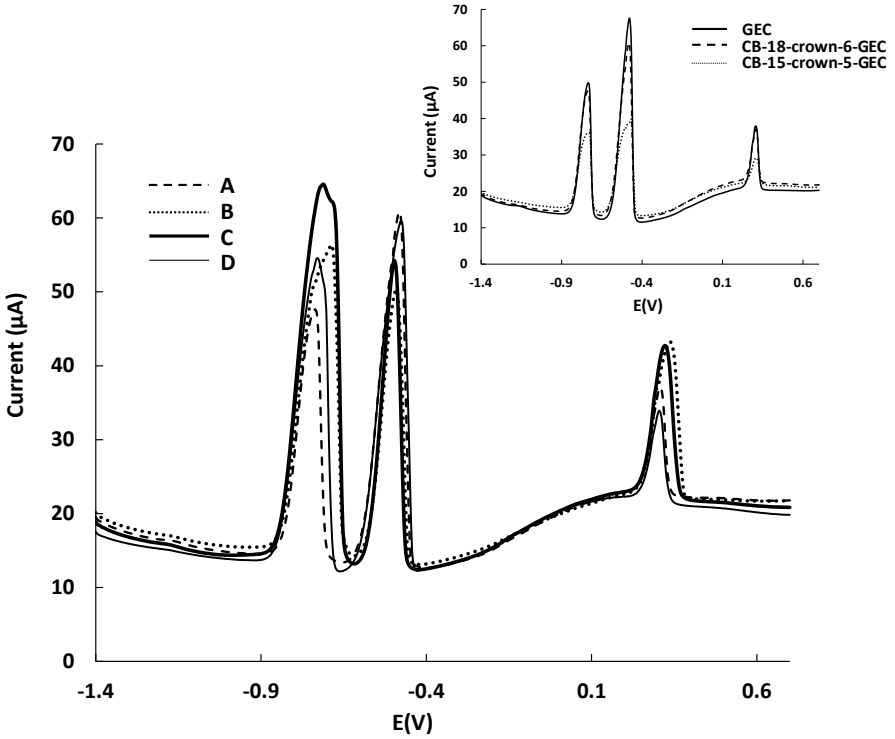


**Figure 4.12**. Some differential pulse anodic stripping voltammograms generated during the building of the response model recorded on a CB-18-crown-6-GEC sensor at pH 4.5 using a $E_d$ of −1.40 V during 300 s and $t_r$ of 10 s. Sample composition: (A) 31.1 µg $L^{-1}$ of Cd(II), 147.1 µg $L^{-1}$ of Pb(II) and 27.5 µg $L^{-1}$ of Hg(II); (B) 124.9 µg $L^{-1}$ of Cd(II), 92.5 µg $L^{-1}$ of Pb(II) and 136.2 µg $L^{-1}$ of Hg(II); (C) 177.4 µg $L^{-1}$ of Cd(II), 70.0 µg $L^{-1}$ of Pb(II) and 80.1 µg $L^{-1}$ of Hg(II); (D) 94.2 µg $L^{-1}$ of Cd(II), 162.9 µg $L^{-1}$ of Pb(II) and 7.5 µg $L^{-1}$ of Hg(II). Inset: comparison between the response of the three-sensor array for sample composition (A).

## 4.3.4 Quantification of the Metal Mixtures

Once the data were compressed by use of Wavelet Transform in this study case, the first step in building the appropriate ANN model is choosing the topology of the neural network used. Normally, given the difficulties to predict the optimal settings in advance this is a trial-and- error process, where several parameters (training algorithms, number of hidden layers, transfer functions, etc.) are fine-tuned in order to find the best configuration that optimizes

the performance of the model [13]. In consequence, the samples from the training subset were used for building the ANN model, and its accuracy was then evaluated towards samples of the external test subset by employing the developed model to predict the concentrations of the metals of those samples (external validation). Taking into account that the external test subset data is not used at all for the modeling, its goodness of fit is a measure of the completed modeling performance. Model prediction abilities are shown in the comparison graphs (obtained vs. expected concentrations) for all ions, both for training subset and testing subsets. The factors considered for the selection of the best model were the accuracy of fit, evaluated as the smaller RMSE (root mean squared error) [14] and additionally, regression parameters from the comparison graphs close to the ideal values (i.e. slope and correlation coefficient equal 1, and intercept equal 0), meaning that there are no significant differences between the values predicted by the ANN model and those expected and provided by the reference method.

In our case, the resolution of the Cd(II), Pb(II) and Hg(II) mixtures was attempted using the data from the three voltammetric sensor array. To this aim, the set of samples was measured with the three electrodes (unmodified GEC, CB-15-crown-5-GEC and CB-18-crown-6-GEC) and the obtained voltammetric responses were compressed employing DWT and the different ANN models were optimized. After a systematic study optimizing the different parameters, the final architecture of the ANN model had 93 neurons in the input layer, 4 neurons and satlins transfer function in the hidden layer and 3 neurons and purelin transfer function in the output layer, providing the concentrations of the three species considered. Figure 4.13 illustrates the comparison graphs of predicted vs. expected concentrations for the considered compounds for training (●, solid line) and testing subsets (○, dashed line). As it can be observed, a satisfactory trend was obtained for all three metal ions with regression lines close to the theoretical ones (long dashed line). Table 4.5 shows the calculated linear comparison parameters being near the ideal value, with correlation coefficients and slopes with values very close to 1 and intercepts quite close to 0.

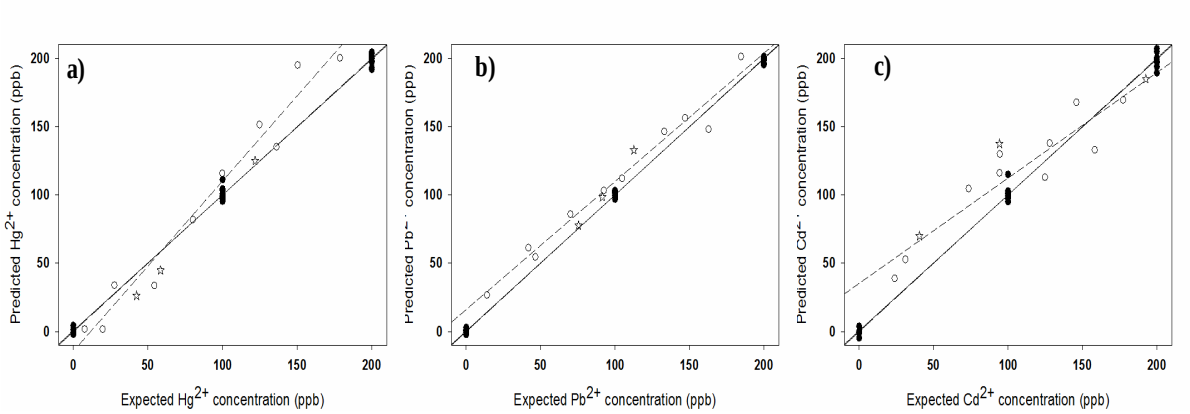


**Figure 4.13.** Modelling ability of the optimized ANN for the three-sensor array. Sets adjustments of obtained vs. expected concentrations for (a) Cd(II), (b) Pb(II) and (c) Hg(II), for training subset (●, solid line), testing subsets (○,dashed line) and certified samples (☆). Long dashed line corresponds to theoretical diagonal line.

Additionally, to assess the applicability of the three sensor array to real samples, an attempt was performed to simultaneously determine Cd(II), Pb(II) and Hg(II) in 3 certified samples, randomly distributed along the experimental domain. Figure 4.13 (empty star) shows the linear regression results for Cd(II), Pb(II) and Hg(II). The general trend is quite satisfactory for all the considered metal ions with slopes and intercepts close to 1 and 0 respectively, and with correlations being also significant (Table 4.5). Although, Cd(II) is the analyte with the worst performance especially with a somewhat lesser correlation and higher confidence interval of the intercept value.

**Table 4.5.** Results of the fitted regression lines for the comparison between obtained vs. expected values, for the training and testing subsets of samples and the different metal species (intervals calculated at the 95% confidence level).

| *c* | *Metal* | *Correlation* | *Slope* | *Intercept (ppb)* | *RMSE (ppb)* | *NRMSE* | *Total RMSE (ppb)* | *Total NRMSE* |
|---|---|---|---|---|---|---|---|---|
| train subset | Hg(II) | 0.999 | 0.99±0.04 | 0.74±4.91 | 3.89 | 0.019 | 3.69 | 0.018 |
| | Pb(II) | 0.999 | 0.99±0.02 | 0.49±2.46 | 1.97 | 0.010 | | |
| | Cd(II) | 0.998 | 0.99±0.05 | 0.71±5.95 | 4.69 | 0.023 | | |
| test subset | Hg(II) | 0.982 | 1.25±0.39 | -14.26±40.44 | 21.71 | 0.109 | 19.35 | 0.096 |
| | Pb(II) | 0.986 | 0.94±0.25 | 16.11±28.66 | 14.10 | 0.071 | | |
| | Cd(II) | 0.927 | 0.77±0.51 | 35.24±58.97 | 23.17 | 0.116 | | |

RMSE: root mean square error; NRMSE: normalized root mean square error

# Article 4:

**Instrumental measurement of wine sensory descriptors using a voltammetric electronic tongue**

Xavier Cetó, Andreu González-Calabuig, Josefina Capdevila, Anna Puig-Pujol and Manel del Valle

*Sensors and Actuators B, 2015, 207, 1053–1059*

The approach presented reports the application of a voltammetric electronic tongue (ET), in contrast with a wine tasting sensory panel, as a tool for standardized wine tasting; concretely, to achieve the discrimination of different wine DOs (Denominación de Origen, a mark related to its geographical region and ensuring high-quality levels) and the prediction of the global score assigned by the trained sensory panel.

To this aim, a voltammetric array of sensors based on metallic and bulk-modified graphite electrodes was used as the sensing part, while chemometric tools such as linear discriminant analysis (LDA) and artificial neural networks (ANNs) were used as the qualitative and quantitative modeling tools. Departure information was the set of voltammograms, which were first preprocessed employing fast Fourier transform (FFT), followed by removal of less-significant coefficients employing a stepwise inclusion method and pruning of the inputs.

### 4.4.1 Voltammetric response

As from the definition of ET of the IUPAC, the first condition for the development of an ET is that we must have an array of low selective sensors with cross-response features that provide some added value in the generation of analytical information. Hence, we should firstly confirm that differentiated signals are observed for the different electrodes, and that those are related to the phenomena under study. That is, generating data rich enough that can be a useful departure point for the multivariate calibration model. In our case, we can see how that can be achieved thanks to the use of the different modifiers and the metal wires (Figure 4.14); even in the case of Pt nanoparticles and Pt wire, where still some differences may be observed. In this case probably due to catalytic phenomena attributable to large surface to volume ratio of the nanoparticles.

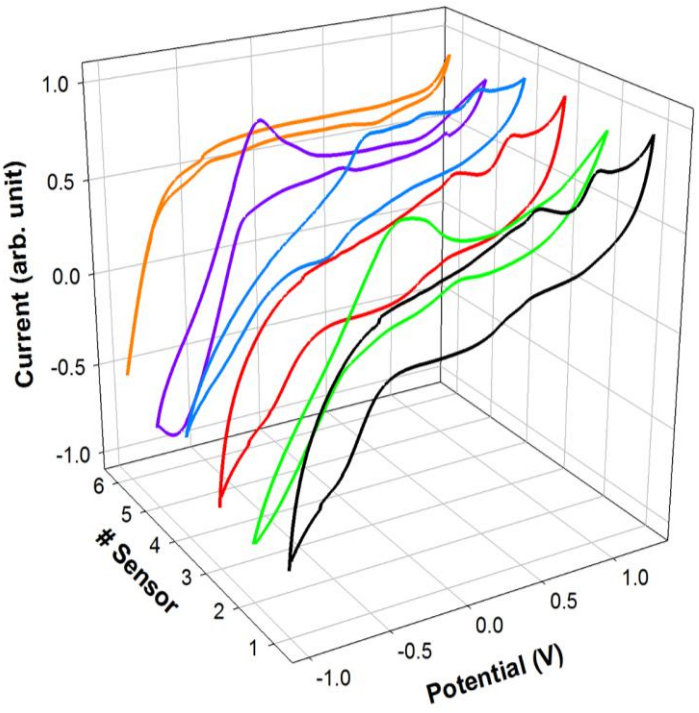


**Figure 4.14.** Example of the different voltammograms obtained with the different sensors forming the ET array for an arbitrary wine sample. Signals provided correspond to: (1) graphite-epoxy sensor, (2) Pt nanoparticle modified sensor, (3) cobalt(II) phthalocyanine modified sensor, (4) Cu nanoparticle modified sensor, (5) Pt metallic sensor and (6) Au metallic sensor.

To provide an objective measure of the differences observed for the different sensors towards wine samples, correlation between their responses was evaluated by means of the comparison factor $f_c$. Thus, obtaining a unique numerical value that provides a measure of its resemblance. In our case, calculated values are summarized in Table 4.6 where, as can be seen, those are around 0.7 and even as low as 0.54.

**Table 4.6.** Averaged values of comparison factor $f_c$ for the sensors employed in the array.

| $f_c$ | **1** | **2** | **3** | **4** | **5** | **6** |
|---|---|---|---|---|---|---|
| **1** | 1 | 0.700 | 0.867 | 0.786 | 0.709 | 0.710 |
| **2** | - | 1 | 0.761 | 0.640 | 0.545 | 0.585 |
| **3** | - | - | 1 | 0.723 | 0.627 | 0.664 |
| **4** | - | - | - | 1 | 0.706 | 0.675 |
| **5** | - | - | - | - | 1 | 0.751 |
| **6** | - | - | - | - | - | 1 |

After this initial confirmation, the next step is to assess whether or not the recorded signals are related to the phenomena under study. However, this cannot always be checked so easily, requiring the use of advanced chemometric tools which, as the IUPAC report reminds us, are the ones extracting and interpreting the relevant information. Therefore, in the next sections we will focus on discerning the richness of the generated data and its suitability for the desired outputs.

At this point, given the complexity of the generated data, FFT was used as a preprocessing step in order to reduce the high dimensionality requirements of the processing, which additionally may result in an improvement of model's performance. In this manner, each voltammogram was compressed down to only 32 coefficients without any loss of significant information (Figure 4.15) [19]; this allowed for a compression of the original data up to 93.75% (from 512 current values down to 32 coeffs.), prior to pattern recognition or numerical modelling.

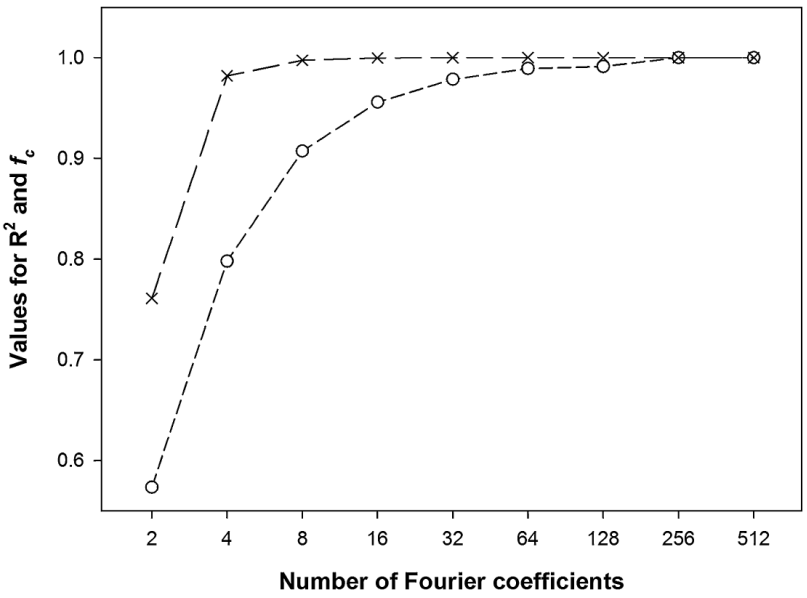


**Figure 4.15.** FFT data pre-processing. Representation of the coefficient of determination, R2(x) and $f_c$ (○) as a measure of the signal reconstruction degree, vs. the number of Fourier coefficients used. For better representation of the data, Y-axis is plotted in linear-scale, while X-axis is in log-scale.

## 4.4.2. Identification of the DO for the same grape variety

As a first attempt to assess whether or not the ET would be capable to distinguish the wine samples based on its DO, we focused on a specific grape variety and analyzed some wine samples from that variety, but produced in different regions. Hence, reducing the source of variability and ensuring the source of the discrimination factor; that is, to asses if there is or not an effect due to its origin.

To this aim, a total subset of nine samples, all from Garnatxa Blanca variety, produced in three different DO regions (Empordà, Terra Alta and Montsant) were initially considered. Samples were analyzed as previously described in Section 3.4, and an extract of the recorded signals has already been shown in Fig. 4.14. Once confirmed the cross-response features of the ET, we should look now for (dis)similarities along the recorded signals that might indicate whether or not analyzed samples might be distinguished by means of the ET. Hence, looking more deeply in the voltammetric responses, we can observe some distinguished features that seem to originate depending on the DO; e.g. some anodic peaks that can be observed around +1.0 V for graphite–epoxy sensor (Fig. 4), but also at the anodic wave in the region from −0.5 to −1.0 V.

To confirm this differentiated behaviour, voltammetric responses were compressed employing FFT, and obtained coefficients were analyzed employing PCA (Figure 4.16); an unsupervised method which provides a better representation of samples (dis)similarities, but not performing its classification. As could be expected from the voltammograms, the PCA plot shows how some samples seem to group in clusters, thus indicating some similarities between those samples and suggesting that the ET should be capable of distinguishing such factor (i.e. the effect of the different DOs in the final wine). Moreover, it should be also noticed that with only the first two PCs, the accumulated explained variance was ca. 79.8%; a large value which means that most of the variance contained in the original information is now represented by only these two new coordinates.

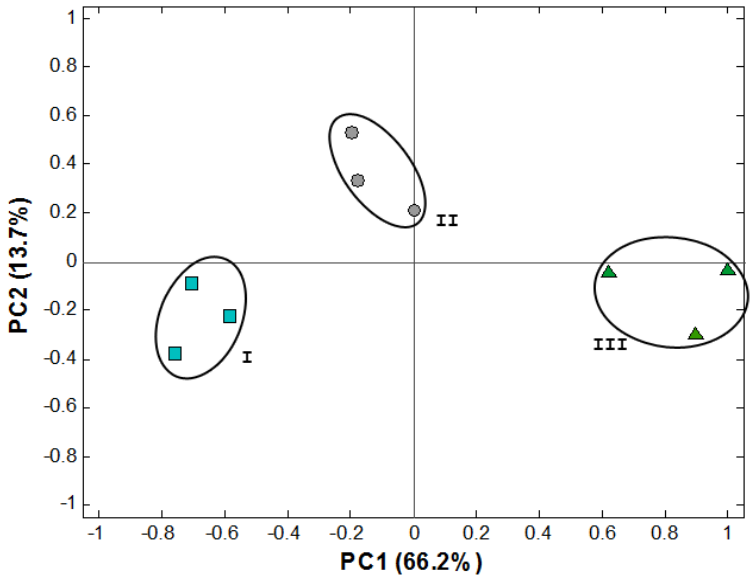


**Figure 4.16.** Score plot of the first two components obtained after PCA analysis of Garnatxa Blanca wine samples: (■), I, Empordà, (●), II, Terra Alta and (▲), III, Montsant.

## 4.4.3. Discrimination of different DOs

Due to the satisfactory trend already observed in the previous analysis, the whole set of samples were analyzed with the ET array and recorded signals compressed employing FFT as previously done, but this time LDA was chosen for pattern recognition of the different DOs. This alternative was chosen given that, unlike PCA which only provides a visualization tool of the variability of the data, LDA is a supervised method that allows to actually build a classification model [20]. That is, LDA explicitly attempts to model the difference between the classes of data, while PCA does not.

Therefore, the whole set of 71 samples was categorized according its DO as follows (number of samples): Empordà (10), Penedès (11), Costers del Segre (8) Terra Alta (16), Priorat (7), Montsant (7), Catalunya (10) and Tarragona (2). Unfortunately, compared to the other classes, very few samples from DO Tarragona were available, and hence it would result problematic to build a proper classification model without overfitting it if those were included. Accordingly, those samples were not considered for further calculations.

Lastly, as LDA is a supervised method, some samples from the set must be left out when building the model so that they can be used to assess its performance. In our case, the model was trained with 80% of the data (training subset), using the remaining 20% of the data (testing subset) to characterize the accuracy of the classification model and obtain unbiased data.

Figure 4.17 displays the distribution of the wine samples along the first three new coordinates, showing an accumulated variance of 94.8%; a high value indicating that nearly all the variance contained in the original information is represented now by only these three new functions. As can be observed, discrimination of the different wines according to its DOs can be achieved with this simple analysis of the new coordinates. Nevertheless, it should be taken into account that the actual LDA model is composed by 6 functions (number of groups - 1) and that all of them are used to perform the classification task; although not being possible to visualize it.

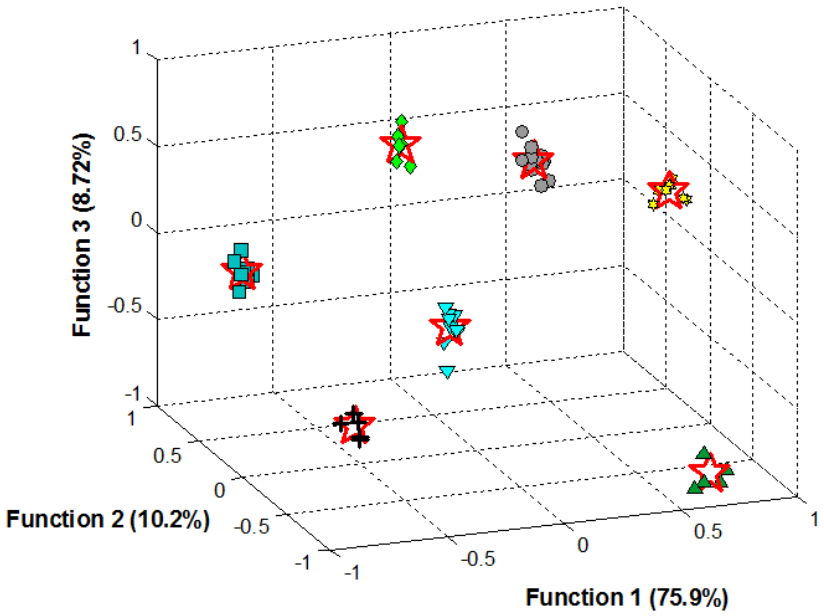


**Figure 4.17**. Score plot of the first three functions obtained after LDA analysis of the wine samples, according to their DO: (■) Empordà, (▼) Penedès, (◆) Costers del Segre, (●) Terra Alta, (+) Priorat, (▲) Montsant and (☆) Catalunya; also the centroid of each class is plotted (⋆).

Despite the good clustering observed in the built pattern recognition model (Figure 4.17), its actual performance should be assessed employing the samples from the testing subset, and not only the ones from the training subset. To this aim, the generated model was used to predict the expected DO for the 14 samples that were left out (not being used at all) during the modeling stage and predicted classes were compared to the expected ones. The corresponding confusion matrix was then built (Table 4.7), allowing to calculate the performance of the model by means of three different indicators: classification rate, sensitivity and specificity.

**Table 4.7.** Confusion matrix built according to the DO category obtained using the LDA model for the testing subset samples.

| | Emp[b] | Pen[b] | CdS[b] | TA[b] | Pri[b] | Mon[b] | Cat[b] |
|---|---|---|---|---|---|---|---|
| **Emp[a]** | 1 | 0 | 0 | 0 | 1 | 0 | 0 |
| **Pen[a]** | 0 | 2 | 0 | 0 | 0 | 0 | 0 |
| **CdS[a]** | 0 | 0 | 2 | 0 | 0 | 0 | 0 |
| **TA[a]** | 0 | 0 | 0 | 2 | 0 | 0 | 0 |
| **Pri[a]** | 0 | 0 | 0 | 0 | 2 | 0 | 0 |
| **Mon[a]** | 0 | 0 | 0 | 0 | 0 | 2 | 0 |
| **Cat[a]** | 0 | 0 | 0 | 0 | 0 | 0 | 2 |

Emp: Empordà; Pen: Penedès; CdS: Costers del Segre; TA: Terra Alta; Pri: Priorat; Mon: Montsant; Cat: Catalunya.
[a] Expected;.[b] Predicted

The former corresponds to the ratio between the number of samples correctly classified and the total number of samples. While the latter two, are related to the number of false positives or false negatives. Sensitivity is calculated as the percentage of objects of each class identified by the classifier model, and specificity as the percentage of objects from different classes correctly rejected by the classifier model; averaging those for the classes. In this case, values reached 92.9%, 92.9% and 98.8% for the classification rate, sensitivity and specificity, respectively.

Similarly, in order to evaluate if the only miss-classified sample could be an outlier, model performance was also evaluated employing the leave-one-out strategy, regardless the fact this has been sometimes criticized as overoptimistic [21]. The idea here is that the use of a larger number of samples in the training subset might improve the model generalization ability. In this manner, LDA model was rebuilt, and as it could be expected given that wines are already subjected to strict DO controls, none of the samples were now miss-classified, achieving a classification rate of 100% in terms of accuracy, sensitivity and specificity.

### 4.4.4. Prediction of global scores of the sensory panel

To further assess the ability of the ET as a tool for wine tasting, the correlation between the ET measurements and the global scores assigned by the sensory panel was also attempted. That is, the average scores assigned to each wine by the sensory panel were modelled from the set of voltammetric responses, previously compressed with FFT, by means of an ANN model.

Unlike the previous cases, where qualitative information was extracted, a quantitative model was built this time. For this, ANN was selected as the modelling tool due to its superior performance compared to linear methods; i.e. more flexible modelling methodologies, since both linear and non-linear functions can be used (or combined) in the processing units [13]. Thus, ANNs are specially suitable to be used with non-linear sensor responses and allow for more complex relationships between a high-dimensional descriptor space and the given retention data; all this leads to a better predictive power of the resulting ANN model compared with other linear methods [14], although if linearity exists, a proper behavior may be obtained also with the latter.

As before, the set of samples were split into two subsets: the training subset (49 samples, 71%) used to build the model and the testing subset (20 samples, 29%) used to assess its performance. Again, this division was randomly performed, taking as only precaution to avoid

that extreme values are used in the testing subset; that is, to avoid extrapolation from the model.

After a systematic study to optimize the topology of the neural network (i.e. training algorithm, number of hidden layers, number of neurons, transfer functions, etc.), the final architecture of the ANN model had 80 neurons (corresponding to the selected FFT coeffs. after CI analysis) in the input layer, 6 neurons and logsig transfer function in the hidden layer and one neuron and tansig transfer function in the output layer, viz. the score assigned by the sensory panel.

Subsequently, comparison graphs of predicted vs. expected scores, both for the training and testing subsets, were built and the linear fitted regression parameters were calculated to easily check the performance of the ANN model (Figure 4.18). As it can be observed, a satisfactory trend was obtained for both subsets, with regression lines close to the theoretical ones; i.e. values of slope and intercept close to 1 and 0, respectively.

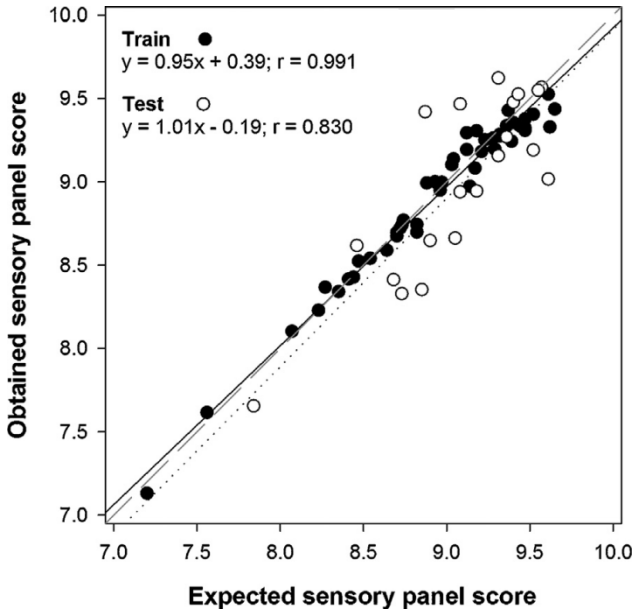


**Figure 4.18.** Modelling ability of the optimized FFT-ANN for the prediction of white wines global scores assigned by the sensory panel. Set adjustments of obtained vs. expected values, both for training (●, solid line) and testing subsets (○, dotted line). The dashed line corresponds to theoretical diagonal line.

To numerically assess the predictive ability of the ET three different parameters were calculated: standard error of prediction (SEP), ratio of standard error of performance to

standard deviation (RPD) and range error ratio (RER) [22]; with obtained values of 0.30, 1.48 and 5.93, respectively.

However, despite the good trend observed, it is true that the observed dispersion, especially for the testing subset, is larger than desirable for a quantitative application; but still good enough to be considered at least as a semi-quantitative approach. It should be highlighted anyhow that still correlation and the followed trend are highly significant. Moreover, considering the subjective nature of the scores, which are provided by the sensory panel.

As an additional verification of the proposed approach, a Student's paired samples t test for the testing subset was performed. Obtained experimental t value was 1.42, while the critical tabulated t value with 95% confidence level and 19 degrees of freedom is 2.09. Therefore, confirming the agreement observed between the ET response and the scores assigned by the sensory panel.

# Article 5:

**Electronic tongues to asses wine sensory descriptors**

Xavier Cetó, Andreu González-Calabuig, Nora Crespo, Sandra Pérez, Josefina Capdevila, Anna Puig-Pujol and Manel del Valle

*Talanta,* 2017, 162, 218–224

This work reports the application of an electronic tongue as a tool towards the analysis of wine in tasks such as its discrimination based on the maturing in barrels or the prediction of the global scores assigned by a sensory panel.

To this aim, red wine samples were first analysed with the voltammetric sensor array, without performing any sample pretreatment. Afterwards, obtained responses were preprocessed employing fast Fourier transform (FFT) for the compression and reduction of signal complexity, and obtained coefficients were then used as inputs to build the qualitative and quantitative models employing either linear discriminant analysis (LDA) or partial least squares regression (PLS), respectively.

### 4.5.1. Voltammetric sensor array

In the present work we have combined metallic electrodes with catalyst-modified carbon electrodes; the goal is to accomplish better complementary and more varied voltammograms with the wines considered; in this sense, example of the voltammetric responses obtained for the selected sensor array are shown in Figure 4.19. As can be seen, differentiated response is achieved thanks to the use of the different modifiers for the epoxy graphite electrodes and the different metallic electrodes; even in the case of Pt, the responses of the electrode modified with Pt nanoparticles and the Pt metal electrode still display some differences, useful for obtaining complementary information from the voltammograms. In this case, differences are probably due to catalytic phenomena attributable to large surface to volume ratio when metal nanoparticles are used.

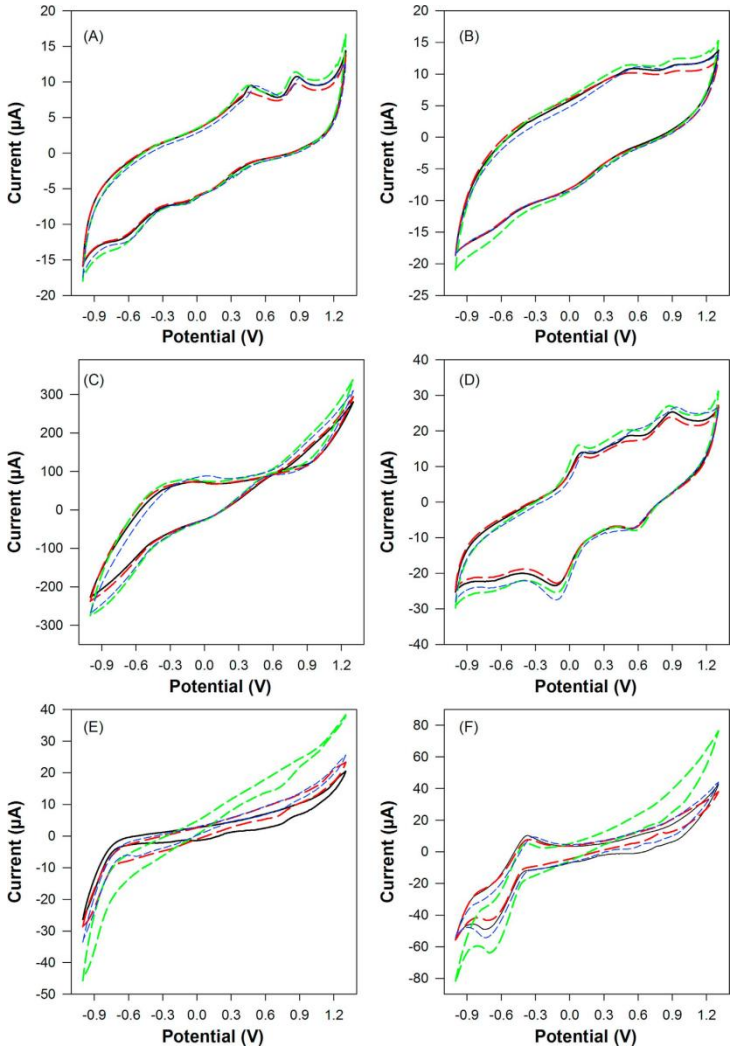


**Figure 4.19.** Example of the different voltammograms obtained with the different sensors forming the ET array for four arbitrary red wine samples. Signals provided correspond to: (A) graphite–epoxy sensor, (B) Cu nanoparticles modified sensor, (C) Pt nanoparticles modified sensor, (D) Co phthalocyanine modified sensor, (E) Au metallic sensor and (F) Pt metallic sensor

Additionally due to the large dimensionality of the generated signals, a preprocessing stage based on the usage of FFT was also performed prior the modelling stage itself, aimed to improve model's robustness and performance. In this manner, prior to the modelling, each voltammogram was compressed from the registered 512 current intensities down to 32 coefficients without any loss of significant information; this allowed a compression of the original data up to 93.8%.

## 4.5.2. Effect of the barrel in wine maturing

In the first study case, we assessed whether there was or not some identifiable trend in the ET response that could be related to the type of barrel used during wine maturing; that is, the type of wood oak used for the construction of the barrel in which the wine will be aged. On this account, Fernández de Simón and colleagues demonstrated that there was a clear effect based on the type of oak used, as they found that wines with different characteristics were obtained from the same base wine after 21 months of ageing [23].

Among the different types of oak barrels, there are mainly two that are used among producers in Catalonia region; namely, French (Quercus robur, Quercus petraea) or American (Quercus alba) oak wood, although also their mixtures might be used. Hence, we will focus on the analysis of different wines aged on those.

As a first attempt to assess the capabilities of the ET to distinguish barrel effect in wine ageing, we initially focused only on wines aged in French and American barrels to asses if there is or not any pattern found. To this aim, a total subset of 16 samples, were initially considered. Samples were analysed as previously described by means of the sensor array. Next, obtained responses were compressed by means of FFT and obtained coefficients were analysed employing PCA (Figure 4.20). This, as an unsupervised method, provides a better representation of samples (dis)similarities, but it does not perform its classification.

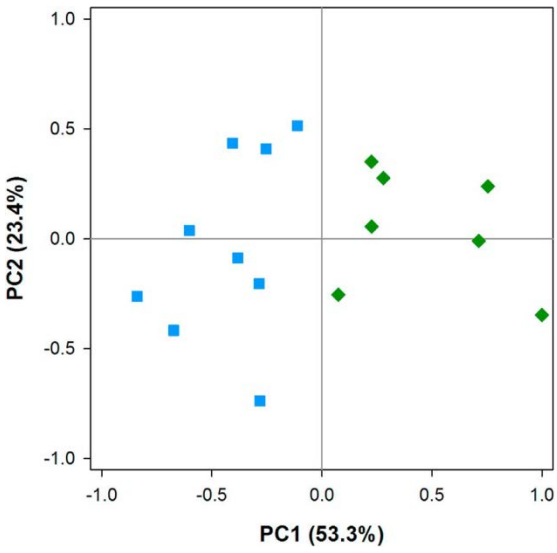


**Figure 4.20.** Score plot of the first two components obtained after PCA analysis of the wine samples: (■) French and (◆) American.

Interestingly, the PCA plot shows how French oak samples seem to group in the left side, whereas the American ones seem to group in the opposite one; thus indicating some effect due to the oak barrel employed and suggesting that the ET should be capable of distinguishing such factor.

To further confirm the observed trend, some additional samples aged in mixed oak barrels were analysed as described with our sensor array. Obtained responses were compressed by means of FFT as before, and the whole set modelled using LDA as the pattern recognition method (Figure 4.21). This was chosen given that LDA is a supervised method that allows to actually build a classification model [20]. That is, LDA looks specifically for differences among the data classes, while unsupervised methods do not.

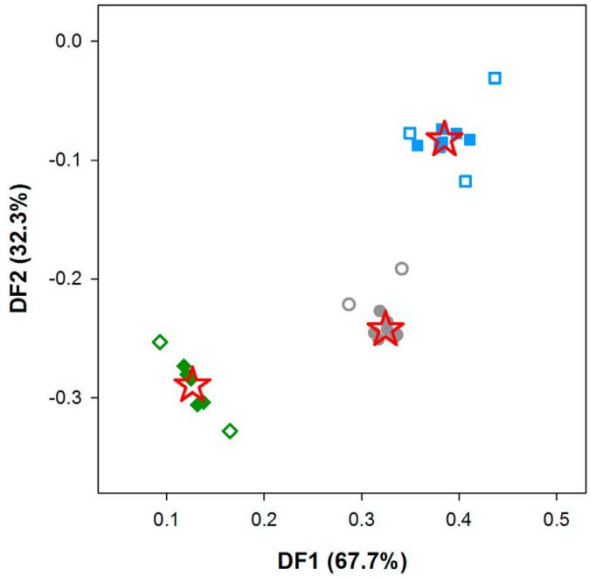


**Figure 4.21.** Score plot of the first two functions obtained after LDA analysis of the wine samples, according to its maturing: (■) French, (●) French/American and (◆) American; with filled symbols for the training subset and empty ones for the testing subset. Additionally, the centroid for each class is plotted (★).

At first sight, it can be seen how the ET is able to distinguish the different types of barrels with this simple analysis of the projected coordinates; however, to numerically assess the performance of the model, cross validation was performed and three different indicators (namely, classification rate, sensitivity and specificity) were calculated. To this aim, the generated model was used to predict the expected group for the test samples that were left out (28% not being used at all during the modelling stage) and predicted classes were compared to the expected ones. The corresponding confusion matrix was then built (Table 1),

and the efficiency of the classification was evaluated for samples of the external test subset as 100% according to classification rate, sensitivity and specificity. With the goal of providing a further measure of the goodness of fit, a Pearson's chi-squared test was calculated for the contingency table (Table 4.7), obtaining a calculated statistic of $\chi^2$=14.0, larger than the tabulated value at the 95% confidence level (9.49). This parameter, plus the calculated coefficient of contingency (0.8165, a 100% of the maximum value for the number of classes considered) describes numerically the ability in the identification of ageing wood used.

**Table 4.7.** Confusion matrix built according to the maturing category obtained using the LDA model for the testing subset. Results provided correspond to the average of the values obtained for each sample after 25 repeated calculations done with random division of samples for train/test subsets each time.

| | **F**[b] | **FA**[b] | **A**[b] |
|---|---|---|---|
| **F**[a] | 100% | 0 | 0 |
| **FA**[a] | 0 | 100% | 0 |
| **A**[a] | 0 | 0 | 100% |

F: French; FA: French/American; A: American. [a] Expected. [b] Found.

## 4.5.3. Prediction of the wine maturing period

As before, another set of samples was analysed with the ET, and responses were modelled employing PLS instead of LDA to quantitatively predict their ageing time. Details of the PLS model, such as number of latent variables used (5) were derived from a leave-one-out cross-validated initial calculation. After model optimization, a more complete cross-validation stage (RSS) with separate training and test subsets was done, whereas comparison graphs of predicted vs. expected ageing months were built to check its prediction ability (Figure 4.22), and regression lines were fitted. To ensure the robustness of the approach, and that the results obtained were not dependant on the specific subdivision of the samples for the train and test subsets, a repeated resampling approach was used (n=24), which in turn allowed us to assign prediction uncertainties to the different samples and to obtain unbiased data, both for training and test subsets.

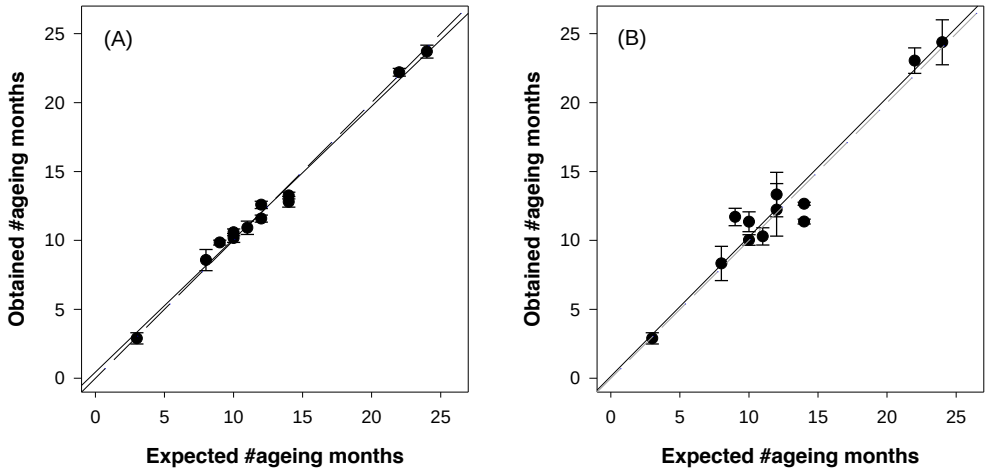


**Figure 4.22.** Performance of the optimized FFT-PLS model for the prediction of red wines ageing time. Set adjustments of obtained vs. expected values, both for (A) training and (B) testing subsets. The dashed line corresponds to theoretical diagonal line. Results provided correspond to the average of the values obtained for each sample after 24 repeated calculations done with random division of samples for train/test subsets each time. Uncertainties calculated at the 95% confidence level.

As can be seen in Table 4.8, a satisfactory trend was obtained for both subsets, with regression lines of the predicted vs. expected comparison plot almost indistinguishable from the theoretical ones; that is, with slope, intercept and correlation values close to 1, 0 and 1, respectively.

**Table 4.8.** Parameters of the fitted regression lines for the comparison between obtained vs. expected values, both for the training and testing subsets of samples for maturing period (intervals calculated at the 95% confidence level).

| | Correlation | Slope | Intercept | NRMSE |
|---|---|---|---|---|
| *Train* | 0.982 | 0.964±0.025 | 0.45±0.33 | 0.048 |
| *Test* | 0.969 | 1.011±0.061 | 0.14±0.84 | 0.077 |

**NRMSE**: Normalized Root Mean Square Error; Intercept values are expressed in months.

In addition, joint confidence intervals were calculated and plotted according to described methodology (Figure 4.24) [2]. Its usage allows to simultaneously assess the goodness of slope and intercept, and therefore represents a rapid visualization tool to detect if there are or not differences between two compared methods. In this direction, uncertainties in both axes are used to calculate the estimated covariance matrix based on an F distribution, and to examine whether or not the theoretical (slope, intercept) comparison point (1,0) is included in the

elliptical region of the 95% joint confidence intervals. Therefore, we can state that there are not significant differences between the actual ageing time and the values predicted by the ET, thus suggesting the ET as a promising approach for the obtaining of an analytical tool to assess the wine ageing process.

### 4.5.4. Prediction of global scores of the sensory panel

Lastly, the capabilities of the ET as a tool able to reproduce the global scores assigned by a trained human sensory panel were also evaluated. This represents a more complex approach compared to the previous ones, as those scores depend from the mouthfeel and flavours perceived when tasting the wine, and can be related to both the presence and absence of several compounds and classes of those. This is why the ET system represents an interesting straightforward approach for this scenario, as its biomimetic nature aligns with the biological scheme. Hence, the hypothesis if the ET can be trained employing the scores assigned by the sensory panel to reproduce the knowledge from the experts is thus assessed.

After analysing the wine samples with the sensor array, obtained responses were processed as previously described; a PLS model was constructed from the FFT coefficients available from each sample and optimized to correlate the ET responses with the average scores assigned to each wine by the sensory panel. Fine tuning of the PLS model, such as number of latent variables used (6) were derived from a separate leave-one-out cross-validated initial calculation. After model optimization, a more complete cross-validation (RRSS) stage with separate training and test subsets was done, whereas comparison graphs of predicted vs. expected scores assigned by the sensory panel were built to check its prediction ability (Figure 4.23), and corresponding regression lines were fitted. Again, to ensure the robustness of the approach, and that the results obtained were not dependant on the specific subdivision of the samples for the train and test subsets, a repeated sampling and calculation (n=30) was performed, which in turn allowed us to assign prediction uncertainties to the different samples and to obtain unbiased data, both for training and test subsets.

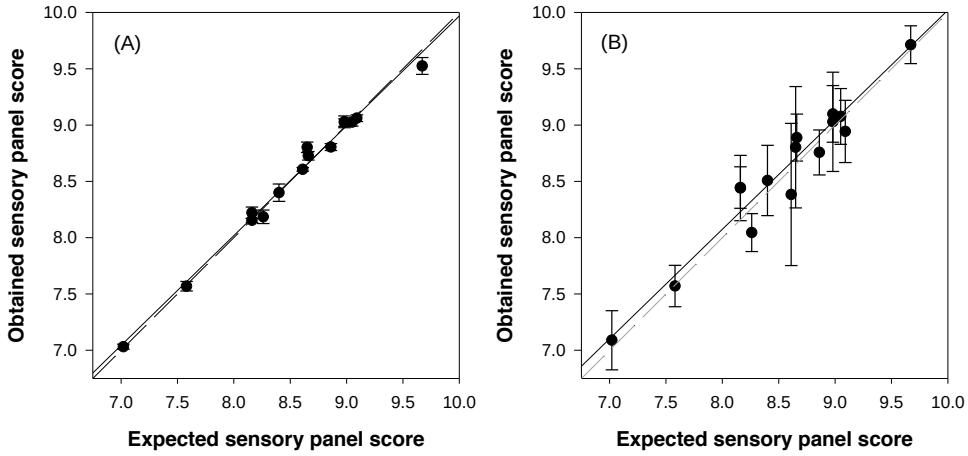


**Figure 4.23.** Performance of the optimized FFT-PLS model for the prediction of red wines global scores assigned by the sensory panel. Set adjustments of obtained vs. expected values, both for (A) training and (B) testing subsets. The dashed line corresponds to theoretical diagonal line. Results provided correspond to the average of the values obtained for each sample after 30 repeated calculations done with random division of samples for train/test subsets each time. Uncertainties calculated at the 95% confidence level.

As can be observed from Figure 4.23, the obtained comparison results are close to the ideal values, with regression lines very close to the theoretical ones. This was further confirmed by numerically assessing the regression parameters (Table 4.9) and building the joint confidence intervals plot (Figure 4.24); which intercepts were close to 0 and slopes and correlation coefficients close to 1, being these theoretical values included in the 95% confidence interval. Thus, meaning there is no significant model bias or differences between the values predicted by the ET and the ones assessed by the panel.

**Table 4.9.** Parameters of the fitted regression lines for the comparison between obtained vs. expected values, both for the training and testing subsets of samplesfor sensory score prediction (intervals calculated at the 95% confidence level).

| | Correlation | Slope | Intercept | NRMSE |
|---|---|---|---|---|
| *Train* | 0.981 | 0.976±0.023 | 0.22±0.20 | 0.045 |
| *Test* | 0.917 | 0.973±0.087 | 0.29±0.74 | 0.110 |

**NRMSE**: Normalized Root Mean Square Error; Intercept values are expressed in arb. unit (0–10).

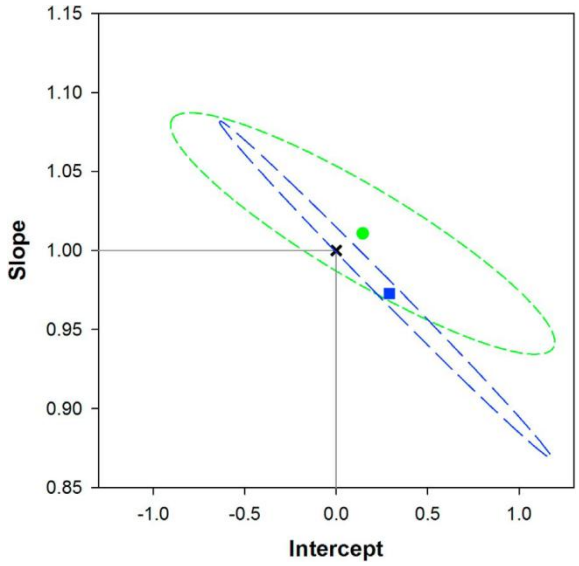


**Figure 4.24.** Joint confidence intervals for the testing subsets: (●, short-dashed line) the ageing time and (■, long-dashed line) the global scores assigned by the sensory panel. Also the ideal point (1,0) is plotted (x); intervals calculated at the 95% confidence level

# Article 6:

**Voltammetric electronic tongue to identify Brett character in wines. On-site quantification of its ethylphenol metabolites**

Andreu González-Calabuig and Manel del Valle

*Talanta,* 2018, 179, 70–74

This work reports the applicability of a voltammetric sensor array able to evaluate the content of the metabolites of the Brett defect: 4-ethylphenol (4-EP), 4-ethylguaiacol (4-EG) and 4-ethylcatechol (4-EC) in spiked wine samples using the electronic tongue (ET) principles.

The ET used cyclic voltammetry signals, obtained from an array of six graphite epoxy modified composite electrodes; these were compressed using Discrete Wavelet transform while chemometric tools, among these artificial neural networks (ANNs), were employed to build the quantitative prediction model. In this manner, a set of standards based on a modified full factorial design and ranging from 0 to 25 mg $L^{-1}$ on each phenol, was prepared to build the model; afterwards, the model was validated with an external test set. The model successfully predicted the concentration of the three considered phenols.

## 4.6.1. Voltammetric array response

The voltammetric responses for each of the electrodes towards the individual compounds were first evaluated, to assure that the generated signals were different enough and the obtained data were rich enough to be the departure point for a multivariate calibration model.

Therefore, under the described conditions in Section 3.4, individual stock solutions of 25 mg $L^{-1}$ of 4-EP, 4-EG and 4-EC in a wine matrix were analyzed (Figure 4.25). No further optimization of the media composition or pH was done, as the simplest procedure possible was desired. Even pH was not regulated, although in this case, being wine a natural fermented product, pH value is within narrow values for a given variety. As a general trend, and as it is already reported in the literature [24], two processes are observed for all the sensors corresponding to the oxidation of the corresponding phenol to its quinone form, and the reduction of the quinone to the phenolic form.

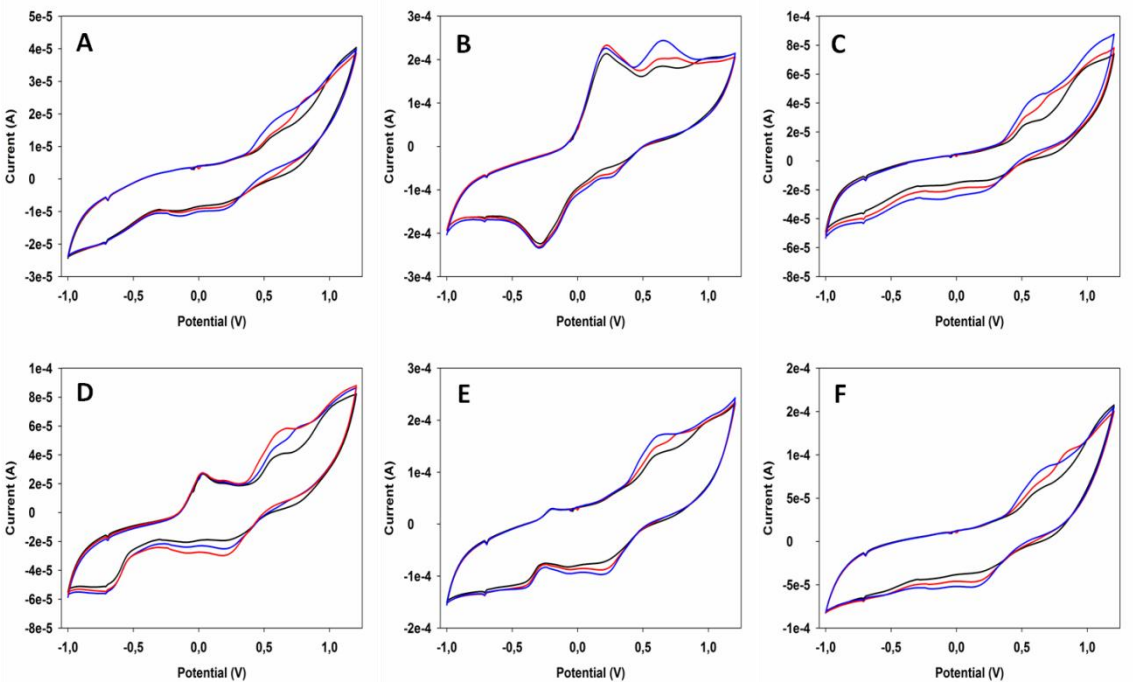


**Figure 4.25.** Voltammograms obtained for 25 ppm of 4-EP (black), 4-EG (red) and 4-EC (blue) in a wine matrix for a (A) Bare epoxy-graphite electrode, and electrodes modified with (B) Cu nanoparticles, (C) $WO_3$ nanoparticles, (D) $Bi_2O_3$ nanoparticles, (E) Polypyrrole and (F) Co(II) phthalocyanine.

Moreover, it can also be seen that the copper nanoparticle modified electrode displayed higher currents, a fact somehow explained by the fact that the main natural phenolic-degrading enzymes, like tyrosinase or laccase, are copper containing redox enzymes [25][26]. Besides, slightly differentiated curves were obtained for each of the compounds, a necessary condition for any ET study.

However, it is not enough to asses visually that each sensor in the array responded in a different manner towards 4-ethylphenol, 4-ethylguaiacol and 4-ethylcatechol a chemometric assay was further done. In order to assess mathematically the complementarities between the voltammetric responses of Figure 4.25, a principal component analysis (PCA) was performed [27]. In Figure 4.26A are plotted the scores of samples corresponding to the two first principal components for the array response towards the 3 ethylphenols; in there, it can be seen that each compound sample is differentiated and clearly clustered. Figure 4.26B also plots the scores of the two first principal components but taking into account each sensor, as it can be seen each sensor provides a distinct signal for each analyte. Moreover, the different sensors appear in different coordinates in the scores plot meaning that they have different responses that complement each other. Perhaps the two electrodes showing the closest response were

these of Co (II) phthalocyanine and $WO_3$ that were kept given the very different nature of the catalysts involved.

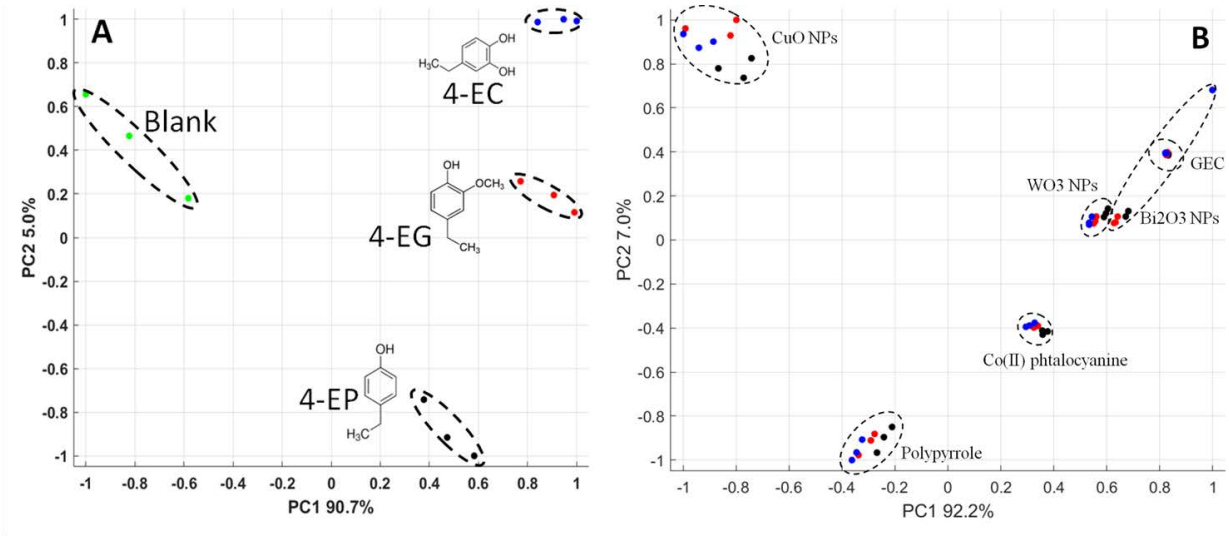


**Figure 4.26.** A) Score plot of the first two components obtained after PCA analysis. A total of 12 samples were analyzed corresponding to triplicate determinations of: 4-EP (black), 4-EG (red), 4-EC (blue) and wine matrix (green). (B) The scores plot of graphite-epoxy electrode (GEC), CuO NPs electrode, WO3 NPs electrode, Bi2O3 NPs electrode, polypyrrole electrode and Co(II)phthalocyanine electrode for 25 ppm of 4-EP (black), 25 ppm of 4-EG (red) and 25 ppm of 4-EC (blue)

The array response towards the compounds of interest, once confirmed the different behaviour of the employed electrodes, allowed the differentiation of the different ethylphenol compounds considered; the next step was to proceed with the design of the architecture of the ANN model capable to quantify these compounds in the wine matrix considered here.

## 4.6.2. Building of the ANN model

The first step in the construction of the artificial neural network model is the definition of the training and test subsets. In this case the chosen experimental design for the train subset was a modified (tilted) $3^3$ factorial design (27 samples); while the validation of the constructed model was done with the test set (10 samples), these were randomly distributed along the experimental domain (0–25 ppm for each phenolic compound). These values are in consistence with typical concentrations of the Brett defect, and also determined by the threshold detected by a trained wine taster, which is around 1 ppm. All standards were prepared on a Don Simon commercial wine matrix as background.

Once the data of the samples in the different subsets was collected the voltammograms were compressed by use of DWT, as result the obtained dataset is suited to be feed to the different ANN models. The next step is to optimize the appropriate ANN architecture, this was done by trial-and-error procedure due to the difficulties to predict the best configuration as there are several parameters involved (compression pretreatment, number of neurons in the hidden layer, transfer functions, etc.).

As previously commented, the samples from the training subset were used to build the ANN model and the performance of the model was evaluated with the prediction of the analyte concentrations in the test subset samples. As mentioned, the test subset is an external set that has not been used in the modeling procedure; the goodness of fit for this subset is a good parameter to evaluate the modeling performance.

After the evaluation of different topologies, the final ANN architecture had 132 neurons (6 sensors × 22 DWT coeffs.) in the input layer, 3 neurons and satlins transfer function in the hidden layer and 3 neurons and purelin transfer function in the output layer, providing simultaneously the concentration of the three compounds considered.

Comparison graphs of predicted vs. expected concentrations for training and testing subsets, for each of the compounds, were built to evaluate the prediction ability of the ANN model (Figure 4.27). A satisfactory trend is obtained for both subsets, with regression lines values very close to the theoretical ones, slope and intercept equal to 1 and 0 respectively. Nevertheless, the training subset showed better correlation coefficients ($r \geq 0.99$) than the test subset ($r \geq 0.95$) but this is expected to be as the train subset is used to optimize the architecture, therefore the model is tailored to fit this data, while the test subset is not used at all during the modeling. The detailed results, described in Table 4.10, showed promising results for the test subset as the NRSME for the three compounds was 0.05, a remarkably low value. From the statistics of comparative graphs (external test subset), an estimation on the reproducibility associated with each determination was 4.6%, 6.5% and 13.0% RSD for 4-EP, 4-EG and 4-EC, respectively. The detection limits obtained for the different ethylphenols were 1.8 ppm, 5.5 ppm and 3.0 ppm for 4-EP, 4-EG and 4-EC, respectively, not far away from the thresholds detected by a human expert. To complement and contrast these results, a PLS treatment was employed to compare the ANN model with the usual chemometric methods, such as partial least squares model. The NRMSE obtained for the test subset with the PLS model was 0.159, clearly worse than the chosen variant. Curiously, the PLS models achieved comparable NRMSE values in quantification of 4-EG, probably this is the electroactive species

with best linearity; with PLS, the individual NRMSE errors were 0.059, 0.062 and 0.135 for 4-EP, 4-EG and 4EC, respectively. The results of the PLS model are detailed in the Table 4.11.

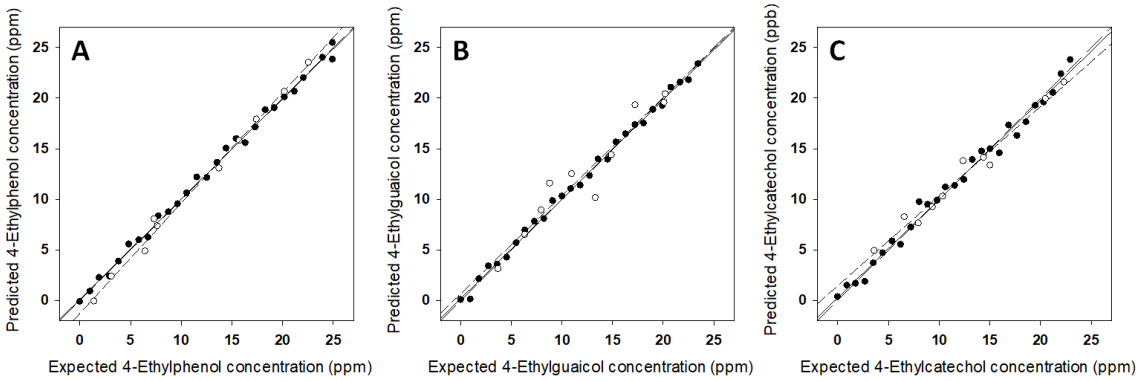


**Figure 4.27.** Modeling ability of the developed DWT-ANN. Adjustments of expected vs. predicted concentrations for (A) 4-EP, (B) 4-EG and (C) 4-EC, both for training (●, solid line) and testing subsets (○, dashed line). Dotted line corresponds to theoretical diagonal line.

**Table 4.10.** Results of the fitted regression lines for the comparison between obtained vs. expected values, both for the training and testing subsets of samples and the three considered species (intervals calculated at the 95% confidence level).

| | | *r* | *Slope* | *Intercept (mg·L$^{-1}$)* | *NRMSE* | *TotalNRMSE* |
|---|---|---|---|---|---|---|
| ***Train*** | *4-Ethylphenol* | *0.998* | *0.990±0.0487* | *0.131±0.715* | *0.019* | *0.022* |
| | *4-Ethylguaiacol* | *0.998* | *0.981±0.0486* | *0.213±0.667* | *0.018* | |
| | *4-Ethylcatechol* | *0.995* | *0.974±0.0816* | *0.282±1.095* | *0.029* | |
| ***Test*** | *4-Ethylphenol* | *0.997* | *1.089±0.133* | *-1.243±1.798* | *0.037* | *0.050* |
| | *4-Ethylguaiacol* | *0.958* | *0.969±0.474* | *0.691±6.400* | *0.069* | |
| | *4-Ethylcatechol* | *0.988* | *0.886±0.227* | *1.461±3.069* | *0.043* | |

NRMSE: Normalized Root Mean Square Error

**Table 4.11.** PLS results of the fitted regression lines for the comparison between obtained vs. expected values, both for the training and testing subsets of samples and the three considered species (intervals calculated at the 95% confidence level).

| | | *r* | *Slope* | *Intercept (mg·L$^{-1}$)* | *NRMSE* | *Total NRMSE* |
|---|---|---|---|---|---|---|
| | *4-Ethylphenol* | *0.999* | *0.999* | *0.005* | *0.006* | |
| ***Train*** | *4-Ethylguaiacol* | *0.999* | *0.999* | *0.018* | *0.005* | *0.013* |
| | *4-Ethylcatechol* | *0.999* | *0.999* | *0.282* | *0.001* | |
| | *4-Ethylphenol* | *0.991* | *0.694* | *1.121* | *-0.917* | |
| ***Test*** | *4-Ethylguaiacol* | *0.975* | *0.969* | *1.036* | *-0.295* | *0.159* |
| | *4-Ethylcatechol* | *0.918* | *0.886* | *1.047* | *0.736* | |

NRMSE: Normalized Root Mean Square Error

Additionally, to visualize the goodness of the fit joint confidence intervals (JCI) were calculated and plotted according to advanced linear regression methodology [3]. The use of JCI plots has been previously employed as a rapid visualization tool to detect if two methods have significant differences [28], allowing simultaneous evaluation of the slope and intercept. The plotting of the JCI takes into account the uncertainties from both axes to calculate the estimated covariance matrix based on a F distribution. In this manner the plots were constructed, for the pooled data of the plots shown in Figure 4.27, and the theoretical comparison point (0,1) was included for comparison purposes. As can be observed in Figure 4.28, the theoretical point is included within the confidence intervals for both for the training and testing subsets; confirming that statistically there are no significant differences for the ET predicted values and the expected ones.

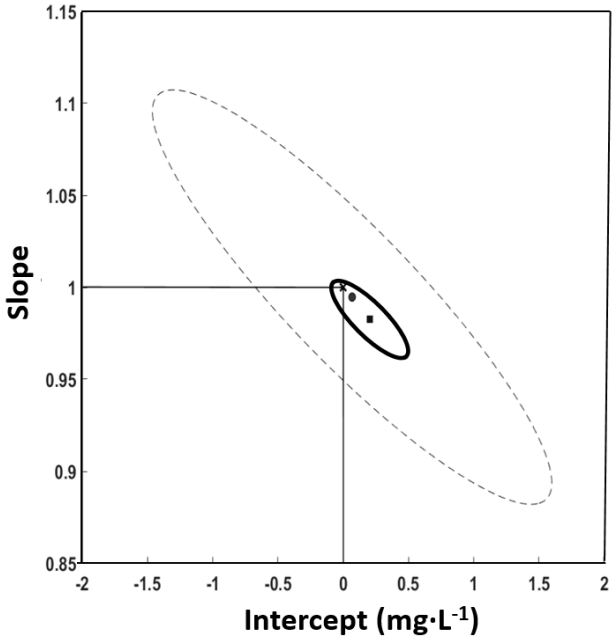


**Figure 4.28.** Joint confidence intervals for the train subset: (red square, solid line) and the test subset (blue circle, dashed line). Also ideal point (1,0) is plotted (x); intervals calculated at the 95% confidence level.

Again, it can be seen that the test subset gives a bigger joint confidence ellipse, this fact can be easily explained; firstly, the test subset is not employed at all during the construction of the model. Moreover, the number of samples in the testing subset is much lower that the train subset, and consequently, the tabulated values of t and F are higher, resulting in higher dispersion and larger confidence intervals.

# Article 7:

**Electronic Tongue for nitro and peroxide explosive sensing**

Andreu González-Calabuig, Xavier Cetó and Manel del Valle

*Talanta,* 2016, 153, 340–346

This work reports the application of a voltammetric electronic tongue (ET) towards the simultaneous determination of both nitro-containing and peroxide-based explosive compounds, two families that represent the vast majority of compounds employed either in commercial mixtures or in improvised explosive devices.

The multielectrode array was formed by graphite, gold and platinum electrodes, which exhibited marked mix-responses towards the compounds examined; namely, 1,3,5-trinitroperhydro-1,3,5-triazine (RDX), octahydro-1,3,5,7-tetranitro-1,3,5,7-tetrazocine (HMX), pentaerythritol tetranitrate (PETN), 2,4,6-trinitrotoluene (TNT), N-methyl-N,2,4,6-tetranitroaniline (Tetryl) and triacetone triperoxide (TATP). Departure information was the set of voltammograms, which were first analyzed by means of principal component analysis (PCA) allowing the discrimination of the different individual compounds, while artificial neural networks (ANNs) were used for the resolution and individual quantification of some of their mixtures.

## 4.7.1. TATP synthesis

Although the conditions are optimized to produce the trimer, the reaction described previously can give the DADP and the TATP mixture. Consequently, a $^{1}H$ NMR spectrum (250 MHz, $CDCl_3$) was acquired to ensure that the product resulting from the reaction was the trimer (Figure 4.29). The resulting peaks in the $^{1}H$ NMR spectra were compared with the ones reported in previous works [29]. The NMR shows a very intense peak corresponding to TATP (δ=1.48 (s)) and various peaks corresponding to the $CDCl_3$ (δ=7.28), $H_2O$ (δ=1.55), HDO (δ=1.37); meanwhile, no peaks corresponding to decomposition products were observed (δ=2.03, δ=1.82, δ=1.80, δ=1.31). Therefore, confirming that TATP was the product obtained.

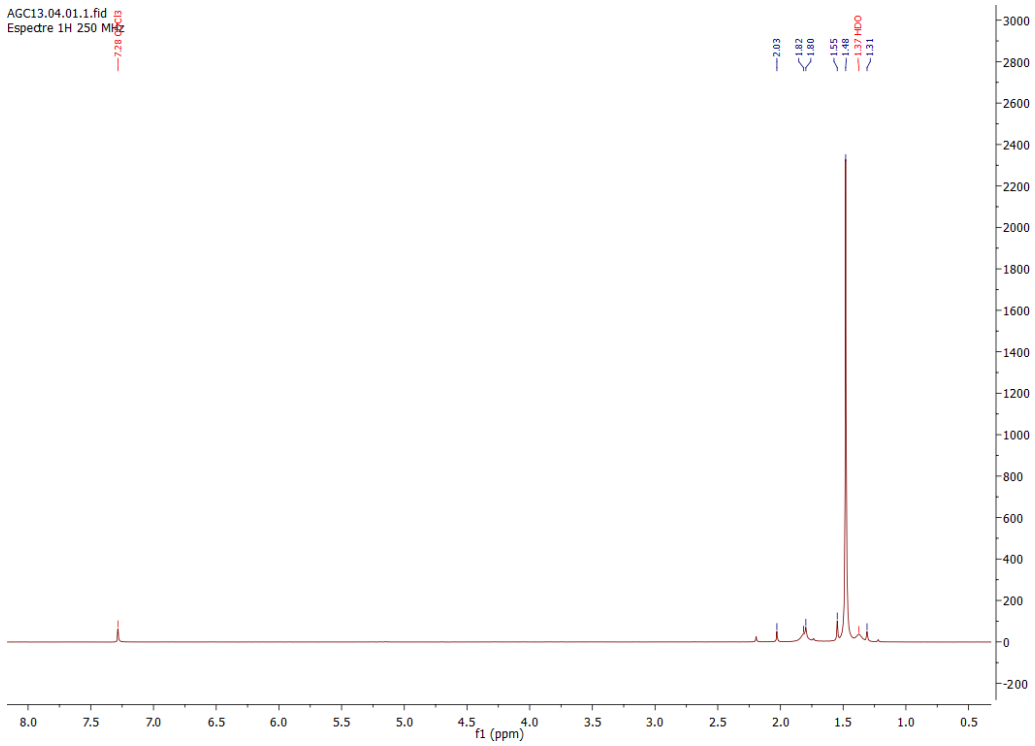


**Figure 4.29.** NMR spectra and synthesis reaction of TATP

## 4.7.2. Voltammetric responses

Following the described procedure, the set of samples was measured employing the multielectrode array, obtaining a whole cyclic voltammogram for each of the sensors from the array. An extract of those results is shown in Figure 4.30. As can be seen, complex and highly overlapped signals are obtained along the whole voltammogram, with differentiated signals obtained for the different kinds of sensors.

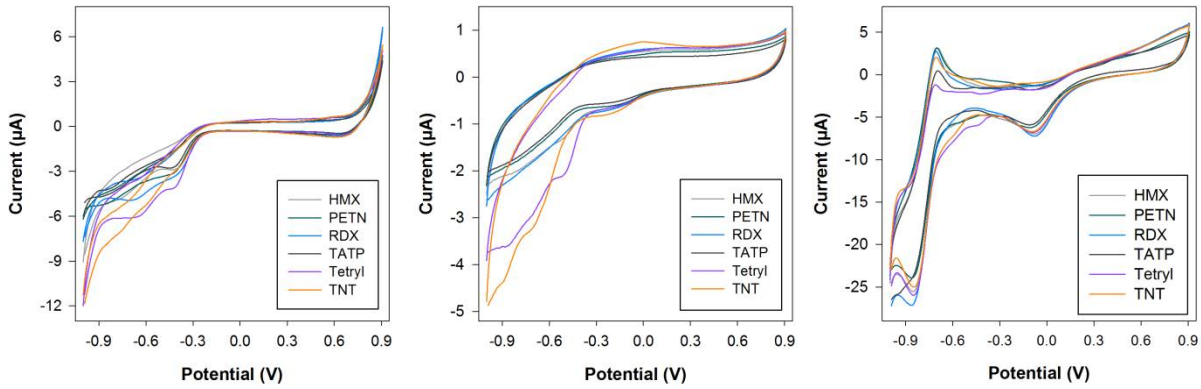


**Figure 4.30.** Voltammograms obtained for (a) epoxy graphite electrode, (b) Au electrode and (c) Pt electrode for 100 µg•mL-1 standard solutions of each of the explosive pure compounds under study (black for TATP, red for RDX, green for HMX, purple for TNT, blue for PETN and orange for Tetryl).

Although at first sight might seem difficult to attribute any peak to a specific compound, characteristic features from the different compounds are still observed. For example, a clear peak corresponding to tetryl can be observed around 0.5 V and a second one at around -0.85 V at the graphite-epoxy electrode, whereas in the case of the gold electrode similar peak might be seen at around -0.4 V and -0.65 V. More significant differences can be found for RDX, where not such clear peaks can be found for the graphite-epoxy electrode, but a clearer peak is observed at around 0.8 V for the gold electrode. This same behavior is observed for the other species such as HMX or TATP for example. Lastly, platinum electrode seems to provide more distinguished features for TATP which oppositely to the other nitro-compounds does not present a reduction peak at around -0.85 V, plus clear response is obtained at the oxidative scan at around -0.70 V. Overall, a situation highly desirable for building an ET application, i.e. when the different sensors display marked distinct features for the different samples.

### 4.7.3. Qualitative analysis of explosives

In a first approach, discrimination of different explosive compounds by means of the ET was attempted. That is, to asses if the system presented herein was able to carry out the identification of the most common explosive compounds.To this aim, voltammetric responses obtained for the stock solutions of each of the pure compounds were analyzed by means of PCA and grouped using cluster analysis tools.

Upon completion of the PCA analysis (Figure 4.31), the accumulated explained variance was calculated with the three first PCs as 99.85%. This large value shows that nearly all the variance contained in the original data can be explained by just using the first new coordinates. In addition, patterns in the figure evidence that samples are clearly grouped based on each explosive compound, with replicas for the same class close one to each other.

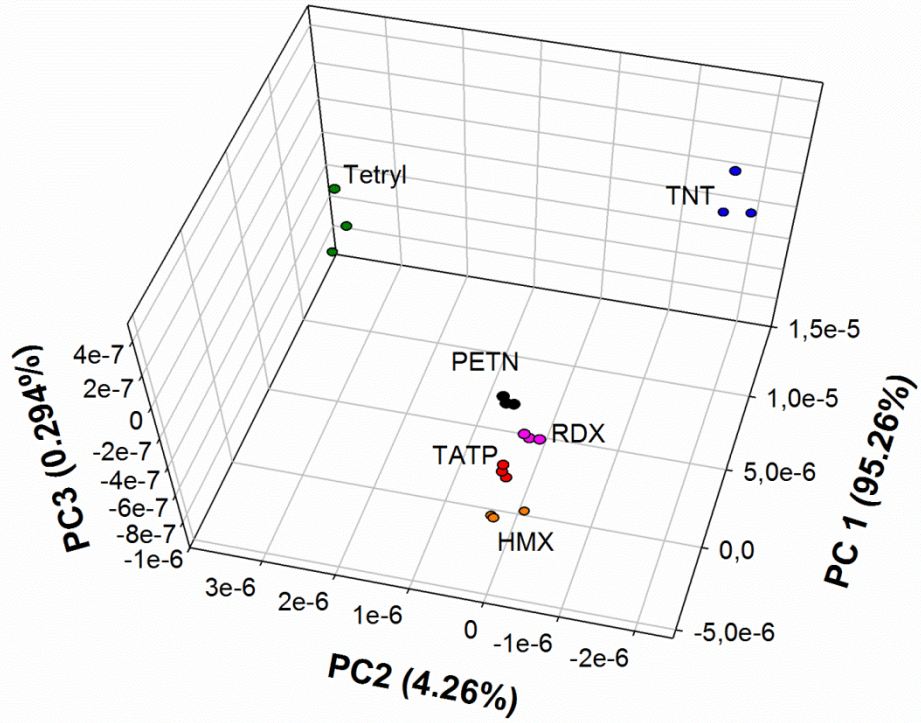


**Figure 4.31.** Score plot of the first three components obtained after PCA analysis. A total of 18 samples were analyzed corresponding to triplicate determinations of: (II) RDX, (II) HMX, (III) PETN, (IV) TNT, (V) Tetryl and (VI) TATP.

After the initial representation of data, a fuzzy ARTMAP ANN model with binary outputs (1/0) was used as classifier, which allowed quantification of the classification performance of the system in contrast to PCA analysis which just provides a visualization of the grouping regions.

The PCA-ANN model was trained with 67% of the data (12 samples) and evaluated using the information of the testing set (remaining 33% of the data; 6 samples) in order to characterize the accuracy of the identification model and obtain unbiased data. From the classification results, the corresponding confusion matrix was built. Correct classification for all the classes was obtained (i.e., a classification rate of 100% for each of the groups), as indicated from the direct visualization of the PCA analysis. The efficiency of the classification obtained was also evaluated according to its sensitivity, i.e., the percentage of objects of each class identified by the classifier model, and to its specificity, the percentage of objects from different classes correctly rejected by the classifier model. The value of sensitivity, averaged for the classes considered, was 100%, and that of specificity was 100%.

With the goal of providing a measure of performance for the identification, a Pearson's chi-squared test was calculated for the contingency table containing the test set samples alone;

this calculation provided, for the six compounds considered, a calculated statistic of χ2¼90.0, significantly larger than the tabulated value at the 95% confidence level (37.7). This statistic also allowed calculation of the contingency coefficient (0.913), equal to the maximum achievable value for the number of samples and classes considered and that describes numerically the power of identification In view of the good results obtained in the qualitative approach, and to further assess the capabilities of the ET to perform its individual quantitative determination, even in the presence of other explosive compounds, the next step was the resolution of ternary mixtures of TNT, tetryl and TATP as the illustrative case. Thus in this way, also demonstrating how the ET would be able to correctly identify each compound regardless of its concentration.

### 4.7.4. Feature selection

As stated, when dealing with voltammetric sensor arrays, the main problem is the huge dimensionality of the recorded set of voltammograms which hinders the modeling step, especially if ANNs are to be used. Therefore, requiring a compression step, which in addition allows to gain advantages in training time, to avoid redundancy in input data and to obtain a model with better generalization ability. In our case this was accomplished by the use of the CI.

Main advantage of this method is the fact that allows the identification of the most relevant features, that is, not only the identification of which sensors most contribute to the discrimination and the quantification of the compounds under scrutiny, but also which points from the voltammograms (i.e. the currents associated to the applied potentials). However, its main drawbacks are the amount of time required for the feature extraction process, the fact that the reduced sets are not unique and the arrival to an optimal set depends on the architecture of the ANN used.

As said, to carry out the selection of the most significant inputs by means of an ANN, first of all, the number of neurons in the hidden layer and the transfer functions (both in the hidden and output layers) are selected in advance to represent the intrinsic dimensionality of the dataset. In this case, and based on previous calculus, the selected ANN architecture to carry out the pruning of the inputs was formed by 5 neurons and *logsig* transfer function in the hidden layer, and 3 neurons and *purelin* transfer function in the output layer. Upon assignation of the weights by the ANN model, the most relevant features were identified, allowing the reduction of the number of inputs by repetitive pruning of the less significant inputs, without any loss of relevant information and an improvement in model robustness as can be seen in Figure 4.32.

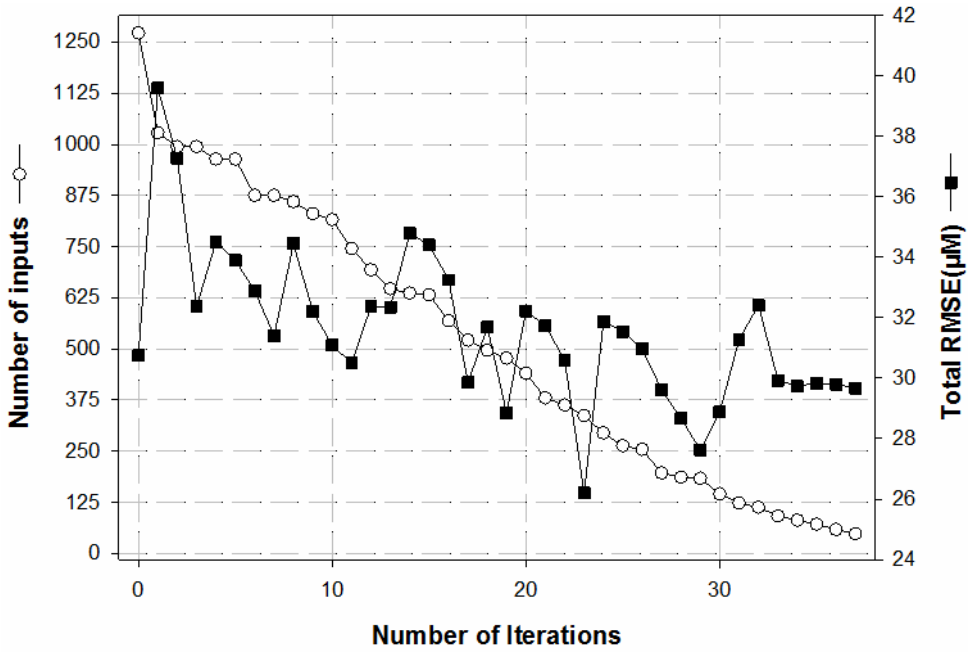


**Figure 4.32.** Feature selection and reduction of the number of inputs by means of CI ANN method.

After this, the final input set was formed by 48 inputs, which meant that a reduction of ca. 96.2% in the size of data to feed the ANN model was achieved. In addition to the large compression ratio, the usage of a pruning strategy of the raw data instead of a compression method such as fast Fourier transform or discrete wavelet transform, offers further advantages as the obtaining of a simpler and more robust model due to non-significant inputs are not included into the model. Even more, allows to identify which sensors mostly contribute to the model. In this direction, the analysis of the selected inputs confirmed the complimentary and cross-response features provided by the chosen sensor array, as all the sensors contributed significantly to the final model. Namely, 12:23:13 were the number of features selected from the responses of the graphite-epoxy, gold and platinum electrodes, respectively.

Hence, once the predictors data matrix was defined, the next step was the optimization of the neural network architecture with the reduced input information by an iterative process varying its configuration (number of neurons in the hidden layer plus transfer functions in the hidden and output layers) in order to generate the best response model.

## 4.7.5. Quantitative analysis of explosive mixtures

Upon completion of an extensive study varying its, the final architecture of the ANN model had 48 neurons (the ones corresponding to the currents previously selected during feature

extraction stage) in the input layer, 8 neurons and logsig transfer function in the hidden layer and three neurons and purelin transfer function in the output layer, providing the concentrations of the three species considered. The accuracy of the generated model was then evaluated towards samples of the external test subset by using the built model to predict the concentrations of the explosives of those samples. Since the external test subset data is not employed at all for the modeling, its goodness of fit is a measure of the accomplished modeling performance. To easily check the prediction ability of the obtained ANN model, comparison graphs of predicted vs. expected concentration for the three compounds were built, both for training subset and testing subsets.

As can be observed in Figure 4.33, a satisfactory trend is obtained for the three compounds, with regression lines close to the theoretical ones. Additionally, regression parameters were calculated (Table 4.12), and as expected from the graphs, a good linear trend is attained for all the cases, but, as usual, with improved behavior for the training subsets due to this subset is the one used to build the model. Despite this, the results obtained for both subsets are close to the ideal values, with intercepts close to 0, and slopes and correlation coefficients close to 1.

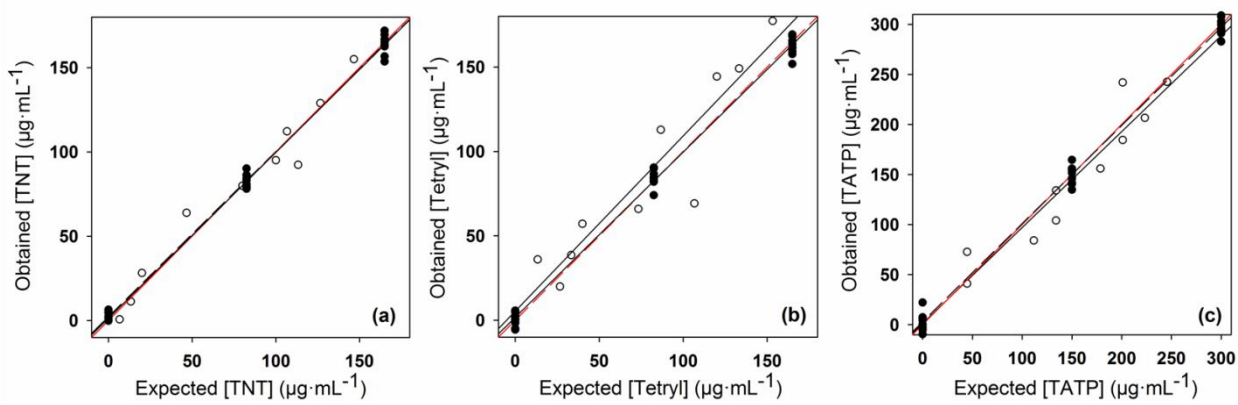


**Figure 4.33.** Modelling ability of the optimized ANN. Sets adjustments of obtained vs. expected concentrations for (a) TNT, (b) Tetryl and (c) TATP, both for training (●, solid line) and testing subsets (○, dotted line). Dashed line corresponds to theoretical diagonal line.

Although not initially considered in this case, individual ANN models may also be developed to separately predict the concentrations of the three species; what would lead to better prediction of the individual concentrations of the three species. However, this configuration was neglected as it does not represent the true nature of the approach and complicates its final application as three models would be used rather than a single one. Nevertheless, this

option may represent an easy way to improve the performance of the final ET approach if required.

**Table 4.12.** Results of the fitted regression lines for the comparison between obtained vs. expected values, both for the training and testing subsets of samples and the three considered explosive compounds (intervals calculated at the 95% confidence level).

| ***Training subset*** | | | | | |
|---|---|---|---|---|---|
| *Explosive* | *Correlation* | *Slope* | *Intercept (μg·mL$^{-1}$)* | *NRMSE* | *Total NRMSE* |
| TNT | 0.997 | 0.984±0.030 | 1.4±3.2 | 0.027 | |
| Tetryl | 0.997 | 0.980±0.030 | 1.7±3.2 | 0.030 | 0.028 |
| TATP | 0.998 | 0.981±0.028 | 2.8±5.6 | 0.027 | |
| ***Testing subset*** | | | | | |
| *Explosive* | *Correlation* | *Slope* | *Intercept (μg·mL$^{-1}$)* | *NRMSE* | *Total NRMSE* |
| TNT | 0.979 | 0.981±0.166 | 2.2±14.9 | 0.064 | |
| Tetryl | 0.929 | 1.038±0.337 | 5.4±30.8 | 0.134 | 0.108 |
| TATP | 0.945 | 0.959±0.269 | 1.2±44.7 | 0.113 | |

*NRMSE: Normalized Root Mean Square Error*

## 4.8 Bibliography


[1] R. Solná, P. Skládal, *Electroanalysis* **2005**, *17*, 2137–2146.

[2] D. C. Montgomery, E. A. Peck, G. G. Vining, *Introduction to Linear Regression Analysis*, John Wiley & Sons, **2012**.

[3] J. Mandel, F. J. Linning, *Anal. Chem.* **1957**, *29*, 743–749.

[4] M. Rodríguez, *Fenton and UV-Vis Based Advanced Oxidation Processes in Wastewater Treatment: Degradation, Mineralization and Biodegradability Enhancement*, Universitat De Barcelona, **2003**.

[5] A. M. Peiro, J. A. Ayllón, J. Peral, X. Doménech, *Appl. Catal. B Environ.* **2001**, *30*, 359–373.

[6] S. Esplugas, J. Gimenez, S. Contreras, E. Pascual, M. Rodríguez, *Water Res.* **2002**, *36*, 1034–1042.

[7] S. Anandhakumar, J. Mathiyarasu, *Microchim. Acta* **2013**, *180*, 1065–1071.

[8] V. S. Ijeri, A. K. Srivastava, *Anal. Sci.* **2001**, *17*, 605–608.

[9] V. S. Ijeri, A. K. Srivastava, *Fresenius. J. Anal. Chem.* **2000**, *367*, 373–377.

[10] T. Navratil, J. Barek, *Crit. Rev. Anal. Chem.* **2009**, *39*, 131–147.

[11] J. W. Steed, J. L. Atwood, *Supramolecular Chemistry*, John Wiley & Sons, **2013**.

[12] J. J. Christensen, J. O. Hill, R. M. Izatt, *Science (80-. ).* **1971**, *174*, 459–467.

[13] F. Despagne, D. L. Massart, *Analyst* **1998**, *123*, 157R–178R.

[14] X. Cetó, F. Céspedes, M. del Valle, *Microchim. Acta* **2013**, *180*, 319–330.

[15] D. Wallach, B. Goffinet, *Ecol. Modell.* **1989**, *44*, 299–306.

[16] G. Zhiqiang, L. Peibiao, Z. Zaofan, *Microchem. J.* **1991**, *43*, 121–132.

[17] J. Wang, M. Bonakdar, *Talanta* **1988**, *35*, 277–280.

[18] N. Serrano, A. González-Calabuig, M. del Valle, *Talanta* **2015**, *138*, 130–137.

[19] L. Moreno-Barón, R. Cartas, A. Merkoçi, S. Alegret, M. del Valle, L. Leija, P. R.

Hernandez, R. Muñoz, *Sensors Actuators B Chem.* **2006**, *113*, 487–499.

[20] R. A. Johnson, D. W. Wichern, *Applied Multivariate Statistical Analysis*, Prentice-Hall New Jersey, **2014**.

[21] D. Kirsanov, O. Mednova, V. Vietoris, P. A. Kilmartin, A. Legin, *Talanta* **2012**, *90*, 109–116.

[22] T. Fearn, *NIR news* **2002**, *13*, 12–13.

[23] B. Fernández de Simón, E. Cadahía, J. Jalocha, *J. Agric. Food Chem.* **2003**, *51*, 7671–7678.

[24] V. Parra, Á. A. Arrieta, J.-A. Fernández-Escudero, M. L. Rodríguez-Méndez, J. A. De Saja, *Sensors Actuators B Chem.* **2006**, *118*, 448–453.

[25] K. Lerch, *Mol. Cell. Biochem.* **1983**, *52*, 125–138.

[26] A. I. Yaropolov, O. V Skorobogat'Ko, S. S. Vartanov, S. D. Varfolomeyev, *Appl. Biochem. Biotechnol.* **1994**, *49*, 257–280.

[27] J. A. Giacometti, F. M. Shimizu, O. Carr, O. N. Oliveira, in *SENSORS, 2016 IEEE*, IEEE, **2016**, pp. 1–3.

[28] X. Cetó, A. González-Calabuig, M. del Valle, *Electroanalysis* **2015**, *27*, 225–233.

[29] J. C. Oxley, J. L. Smith, H. Chen, *Propellants, Explos. Pyrotech.* **2002**, *27*, 209–216.

# Conclusions

## 5. Conclusions

In the presented doctoral thesis were developed a variety of voltammetric ETs that were then used with success in a wide range of applications. Therefore, ETs have a high potential and really shine in situations where conventional analysis and sensor suffer to achieve acceptable results.

The conclusions of this thesis are divided in three sections according to the respective fields:

**1.** Beverage field:

- **1.1.** The ETs developed was able to qualitatively discriminate different red wine DOs and the quantify the global score assigned by a sensory panel; the latter corresponding to the first attempt to correlate such parameter in wines from Catalonia.
- **1.2.** The proposed ET has been successfully applied in the discrimination of white wines from Catalonia based on its maturing in barrels and the prediction of the global scores assigned by a sensory panel.
- **1.3.** An ET was developed for the early identification of *Brett* defect, allowing the quantification of the main volatile chemicals that cause the defect: 4-ethylphenol, 4ethylguaicol and 4-ethylcatechol. The ET developed provides a promising tool for on-site analysis for winemakers.

**2.** Environmental monitoring:

**2.1.** It has been demonstrated that CB-15-crown-5 and CB-18-crown-6 could be successfully immobilized through the assistance of lysine on aryl diazonium salt monolayers anchored on a graphite epoxy composite electrode surface, constituting an alternative to other more widespread ether crown modified electrodes.

**2.2.** The combination of the set of voltammetric measurements with chemometric tools was able to determine the considered metal ions despite the complexity of the signals. Thus, ET permitted to obtain satisfactory results for the quantification of Cd(II), Pb(II) and Cu(II) and Hg(II), Pb(II) and Cd(II).

**2.3.** The complex responses obtained from the biosensor array were successfully processed employing a multilayer ANN using the bio-ET approach. The developed ET was then applied to the monitoring of phenol pollutants mixtures in artificial wastewater during a photo-Fenton process.

**3.** Homeland security:

**3.1.** The electronic tongue developed was capable of the identification of the most used explosive compounds, nitro and peroxo containing compounds. The ET was able to identify: TNT, HMX, RDX, Tetryl, PETN and TATP.

**3.2.** The ETs was able to quantify the concentration of 2,4,6-trinitrotoluene, pentaerythritol tetranitrateand and triacetone triperoxide in of ternary mixtures of the mentioned compounds.

## On going and Future Work

As future perspectives, the integration of new materials, such as molecularly imprinted polymers or graphene, with the aim of increase the performance of the sensor array will surely be an interesting path in the search of developing new sensors for specific applications

As they are now the electrochemical sensors present a signal drift when the sensors are used during long periods of time, this fact and the nature of prediction models made the correction of the drifts and the re-calibration (re-trainning) of the model an issue to be addressed for realistic applications outside laboratory designed experiments.

The inclusion of a $4^{th}$ dimension in the model, such as the sample pH, certainly is an interesting option to contemplate as the models presented in this thesis only take current, sensors and chemical species into account.

# Publications

# Article 1:

**Use of a Bioelectronic Tongue for the Monitoring of the Photodegradation of Phenolic Compounds**

Xavier Cetó, Andreu González-Calabuig and Manel del Valle

*Electroanalysis*, 2015, 27, 225 – 233

DOI: 10.1002/elan.201400394

Full Paper

Wiley Online Library

ELECTROANALYSIS

Special Issue ESEAC

DOI: 10.1002/elan.201400394

# Use of a Bioelectronic Tongue for the Monitoring of the Photodegradation of Phenolic Compounds

Xavier Cetó,[a, b] Andreu González-Calabuig,[a] and Manel del Valle*[a]

**Abstract**: The application of a voltammetric bioelectronic tongue for the simultaneous monitoring of catechol, *m*-cresol and guaiacol in wastewater is reported. Voltammetric responses obtained from an array of bulk modified (bio)sensors, containing enzymes such as tyrosinase and laccase, were combined with chemometric tools such as artificial neural networks (ANNs) for building the quantitative prediction model. To this end, the chemometric model was first built employing a factorial design, validated employing an external test set of samples ($n=14$; total *NRMSE* of 0.076), and afterwards applied to the monitoring of the mineralization of the three phenol pollutants during a photo-Fenton advanced oxidation process.

**Keywords:** Electronic tongue · Artificial neural network · Voltammetric biosensor · Phenolic compounds · Wastewater

## 1 Introduction

Phenolic compounds are widely used in industry as chemical antioxidants, chemical intermediates, additives to lubricants and gasoline, disinfectants, tanning agents, photographic developers or in the production of drugs and pesticides, among others [1–3]. However, despite its extensive usage, some of them are avowed to possess adverse health effects and are consequently regulated, for example by the US Environmental Protection Agency (EPA) or the European Union (EU), as priority pollutants due to their toxicity and persistence in the environment [4,5].

Besides industrial sources, large quantities of phenol-polluted waters are also formed from e.g. the production of olive oil (olive oil mill wastewater, OMW) in the main olive oil producing countries of the Mediterranean region [6]. The phenolic compounds present on those are considered major contributors to the toxicity and the antibacterial activity of OMW, and limit their microbial degradability [7].

For these reasons, removal and control of phenolic compounds from wastewaters is a critical issue, affecting many different industrial sources. On that account, several methods have been reported in the literature to tackle elimination of organic pollutants in water [3,8–11]; e.g. incineration, air stripping, air desorption, liquid-liquid extraction, adsorption of the organic compounds onto activated carbon, inverse osmosis, ultra-filtration, biological treatment, wet oxidation, electrochemical oxidation, photochemical oxidation or chemical oxidation, etc. Even, in some cases, the elimination of organic pollutants needs the coupling of two or more of those basic treatment techniques [9,12].

Among the different alternatives, advanced oxidation processes (AOPs) have been reported as very promising methods for the treatment of hardly biodegradable organic pollutants [13,14]. AOPs are based on the generation of highly reactive radicals (especially hydroxyl radicals) in near ambient temperature and pressure conditions, which are extraordinarily reactive species that attack most of the organic molecules. The most common AOPs are UV-based and $H_2O_2$-based processes like the heterogeneous photocatalysis with UV/$TiO_2$, or the Fenton and photo-Fenton reactions [13,14].

Concerning the detection of phenolic compounds [15], the official analytical methods are based on liquid-liquid extraction for liquid samples, and Soxhlet extraction for solid samples, followed by gas chromatography using different detection devices, normally requiring a derivatization step [2]. Unfortunately, these methods take long time, and require expensive and hazardous organic solvents, which are undesirable for health and disposal reasons. Hence, there is a general trend to change these procedures to solid phase extraction (SPE) and liquid chromatography, or capillary electrophoresis methods, to avoid some of these inconvenients [15]; still, these require the use of heavy laboratory equipment, long time analysis and are unsuitable for on-site analyses.

In this direction, biosensors provide an alternative solution for the determination of phenolic compounds thanks to their low cost, fast response and because they can be easily used to carry out on-field analyses [16]. Even more, the usage of chemometric tools such as artificial neural networks (ANNs) might help to avoid and/or take into account any interference problem derived from addi-

[a] X. Cetó, A. González-Calabuig, M. del Valle
Sensors and Biosensors Group, Department of Chemistry, Universitat Autònoma de Barcelona
Edifici Cn, 08193 Bellaterra, Barcelona, Spain
*e-mail: manel.delvalle@uab.cat

[b] X. Cetó
Mawson Institute, University of South Australia
Mawson Lakes, South Australia 5001, Australia

Supporting information for this article is available on the WWW under http://dx.doi.org/10.1002/elan.201400394.

tional species [17]; the coupling of the two concepts leads to an approach known as (bio)electronic tongue (BioET) [18]. That is, a new class of ETs characterized by the incorporation of one or several biosensors into the sensor array, which might be combined with common chemosensors [19]. Thus, with this methodology, it is possible to achieve a parallel determination of a large number of different species, while any interference effect is solved using these advanced chemometric tools [20].

Based on the foregoing, the aim of this work is to demonstrate the applicability of a voltammetric system employing the electronic tongue principles for the monitoring of different phenolic pollutants in wastewaters. The proposed approach is based on the coupling of cyclic voltammetric responses obtained from an array of enzymatic voltammetric (bio)sensors, with chemometric tools such as ANNs for building the quantitative prediction model. To this aim, catechol, *m*-cresol and guaiacol mixtures were selected as the study case, as they are common phenolic compounds present in various industrial effluents but of difficult removal by conventional wastewater treatment schemes [21]. Firstly, an ANN response to predict the three concentrations was built and validated, while, at a second stage, a monitoring application during the mineralization of a mixture with the three compounds was performed.

## 2 Experimental

### 2.1 Reagents and Solutions

All reagents used were analytical reagent grade; all solutions were prepared using deionised water from a Milli-Q system (Millipore, Billerica, MA, USA). Tyrosinase from mushroom (EC 1.14.18.1, 4276 U $mg^{-1}$), laccase from *Trametes versicolor* (EC 1.10.3.2, 21 U $mg^{-1}$), copper nanoparticles (< 50 nm), catechol, *m*-cresol, guaiacol, potassium dihydrogen-phosphate, potassium monohydrogen-phosphate and hydrogen peroxide 30 % (w/w) were purchased from Sigma-Aldrich (St. Louis, MO, USA). Ammonium sulfate was purchased from JT Baker (Deventer, Netherlands). Magnesium sulfate heptahydrate, manganese(II) sulfate monohydrate and iron(II) sulfate heptahydrate were purchased from Panreac Química (Barcelona, Spain). Potassium chloride was obtained from Merck KGaA (Darmstadt, Germany). Graphite powder (particle size 50 μm) was used as received (BDH Laboratory Supplies, Poole, UK). Epotek H77 resin and its corresponding hardener were supplied from Epoxy Technology (Billerica, MA, USA). Compact UV bulb lights (254 nm wavelength peak, 25 W) were purchased from a local distributor (Eventlights, Barcelona, Spain).

Artificial wastewater (AWW) was prepared by mixing 0.50 g of $(NH_4)_2SO_4$, 1.00 g of $MgSO_4 \cdot 7H_2O$, 0.10 g of $MnSO_4 \cdot H_2O$, 0.005 g of $FeSO_4 \cdot 7H_2O$ per liter of tap water [22].

### 2.2 Building the Response Model – Experimental Design

Before using the BioET as a tool for the monitoring of the photodegradation process, the quantitative response model to predict the phenolics mixture composition from the cyclic voltammograms had first to be built. The objective of this step is to determine the ANN configuration that best describes the response of the system towards the composition of the phenolic mixtures. Additionally, the performance of the built model has to be validated towards new samples; that is, to ensure its accuracy and precision with unbiased data.

To build the response model, a $3^3$ factorial design was used to define the set of samples for the training subset (27 samples) [23,24]; while the set of samples used for the testing subset (14 samples) were randomly distributed along the experimental domain (with concentrations from 0 to 80 mg $L^{-1}$ for each phenolic compound). Besides, as the response of the enzymatic sensors is pH-sensitive, all the samples were prepared in buffered media (0.1 M phosphate buffer at pH 6.50 and 0.1 M KCl saline background).

### 2.3 Photodegradation Process

Several methods are reported in the literature to tackle the elimination of organic pollutants in aqueous solutions [9,11,13,25]. However, as the aim of the present work was to demonstrate the capabilities of BioETs as a tool for the monitoring of water contaminants, rather than focusing on the methods used for its removal, the photo-Fenton process was chosen as the treatment method due to its simplicity and efficiency [9,12].

Experimental conditions were adapted from previous works [9,26]; and a representation of the experimental set-up used is sketched in Figure 1. Briefly, a mixture of the phenolic compounds under study was prepared in AWW as the medium, in order to better simulate a real monitoring application. The oxidation process was performed in a stirred batch photoreactor equipped with two 25 W UV lights, and protected from the incidence of direct sunlight. The use of a thermostated bath was discarded as any appreciable increase of the temperature was not noticed, in part thanks to the short reaction time; therefore, reaction took place at room temperature (25 ± 3 °C). The beginning of the experiment corresponded to the simultaneous addition of hydrogen peroxide and the start of irradiation.

In a typical run, 1 L of a AWW solution containing the ternary mixture of phenolic compounds was mixed with 36 mg of $FeSO_4 \cdot 7H_2O$ and 1440 μL of $H_2O_2$ 30 %.

For the monitoring of the photodegradation process with the BioET, a 9 mL aliquot of the reaction mixture was taken from the reactor at specific times with a micropipette, and diluted 1 : 1 with buffer solution (0.1 M phosphate buffer + 0.1 M KCl at pH 6.50) to avoid any discrepancies in the biosensors response due to variation of the pH. This was preferred rather than adjusting the pH

  

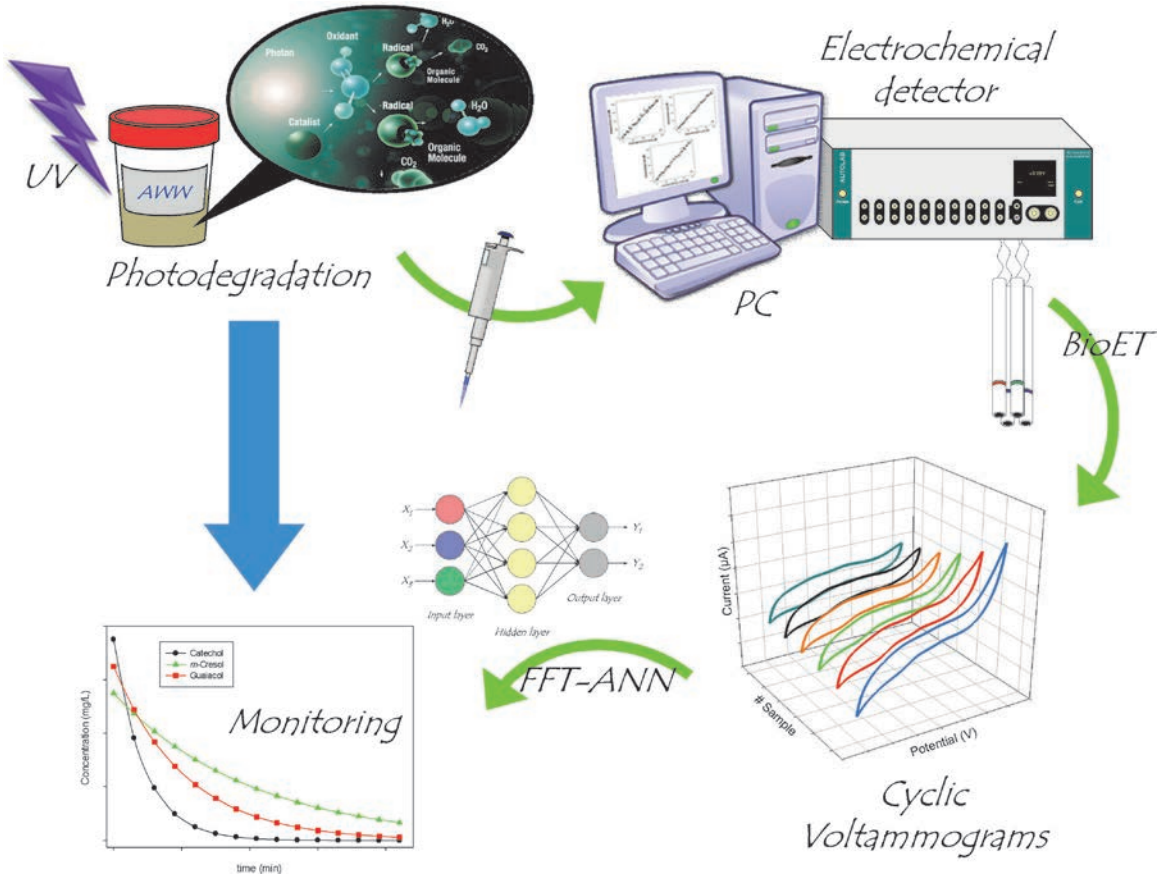


Fig. 1. Scheme of the experimental setup used for the photodegradation and monitoring of the phenolic compounds.

of the AWW or the aliquot as this would simplify its future operation; that is, avoiding the need to perform any other sample step or pre-treatment rather than its mere dilution. Then, the diluted sample was measured with the voltammetric BioET. In this way, *at-line* monitoring was achieved with a delay in the measurements of ca. 15–20 s.

Lastly, after sample measurement, voltammetric responses were input to the ANN model through its preprocessing with Fourier transform for feature extraction/data compression, and final concentration of each compound was obtained by multiplying the resulting values by the proper dilution factor.

### 2.4 Electronic Tongue Approach

The voltammetric BioET was formed by an array of 4 (bio)sensors, plus a reference double junction Ag/AgCl electrode (Thermo Orion 900200, Beverly, MA, USA) and a commercial Pt counter electrode (Model 52-67, Crison Instruments, Barcelona, Spain).

Working electrodes were bulk-modified graphite–epoxy composites, which were prepared by mixing the resin, graphite powder and the modifier/enzyme in the ratio 83 : 15 : 2 (w/w), or 81.5 : 15 : 2 : 1.5 in the case of the bienzymatic biosensor (laccase and tyrosinase, respectively) [27,28]. Afterwards, resin was allowed to harden at 40 °C for seven days, and electrode surfaces were polished with different sandpapers of decreasing grain size; with a final geometric area of 28 $mm^2$.

In this manner, the array of 4 voltammetric electrodes was prepared, consisting in one blank electrode plus three (bio)composite electrodes modified with tyrosinase, tyrosinase + laccase and Cu nanoparticles. This choice was intended as to maximize the response of the (bio)sensor array towards phenolic compounds. That is, on one side, tyrosinase and laccase were chosen as they are extensively used for the development of amperometric biosensors aimed to the detection of phenolic compounds [29]. Whereas, on the other side, copper nanoparticles were also considered as the two enzymes are copper-containing oxidases; hence, due to the well-known catalytic properties of nanoparticles and the importance of copper in the enzymes catalytic center, its inclusion was considered of potential interest.

Electrochemical measurements were performed at room temperature (25 °C), using a 6-channel AUTOLAB PGSTAT20 (Ecochemie, Netherlands) controlled with GPES Multichannel 4.7 software package. A complete voltammogram was recorded for each sample by cycling the potential between −0.4 V and +0.8 V vs. Ag/AgCl with a step potential of 9 mV and a scan rate of 100 $mV s^{-1}$.

In order to get stable voltammetric responses, and to ensure reproducible signals from the BioET array along

  

the whole experiment, two extra precautions were taken. Firstly, electrodes were cycled in buffer solution after its polishing and beginning of sample measurements. Secondly, an electrochemical cleaning stage was carried out between measurements to prevent any fouling or accumulation of impurities on the working electrode surfaces. To this end, a conditioning potential of +1.0 V was applied during 40 s in a cell containing 20 ml of distilled water [30].

### 2.5 Data Processing

Chemometric processing of the data was done in MATLAB 7.1 (MathWorks, Natick, MA, USA) using specific routines written by the authors, and its Neural Network Toolbox (v.4.0.6); while representation and analysis of the results was performed using Sigmaplot (Systat Software Inc., San Jose, CA, USA).

To fully exploit all the information obtained from each voltammogram and to prevent the under-determination problem encountered with an oversized ANN with excessively complex data (i.e. when too few data points are available compared with the number of adjustable parameters) [31], a compression step was performed to decrease the dimensionality of the electrochemical signatures. The main objective of this step is to reduce the complexity of the input signal while preserving the relevant information, which in addition allows to gain advantages in training time, to avoid redundancy in input data and to obtain a model with better generalization ability [31,32].

In our case, compression of voltammetric data was achieved by means of fast Fourier transform (FFT) [27], while ANNs were chosen as the modeling tool to achieve the individual quantification of each of the compounds. In this manner, each voltammogram was compressed down to 32 coefficients without a significant loss of information (details provided in Supporting information), and obtained coefficients were then used as inputs to the ANN model.

Moreover, to contrast the performance of FFT as preprocessing tool, discrete Wavelet transform (DWT) was also used for data compression (with Daubechies mother wavelet) and its results were used as reference to compare with the ones obtained with FFT [33]. Details from the compression to the model optimization and performance, for both strategies, can be found in Supporting information.

## 3 Results and Discussion

### 3.1 BioET Array Response

As already stated, prior to using the BioET as a monitorization tool for the photodegradation process of the phenolic compounds photodegradation process, a response model was built. To this aim, a total set of 41 phenolic ternary mixtures, with concentrations ranged from 0 to 80 mg $L^{-1}$ for each compound, were first analyzed and used to build and validate the ANN model; so that afterwards, it may be used for the simultaneous monitoring of the compounds under scrutiny during its mineralization.

In first instance, voltammetric responses for each of the electrodes towards individual compounds should also be checked. That is, to ensure that enough differentiated signals were observed for the different electrodes, generating rich data that might be a useful departure point for the multivariate calibration model.

To this aim, under the described conditions in Section 2.4, individual stock solutions of catechol, *m*-cresol and guaiacol were analyzed and their voltammograms inspected (Figure 2). Basically, two processes could be observed there: the oxidation of the corresponding phenol to its quinone form, and the reduction of the quinone to the phenolic form, as previously reported [29]. Besides, clearly differentiated curves are obtained for each of the considered compounds and for each electrode, the desirable condition for an ET study.

In addition, the benefits derived from the incorporation of the enzymatic biosensors may also be noticed, for which higher currents were obtained, especially in the reduction region close to 0 V where obtained net current is clearly enlarged; a situation more patent for catechol and *m*-cresol, which do not show any response with the bare electrode in that region. Similarly, some catalytic effect can also be observed for the sensor modified with copper nanoparticles, a fact somehow explained given both tyrosinase and laccase are copper containing redox enzymes.

Therefore, once it was confirmed that differentiated behavior was observed by the BioET array towards the different compounds under study, the next step was to proceed with the building of the ANN model.

### 3.2 Building of the ANN Model

Under the conditions previously described, the training and testing sets of samples were measured employing the multielectrode array, obtaining a complete voltammogram for each of the (bio)sensors, and each sample.

However, the large dimensionality of the data generated when voltammetric sensors are used (i.e. samples x sensors x polarization potentials) hinders their treatment; especially if ANNs are to be used. Therefore, raw voltammetric responses were compressed down to 32 coefficients by means of FFT, which allowed for a compression of the original information up to 88.1 % (details provided in Supporting information). Besides the high compression ratio, FFT is also particularly useful because of its ability to compress data and to remove noise (high frequency changes in signal) at the same time [32].

The next step was the building and optimization of the ANN model, which is a trial-and-error process where several parameters (e.g. training algorithm, number of hidden layers, number of neurons, transfer functions, etc.) are fine-tuned in order to find the best configuration that optimizes the performance of the model. For this, the ANN model was first trained employing data from the

  

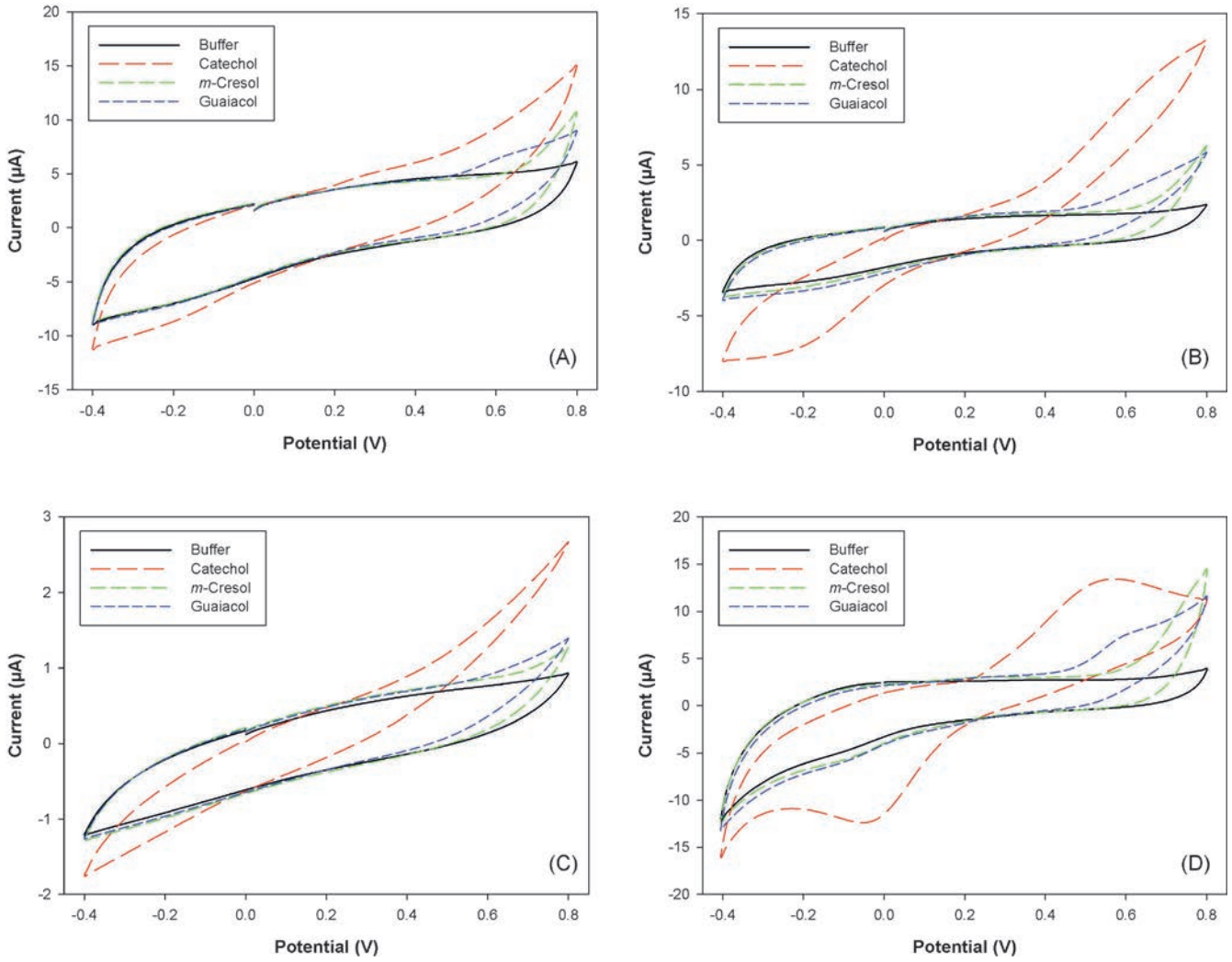


Fig. 2. Example of the different voltammograms obtained with (A) graphite–epoxy sensor, (B) tyrosinase modified biosensor, (C) tyrosinase + laccase modified biosensor and (D) Cu nanoparticle modified sensor for buffer and stock solutions of each of the three phenolic compounds considered (23 mg $L^{-1}$).

training subset, and its performance evaluated employing the samples from the testing subset; this allowed to characterize the accuracy of the quantification model and to detect any overfitting situation due to the use of unbiased data.

After a systematic evaluation of different topologies, from a total number of 90 different configurations (details provided in Supporting information), the final architecture of the ANN model had 128 neurons (4 sensors × 32 FFT coefficients) in the input layer, 5 neurons and *logsig* transfer function in the hidden layer and 3 neurons and *tansig* transfer function in the output layer, providing simultaneously the concentration of the three phenolic compounds considered.

Subsequently, comparison graphs of predicted vs. expected concentrations, both for training and testing subsets, for each of the compounds were then built to check the prediction ability of the obtained ANN model (Figure 3). It may be seen that a satisfactory trend is obtained, with regression lines almost indistinguishable from the theoretical ones (slope = 1, intercept = 0), this condition especially significant for the external test set.

### 3.3 Accuracy and Precision of the ANN Model

After optimization and selection of the ANN architecture, next step was to evaluate its performance and accuracy employing the data from the testing subset. That is, to determine whether or not the concentrations estimated by the ANN model statistically differ from the nominal concentrations, when presenting new samples to it. To this aim, regression statistics were evaluated in two different manners, using *t* and *F* distribution based tests [34].

Firstly, regression parameters of the comparison graphs were calculated (Table 1), and as deduced from the graphs, a satisfactory linear trend is observed for all the cases, with regression lines almost indistinguishable from the theoretical ones. But, as usual in data modeling, with an improved behavior for the training subset due to the lower dispersion attained. However, since the external

  

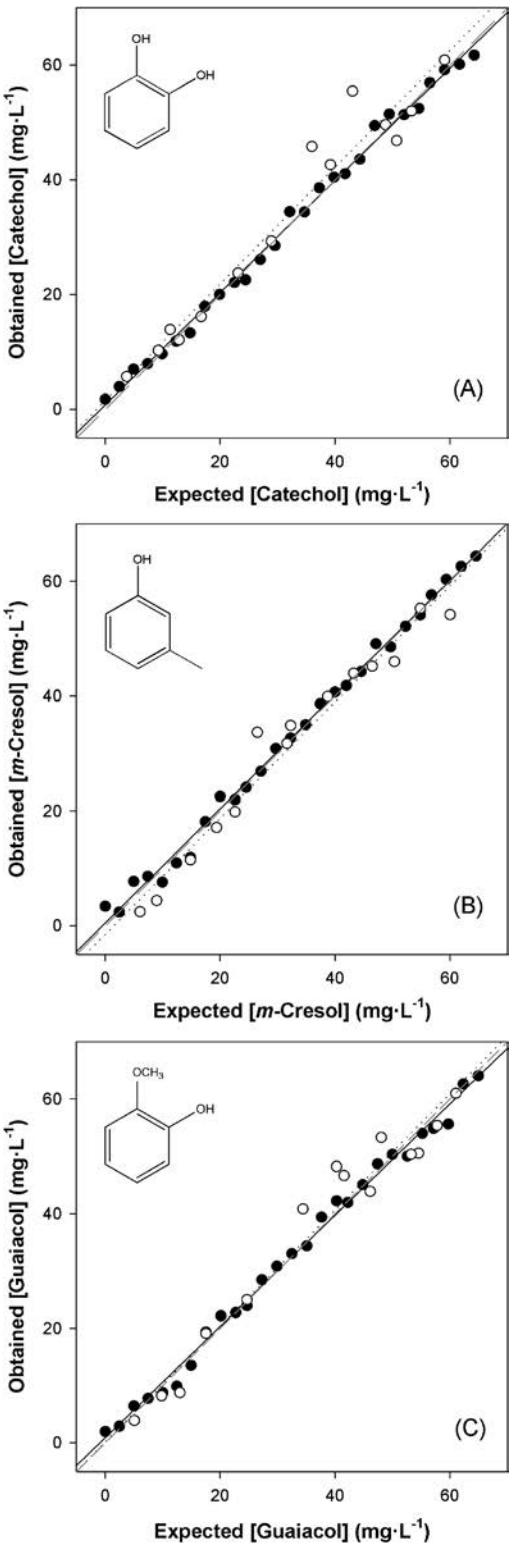


Fig. 3. Modelling ability of the optimized FFT-ANN. Comparison graphs of obtained vs. expected concentrations for (A) catechol, (B) *m-cresol* and (C) guaiacol, both for training (●, solid line) and testing subsets (○, dotted line). Dashed line corresponds to theoretical $Y=X$ diagonal line.

testing subset data is not employed at all for the modeling, its goodness of fit is a more correct indicator of the accomplished modeling performance. Nevertheless, the results obtained for both subsets are close to the ideal comparison values (slope 1, intercept 0 and correlation coefficient 1), being these values included in the confidence intervals.

Table 1. Results of the fitted regression lines for the comparison between obtained vs. expected values, both for the training and testing subsets of samples and the three considered species (intervals calculated at the 95% confidence level). *RMSE*: Root Mean Square Error; Intercept and *RMSE* values are expressed in mg $L^{-1}$.

| Training subset | | | | | |
|---|---|---|---|---|---|
| Compound | *r* | *Slope* | *Intercept* | *RMSE* | *Total RMSE* |
| Catechol | 0.998 | 0.979 ± 0.028 | 0.76 ± 1.05 | 0.025 | 1.50 |
| *m*-Cresol | 0.997 | 0.995 ± 0.030 | 0.50 ± 1.12 | 0.029 | |
| Guaiacol | 0.997 | 0.972 ± 0.031 | 0.90 ± 1.19 | 0.023 | |
| **Testing subset** | | | | | |
| Compound | *r* | *Slope* | *Intercept* | *RMSE* | *Total RMSE* |
| Catechol | 0.975 | 1.017 ± 0.146 | 1.54 ± 5.23 | 4.80 | 4.20 |
| *m*-Cresol | 0.981 | 1.012 ± 0.127 | −1.46 ± 4.63 | 3.63 | |
| Guaiacol | 0.979 | 1.012 ± 0.134 | 0.17 ± 5.43 | 4.09 | |

Additionally, joint confidence intervals were calculated and plotted according to advanced linear regression methodology [34]. The usage of this plot constitutes a rapid visualization tool to detect if there are or not differences between two compared methods, judging simultaneously the goodness of slope and intercept. Thus, taking into account the uncertainties in both axes to calculate the estimated covariance matrix based on an F distribution. Hence, we examined whether the theoretical comparison point (1,0) was included in the elliptical region of the joint confidence intervals of slope and intercept for plots shown in Figure 3. As can be observed in Figure 4, the point (1,0) is included in the confidence intervals for the three species, both for the training and testing subsets; thus confirming that statistically, there are no significant differences for the BioET predicted values and the real ones. Again, it can be seen how results obtained for the training subset are more precise, but with remarkable satisfactory accuracy for both subsets; being all of them close to the ideal point (1,0). The fact that bigger confidence intervals are obtained for the external test subset can be explained by two simple facts. On one side, this data is not employed at all during the building of the model, then being a true test of its generalization ability. On the other side, the number of samples in the testing subset is lower, and consequently, the tabulated values of *t* and *F* are higher, which implies higher confidence intervals.

Lastly, as an additional verification of the proposed approach, a Student's paired samples *t* test for the external test subset was performed. Obtained experimental *t* values were 1.73, 1.13 and 0.54 for catechol, *m*-cresol and guaiacol respectively, while the critical tabulated *t* value with 95% confidence level and 13 degrees of freedom is 2.16. Therefore, from the comparison graphs and these *t*-

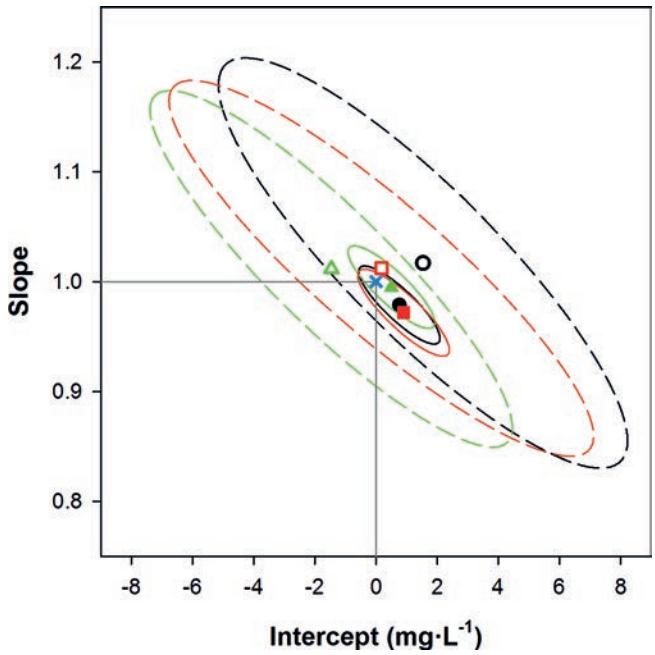


Fig. 4. Joint confidence intervals for the three species: (black ●) catechol, (green ▲) *m-cres*ol and (red ■) guaiacol, both for training (filled symbols, solid lines) and testing (empty symbols, dashed lines) subsets. Also ideal point (1,0) is plotted (blue ×); intervals calculated at the 95 % confidence level.

test results, it could be again concluded that there are no significant differences between the BioET predicted values and the real ones.

### 3.4 Monitoring of Phenolics Mineralization

After building and validating the generated model, the next step was the application of the proposed ET towards the monitoring of the photodegradation process of phenolic compounds mixtures.

To this aim, a ternary mixture of catechol, *m*-cresol and guaiacol (72.8 mg $L^{-1}$, 69.4 mg $L^{-1}$ and 65.6 mg $L^{-1}$, respectively) was prepared in AWW. Then, its photodegradation was carried out as described in section 2.3. During the process, aliquots of the solution from the photoreactor were removed at specific times from the beginning to up to ca. 200 min, and measured with the BioET with no further pretreatment than its mere dilution 1:1 with buffer solution. Recorded voltammetric responses were then preprocessed with FFT, and obtained coefficients were input into the previously built model which allowed the simultaneous determination of the three compounds. Lastly, actual concentration of each compound in the reactor batch was obtained by multiplying by the proper dilution factor.

An extract of the recorded signals obtained during the photodegradation process is shown in Figure 5, where it can be clearly seen how currents decreased monotonously as reaction progressed. Thus, even from the raw voltammetric responses, it would be possible to monitor the mineralization process (and detect its end point). However, in that case, not allowing the resolution of the different phenolic compounds.

Besides, the use of the BioET might not be limited to monitor the mineralization process, but also to detect whether or not some residual wastewater must be treated. Thus, requiring in that case the quantification of each of the compounds, to determine if their levels are under the required ones; what will be achieved thanks to the use of the chemometric model.

Evolution along time of the photo-Fenton mineralization process is plotted in Figure 6. At first sight, it can be seen how the ANN model confirms what was already ex-

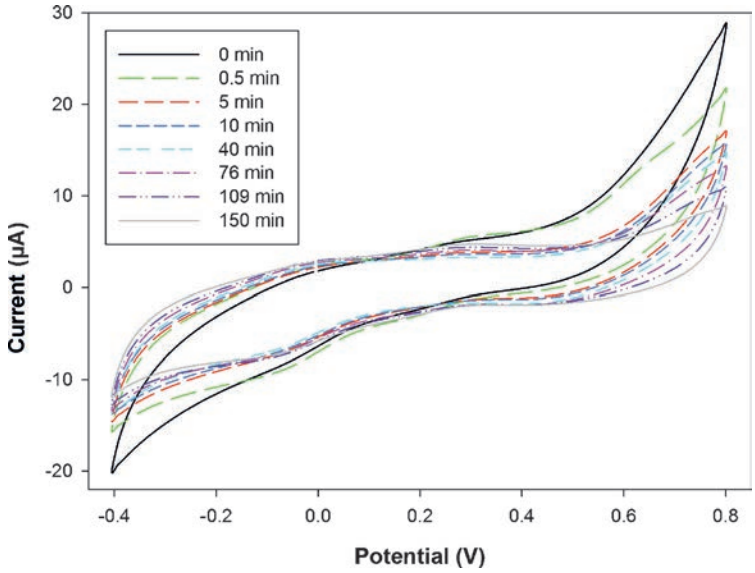


Fig. 5. Voltammetric responses obtained for some samples collected during the photodegradation process with the Cu nanoparticle modified sensor, as example.

  

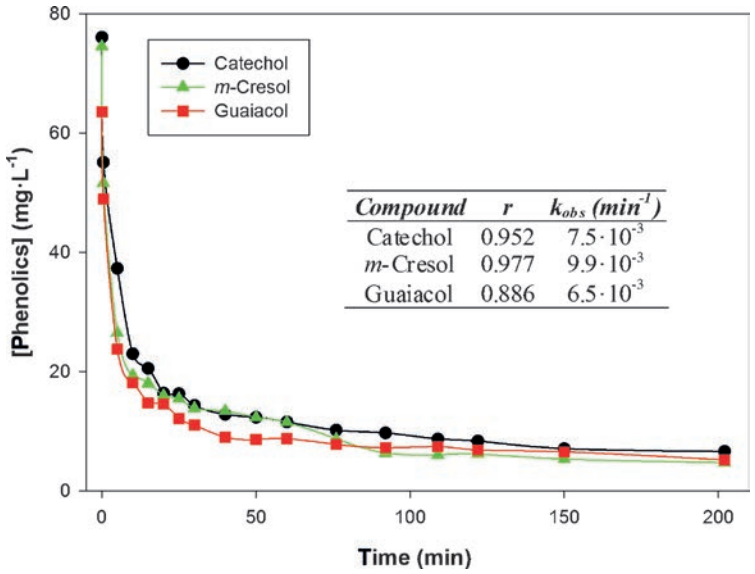


Fig. 6. Photo-Fenton mineralization and its monitoring with the BioET. Representation of the found values for each of the considered species: (black ●) catechol, (green ▲) *m-cresol* and (red ■) guaiacol. Inset: Corresponding calculated apparent pseudo-first-order rate constants ($k_{obs}$), determined from the linearizations.

pected from the voltammetric responses; that is, an exponential decrease in the concentration of each of the compounds. Moreover, the trends observed agree with previous reported results [9], where degradation rate is described by a first-order kinetics with respect to phenols concentration.

In this direction, and considering an independent behavior of each phenolic compound (i.e. the compounds not interacting with the others during the degradation) [35], degradation rate for each compound can be described by a pseudo-first order kinetics with respect to its concentration according to Equation 1, where $k_{obs}$ corresponds to the apparent pseudo-first-order rate constant.

$$\ln C = \ln C_0 - k_{obs}\, t \quad (1)$$

Thus, the plotting of the ln of the concentration of each compound vs. time in every experiment leads to a straight line whose slope is $k_{obs}$. Calculated values are summarized in the inset table in Figure 6, where also the obtained correlation coefficients for the linearized least squares regression are detailed, corroborating the pseudo-first order kinetics. As an extra validation, it has to be said that these results coincide with those reported in the literature, e.g. [9,12].

Therefore, it has been demonstrated that ETs (i.e. the combination of voltammetric measurements with chemometric tools) are an analytically powerful approach for the speciation of different phenolic compounds in wastewater and the monitoring of its mineralization. This approach is particularly useful since it does not only allow the identification of the presence of the phenolic compounds, but also the individual quantification of the amount present in the mixtures analyzed. Besides, with the same experimental setup, the approach proposed herein might be alternatively applied for the quantification of analogous or different mixtures, even quaternary or more complex mixtures, with a proper retraining set of samples. Lastly, this also represents a viable system with significant promise for on-field measurements given its simplicity, rapidity and portability; therefore, really suitable for screening analysis.

## 4 Conclusions

In this work, the application of an ET-based system for the simultaneous monitoring of various phenolic pollutants in wastewater has been reported. More specifically, the approach presented herein combines an array of voltammetric (bio)sensors to extract the fingerprints of the samples along with an ANN model that allows the resolution of signal overlapping and quantification of the individual species. On that account, the complex responses obtained from the (bio)sensor array were successfully processed employing a multilayer ANN; which has proved to be especially suited for building the response models. Lastly, proposed BioET array was then applied to the monitoring of phenol pollutants mixtures degradation during a photo-Fenton process.

Overall, reported approach herein represents a proof of concept for the versatility of the proposed system and its capabilities as on-field screening tool, demonstrating that ETs can be a viable option to monitor several analytes on-site, with the added advantages of simplicity, the low cost of both the system and the analysis, speed of response, versatility, simple measuring setup, etc. With this approach, a quantitative multideterminations of a number of chemical species is easily attainable with rather simple equipment, shifting the complexity from the sensors to the software side.

  

## Acknowledgements

Financial support for this work was provided by the *Spanish Ministry of Science and Innovation*, *MCINN* (Madrid) through Project CTQ2010-17099. Manel del Valle thanks the support from *Generalitat de Catalunya* and from the *Program ICREA Academia*. Andreu González-Calabuig thanks *Universtitat Autònoma de Barcelona* for the PIF fellowship. X. Cetó thanks the support from the Australian Research Council's Linkage Project Scheme.

## References

[1] L. Moreno-Baron, R. Cartas, A. Merkoçi, S. Alegret, J. M. Gutierrez, L. Leija, P. R. Hernandez, R. Muñoz, M. del Valle, *Anal. Lett.* **2005**, *38*, 2189.
[2] K. Farhod Chasib, *J. Chem. Eng. Data* **2013**, *58*, 1549.
[3] S. Mukherjee, B. Basak, B. Bhunia, A. Dey, B. Mondal, *Rev. Environ. Sci. Biotechnol.* **2013**, *12*, 61.
[4] EPA, *Steam Electric Power Generating Point Source Category*, Vol. 47, Federal Register, **1982**, p. 52290.
[5] Commission Regulation (EEC) Official Journal L 129, Publication Office of the European Union, 18 May **1976**, pp. 23.
[6] L. Gianfreda, G. Iamarino, R. Scelza, M. A. Rao, *Biocatal. Biotransfor.* **2006**, *24*, 177.
[7] R. Capasso, *Curr. Top. Phytochem.* **1997**, *1*, 145.
[8] G. Busca, S. Berardinelli, C. Resini, L. Arrighi, *J. Hazard. Mater.* **2008**, *160*, 265.
[9] M. Rodríguez, *Fenton and UV-VIS based advanced oxidation processes in wastewater treatment: Degradation, mineralization and biodegradability enhancement*, *PhD Thesis,* Universitat de Barcelona, Barcelona, **2003**.
[10] J. M. Britto, M. d. C. Rangel, *Quím. Nova* **2008**, *31*, 114.
[11] S. J. Kulkarni, J. P. Kaware, *Int. J. Sci. Res. Public.* **2013**, *3*, 1.
[12] S. Esplugas, J. Giménez, S. Contreras, E. Pascual, M. Rodríguez, *Water Res.* **2002**, *36*, 1034.
[13] S. Ahmed, M. G. Rasul, W. N. Martens, R. Brown, M. A. Hashib, *Desalination* **2010**, *261*, 3.
[14] I. Magario, F. S. García Einschlag, E. H. Rueda, J. Zygadlo, M. L. Ferreira, *J. Mol. Catal. A* **2012**, *352*, 1.
[15] D. Puig, D. Barceló, *TrAC – Trends Anal. Chem.* **1996**, *15*, 362.
[16] F. Karim, A. N. M. Fakhruddin, *Rev. Environ. Sci. Biotechnol.* **2012**, *11*, 261.
[17] Y. Ni, S. Kokot, *Anal. Chim. Acta* **2008**, *626*, 130.
[18] E. Tønning, S. Sapelnikova, J. Christensen, C. Carlsson, M. Winther-Nielsen, E. Dock, R. Solna, P. Skladal, L. Nørgaard, T. Ruzgas, J. Emnéus, *Biosens. Bioelectron.* **2005**, *21*, 608.
[19] J. Zeravik, A. Hlavacek, K. Lacina, P. Skládal, *Electroanalysis* **2009**, *21*, 2509.
[20] M. del Valle, *Electroanalysis* **2010**, *22*, 1539.
[21] C.-H. Ko, S.-S. Chen, *Bioresource Technol.* **2008**, *99*, 2293.
[22] K. Volkan Özdokur, L. Pelit, H. Ertaş, S. Timur, F. Nil Ertaş, *Talanta* **2012**, *98*, 34.
[23] L. Zhang, Y. Z. Liang, J. H. Jiang, R. Q. Yu, K. T. Fang, *Anal. Chim. Acta* **1998**, *370*, 65.
[24] X. Cetó, F. Céspedes, M. I. Pividori, J. M. Gutiérrez, M. del Valle, *Analyst* **2012**, *137*, 349.
[25] O. K. Dalrymple, D. H. Yeh, M. A. Trotz, *J. Chem. Technol. Biotech.* **2007**, *82*, 121.
[26] M. Rodríguez, N. B. Abderrazik, S. Contreras, E. Chamarro, J. Gimenez, S. Esplugas, *Appl. Catal. B: Environ.* **2002**, *37*, 131.
[27] X. Cetó, F. Céspedes, M. del Valle, *Talanta* **2012**, *99*, 544.
[28] M. Elkaoutit, I. Naranjo-Rodriguez, K. R. Temsamani, M. D. La Vega, J. L. H. De Cisneros, *J. Agric. Food Chem.* **2007**, *55*, 8011.
[29] R. Solná, P. Skládal, *Electroanalysis* **2005**, *17*, 2137.
[30] X. Cetó, J. M. Gutiérrez, L. Moreno-Barón, S. Alegret, M. del Valle, *Electroanalysis* **2011**, *23*, 72.
[31] F. Despagne, D. L. Massart, *Analyst* **1998**, *123*, 157R.
[32] X. Cetó, F. Céspedes, M. del Valle, *Microchim Acta* **2013**, *180*, 319.
[33] L. Moreno-Barón, R. Cartas, A. Merkoçi, S. Alegret, M. del Valle, L. Leija, P. R. Hernandez, R. Muñoz, *Sens. Actuators B, Chem.* **2006**, *113*, 487.
[34] D. C. Montgomery, E. A. Peck, G. G. Vining, *Introduction to Linear Regression Analysis*, Wiley, Chichester, **2012**.
[35] A. M. Peiró, J. A. Ayllón, J. Peral, X. Doménech, *Appl. Catal. B: Environ.* **2001**, *30*, 359.

Received: July 31, 2014
Accepted: October 27, 2014
Published online: December 4, 2014

  

# Article 2:

**Crown ether-modified electrodes for the simultaneous stripping voltammetric determination of Cd(II), Pb(II) and Cu(II)**

Núria Serrano, Andreu González-Calabuig and Manel del Valle

*Talanta* 138 (2015) 130–137

DOI: 10.1016/j.talanta.2015.01.044

Talanta 138 (2015) 130–137

Contents lists available at ScienceDirect

Talanta

journal homepage: www.elsevier.com/locate/talanta

# Crown ether-modified electrodes for the simultaneous stripping voltammetric determination of Cd(II), Pb(II) and Cu(II)

Núria Serrano [a,b], Andreu González-Calabuig [b], Manel del Valle [b,*]

[a] Department of Analytical Chemistry, Faculty of Chemistry, Universitat de Barcelona, Martí i Franquès 1-11, 08028 Barcelona, Spain
[b] Sensors & Biosensors Group, Department of Chemistry, Universitat Autònoma de Barcelona, Edifici Cn, 08193 Bellaterra, Spain

ARTICLE INFO

*Article history:*
Received 10 December 2014
Received in revised form
23 January 2015
Accepted 31 January 2015
Available online 9 February 2015

*Keywords:*
Crown ether-modified sensors
Electrochemical grafting
Metal determination
Stripping voltammetry
Artificial neural network

ABSTRACT

This work describes the immobilization of 4-carboxybenzo-18-crown-6 (CB-18-crown-6) and 4-carboxybenzo-15-crown-5 (CB-15-crown-5) assisted by lysine on aryl diazonium salt monolayers anchored to the surface of graphite–epoxy composite electrodes (GEC), and their use for the simultaneous determination of Cd(II), Pb(II) and Cu(II) by differential pulse anodic stripping voltammetry (DPASV). These modified electrodes display a good repeatability and reproducibility with detection and quantification limits at levels of $\mu g\ L^{-1}$ (ppb), confirming their suitability for the determination of Cd (II), Pb(II) and Cu(II) ions in environmental samples. The overlapped nature of the multimetal stripping measurements was resolved by employing the two-sensor array CB-15-crown-5-GEC and CB-18-crown-6-GEC, since the metal complex selectivity exhibited by the considered ligands could add some discrimination power. For the processing of the voltammograms, Discrete Wavelet Transform and Causal Index were selected as preprocessing tools for data compression coupled with an artificial neural network for the modeling of the obtained responses, allowing the resolution of mixtures of these metals with good prediction of their concentrations (correlation with expected values for an external test subset better than 0.942).



## 1. Introduction

Determination of trace heavy metal ions in environmental samples is nowadays an area of major concern, since heavy metals from pollution sources can affect people's health when absorbed or inhaled interfering with organ system function. Heavy metals are especially hazardous since they tend to bioaccumulate in animals and human organisms, this means that they become toxic when they are not metabolized by the body and accumulate in the soft tissues [1].

Stripping voltammetry methods are the most efficient electrochemical techniques for trace and species analysis due to their high sensitivity and selectivity, being particularly suitable for the determination of trace heavy metal ions in environmental samples [2]. The performance of voltammetry is strongly influenced by the working electrode material. For many years, electrochemical stripping methods were associated with the use of working mercury electrodes for the determination of trace metal ions due to the extensive cathodic potential range [3]. However, the disposal of the mercury containing device and the incorrect handling can lead to the formation of mercury vapors that as solution of soluble mercury salts are toxic and represent a significant health and environmental hazard. Thus, the development and use of chemically modified electrodes as working electrodes for the detection and quantification of metal ions in natural samples is also a subject of high interest.

Macrocyclic compounds, as crown ethers, can be employed as modifiers for metal determination, where crown compound acts as host, complexing its metal. Compounds of this type may be introduced into the electrode to enhance its selectivity and to lower its detection limits. Moreover, crown ethers have a high degree of selectivity being able to strongly bind certain metals, since their structural properties allow the complex formation by means of ion–dipole interaction with these metal ions [4]. So, the complexing ability, coordination geometry and crown cavity size suitable for a particular analyte have to be considered for the selective detection of metal ions. Particularly, crown ethers are well-known to form complexes with alkaline ions, alkaline earth metals, lanthanides and transition metal ions. Surprisingly, studies devoted to complexation with transition metal ions are scarce and only a few works using crown ether-modified electrodes are published for the determination of lead [5–7], mercury [8,9], silver [10], thallium [11], palladium [12] and copper [13]. Interference effect of metal detection using crown ether-modified electrodes in the presence of other

* Corresponding author. Tel.: +34 93 581 10 17; fax: +34 93 581 24 77.
*E-mail address:* manel.delvalle@uab.es (M. del Valle).

http://dx.doi.org/10.1016/j.talanta.2015.01.044
0039-9140/

heavy metals such as Ni(II), Co(II), Mn(II), Cd(II), Pb(II) Fe(II), Ag(I), Ca (II) etc. was also discussed in previous works [6,7,11,13].

An important aspect in the design of these electrodes is the chemical modification procedure. In this sense, a few approaches are described in the literature to present day including the crown ethers coating with graphite powders and the modification of a gold electrode with a crown ether yielding a self-assembled monolayer (SAM) [14]. Nevertheless, as reported for peptides, an alternative strategy would be the crown ether immobilization on aryl diazonium salt monolayers anchored on the electrode surface resulting in a simple, flexible and valuable alternative for forming stable complexing monolayers [15,16].

Crown ether-modified electrodes can be used for metal determination as a single-electrode sensor or in combination with others forming a multi-sensor array, in which each electrode in the array is modified with a recognition crown ether that is largely selective for one of the metal ions to provide a multivariate response [17].

The aim of this work is to report the modification and analytical characterization of graphite–epoxy composite electrodes (GEC) with 4-carboxybenzo-18-crown-6 (CB-18-crown-6) and 4-carboxybenzo-15-crown-5 (CB-15-crown-5), which were immobilized on aryl diazonium salt monolayers anchored to the electrode surface, for the simultaneous determination of Cd(II), Pb(II) and Cu(II) using differential pulse anodic stripping voltammetry (DPASV). An artificial neural network model was proposed as a tool to maximize the information obtained from the voltammetric data sets using CB-18-crown-6-GEC and CB-15-crown-5-GEC sensors that a priori are difficult to understand.

## 2. Experimental

### 2.1. Chemicals

Potassium ferricyanide $K_3[Fe(CN)_6]$, potassium ferrocyanide $K_4[Fe(CN)_6]$, 2-(N-morpholino)-ethanesulfonic acid (MES), potassium dihydrogen phosphate, sodium monophosphate, methanol, perchloric acid, hydrochloride acid, *N*-hydroxysulfosuccinimide (sulfo-NHS), *N*-(3-dimethylaminopropyl)-*N′*-ethylcarbodiimide hydrochloride (EDC) and sodium nitrite were purchased from Sigma (St. Louis, MO, USA). 4-aminobenzoic acid (ABA) and DL-lysine monohydrochloride were provided by Acros (Geel, Belgium). 4-carboxybenzo-18-crown-6 with a purity of 99% and 4-carboxybenzo-15-crown-5 with purity greater than 98% were provided by Acros and Sigma, respectively. All other reagents used were from Merck (Darmstadt, Germany) and Fluka (Buchs, Switzerland). All reagents were of analytical grade. Pb(II), Cd(II) and Cu(II) stock solutions $10^{-2}$ M were prepared from $Pb(NO_3)_2 \cdot 4H_2O$, $Cd(NO_3)_2 \cdot 4H_2O$ and $Cu(NO_3)_2 \cdot 3H_2O$, respectively and standardized complexometrically [18]. 0.1 M acetate buffer solution (pH 4.5) was used for pH control. Ultrapure water from MilliQ System (Millipore, Billerica, MA, USA) was used in all experiments.

### 2.2. Apparatus

Cyclic voltammetric (CV) measurements were carried out using a μSTAT 200 potentiostat from Dropsens (Oviedo, Spain) using Dropview (Dropsens) software for data acquisition and control of the experiments. A three electrode configuration was used to perform the CV measurements for modification and characterization of the electrodes: a commercial platinum counter electrode (Model 52-67, Crison Instruments, Barcelona, Spain), a reference double junction Ag/AgCl electrode (Thermo Orion 900200, Beverly, MA, USA) and the modified GEC as the working electrode.

Differential pulse anodic stripping voltammetric (DPASV) measurements were performed in an Autolab System PGSTAT 30 (EcoChemie, The Netherlands), in a multichannel configuration, using GPES Multichannel 4.7 software package (EcoChemie). The voltammetric cell was formed by the two working graphite epoxy electrodes (GECs) modified with 4-carboxybenzo-18-crown-6 (CB-18-crown-6) and 4-carboxybenzo-15-crown-5 (CB-15-crown-5) respectively, a commercial platinum counter electrode and a double junction Ag/AgCl reference electrode.

A pH meter GLP 22 (Crison Instruments, Barcelona, Spain) was used for pH measurements. All measurements were carried out at room temperature (20 °C).

### 2.3. Procedures

#### 2.3.1. Preparation of graphite epoxy electrodes

Graphite epoxy composite electrodes (GECs) were fabricated by using a PVC tube body (6 mm i.d.) and a small copper disk soldered at the end of an electrical connector. The working surface is an epoxy–graphite conductive composite, formed by a mixture of 20% graphite powder (Merck, Darmstadt, Germany) and 80% of epoxy resin, Epotek H77, and its corresponding hardener (both from Epoxy Technology, Billerica, MA, USA), deposited on the cavity of the plastic body [19], as usual design from our laboratory. The composite material was cured at 80 °C for 3 days. Prior to their functionalization, the electrode surface was moistened with MilliQ water and then polished on abrasive sandpaper (400, 600, 800, 1000, and 1200 grit) and finally on alumina polishing strips (301044-001, Orion) in order to obtain a reproducible electrochemical surface.

#### 2.3.2. Preparation of modified GECs

The principle of the modification of the GEC is illustrated in Fig. 1, with specific steps described below [20].

*2.3.2.1. Diazonium salt electrochemical grafting.* The *in situ* generation of the aryl diazonium was performed by adding $5 \times 10^{-3}$ equivalents of sodium nitrite to an acidic solution (1 M aqueous HCl) of ABA. These solutions were mixed for about 30 min in an ice bath, prior to the electrochemical grafting process [21], conducted by scanning the potential at 0.2 V $s^{-1}$ from 0 V to −1 V for 100 cycles. The functionalized electrodes were thoroughly rinsed with Milli-Q water and methanol to remove any physisorbed compounds.

*2.3.2.2. Covalent immobilization of crown ethers via carbodiimide coupling.* The carboxyl groups of the electrografted diazonium salt were activated by incubating the functionalized electrodes in a 26 mM EDC and 35 mM sulfo-NHS solution in 100 mM MES buffer (pH 4.5) for 1 h. In order to conjugate the carboxy-fucntionalized electrode with the carboxy-modified ligands, a lysine spacer was intercalated in between, by using its two amino functionalities to form amido bonds [22–25]. The surface activated groups reacted overnight with the α-amine group of the lysine at 4 °C. Prior to cross linking with EDC/sulfo-NHS, 2.9 mg of 4-carboxybenzo-18-crown-6 or 4-carboxybenzo-15-crown-5 were incubated with 100 μL 5 mM lysine in 0.1 M MES buffer for 3 h.

#### 2.3.3. DPASV measurements

Before each set of measurements, the electrodes were scanned in acetate buffer solution in order to get stable voltammetric responses.

DPASV determinations using CB-18-crown-6-GEC and CB-15-crown-5-GEC of Cd(II), Pb(II) and Cu(II), were done at a deposition potential ($E_d$) of −1.4 V, applied with stirring during a deposition time ($t_d$) of 300 s and followed for a rest period ($t_r$) of 10 s. Determinations were done by scanning potential from −1.4 to +0.2 V using a step potential of 4 mV and pulse amplitude of 50 mV. Calibration plots were obtained by increasing metal concentrations in pH 4.5 acetate buffer media.

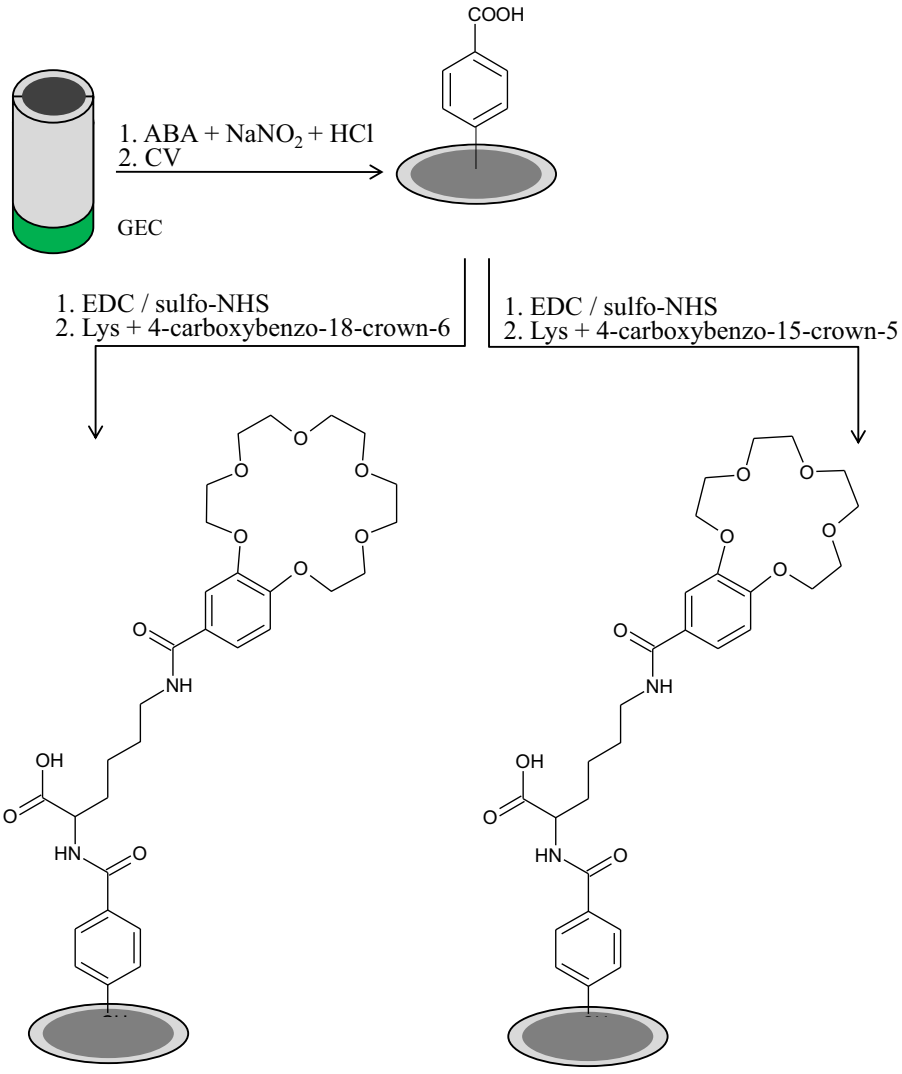


**Fig. 1.** Scheme of the preparation of the two modified electrodes, CB-15-crown-5-GEC and CB-18-crown-6-GEC, by electrochemical grafting.

In order to eliminate any remaining bound metals from the electrode, an electrochemical cleaning stage was considered between measurements. This stage was performed by applying a conditioning potential ($E_{cond}$) of 0.5 V for 30 s after each measurement, in a cell containing fresh buffer solution.

To allow the multimetal simultaneous determination, a response model was built using artificial neural networks (ANN) and voltammetric data compression. For this aim, DPASV scans of a total set of 35 samples in the concentration range 1.5–200 ppb, manually prepared by appropriate dilution from the mother metal stock solutions in pH 4.5 acetate buffer, were recorded at the same experimental conditions as calibration plots. The set of samples was divided into two data subsets: a training subset formed by 27 samples (79.4%), which were distributed in a cubic design [26] and used to establish the response model; plus 7 additional samples (20.6%) for the testing subset, randomly distributed along the experimental domain, and used to evaluate the model predictive response (Fig. 2). All experiments were carried out without any oxygen removal.

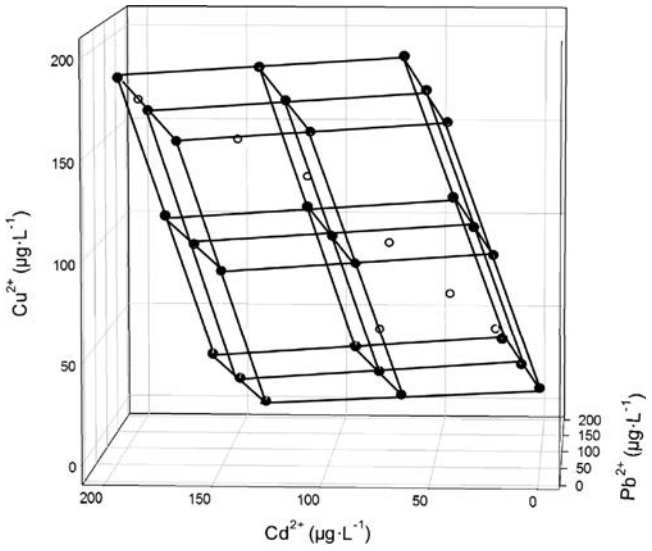


**Fig. 2.** Experimental design using for training (•, solid line) and testing (○) data subsets.

### 2.3.4. Data processing

In order to reduce the large amount of information generated for each sample (2 sensors × 390 current values at different potential) a preprocessing stage was necessary to compress the original data. The objective of this step is to reduce the complexity of the input data while preserving the relevant information; also the compression of the data allows to reduce the training time, avoid redundancy in input data and to obtain a model with better generalization ability.

The chosen method was the Discrete Wavelet Transform (DWT) [27]; each voltammogram was normalized and then compressed using *Daubechies 4* wavelet mother function and a fourth decomposition level. In this manner, the original data was reduced to 60 coefficients without any loss of relevant information. In addition Causal Index [28] was employed to further refine the model by eliminating the inputs that make relatively small contributions. With this double compression–pruning approach, the 780 inputs per sample were reduced down to 21 coefficients, achieving a compression ratio up to 97.31%.

Chemometric processing of data was performed by specific routines written by the authors using MATLAB 7.1 (MathWorks, Natick, MA) and its Neural Network Toolbox (v.4.0.6).

## 3. Results and discussion

### 3.1. GEC characterization

The electrochemical response using 2 mM ferrocyanide/ferricyanide as redox probe in 100 mM phosphate buffer (pH 7.4) was investigated at each functionalization step using cyclic voltammetry (CV). CV measurements were performed in unstirred conditions scanning the potential at $0.1\ V\ s^{-1}$ from $-0.7$ to 1 V. Electrografting resulted in decreasing current as expected (Fig. 3). Covalent binding of complexing agents through the α-amine group of the lysine also resulted in lower current peaks compared to bare electrode, as shown in Fig. 3 for CB-18-crown-6-GEC. These observed changes in the voltammograms confirmed the modifications occurring on the electrode surface.

### 3.2. Repeatability and reproducibility

The selected $E_d$, $t_d$ and $t_r$ were firstly optimized to ensure the detection of each metal at each ligand-modified electrode in the selected concentration range; the compromise conditions were for all cases: $-1.4$ V as the applied accumulation voltage with stirring during a $t_d$ of 300 s and followed by a rest stage of 10 s at the same applied potential. Three different pH values 4.5, 6.0, and 6.8 were also tested for the simultaneous determination of Cd(II), Pb(II) and Cu(II). At pH values of 6.0 and 6.8 a significant decrease in the peak current of Cu(II) was detected with respect to the obtained at pH 4.5 suggesting some degree of metal hydrolysis. According to this study, an optimal pH value of 4.5 was selected.

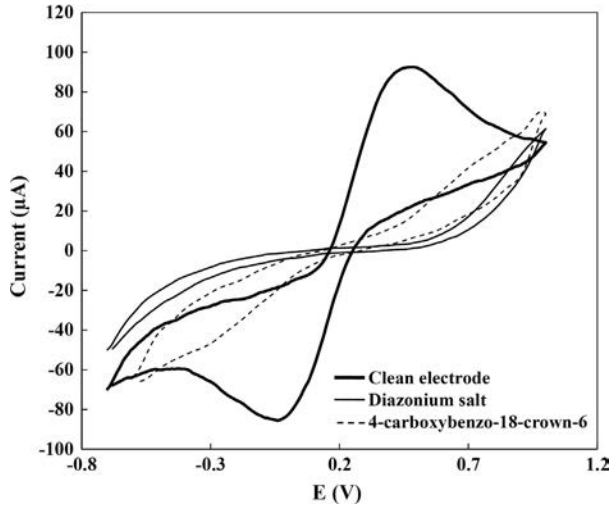


**Fig. 3.** CVs plots recorded at each electrode functionalization step. Measurements were performed in a 2 mM ferrocyanide/ferricyanide solution in phosphate buffer.

Stripping measurements of a 125 $\mu g\ L^{-1}$ Cd(II), Pb(II) and Cu(II) solution (mixed solution) by applying the optimized voltammetric conditions were carried out using both ligand-modified electrodes in order to test their repeatability and reproducibility. The reproducibility calculated from three different modified GEC units for each complexing agent within a series of five repetitive yielded RSD of 3.1%, 2.1%, and 2.2% for Cd(II), Pb(II) and Cu(II), respectively for the CB-18-crown-6-GEC and 6.4%, 2.7%, and 3.0% for Cd(II), Pb (II) and Cu(II), respectively for the CB-15-crown-5-GEC. The repeatability estimated using for each complexing agent the same electrode unit for five repetitive measurements produced RSD of 3.1%, 4.3%, and 2.2% for Cd(II), Pb(II) and Cu(II), respectively for the CB-18-crown-6-GEC and 5.2%, 3.3%, and 1.6% for Cd(II), Pb(II) and Cu(II), respectively for the CB-15-crown-5-GEC.

### 3.3. Linearity, limit of detection (LOD) and limit of quantification (LOQ)

First of all, separate calibration of Cd(II), Pb(II) and Cu(II) ions by stripping voltammetry (DPASV) was carried out on each CB-18-crown-6-GEC and CB-15-crown-5-GEC respectively. The LOD was calculated as 3 times the standard deviation of the intercept over the slope of the calibration curve of the target ions. LOQ was evaluated by considering 10 times the previous ratio. The lowest value of the linear concentration range was established from the corresponding limit of quantification (LOQ). For LOD and LOQ determinations, 10 different standards of the considered ions were used to build the calibration lines. Fig. 4a–c shows, as an example, the evolution of DPASV signals of each metal using the CB-15-crown-5-GEC sensor when the concentration of Cd(II), Pb(II) and Cu(II) respectively increases (CB-18-crown-6-GEC with equivalent behavior). In all cases, well defined stripping peaks without any clear evidence of signal splitting were observed over the considered concentration range. Linear calibration curves were obtained for Cd(II), Pb(II) and Cu(II) up to a maximum concentration level of 191.1, 186.5, and 177.3 $\mu g\ L^{-1}$ respectively. The corresponding regression equations and the correlation coefficients for both sensors are shown in Table 1. It must be pointed out that similar voltammetric responses for Pb(II), Cd(II) and Cu(II) were also observed using CB-18-crown-6-GEC sensor at the same experimental conditions. Nevertheless, regarding the sensitivities considered as the value obtained from the slope of the calibration curves, it can be mentioned that: i) using CB-18-crown-6-GEC, Pb (II) was the metal ion showing better sensitivity; and ii) using CB-15-crown-5-GEC, Cu(II) was the most sensitive metal. The LOD of the assay for the three metal ions in both modified electrodes varied from 1.5 to 4.7 $\mu g\ L^{-1}$ depending on the metal ion (Table 1) and the LOQ ranged from 5.0 to 15.7 $\mu g\ L^{-1}$ depending on the metal ion (Table 1). For Pb(II) and Cu(II) the obtained results are comparable with the values reported in earlier studies [6,7,13]. In the case of Cd(II) no previous LOD and LOQ data are available in the literature. In comparison with previous results achieved using others solid composite electrodes, *e.g.*, graphite solid composite electrode, solid composite silver electrode, carbon composite solid electrode modified with silica gel… [in Ref. [29], Table 3], the LODs obtained in this work are similar or even significantly lower depending on the solid composite electrode considered. Furthermore, lower concentrations ranges and better detection limits could easily be achieved using the proposed method by increasing the deposition time. Therefore the reported calibration data suggest that both CB-18-crown-6-GEC and CB-15-crown-5-GEC sensors could be fully suitable for the determination of Cd(II), Pb (II) and Cu(II) at the ultra-trace level in environmental samples. The second observation is that the use of the two electrodes as an array could add some discrimination power to resolve a multi-metal mixture.

### 3.4. Metal complex selectivity

Taking into account that the immobilized crown ethers on the GEC surface are used as molecular collectors with ability to selectively coordinate with the metal ions, both the ionic diameter of metal ions and the cavity size/structure of the crown ethers play a crucial role for the complex formation by means of ion–dipole interaction with metal ions. The ability of each considered metal ions for forming the complex with both CB-18-crown-6 and CB-15-crown-5 is displayed in Fig. 5a. Voltammetric peak current responses for equal concentrations of metal ion solution (175 μg $L^{-1}$ of Cd(II), Pb(II) and Cu(II)) show that CB-18-crown-6 exhibits the highest selective complex forming ability with Pb(II) followed by Cu(II); on the contrary, CB-15-crown-5

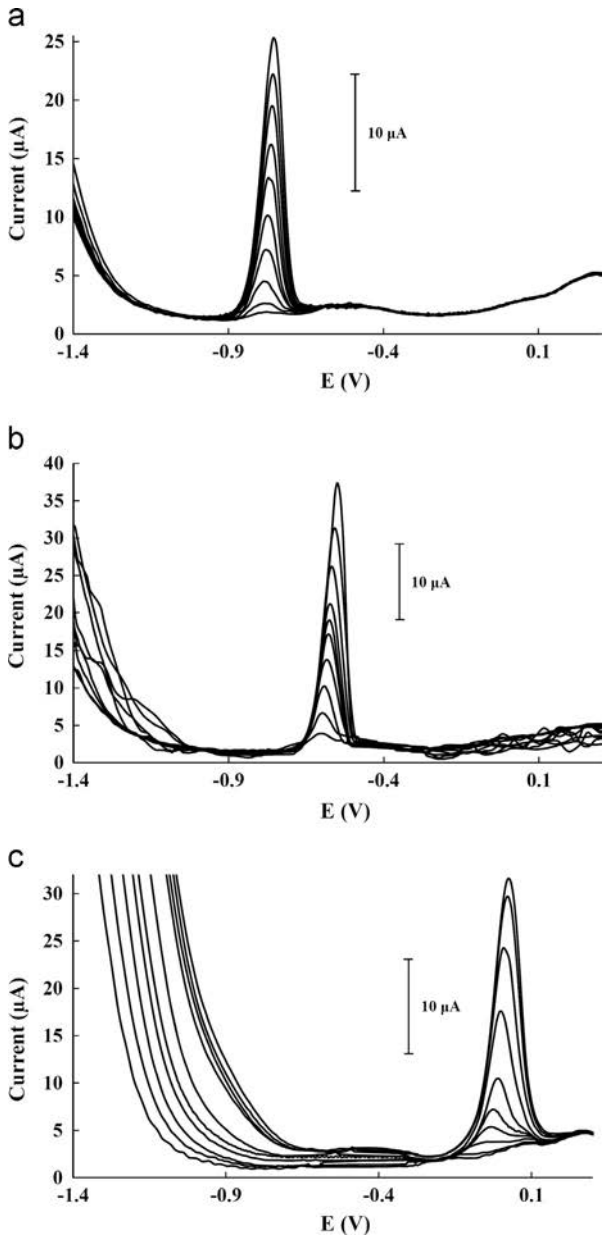


**Fig. 4.** DPASV measurements of (a) Cd(II), (b) Pb(II), and (c) Cu(II) alone (0–200 μg $L^{-1}$ concentration range) recorded on a CB-15-crown-5-GEC sensor at pH 4.5 using a $E_d$ of −1.40 V during 300 s and $t_r$ of 10 s.

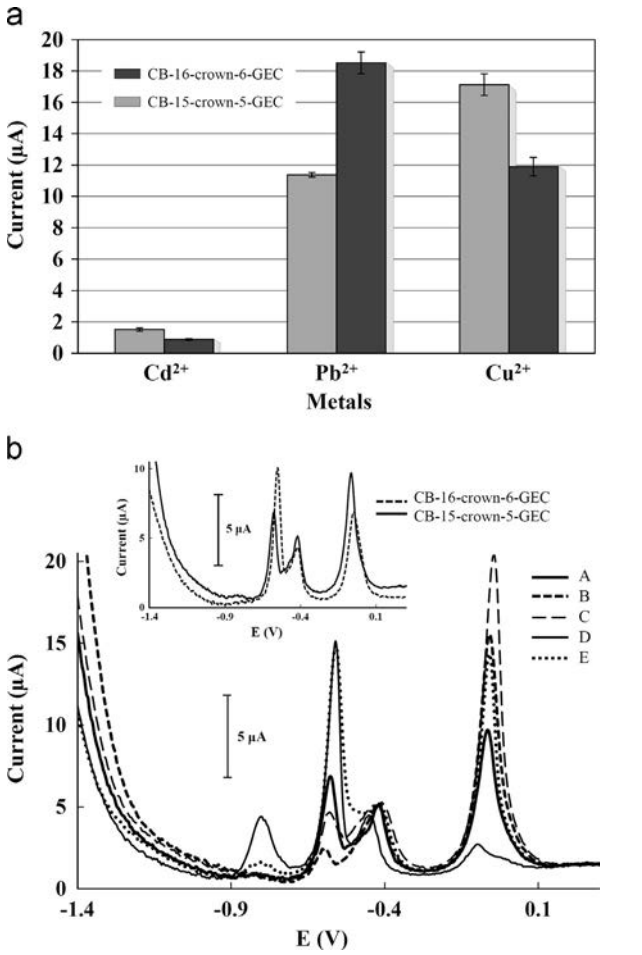


**Fig. 5.** (a) Differential pulse anodic stripping voltammetric peak current of 175 μg $L^{-1}$ of Cd(II), Pb(II) and Cu(II) using both CB-15-crown-5-GEC and CB-18-crown-6-GEC sensors. (b) Some voltammograms generated during the build of the response model recorded at the same conditions as Fig. 4. Sample composition: (A) 100.7 μg $L^{-1}$ of Cd(II), Pb(II) and Cu(II); (B) 54.9 μg $L^{-1}$ of Cd(II), 85.5 μg $L^{-1}$ of Pb(II) and 177.1 μg $L^{-1}$ of Cu(II); (C) 123.6 μg $L^{-1}$ of Cd(II), 108.4 μg $L^{-1}$ of Pb(II) and 169.4 μg $L^{-1}$ of Cu(II); (D) 146.5 μg $L^{-1}$ of Cd(II), 116.0 μg $L^{-1}$ of Pb(II) and 24.4 μg $L^{-1}$ of Cu(II); (E) 169.4 μg $L^{-1}$ of Cd(II), 123.6 μg $L^{-1}$ of Pb(II) and 93.1 μg $L^{-1}$ of Cu(II). Inset in (b): comparison between the response of both sensors for sample composition (A).

**Table 1**
Calibration data ($y$ *vs.* $x$) for the separate determination of Cd(II), Pb(II) and Cu(II) on CB-18-crown-6-GEC and CB-15-crown-5-GEC at $E_d$ of −1.4 V using a $t_d$ of 120 s at pH 4.5.

| | Cd (II) | | Pb (II) | | Cu (II) | |
|---|---|---|---|---|---|---|
| | CB-18-crown-6-GEC | CB-15-crown-5-GEC | CB-18-crown-6-GEC | CB-15-crown-5-GEC | CB-18-crown-6-GEC | CB-15-crown-5-GEC |
| **Regression**[a] | $y=0.016x-0.13$ | $y=0.011x-0.11$ | $y=0.021x+0.31$ | $y=0.014x-0.013$ | $y=0.015x-0.052$ | $y=0.020x-0.39$ |
| $R^2$ | 0.999 | 0.998 | 0.999 | 0.999 | 0.999 | 0.999 |
| **Linear range (μg $L^{-1}$)**[b] | 7.9–191.1 | 15.7–191.1 | 5.0–186.5 | 10.9–186.5 | 5.1–177.3 | 7.7–177.3 |
| **LOD (μg $L^{-1}$)** | 2.4 | 4.7 | 1.5 | 3.3 | 1.5 | 2.3 |

[a] $y$ is the peak area (a.u.) and $x$ is the concentration (μg $L^{-1}$).
[b] The lowest value of the linear range was considered from the LOQ

offers the highest interaction with Cu(II) followed by Pb(II). In both considered crown ethers, Cd(II) shows the smallest ion–dipole interaction being CB-15-crown-5 a little bit more selective than CB-18-crown-6. Comparing the ionic diameter of the considered metal ions (1.5 Å for Cu(II), 1.9 Å for Cd(II), and 2.4 Å for Pb(II) ) with the cavity size of both crown ethers (cavity diameter, 1.7–2.2 Å for CB-15-crown-5 and 2.6–3.2 Å for CB-18-crown-6), the described behavior is consistent with studies by Christensen et al. in 1971 who suggested that cation diameter to host cavity size ratios of 0.75–0.90 are favorable for direct ion–crown ether binding [4,30]. Thus, for Pb(II) a ratio of 0.75–0.92 was achieved for CB-18-crown-6 reflecting the size match for that ion. Likewise, ratios of 0.86–1.11 and 0.68–0.88 for CB-15-crown-5 were obtained for Cd(II) and Cu(II), respectively, consistent with the observed selectivities. The hypothesis is, therefore, that the use of the two electrodes as an array will provide higher information to resolve a multimetal mixture than that obtained from a single electrode. Two were the electrodes considered here, given that these are the ligands commercially available. With synthetic approaches, the number of differently modified sensors might be increased at will.

### 3.5. Multimetal stripping voltammetric measurements

The behavior of the stripping signals of different mixtures of Cd(II), Pb(II) and Cu(II) was studied in the concentration range 1.5–200 μg $L^{-1}$ using both CB-18-crown-6-GEC and CB-15-crown-5-GEC sensors in order to detect possible interactions between metal ions. As an example, a sample of five stripping voltammograms obtained using CB-15-crown-5-GEC (arbitrary concentrations) is displayed in Fig. 5b. As it can be seen, in contrast to the individual signals of metals (Fig. 4), an overlapping effect and the formation of some intermetallic compounds hinder the direct determination of the mixtures. Comparing both individual and multimetal stripping measurements the potential of the oxidation peak of each considered metal in the complex voltammograms could be assigned at *ca.* −0.75 V, −0.55 V, and 0.03 V for Cd(II), Pb(II) and Cu(II), respectively. A comparison between the voltammograms provided by both modified sensors displayed no significant differences in metal peak shapes and peak potentials, however different levels of metal interactions were observed in agreement with metal complex selectivity. Thus, for example, in the calibration mixture of 100.7 μg $L^{-1}$ of Cd(II), Pb(II) and Cu(II) the greatest voltammetric peak currents were obtained for Cu(II) and Cd(II) using the CB-15-crown-5-GEC, and for Pb(II) using CB-18-crown-6-GEC (inset in Fig. 5b). In this way, the stripping voltammetric response will be different depending on the metal ion concentration in each calibration mixture, the used modified sensor and the metal complex selectivity. For example, in the calibration mixture of 146.5, 116.0, and 24.4 μg $L^{-1}$ of Cd(II), Pb(II) and Cu(II) using the CB-15-crown-5-GEC (Fig. 5b, (D) thin line), the peak current of Cd(II) and Pb(II) increases substantially with respect to the mixture of equal concentration of metal ions (Fig. 5b, (A) thick line), whereas the peak current of Cu(II) decreases considerably.

Apart from the initially observed complexity, as the next step, the sets of voltammograms of heavy metal mixtures obtained from the two-sensor array were postulated to be used to calibrate Cd(II), Pb(II) and Cu(II) using an appropriate ANN model that may consider any non-linearity or overlapping in the determination of the considered metal ions.

### 3.6. Quantification of the metal mixtures

Once the data were compressed by use of Wavelet Transform and Causal Index in this study case, the first step in building the appropriate ANN model is choosing the topology of the neural network to be used. Normally, given the difficulties to predict the optimal settings in advance this is a trial-and-error process, where several parameters (training algorithms, number of hidden layers, transfer functions, etc.) are fine-tuned in order to find the best configuration that optimizes the performance of the model [31].

In consequence, the samples from the training subset were used for building the ANN model, and its accuracy was then evaluated towards samples of the external test subset by employing the built model to predict the concentrations of the metals of those samples (external validation). Taking into account that the external test subset data is not used at all for the modeling, its

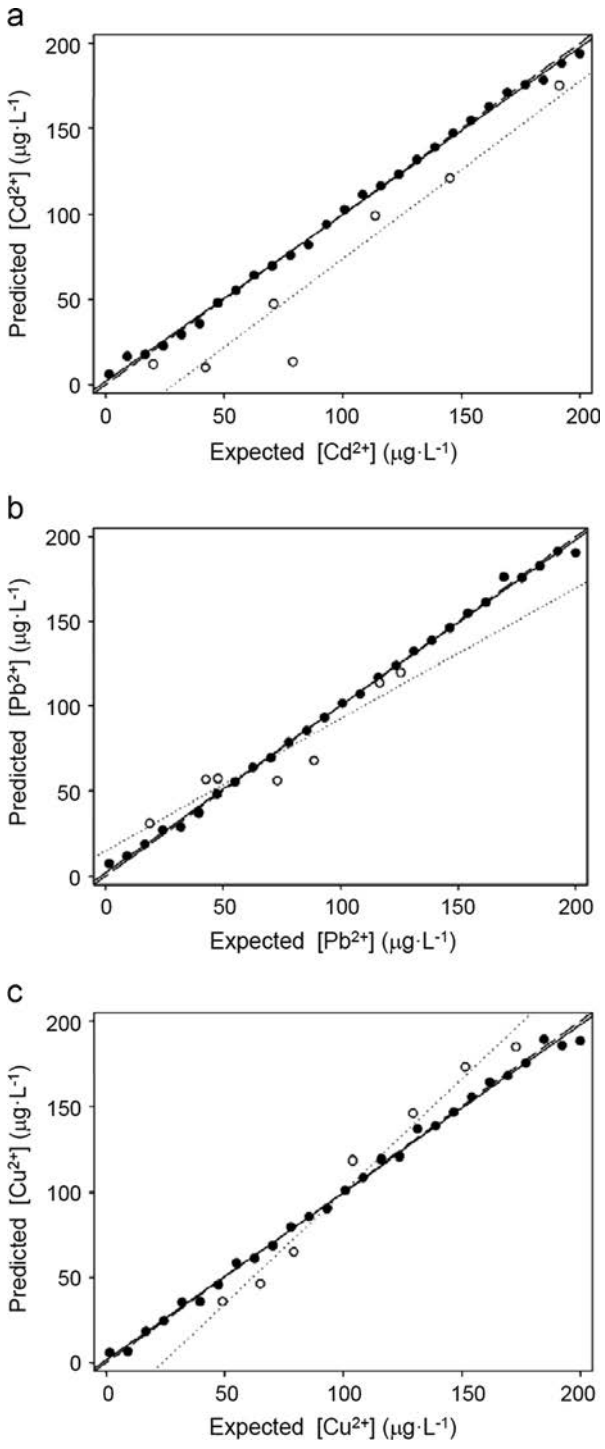


**Fig. 6.** Modeling ability of the optimized ANN for the two-sensor array. Comparison graphs of obtained *vs.* expected concentrations for (a) Cd(II), (b) Pb(II) and (c) Cu(II) metals, both for training (•, solid line) and testing subsets (○, dotted line). Dashed line corresponds to theoretical diagonal line ($Y=X$).

**Table 2**
Results of the fitted regression lines for the comparison between obtained *vs.* expected values, both for the training and testing subsets of samples and the different metal species (intervals calculated at the 95% confidence level).

| | Metal | Correlation | Slope | Intercept ($\mu g\ L^{-1}$) | RMSE ($\mu g\ L^{-1}$) | NRMSE | Total RMSE ($\mu g\ L^{-1}$) | Total NRMSE |
|---|---|---|---|---|---|---|---|---|
| **tr** | Pb(II) | 0.999 | $0.98 \pm 0.04$ | $1.9 \pm 4.3$ | 2.91 | 0.015 | 3.17 | 0.016 |
| | Cd(II) | 0.999 | $0.98 \pm 0.04$ | $1.9 \pm 4.3$ | 3.02 | 0.015 | | |
| | Cu(II) | 0.996 | $0.98 \pm 0.05$ | $1.5 \pm 5.5$ | 3.66 | 0.018 | | |
| **ts** | Pb(II) | 0.942 | $0.77 \pm 0.64$ | $15 \pm 52$ | 14.2 | 0.071 | 22.4 | 0.12 |
| | Cd(II) | 0.957 | $1.04 \pm 0.72$ | $-30 \pm 49$ | 34.1 | 0.170 | | |
| | Cu(II) | 0.989 | $1.31 \pm 0.45$ | $-31 \pm 52$ | 17.3 | 0.087 | | |

tr: training subset; ts: testing subset; RMSE: root mean square error; and NRMSE: normalized root mean square error

goodness of fit is a measure of the completed modeling performance. With the aim of facilitating the verification of the prediction ability of the obtained ANN model, comparison graphs of predicted *vs.* expected concentrations for the considered compounds were plotted, both for training subset and testing subsets. Once calculated the root mean square error (RMSE) [32], the best model will be the one that has the lowest RMSE values and additionally, regression parameters from the comparison graphs are close to the ideal values (*i.e.* slope and correlation coefficient equal 1, and intercept equal 0).

In our case, the resolution of the Cd(II), Pb(II) and Cu(II) mixtures was attempted using the data from the two voltammetric sensors. To this aim, the set of samples was measured with the two electrodes (CB-15-crown-5-GEC and CB-18-crown-6-GEC) and the obtained voltammetric responses were compressed employing DWT+CI and the different ANN models were optimized. After a systematic study for the fine tuning of the different parameters, the final architecture of the ANN model had 21 neurons in the input layer, 4 neurons and *logsig* transfer function in the hidden layer and three neurons and *tansig* transfer function in the output layer, providing the concentrations of the three species considered. Afterwards, comparison graphs of predicted *vs.* expected concentrations for the considered compounds were built (Fig. 6). As it can be observed, a satisfactory trend was obtained for all three metal ions with regression lines close to the theoretical ones. In addition, the obtained linear comparison parameters were calculated (Table 2) resulting close to the ideal values, with intercepts close to 0 and slopes and correlation coefficients close to 1, meaning that there are no significant differences between the values predicted by the ANN model and those expected and provided by the reference method.

## 4. Conclusions

In this work, it has been demonstrated that CB-15-crown-5 and CB-18-crown-6 could be successfully immobilized through the assistance of lysine on aryl diazonium salt monolayers anchored on a graphite epoxy composite electrode surface, constituting an alternative to the more widespread ether crown modified electrodes. These proposed modified electrodes exhibited a good repeatability and reproducibility and may be used for a large set of measurements without signs of degradation or loss of sensitivity, allowing the simultaneous determination of Cd(II), Pb(II) and Cu(II). In agreement with their good performance, these modified electrodes could be a promising implement for the determination of heavy metals in real samples as a healthier alternative to mercury electrodes. Related to their analytical performances, normal-shaped stripping signals were obtained for individual stripping measurements of Cd(II), Pb(II) and Cu(II) achieving LODs and LOQs at levels of $\mu g\ L^{-1}$, whereas an overlapping effect and the formation of some intermetallic compounds were observed in the stripping measurements of Cd(II), Pb(II) and Cu(II) mixtures in both CB-15-crown-5-GEC and CB-18-crown-6-GEC.

These considered crown ethers exhibit a high metal complex selectivity. In agreement with propitious cation diameter to host cavity size ratios, Pb(II) shows a more favorable complex forming ability with CB-18-crown-6 whereas Cu(II) fits snugly into CB-15-crown-5. For Cd(II), CB-15-crown-5 is a little bit more selective than CB-18-crown-6.

Taking as advantage of the crown ethers selective complex forming ability with metal ions, the use of the two-sensor array CB-15-crown-5-GEC and CB-18-crown-6-GEC can add some discrimination power to resolve the metal ion mixture. In this sense, the results provided in this work prove that the combination of the set of voltammetric measurements with chemometric tools helps us to determine the considered metal ions despite the intricate origin of the signals. Thus, voltammetric data preprocessed by DWT+CI and coupled with an artificial neural network permitted to obtain satisfactory results for the quantification of Cd(II), Pb(II) and Cu(II). The experiments exhibited similar performance in all training and testing correlation coefficients, obtained from the predicted *vs.* expected concentrations comparison graphs, which were in all cases higher than 0.942. The multivariate models created with ANN properly describe the complexity in the voltammograms caused by the overlapped peaks.

In conclusion, the present work considers a problem that can be encountered in the analysis of natural samples containing a mixture of different heavy metals. At the view of the satisfactory results obtained in this work, the proposed methodology seems to be perfectly suitable for the determination of heavy metals ions in environmental and biological samples at the ultra-trace level. Nevertheless, further research focused on the application of the analysis of multi-way data from an array of crown ethers-modified electrodes for the determination of heavy metals ions in real samples is required.

## Acknowledgments

The authors acknowledge financial support from the Spanish Ministry of Economy and Competitiveness (MINECO, projects CTQ2013-41577-P and CTQ2012-32863) and from the Catalonia program ICREA Academia (year 2010).

## References

[1] E. Lawrence, A.R.W. Jackson, J.M. Jackson, Logman Dictionary of Environmental Science, Addison Wesley Longman, Harlow, UK, 1998.
[2] J. Wang, Stripping Analysis: Principles, Instrumentation and Applications, VCH, Deerfield Beach, FL, 1985.
[3] J. Barek, A.G. Fogg, A. Muck, J. Zima, Crit. Rev. Anal. Chem. 31 (2001) 291–309.
[4] J.W. Steed, J.L. Atwood, Supramolecular Chemistry, Wiley, Chichester, UK, 2009.
[5] S.V. Prabhu, R.P. Baldwin, L. Kryger, Electroanalysis 1 (1989) 13–21.
[6] S. Anandhakumar, J. Mathiyarasu, Microchim. Acta 180 (2013) 1065–1071.
[7] V.S. Ijeri, A.K. Srivastava, Anal. Sci. 17 (2001) 605–608.
[8] J. Wang, M. Bonakdar, Talanta 35 (1988) 277–280.

[9] G. Zhiqiang, L. Peibiao, Z. Zaofan, Microchem. J. 43 (1991) 121–132.
[10] S. Tanaka, H. Yoshida, Talanta 36 (1989) 1044–1046.
[11] S. Cheraghi, M.A. Taher, H. Fazelirad, Microchim. Acta 180 (2013) 1157–1163.
[12] M.V. Tsymbal, I.Ya. Tuijan, Z.A. Temerdashev, K.Z. Brainina, Electroanalysis 6 (1994) 113–117.
[13] V.S. Ijeri, A.K. Srivastava, Fresenius J. Anal. Chem. 367 (2000) 373–377.
[14] A.M. Kijak, J.A. Cox, Anal. Chim. Acta 489 (2003) 13–19.
[15] J. Gooding, D. Hibbert, W. Yang, Sensors 1 (2001) 75–90.
[16] N. Serrano, B. Prieto-Simón, X. Cetó, M. del Valle, Talanta 125 (2014) 159–166.
[17] M. del Valle, Int. J. Electrochem. 2012 (2012) (Article ID 986025).
[18] A.I. Vogel, Textbook of Quantitative Chemical Analysis, 5th ed., Pearson Education Limited, Harlow, UK, 1989.
[19] A. Bonanni, M.J. Esplandiu, M.I. Pividori, S. Alegret, M. del Valle, Anal. Bioanal. Chem. 385 (2006) 1195–1201.
[20] C. Ocaña, M. del Valle, Microchim. Acta 181 (2014) 355–363.
[21] D. Belanger, J. Pinson, Chem. Soc. Rev. 40 (2011) 3995–4048.
[22] T.H. Young, J.N. Lu, D.J. Lin, C.L. Chang, H.H. Chang, L.P. Cheng, Desalination 234 (2008) 134–143.
[23] R. Usha, K.J. Sreeram, A. Rajaram, Colloid Surf. B: Biointerfaces 90 (2012) 83–90.
[24] N.R. Shenoy, J.M. Bailey, J.E. Shively, Protein Sci. 1 (1992) 58–67.
[25] J.D. Wade, T. Domagala, J. Rothacker, B. Catimel, E. Nice, Lett. Pept. Sci. 8 (2002) 211–220.
[26] X. Cetó, F. Céspedes, M.I. Pividori, J.M. Gutiérrez, M. del Valle, Analyst 137 (2012) 349–356.
[27] M. del Valle, R. Muñoz, J.M. Gutiérrez, Wavelets: Classification, Theory and Applications, Nova Science Pub Inc, New York, US, 2011.
[28] R.A. Johnson, D.W. Wichestein, Applied multivariate statistical analysis, Pearson Education, Harlow, UK, 2007.
[29] T. Navratil, J. Barek, Crit. Rev. Anal. Chem. 39 (2009) 131–147.
[30] J.J. Christensen, J.O. Hill, R.M. Izatt, Science 174 (1971) 459–467.
[31] F. Despagne, D.L. Massart, Analyst 123 (1998) 157R–178R.
[32] X. Cetó, F. Céspedes, M. del Valle, Microchim. Acta 180 (2013) 319–330.

# Article 3:

**Simultaneous Voltammetric Determination of Heavy Metals by Use of Crown Ether-modified Electrodes and Chemometrics**

Andreu González-Calabuig, David Guerrero, Núria Serrano and Manel del Valle

*Electroanalysis*, 2016, 28, 663 – 670

DOI: 10.1002/elan.201500512

Full Paper Wiley Online Library ELECTROANALYSIS

DOI: 10.1002/elan.201500512

# Simultaneous Voltammetric Determination of Heavy Metals by Use of Crown Ether-modified Electrodes and Chemometrics

Andreu González-Calabuig,[a] David Guerrero,[a] Núria Serrano,[b] and Manel del Valle*[a]

**Abstract**: A three-sensor array consisting of a graphite-epoxy composite electrode (GEC), 4-carboxybenzo-18-crown-6-GEC and 4-carboxybenzo-15-crown-5-GEC was employed for the simultaneous determination of Cd(II), Pb(II) and Hg(II) by differential pulse anodic stripping voltammetry (DPASV). Sensors were firstly studied for the determination of Hg(II); secondly, peak current responses confirmed that all sensors showed differentiated response for the three considered metals. A response model was developed to resolve mixtures of Cd(II), Pb(II) and Hg(II) at the μg $L^{-1}$ level; Discrete Wavelet Transform was selected as preprocessing tool and artificial neural network used for the modelling of the obtained responses.

**Keywords:** crown ether-modified sensors · electrochemical grafting · heavy metal · stripping voltammetry · artificial neural network

## 1 Introduction

The determination of heavy metal ions at trace levels is becoming more important day by day because of the health problems that they can cause in living systems, since they tend to bioaccumulate in their organisms and severe illnesses may be originated. Heavy metals become toxic when they are not metabolized by the body and accumulate in the soft tissues [1]. The main threats to human health from heavy metals are associated with exposure to lead, cadmium, mercury and arsenic. The general population is primarily exposed to mercury via food; fish is the major source of methyl mercury exposure, as also is relevant the use of dental amalgam. Related to cadmium exposure, cigarette smoking is the major source, whereas in non-smokers, food is the most important source. Exposure to lead is mainly via air and food in approximately equal proportions, being children particularly vulnerable [2].

Atomic absorption spectrometry (AAS), inductively coupled plasma optical emission spectrometry (ICP-OES), X-ray fluorescence (XRF), inductively coupled plasma mass spectrometry (ICP-MS), and stripping voltammetric techniques (anodic stripping voltammetry (ASV) and adsorptive stripping voltammetry (AdSV)) are some of the available techniques for the determination of heavy metals in natural samples. Particularly, stripping voltammetry techniques are the most suitable techniques for trace metals analysis in natural samples [3], due to their excellent detection limits, their sensitivity to the presence of different metal species, their capacity to multielement determination, and their relative low cost. Nevertheless, the performance of voltammetry is strongly influenced by the working electrode material. With the aim of developing alternative electrodes for classic mercury electrodes, chemically modified electrodes were considered for metal ion determination.

Thiol rich peptides and macrocyclic compounds, as crown ethers, can be employed as modifiers for metal determination. A simple and flexible approach to attach these compounds to an electrode surface is based on their immobilization on aryl diazonium salt monolayers anchored on the electrode surface, also referred in the literature as electrochemical grafting, which is a valuable alternative to the use of self-assembled monolayers (SAM) for forming stable complexing surfaces [4–7].

Particularly, crown ethers may act as a host, complexing a centre metal, and once introduced into the electrode enhance its selectivity and lower the metal detection limit. To achieve high degree of selectivity one may think to modify them to strongly bind certain metals allowing the complex formation by means of ion-dipole interaction with these metal ions [8]. So, the complexing ability and crown cavity size which is suitable for a particular metal ion have to be considered for its selective detection.

Although some studies devoted to the application of crown ether-modified electrodes for the individual determination of lead [9–11], mercury [12,13], silver [14], thallium [15], palladium [16] and copper [17] can be found in the literature, related works entailing the simultaneous

[a] A. González-Calabuig, D. Guerrero, M. del Valle
Sensors & Biosensors Group, Department of Chemistry
Universitat Autònoma de Barcelona
Edifici Cn, 08193 – Bellaterra (Spain)
*e-mail: manel.delvalle@uab.es

[b] N. Serrano
Department of Analytical Chemistry, Faculty of Chemistry
Universitat de Barcelona, Martí i Franquès 1–11
08028 – Barcelona (Spain)

  

determination of different heavy metal ions are scarce [6].

Crown ether-modified electrodes not only can be used for metal determination as a single-electrode sensor but also in combination with others forming an electrode arrays with semi-selective ligands for the determination of several metal ions. Such a strategy relies on the modification of electrodes in the array with different complexing agents to provide a highly variate response [18]. The main advantage of a multi-sensor array over the classical one-electrode is that the information provided by the electrode array is significantly higher than that obtained from a single electrode; in this way, multimetal interactions or interfering effects can be modelled and resolved.

In this work, a three-sensor array consisting of one graphite-epoxy composite electrode (GEC) and two GECs modified with 4-carboxybenzo-18-crown-6 (CB-18-crown-6) and 4-carboxybenzo-15-crown-5 (CB-15-crown-5) respectively, which were immobilized through aryl diazonium salt monolayers anchored to the electrode surface was firstly analytically studied for the determination of Hg(II) using voltammetric techniques. Subsequently, this three-sensor array was applied for the first time for the simultaneous determination of Cd(II), Pb(II) and Hg(II) ions in certified samples by voltammetric techniques. An artificial neural network model was proposed as a tool to maximize the information obtained from the voltammetric data.

## 2 Experimental

### 2.1 Chemicals

Potassium ferricyanide $K_3[Fe(CN)_6]$, potassium ferrocyanide $K_4[Fe(CN)_6]$, 2-(N-morpholino)-ethanesulfonic acid (MES), potassium dihydrogen phosphate, sodium monophosphate, methanol, perchloric acid, hydrochloride acid, *N*-hydroxysulfosuccinimide (sulfo-NHS), *N*-(3-dimethylaminopropyl)-*N*′-ethyl-carbodiimide hydrochloride (EDC) and sodium nitrite were purchased from Sigma (St. Louis, MO, USA). 4-aminobenzoic acid (ABA) and DL-lysine monohydrochloride were provided by Acros (Geel, Belgium). 4-carboxybenzo-18-crown-6 with a purity of 99% and 4-carboxybenzo-15-crown-5 with purity greater than 98% were provided by Acros and Sigma respectively. All other reagents used were from Merck (Darmstadt, Germany) and Fluka (Buchs, Switzerland). All reagents were of analytical grade. Pb(II), Cd(II) and Hg(II) stock solutions $10^{-2}\,mol\cdot L^{-1}$ were prepared from $Pb(NO_3)_2\cdot 4H_2O$, $Cd(NO_3)_2\cdot 4H_2O$ and $Hg(NO_3)_2\cdot H_2O$ respectively and standardized complexometrically. Pb(II), Cd(II) and Hg(II) 1000 $mg\cdot L^{-1}$ certified standard solutions were purchased from Fluka. 0.1 $mol\cdot L^{-1}$ acetic acid/acetate buffer solution (pH 4.5) was used for pH control. Ultrapure water from MilliQ System (Millipore, Billerica, MA, USA) was used in all experiments.

### 2.2 Apparatus

Voltammetric measurements were performed in an Autolab System PGSTAT 30 (EcoChemie, The Netherlands), in a multichannel configuration, using GPES Multichannel 4.7 software package (EcoChemie). The voltammetric cell was formed by one working graphite epoxy electrode (GEC) and two working graphite epoxy electrodes modified with 4-carboxybenzo-18-crown-6 (CB-18-crown-6) and 4-carboxybenzo-15-crown-5 (CB-15-crown-5) respectively, a commercial platinum counter electrode (Model 52-67, Crison Instruments, Barcelona, Spain), and a double junction Ag/AgCl reference electrode (Thermo Orion 900200, Beverly, MA, USA).

A pH meter GLP 22 (Crison Instruments, Barcelona, Spain) was used for pH measurements.

All measurements were carried out at room temperature (20°).

### 2.3 Procedures

#### *2.3.1 Preparation of Graphite Epoxy Electrodes*

Graphite epoxy composite electrodes (GECs) were fabricated by using a PVC tube body (6 mm i. d.) and a small copper disk soldered at the end of an electrical connector. The working surface is an epoxy-graphite conductive composite, formed by a mixture of 20% graphite powder (Merck, Darmstadt, Germany) and 80% of epoxy resin, Epotek H77, and its corresponding hardener (both from Epoxy Technology, Billerica, MA, USA), deposited on the cavity of the plastic body [19]. The composite material was cured at 80 °C for 3 days. Prior to their functionalization, the electrode surface was moistened with MilliQ water and then polished on abrasive sandpaper (400, 600, 800, 1000, and 1200 grit) and finally on alumina polishing strips (301044-001, Orion) in order to obtain a reproducible electrochemical surface.

#### *2.3.2 Preparation of Modified GECs*

The specific steps for the modification of the GEC are described below [20].

– *Diazonium salt electrochemical grafting:* The *in situ* generation of the aryl diazonium was performed by adding $5\cdot 10^{-3}$ equivalents of sodium nitrite to an acidic solution (1 M aqueous HCl) of ABA. These solutions were mixed for about 30 min in an ice bath, prior to the electrochemical grafting process [21] conducted by scanning the potential at 0.2 $V\,s^{-1}$ from 0 V to −1 V for 100 cycles. The functionalized electrodes were thoroughly rinsed with Milli-Q water and methanol to remove any physisorbed compounds.

– *Covalent immobilization of crown ethers via carbodiimide coupling:* The carboxyl groups of the electrografted diazonium salt were activated by incubating the functionalized electrodes in a 26 mM EDC and 35 mM sulfo-NHS solution in 100 mM MES buffer (pH 4.5) for 1 h. In order to conjugate the carboxy-functionalized electrode with

  

the carboxy-modified ligands, a lysine spacer was intercalated in between, by using its two amino functionalities to form amido bonds [6]. The surface activated groups reacted overnight with the α-amine group of the lysine at 4°. Prior to cross linking with EDC/sulfo-NHS, 2.9 mg of 4-carboxybenzo-18-crown-6 or 4-carboxybenzo-15-crown-5 were incubated with 100 µL 5 mM lysine in 0.1 M MES buffer for 3 h.

Figure 1 illustrates the CB-15-crown-5-GEC and CB-18-crown-6-GEC electrodes modified by electrochemical grafting.

The electrochemical response using 2 mM ferrocyanide/ferricyanide as redox probe in 100 mM phosphate buffer (pH 7.4) was investigated at each functionalization step using cyclic voltammetry (CV) leading voltammograms that confirm the modifications occurring on the electrode surface (Figure not shown). This procedure has been tested [6] with a high repeatability and a noticeable reproducibility.

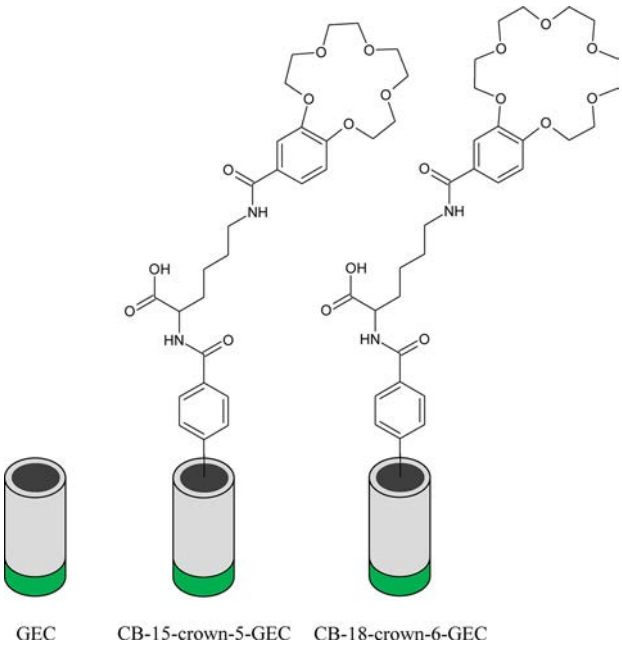


Fig. 1. Scheme of the three-sensor array: GEC, CB-15-crown-5-GEC and CB-18-crown-6-GEC.

### 2.3.3 Voltammetric Measurements

Before each set of measurements, the electrodes were scanned in acetic acid/acetate buffer solution in order to get stable voltammetric responses.

Voltammetric determinations using GEC, CB-18-crown-6-GEC and CB-15-crown-5-GEC of Cd(II), Pb(II) and Hg(II), were done, without the need of any oxygen removal, at a deposition potential ($E_d$) of −1.4 V, applied with stirring during a deposition time ($t_d$) of 300 s and followed for a rest period ($t_r$) of 10 s. Determinations were done by scanning potential from −1.4 to +0.7 V using a step potential of 4 mV and pulse amplitude of 50 mV. Calibration plots were obtained by increasing metal concentrations in pH 4.5 acetic acid/acetate buffer media.

In order to eliminate any remaining bound metals from the electrode, an electrochemical cleaning stage was considered between measurements. This stage was performed by applying a conditioning potential ($E_{cond}$) of 1.20 V for 240 s after each measurement, in a cell containing fresh buffer solution.

To allow the multimetal simultaneous determination, a response model was built using artificial neural networks (ANN). For this aim, voltammetric scans of a total set of 37 multimetal mixed samples in the concentration range 0–200 $\mu g \cdot L^{-1}$ were recorded at the same experimental conditions as calibration plots. The set of samples was divided into two data subsets: a training subset formed by 27 samples (72.9 %), which were distributed in a factorial design [22] with 3 factors and 3 levels, and used to establish the response model and the testing subset formed by 10 samples (27.1 %), randomly distributed along the experimental domain, used to evaluate the model predictive response; additionally 3 certified samples, also containing the three metals randomly distributed along the experimental domain, were used to evaluate the applicability of the three-sensor array for the simultaneous determination of Pb(II), Cd(II) and Hg(II) in real samples.

Training and testing subset samples were manually prepared by appropriate dilution from the prepared metal stock solutions $10^{-2}$ $mol \cdot L^{-1}$ in pH 4.5 acetic acid/acetate buffer, whereas certified samples were manually prepared by appropriate dilution from 1000 $mg \cdot L^{-1}$ certified standard solutions in pH 4.5 acetic acid/acetate buffer.

### 2.3.4 Data Processing

In order to reduce the large amount of information generated for each sample (3 sensors x 431 current values at different potential) and its multiway nature a preprocessing stage was necessary to compress the original data. The objective of this step is to reduce the complexity of the input data while preserving the relevant information; also the compression of the data allows to reduce the training time, avoid redundancy in input data and to obtain a model with better generalization ability.

The chosen method was the Discrete Wavelet Transform (DWT) [23], each voltammogram was compressed using Daubechies 3 wavelet mother function and a 4 decomposition level. In this manner, the original data was reduced to 93 coefficients without losing relevant information, achieving a compression ratio up to 92.3 %.

Chemometric processing of data was performed by specific routines written by the authors using MATLAB 8.4 (MathWorks, Natick, MA) and its Neural Network Toolbox (v.8.2.1).

  

## 3 Results and Discussion

As the most novel part of the present work is the part concerning Hg(II) sensing, this was studied in detail; next, the sensor array was employed for the simultaneous determination of the three considered metals, in an electronic tongue approach.

### 3.1 Calibration Data

Most influential parameters in the ASV voltammetric response for a given metal are the operating parameters, such as deposition potential ($E_d$), the accumulation potential ($t_d$) and pH of the medium. The optimized compromise conditions for the simultaneous determination of Pb(II), Cd(II) and Hg(II) using the three-sensor array were an $E_d$ of −1.4 V with stirring during a $t_d$ of 300 s and followed by a rest period of 10 s at the same applied potential in 0.1 mol $L^{-1}$ acetic acid/acetate buffer pH 4.5.

Once stablished the working conditions, the electrodes of the array (GEC, CB-18-crown-6-GEC and CB-15-crown-5-GEC) were analytically characterized for the determination of Hg(II) given that there are no previous studies in this regard; on the other hand, responses towards Cd(II) and Pb(II) were already studied in a related work, involving the triad of metals Cd(II), Pb(II) and Cu(II) [6].

First of all, individual calibration of Hg(II) ion by stripping voltammetry (DPASV) was carried out using the three-sensor array. The LOD was calculated as 3 times the standard deviation of the intercept over the slope of the calibration curve of the target ions. LOQ was evaluated by considering 10 times the previous ratio. The lowest value of the linear concentration range was established from the corresponding limit of quantification (LOQ). For LOD and LOQ determinations, eleven different standards of the considered ion were used to build the calibration lines.

The three sensors evaluated provided a well-defined stripping peak over the considered concentration range. Excellent linear responses of peak currents *versus* Hg(II) concentrations were obtained for GEC, CB-18-crown-6-GEC and CB-15-crown-5-GEC up to a maximum concentration level of 200 μg $L^{-1}$. The corresponding regression equations and the correlation coefficient for the sensors of the array are shown in Table 1.

With respect to the sensitivities considered as the value obtained from the slope of the calibration curves, it can be stated that: Hg(II) shows a very similar sensitivity for the three considered sensors suggesting that the three electrodes respond in the same way versus Hg(II). However, comparing the two crown ether-modified sensors it can be observed that their sensitivities are slightly different suggesting that CB-18-crown-6-GEC offers a higher interaction than CB-15-crown-5-GEC with Hg(II). Related to the unmodified GEC it has a sensitivity slightly higher than other sensors, this fact is because the graphite structure where the mercury can be introduced into the own structure of the graphite making it especially sensitive. As shown in Table 1, both LOD and LOQ were at the level of μg $L^{-1}$ for all considered sensors. In comparison with previous results achieved at other crown ether-modified electrodes, the LODs provided by CB-18-crown-6-GEC and CB-15-crown-5-GEC sensors were similar than the LOD obtained using a ferrocenoylpolythia crown ether—Nafion-modified glassy carbon electrode [13], and much lower than the LOD achieved using a carbon-paste electrodes modified with 18-crown-6 [12]. It must be point out that in this work an enrichment time of 300 s was selected looking for a compromise between the peak currents and the time of the analysis, nevertheless lower concentrations ranges and better detection limits could easily be achieved using the proposed method by increasing the enrichment time.

Table 1. Calibration data for the determination of Hg(II) on GEC, CB-18-crown-6-GEC and CB-15-crown-5-GEC at $E_d$ of −1.4 V using a $t_d$ of 120 s at pH 4.5.

| | GEC | CB-18-crown-6-GEC | CB-15-crown-5-GEC |
|---|---|---|---|
| Regression [a] | $y = 0.157\,x + 2.88$ | $y = 0.146 + 3.26$ | $y = 0.128 + 4.76$ |
| $R^2$ | 0.985 | 0.995 | 0.995 |
| Linear range (μg $L^{-1}$) [b] | 37–200 | 43–200 | 40–200 |
| LOD (μg $L^{-1}$) | 11 | 13 | 12 |

[a] y is the peak height (μA) and x the concentration (μg $L^{-1}$). [b] The lowest value of the linear range was considered from the LOQ.

Comparing both unmodified GEC and crown ether modified GEC it can be observed that the LOD and LOQ values obtained for both CB-18-crown-6-GEC and CB-15-crown-5-GEC sensors are in the range of those obtained for the unmodified graphite composite electrode. Therefore the reported calibration data suggest that all considered sensors could be fully suitable for the determination of Hg(II) at low μg·$L^{-1}$ level in natural samples. However, until no simultaneous determinations of Hg(II) with other heavy metal ions such as Cd(II) and Pb(II) are performed, it cannot be established which of the considered sensor is the best especially in terms of selectivity for Hg(II) determination.

### 3.2 Multimetal Stripping Voltammetric Measurements

Before the application of the three considered sensors as an array for the simultaneous determination of Cd(II), Pb(II) and Hg(II) is import to know if this array can add some discrimination power to resolve the mixture. Therefore, the cross-response of these sensors was examined.

Considering that the immobilized crown ethers on the GEC surface are used as molecular collector with ability to selectively coordinate with the metal ions, both the ionic diameter of metal ions and the cavity size of the crown ethers play a crucial role for the complex formation by means of ion-dipole interaction with metal ions.

  

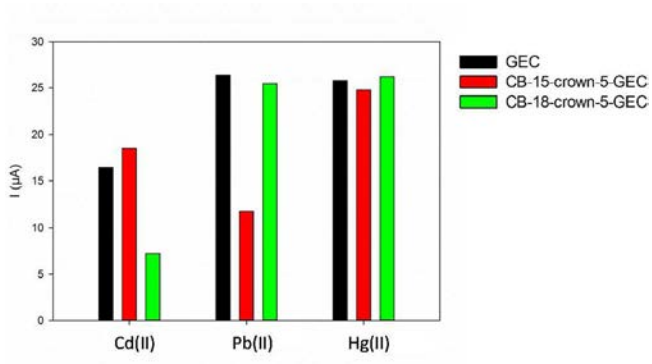


Fig. 2. Differential Pulse anodic stripping voltammetric sensitivity, from peak current of 175 µg $L^{-1}$ of Cd(II), Pb(II) and Hg(II) using the three-sensor array. Black: graphite epoxy composite electrode (GEC); red: CB-15crown-5-GEC; green: CB-18-crown-6-GEC.

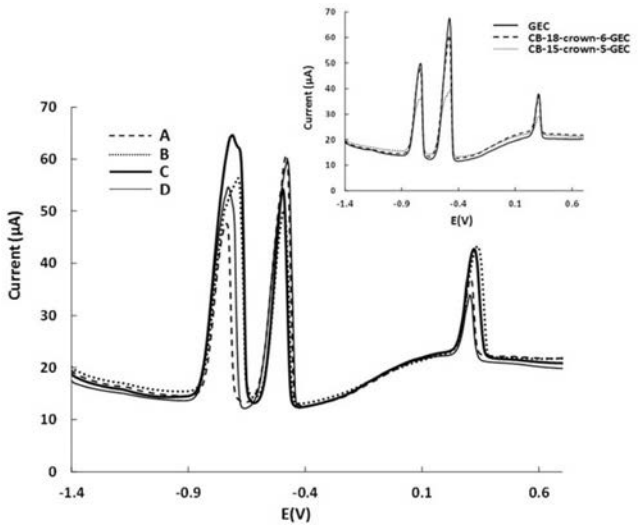


Fig. 3. Some differential pulse anodic stripping voltammograms generated during the building of the response model recorded on a CB-18-crown-6-GEC sensor at pH 4.5 using a $E_d$ of −1.40 V during 300 s and $t_r$ of 10 s. Sample composition: (A) 31.1 µg $L^{-1}$ of Cd(II), 147.1 µg $L^{-1}$ of Pb(II) and 27.5 µg $L^{-1}$ of Hg(II); (B) 124.9 µg $L^{-1}$ of Cd(II), 92.5 µg $L^{-1}$ of Pb(II) and 136.2 µg $L^{-1}$ of Hg(II); (C) 177.4 µg $L^{-1}$ of Cd(II), 70.0 µg $L^{-1}$ of Pb(II) and 80.1 µg $L^{-1}$ of Hg(II); (D) 94.2 µg $L^{-1}$ of Cd(II), 162.9 µg $L^{-1}$ of Pb(II) and 7.5 µg $L^{-1}$ of Hg(II). Inset: comparison between the response of the three-sensor array for sample composition (A).

Although, it is known that both CB-18-crown-6 and CB-15-crown-5 exhibit a cross-response for Cd(II) and Pb(II) [6], it is unknown whether with Hg(II) has this characteristic response. With this aim voltammetric peak current responses for equal concentrations of metal ion solution (175 µg $L^{-1}$ of Cd(II), Pb(II) and Hg(II)) were recorded using the three-sensor array. Figure 2 shows that, on the one hand, CB-18-crown-6-GEC and GEC exhibit the highest interaction with Pb(II) and Hg(II) being the ion-dipole interaction of CB-18-crown-6-GEC with Hg(II) slightly higher than with Pb(II); on the other hand, CB-15-crown-5-GEC offers the highest selective complex forming ability with Hg(II) followed by Cd(II). Although, for the three considered sensors Hg(II) shows a similar interaction, it can be seen that CB-18-crown-6-GEC is a little bit more selective than CB-15-crown-5-GEC. Comparing the ionic diameter of the considered metal ions (1.9 Å for Cd(II), 2.1 Å for Hg(II), and 2.4 Å for Pb(II)) with the cavity size of both crown ethers (cavity diameter, 1.7–2.2 Å for CB-15-crown-5 and 2.6–3.2 Å for CB-18-crown-6), the described behavior is consistent with studies by Christensen *et al.* in 1971 who suggested that cation diameter to host cavity size ratios of 0.75–0.90 are favorable for direct ion-crown ether binding [24]. Thus, ratios of 0.66–0.81 and 0.75–0.92 for Hg(II) and Pb(II), respectively, were achieved for CB-18-crown-6 reflecting the size match for those ions. Likewise, a ratio of 0.86–1.11 for CB-15-crown-5 were obtained for Cd(II) consistent with the observed selectivities.

Therefore, from Figure 2 it can be evidenced the existence of cross-response between the three metal ions and the considered sensors. In this way, whereas additionally a maximum signal for each metal is obtained for a different electrode, the use of the three-sensor array would provide higher information to resolve the multimetal mixture than that obtained from a single electrode. As an example, a sample of four stripping voltammograms obtained using CB-18-crown-6-GEC (arbitrary concentrations) is displayed in Figure 3. Relatively well-defined stripping peaks without any clear evidence of signal splitting or overlapping effect were observed over the considered concentration range. The potential of the oxidation peak of each considered metal in the complex voltammograms was assigned at *ca.* −0.73 V, −0.48 V, and 0.31 V for Cd(II), Pb(II) and Hg(II) respectively. A comparison between the voltammograms provided by unmodified GEC and both crown ethers-modified sensors displayed no significant differences in metal peak shapes and peak potentials (at shown concentration levels), however different degree of metal interactions were observed in agreement with metal complex selectivity (inset in Figure 3). Thus, the stripping voltammetric response will be different depending on the metal ion concentration in each calibration mixture, the used sensor and the metal complex selectivity.

As the next step, the sets of voltammograms of heavy metal mixtures obtained from the three-sensor array were postulated to be used to calibrate Cd(II), Pb(II) and Hg(II) using an appropriate ANN model that may consider any non-linearity or splitting in the determination of the considered metal ions.

### 3.3 Quantification of the Metal Mixtures

Once the data were compressed by use of Wavelet Transform in this study case, the first step in building the appropriate ANN model is choosing the topology of the neural network used. Normally, given the difficulties to predict the optimal settings in advance this is a trial-and-

  

error process, where several parameters (training algorithms, number of hidden layers, transfer functions, etc.) are fine-tuned in order to find the best configuration that optimizes the performance of the model [25].

In consequence, the samples from the training subset were used for building the ANN model, and its accuracy was then evaluated towards samples of the external test subset by employing the developed model to predict the concentrations of the metals of those samples (external validation). Taking into account that the external test subset data is not used at all for the modelling, its goodness of fit is a measure of the completed modelling performance.

Model prediction abilities are shown in the comparison graphs (obtained vs. expected concentrations) for all ions, both for training subset and testing subsets. The factors considered for the selection of the best model were the accuracy of fit, evaluated as the smaller RMSE (root mean squared error) [26] and additionally, regression parameters from the comparison graphs close to the ideal values (i.e. slope and correlation coefficient equal 1, and intercept equal 0), meaning that there are no significant differences between the values predicted by the ANN model and those expected and provided by the reference method.

In our case, the resolution of the Cd(II), Pb(II) and Hg(II) mixtures was attempted using the data from the three voltammetric sensor array. To this aim, the set of samples was measured with the three electrodes (unmodified GEC, CB-15-crown-5-GEC and CB-18-crown-6-GEC) and the obtained voltammetric responses were compressed employing DWT and the different ANN models were optimized. After a systematic study optimizing the different parameters, the final architecture of the ANN model had 93 neurons in the input layer, 4 neurons and *satlins* transfer function in the hidden layer and 3 neurons and *purelin* transfer function in the output layer, providing the concentrations of the three species considered. Figure 4 illustrates the comparison graphs of predicted *vs.* expected concentrations for the considered compounds for training (●, solid line) and testing subsets (○, dashed line). As it can be observed, a satisfactory trend was obtained for all three metal ions with regression lines close to the theoretical ones (long dashed line). Table 2 shows the calculated linear comparison parameters being near the ideal value, with correlation coefficients and slopes with values very close to 1 and intercepts quite close to 0.

Additionally, to assess the applicability of the three-sensor array to real samples, an attempt was performed to simultaneously determine Cd(II), Pb(II) and Hg(II) in 3 certified samples, randomly distributed along the experimental domain. Figure 4 (empty star) shows the linear regression results for Cd(II), Pb(II) and Hg(II). The general trend is quite satisfactory for all the considered metal ions with slopes and intercepts close to 1 and 0 respectively, and with correlations being also significant (Table 2). Although, Cd(II) is the analyte with the worst performance especially with a somewhat lesser correlation and higher confidence interval of the intercept value.

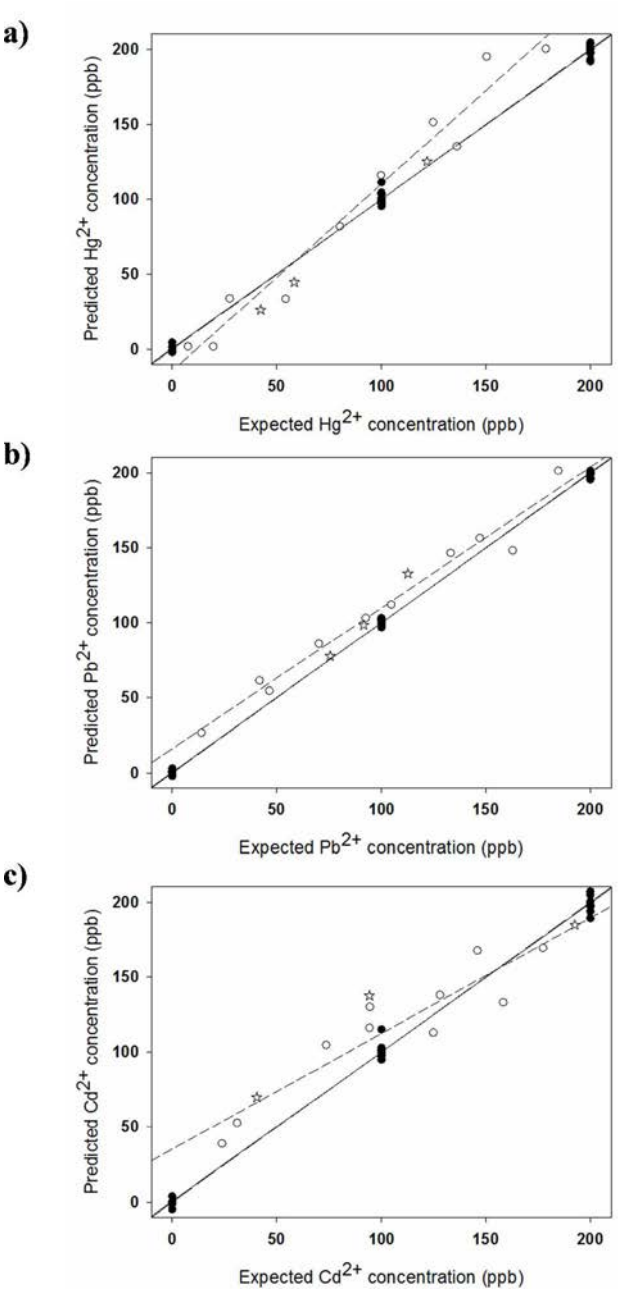


Fig. 4. Modelling ability of the optimized ANN for the three–sensor array. Sets adjustments of obtained vs. expected concentrations for (a) Cd(II), (b) Pb(II) and (c) Hg(II), for training subset (●, solid line), testing subsets (○, dashed line) and certified samples (empty star). Long dashed line corresponds to theoretical diagonal line.

## 4 Conclusions

In this work, a three-sensor array constituted by an unmodified GEC and two GECs modified with CB-18-crown-6 and CB-15-crown-5 respectively, which were immobilized on aryl diazonium salt monolayers anchored to

  

Table 2. Results of the fitted regression lines for the comparison between obtained vs. expected values, for the training and testing subsets of samples and the different metal species (intervals calculated at the 95 % confidence level).

| | Metal | Correlation | Slope | Intercept (ppb) | RMSE (ppb) | NRMSE | Total RMSE (ppb) | Total NRMSE |
|---|---|---|---|---|---|---|---|---|
| | Hg(II) | 0.999 | 0.99 ± 0.04 | 0.74 ± 4.91 | 3.89 | 0.019 | | |
| **train subset** | Pb(II) | 0.999 | 0.99 ± 0.02 | 0.49 ± 2.46 | 1.97 | 0.010 | 3.69 | 0.018 |
| | Cd(II) | 0.998 | 0.99 ± 0.05 | 0.71 ± 5.95 | 4.69 | 0.023 | | |
| | Hg(II) | 0.982 | 1.25 ± 0.39 | −14.26 ± 40.44 | 21.71 | 0.109 | | |
| **test subset** | Pb(II) | 0.986 | 0.94 ± 0.25 | 16.11 ± 28.66 | 14.10 | 0.071 | 19.35 | 0.096 |
| | Cd(II) | 0.927 | 0.77 ± 0.51 | 35.24 ± 58.97 | 23.17 | 0.116 | | |

RMSE: root mean square error; NRMSE: normalized root mean square error

the electrode surface, was successfully applied for the simultaneous determination of Cd(II), Pb(II) and Hg(II) by DPASV. The three-sensor array was firstly analytical studied for the determination of Hg(II) providing a well-shaped stripping peak over the considered concentration range. The achieved LODs and LOQs were at levels of $\mu g\,L^{-1}$, which are similar or even much lower to those obtained for the determination of Hg(II) with other crown ether-modified electrodes [12–13].

Taking advantage of the crown ethers complex forming ability with the considered metal ions, the use of the three-sensor array allows the existence of a cross-response between the three metal ions and the considered sensors adding the discrimination power to resolve the Cd(II), Pb(II) and Hg(II) mixture.

In this sense, in this work, the simultaneous quantification of Cd(II), Pb(II) and Hg(II) was satisfactory achieved by combining the set of voltammetric measurements with chemometric tools. Thus, voltammetric data obtained using the three-sensor array was preprocessed by DWT and coupled with an artificial neural network. The experiments exhibited similar performance in all training and testing correlation coefficients, obtained from the predicted *vs.* expected concentrations comparison graphs, which were in all cases higher than 0.927. Under the above mentioned conditions, the simultaneous determination of Cd(II), Pb(II) and Hg(II) in certified samples using the three-sensor array was successfully attempted obtaining a satisfactory trend for the three considered metal ions with correlation coefficients of 0.998 and 0.999 for Pb(II) and Hg(II), respectively, whereas for Cd(II) a lower correlation (0.964) and a higher confidence interval of the intercept value are achieved, the recovery values were 80.7 %, 109.4 % and 138.1 % for Hg(II), Pb(II) and Cd(II) respectively. In similar works performed, Cd(II) has been always the worst performing metals probably because of non-linearities in measured signals originated at intermetallic reduced compounds [6,27].

At the sight of the satisfactory results reached in this work, the proposed methodology seems to be perfectly suitable for the determination of heavy metals ions in environmental and biological samples at the ultra-trace level. Even so, further research focused on the application of the proposed method for drinking water analysis is required taking into consideration the guidelines for drinking water quality [28]; since Cd(II) and Pb(II) could be successfully determined according to the proposed experimental conditions [6], whereas for Hg(II) determination an increase of the deposition time would still be required.

## Acknowledgements

The authors acknowledge financial support from the Spanish Ministry of Science and Innovation (MINECO, through projects CTQ2013-41577-P and CTQ2012-32863). M. del Valle acknowledges support by the Catalonia program ICREA Academia.

## References

[1] E. Lawrence, A. R.W. Jackson, J. M. Jackson, *Longman Dictionary of Environmental Science*, Addison Wesley Longman, Harlow, UK, **1998**.
[2] L. Järup, *British Medical Bulletin* **2003**, *68*, 167–182.
[3] J. Wang, Stripping Analysis: Principles, Instrumentation and Applications, VCH, Deerfield Beach, FL **1985**.
[4] J. Gooding, D. Hibbert, W. Yang, *Sensors* **2001**, *1*, 75–90.
[5] N. Serrano, B. Prieto-Simón, X. Cetó, M. del Valle, *Talanta* **2014**, *125*, 159–166.
[6] N. Serrano, A. González-Calabuig, M. del Valle, *Talanta* **2015**, *138*, 130–137.
[7] C. Pérez-Ràfols, N. Serrano, J. M. Díaz-Cruz, C. Ariño, M. Esteban, *Talanta* **2015**, *144*, 569–573.
[8] J. W. Steed, J. L. Atwood, *Supramolecular Chemistry*, Wiley, Chichester, UK **2009**.
[9] S. V. Prabhu, R. P. Baldwin, L. Kryger, *Electroanalysis* **1989**, *1*, 13–21.
[10] S. Anandhakumar, J. Mathiyarasu, *Microchim. Acta* **2013**, *180*, 1065–1071.
[11] V. S. Ijeri, A. K. Srivastava, *Anal. Sci.* **2001**, *17*, 605–608.
[12] J. Wang, M. Bonakdar, *Talanta* **1988**, *35*, 277–280.
[13] G. Zhiqiang, L. Peibiao, Z. Zaofan, *Microchem. J.* **1991**, *43*, 121–132.
[14] S. Tanaka, H. Yoshida, *Talanta* **1989**, *36*, 1044–1046.
[15] S. Cheraghi, M. A. Taher, H. Fazelirad, *Microchim. Acta* **2013**, *180*, 1157–1163.
[16] M. V. Tsymbal, I. Ya. Tuijan, Z. A. Temerdashev, K. Z. Brainina, *Electroanalysis* **1994**, *6*, 113–117.
[17] V. S. Ijeri, A. K. Srivastava, *Fresenius J. Anal. Chem.* **2000**, *367*, 373–377.
[18] M. del Valle, *Electroanalysis* **2010**, *22*, 1539–1555.
[19] A. Bonanni, M. J. Esplandiu, M. I. Pividori, S. Alegret, M. del Valle, *Anal. Bioanal. Chem.* **2006**, *385*, 1195–1201.

  

[20] C. Ocaña, M. del Valle, *Microchim. Acta* **2014**, *181*, 355–363.
[21] D. Belanger, J. Pinson, *Chem. Soc. Rev.* **2011**, *40*, 3995–4048.
[22] X. Cetó, F. Céspedes, M. I. Pividori, J. M. Gutiérrez, M. del Valle, *Analyst* **2012**, *137* 349–356.
[23] M. del Valle, R. Muñoz, J. M. Gutiérrez, *Wavelets: Classification, Theory and Applications*, Nova Science Pub Inc, New York, US, **2011**.
[24] J. J. Christensen, J. O. Hill, R. M. Izatt, *Science* **1971**, *174*, 459–467.
[25] F. Despagne, D. L. Massart, *Analyst* **1998**, *123*, 157R-178R.
[26] X. Cetó, F. Céspedes, M. del Valle, *Microchim. Acta*, **2013**, *180*, 319–330.
[27] J. M. Gutierrez, L. Moreno-Baron, F. Cespedes, R. Muñoz, M. del Valle, *Electroanalysis* **2009**, *21*, 445–451.
[28] *Guidelines for Drinking-water Quality -- 4th ed*, World Health Organization, Geneva, Switzerland, **2011**.

Received: July 28, 2015
Accepted: September 14, 2015
Published online: October 12, 2015

  

# Article 4:

**Instrumental measurement of wine sensory descriptors using a voltammetric electronic tongue**

Xavier Cetó, Andreu González-Calabuig, Josefina Capdevila, Anna Puig-Pujol and Manel del Valle

*Sensors and Actuators B* 207 (2015) 1053–1059

DOI: 10.1016/j.snb.2014.09.081

Sensors and Actuators B 207 (2015) 1053–1059

Contents lists available at ScienceDirect

Sensors and Actuators B: Chemical

journal homepage: www.elsevier.com/locate/snb

# Instrumental measurement of wine sensory descriptors using a voltammetric electronic tongue

Xavier Cetó[a], Andreu González-Calabuig[a], Josefina Capdevila[b], Anna Puig-Pujol[b], Manel del Valle[a,*]

[a] Sensors and Biosensors Group, Department of Chemistry, Universitat Autònoma de Barcelona, Edifici Cn, 08193 Bellaterra, Barcelona, Spain
[b] Department of Enological Research, INCAVI-IRTA, 08720 Vilafranca del Penedes, Spain

ARTICLE INFO

*Article history:*
Available online 30 September 2014

*Keywords:*
Electronic tongue
Linear discriminant analysis
Artificial neural network
Voltammetric sensor
Wine
Sensory panel

ABSTRACT

The approach presented herein reports the application of a voltammetric electronic tongue (ET), in contrast with a wine tasting sensory panel, as a tool for standardized wine tasting; concretely, to achieve the discrimination of different wine DOs (*Denominación de Origen*, a mark related to its geographical region and ensuring high-quality levels) and the prediction of the global score assigned by the trained sensory panel. To this aim, a voltammetric array of sensors based on metallic and bulk-modified graphite electrodes was used as the sensing part, while chemometric tools such as linear discriminant analysis (LDA) and artificial neural networks (ANNs) were used as the qualitative and quantitative modelling tools. Departure information was the set of voltammograms, which were first preprocessed employing fast Fourier transform(FFT), followed by removal of less-significant coefficients employing a stepwise inclusion method and pruning of the inputs. The trend, in global scores, was modelled successfully with a 92.9% of correct identification for the qualitative application, and a correlation coefficient of 0.830 for the quantitative one (with 14 and 20 samples for the external test subsets, respectively).



## 1. Introduction

Over the last decades, there have been important advances in the design of new sensors and biosensors, normally directed to the implementation of new concepts, designs, or configurations, in all cases heading to improved biodevices showing perfect selectivity [1,2]. Unfortunately, there are many factors hindering their application in the required conditions (e.g. matrix effects, secondary responses, irreversible fouling, etc.).

Opposite to that trend, there is a different approach that appeared in the late 1990s that proposes the use of arrays of sensors in order to obtain some added value in the generation of analytical information [3]. Then, generated information is processed by means of advanced chemometric tools able to interpret and extract meaningful data from the complex readings. Curiously, this approach represents a shift of the complexity of the analysis from the chemical to the data processing field [4]; this approach is known as electronic tongue (ET).

According to the agreed IUPAC definition [3], an electronic tongue is "a multisensor system, which consists of a number of low-selective sensors and uses advanced mathematical procedures for signal processing based on pattern recognition (PARC) and/or multivariate data analysis [artificial neural networks (ANNs), principal component analysis (PCA), etc.]". In this way, the underlying motivation of ETs is different from the general trend in the sensor field; that is, instead of pursuing the perfectly selective sensor, to use low-selectivity sensors or with cross-response features, a prerequisite for the development of these biomimetic systems.

Furthermore, given its biomimetic behaviour, ETs represent a straightforward solution when trying to analytically reproduce the sensory information perceived by subjects or tasters towards natural samples, food, beverages, etc. (Fig. 1); e.g. a taste perception, identifying a variety, noticing a defect, etc. [5–8]. That is, even with absence of the knowledge about which compounds are primarily responsible for some sensations, the perceptions are mimicked.

Within this context, ETs have already been successfully applied to the classification or identification of several beverages such as mineral waters, milk, juices, wine, or coffee, between others [9–12]. Within those, wine is a specially regulated beverage, being, in many cases, subjected to a PDO (protected designation of origin) status

* Corresponding author. Tel.: +34 93 5811017; fax: +34 93 5812379.
*E-mail address:* manel.delvalle@uab.cat (M. del Valle).

http://dx.doi.org/10.1016/j.snb.2014.09.081
0925-4005/

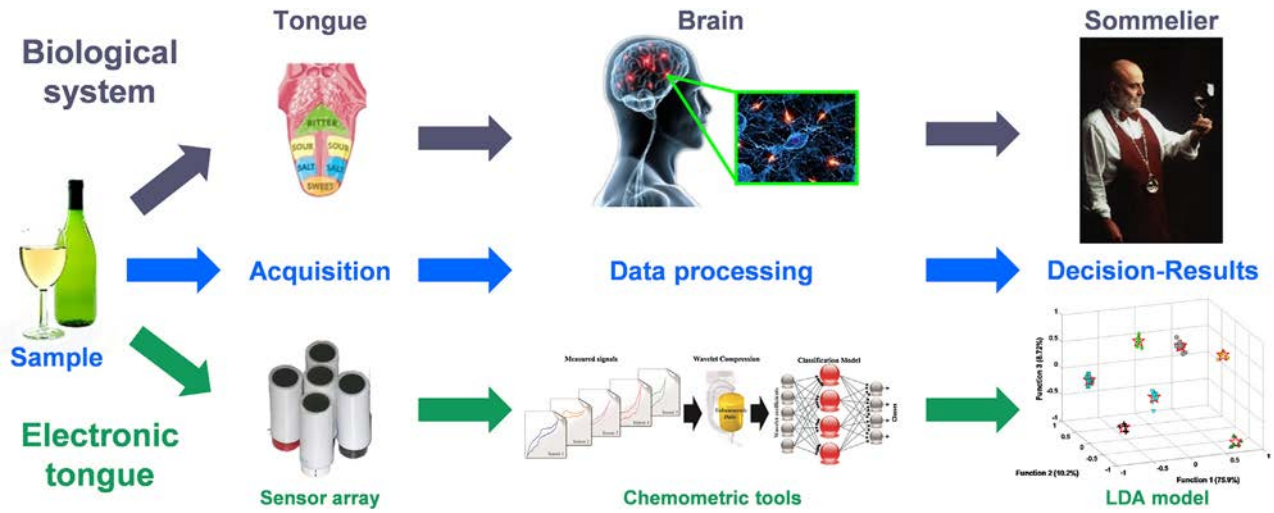


**Fig. 1.** Comparison of the recognition process of a sample by the biological (top) and the biomimetic system (bottom).

and its regulations [13]; in the case of Spain, receiving the appellation DO (*Denominación de Origen*). Therefore its identification has received special attention, together with methodologies for its characterization and elaboration control [11].

However, most of the papers devoted to the application of ETs to wine analysis deal with classification tasks or the numerical prediction of specific chemical parameters or individual taste descriptors (e.g. phenolic content or bitterness level); to the best of authors' knowledge, none of them have achieved the correlation between ET measurements and the global score assigned to wines by a sensory panel.

DOs (or PDOs as defined by the European Union Regulations) are a labelling system established to regulate the quality of Spanish (or the respective European country) foodstuffs based on its region (with well established geographical limits) and food type, which is controlled by a governing body that controls the quality, ingredients and production process of each product in order to ensure attaining specific quality levels in the final food or beverage [14]. Products labelled DOs (or the respective PDOs), apart from being of superior quality, are expected to carry specific characteristics of geographical region or individual producer and be derived from raw materials originating within the region. Like most of these designations, a fundamental tenet of a DO label is that no product outside of that region is permitted to bear that name.

From an analytical point of view, wine is a complex mixture of diverse substances, which exhibit considerable influence on wine's taste and other features. Although declaring the interest, its quality control is still under development and still very much based on wine tasters [11], whose taste and olfaction play an important role in the evaluation of the quality of wine. Therefore, it should be expected that the ability to simultaneously detect a large spectrum of compounds in one step and provide a comprehensive information on the sample within a few seconds can be considered as a basic feature/requirement for the design of an artificial analytical system; a situation that suits perfectly with the concept of ETs.

In this sense, the main goal of this work is to demonstrate the huge capabilities of ET-based systems to mimic the human taste perception and provide an analytical tool for its assessment. More specifically, proposed approach herein is based on the application of a voltammetric ET formed by bulk-modified graphite–epoxy composites and metallic electrodes towards the discrimination of different wine DOs and the prediction of the global score assigned by a standardized sensory panel.

## 2. Experimental

### 2.1. Reagents and solutions

All reagents used were analytical reagent grade and all solutions were prepared using deionised water from a Milli-Q system (Millipore, Billerica, MA, USA). Cobalt(II) phthalocyanine(CoPc), copper and platinum nanoparticles (<50 nm), which were used as electrode modifiers, were purchased from Sigma–Aldrich (St. Louis, MO, USA). Au and Pt metal wires were obtained from Goodfellow (Huntington, UK). Graphite powder (particle size < 50 μm) was received from BDH (BDH Laboratory Supplies, Poole, UK). Epotek H77 resin and its corresponding hardener were supplied from Epoxy Technology (Billerica, MA, USA). Potassium chloride was purchased from Merck KGaA (Darmstadt, Germany).

### 2.2. Samples under study

A total set of 71 wines from different producers were analyzed. All wine samples considered were white bottled wines produced in Catalonia region and commercially available. Those samples were selected according to its DO (that is, the region where the wine is produced), but also taking into account other factors such as grape varieties, vintage, etc. Thus, in order to have a more representative set of samples.

In this sense, Table S2 (supplementary data) summarizes information about the producers and trademarks of the wine samples analyzed; so that, complete information of them (e.g. vintage, grape varieties, DO, fermentation method, etc.) can be checked in *La guia de vins de Catalunya* (the 2014 guide of Catalan wines) [15]. Besides, and if only focusing in their DO, the samples can be categorized as (number of samples belonging to each class in brackets): *Empordà* (10), *Penedès* (11), *Costers del Segre* (8) *Terra Alta* (16), *Priorat* (7), *Montsant* (7), *Catalunya* (10) and *Tarragona* (2). Detailed information on each DO (geographical, climatic, soil, etc.) might be found in [16].

Additionally, parameters such as alcohol by volume (abv), volatile acidity, pH or the amount of sugar between others were analyzed following regulated methods to further characterize samples under study and to guarantee they fulfil required standards by the DO [17]. This information, although not used in this study, is presented also in Table S2.

### 2.3. Sensory panel evaluation

Taste attributes of the wines considered were assessed by a panel of 8 wine experts under usual established procedures [18]. The panellists were professional wine tasters from the panel tasting of the different DOs included in this study. All of them were fully trained and with more than five years of experience in evaluating the wines for the different editions of the Catalan wines guide.

Briefly, the 71 wine samples were randomly divided in groups of 8, evaluating one group per day. Randomized samples of 25–30 ml were served in clear glasses NF V09-110 (AFNOR 1995) marked with three digit random numbers and covered with Petri dishes. Water was provided for rinsing the palate during tasting. Evaluations were conducted at 20–22 °C. No information of the type of wine or its DO was provided to the panellists.

In this way, the subjects were asked to rate the global sensory quality of the wines (sight, aroma and taste) by assigning it a value ranging from 0 to 10 (for each of the three parameters); and the assigned score given to each wine was calculated as the weighted mean as follows: sight × 0.3 + aroma × 0.35 + taste × 0.35. Afterwards, the final score was obtained from the mean of the eight panellists. On that account, such information of considered samples can be found in Table S2 (supplementary data) as well as in *La guia de vins de Catalunya* (the 2014 guide of Catalan wines) [15].

### 2.4. Electronic tongue sensor array

A hybrid electronic tongue formed by both bulk-modified graphite composites and metal wire electrodes was used for samples measurement. The latter consisted of 1 mm diameter metal wires casted into the epoxy resin [19], while the formers were prepared by mixing the resin, graphite powder and a modifier in a ratio 83:15:2 (w/w) [20]. In both cases, resin was allowed to harden at 80 °C for three days, and afterwards, electrode surfaces were polished with different sandpapers of decreasing grain size. Final electrodes area was 28 and 0.79 $mm^2$ for composite and metal electrodes, respectively.

In this manner an array of 6 voltammetric electrodes was prepared, consisting in two metallic Au and Pt electrodes plus four composite electrodes, one unmodified epoxy-graphite electrode and three using Cu nanoparticles, Pt nanoparticles and cobalt(II) phthalocyanine as the modifiers.

These modifiers/catalysts were selected based on previously reported studies with wines, either from other research groups or from our laboratories, in order to obtain a variety of electrodes with significant cross-selectivity and complementary electroactive properties that allow the obtaining of rich information to enhance modelling capabilities [21,22]. The desired situation in ETs applications.

Electrodes modified with phthalocyanines (mainly CoPc and its derivatives) are interesting for being efficient electrocatalysts in the determination of many important inorganic, organic or biological compounds [21]; while nanoparticles have emerged as interesting electroactive material in electroanalysis; these are alternative to bulk metals, with catalytic and electrocatalytic peculiarities, mainly derived from their higher surface/mass ratio [22]. Lastly, the usage of bare metallic electrodes respond to some approaches followed by some research groups in the field of ETs [23], while also provides an opportunity to assess the differences found between those and the nanoparticles-modified electrodes.

### 2.5. Voltammetric measurements

The measurement cell was formed by the 6-sensor voltammetric array and a reference double junction Ag/AgCl electrode (Thermo Orion 900200, Beverly, MA, USA) plus a commercial platinum counter electrode (Model 52-67, Crison Instruments, Barcelona, Spain).

Cyclic voltammetry measurements were carried out at room temperature (25 °C), in a multichannel configuration, using a 6-channel AUTOLAB PGSTAT20 (Ecochemie, Netherlands) controlled with GPES Multichannel 4.7 software package.

In order to get stable voltammetric responses, ensuring reproducible signals from the ET array along the whole experiment, electrodes were first cycled in saline solution (i.e. 10 mM KCl). Afterwards, an aliquot of 25 ml of wine was directly used for each measurement, without any sample pretreatment.

In this manner, a complete voltammogram was recorded for each sample by cycling the potential between −1.0 V and +1.3 V vs. Ag/AgCl with a step potential of 9 mV and a scan rate of 100 mV $s^{-1}$. Additionally, an electrochemical cleaning stage was carried out between each measurement to prevent any cumulative effect of impurities on the working electrode surfaces, and avoiding to perform any physical surface regeneration of those. To this end, a conditioning potential of +1.5 V was applied during 40 s in a cell containing 25 ml of distilled water [24]. As in the case of the panel of experts, all samples were analyzed in random order.

### 2.6. Data processing

Chemometric processing of the data was done in MATLAB 7.1 (MathWorks, Natick, MA, USA) using specific routines written by the authors, and its Neural Network Toolbox (v.4.0.6). Concretely, principal component analysis (PCA) and linear discriminant analysis (LDA) were used for qualitative analysis of the results, while quantitative analysis was achieved by means of artificial neural networks (ANNs).

In the case considered, the large dimensionality of the data generated due to the usage of voltammetric sensors (that is, when a complete voltammogram is recorded for each sensor from the array) hinders their treatment; especially if ANNs are to be used. This is because it is widely recommended to employ a dataset for training with larger number of samples than the number of interconnection weights that are then needed to be calculated. If a single voltammogram is formed by hundreds of current values, and a sensor array is then used, the difficulty of the problem is made evident. Therefore, one solution when dealing with a set of voltammograms is to employ a preprocessing stage for data reduction. The main objective of such a step is to reduce the complexity of the input signal while preserving the relevant information, which in addition allows to gain advantages in training time, to avoid redundancy in input data and to obtain a model with better generalization ability [25].

In addition, removal of less significant coefficients that barely contribute to the model (i.e. with low information content) might also improve model performance. That is, having a list of independent variables, some of which may be useful predictors, but some of which are almost certainly useless, the aim is to find the best subset to do the prediction task as well as possible, with as few variables as possible.

In our case, compression of voltammetric data was achieved by means of fast Fourier transform (FFT) [26], while pruning of the inputs was done either using a stepwise inclusion method for LDA [27] or causal index (CI) pruning for ANN model [25,28]. More specifically, a feed-forward network with a back-propagation algorithm which is used to train it according to a learning rule, what is known as multilayer perceptron (MLP) [29].

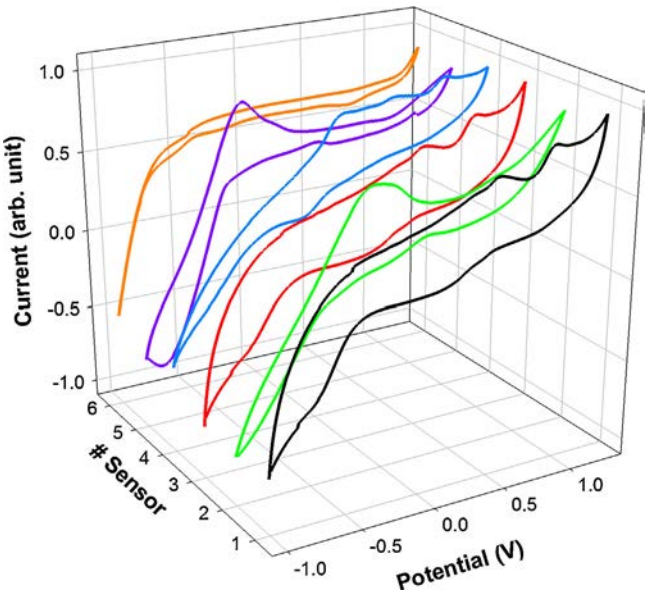


**Fig. 2.** Example of the different voltammograms obtained with the different sensors forming the ET array for an arbitrary wine sample. Signals provided correspond to: (1) graphite–epoxy sensor, (2) Pt nanoparticle modified sensor, (3) cobalt(II) phthalocyanine modified sensor, (4) Cu nanoparticle modified sensor, (5) Pt metallic sensor and (6) Au metallic sensor.

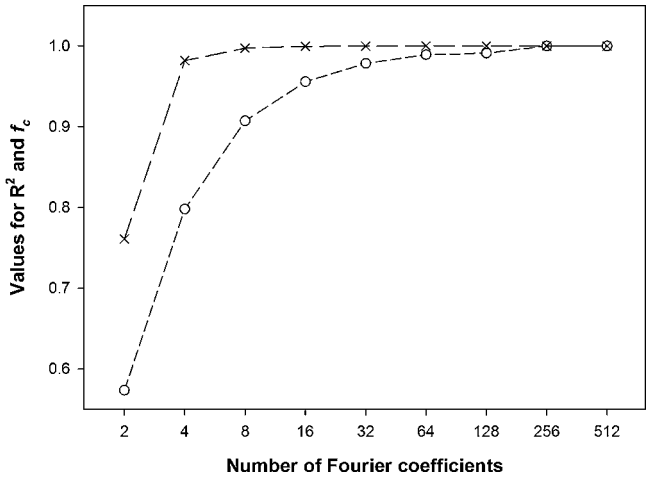


**Fig. 3.** FFT data pre-processing. Representation of the coefficient of determination, $R^2(x)$ and $f_c$ (○) as a measure of the signal reconstruction degree, vs. the number of Fourier coefficients used. For better representation of the data, *Y*-axis is plotted in linear-scale, while *X*-axis is in log-scale.

Sigmaplot (Systat Software Inc., San Jose, CA) was used for graphic representations of data and results.

## 3. Results and discussion

As already commented, the aim of this work was to demonstrate the capabilities of ET-based systems as an analytical tool capable of reproducing the expertise of wine tasters. In this direction, we focused in two specific cases. On the one hand, we evaluated the discrimination of different wine DOs; while on the other hand, we attempted the correlation of ET response with the scores assigned by a sensory panel. Both examples would show the potentialities of ET-systems to translate the subjective evaluations of a sensory panel into conventional qualitative or quantitative information (Fig. 1).

As from the definition of ET of the IUPAC, the first condition for the development of an ET is that we must have an array of low-selective sensors with cross-response features that provide some added value in the generation of analytical information.

Hence, we should firstly confirm that differentiated signals are observed for the different electrodes, and that those are related to the phenomena under study. That is, generating data rich enough that can be a useful departure point for the multivariate calibration model. In our case, we can see how that can be achieved thanks to the use of the different modifiers and the metal wires (Fig. 2); even in the case of Pt nanoparticles and Pt wire, where still some differences may be observed. In this case probably due to catalytic phenomena attributable to large surface to volume ratio of the nanoparticles.

To provide an objective measure of the differences observed for the different sensors towards wine samples, correlation between their responses was evaluated by means of the comparison factor *fc* which considers the area under both signals when superimposed (Fig. S1, supplementary data). Briefly, *fc* is defined as the ratio of the area intersected by both curves to the total area under them, and ranges from 0 to 1 depending on signals similarity; it values 0 when the two signals have nothing in common and increases its value as similarity does. Thus, obtaining a unique numerical value that provides a measure of its resemblance. In our case, calculated values are summarized in Table S1 (supplementary data) where, as can be seen, those are around 0.7 and even as low as 0.54. These numeric values corroborate and objectivize what is already seen in Fig. 2.

After this initial confirmation, the next step is to assess whether or not the recorded signals are related to the phenomena under study. However, this cannot always be checked so easily, requiring the use of advanced chemometric tools which, as the IUPAC report reminds us, are the ones extracting and interpreting the relevant information. Therefore, in the next sections we will focus on discerning the richness of the generated data and its suitability for the desired outputs.

At this point, given the complexity of the generated data, FFT was used as a preprocessing step in order to reduce the high dimensionality requirements of the processing, which additionally may result in an improvement of model's performance. In this manner, each voltammogram was compressed down to only 32 coefficients without any loss of significant information (Fig. 3) [30]; this allowed for a compression of the original data up to 93.75% (from 512 current values down to 32 coeffs.), prior to pattern recognition or numerical modelling.

### 3.1. Identification of the DO for the same grape variety

As a first attempt to assess whether or not the ET would be capable to distinguish the wine samples based on its DO, we focused on a specific grape variety and analyzed some wine samples from that variety, but produced in different regions. Hence, reducing the source of variability and ensuring the source of the discrimination factor; that is, to asses if there is or not an effect due to its origin.

To this aim, a total subset of nine samples, all from *Garnatxa Blanca* variety, produced in three different DO regions (*Empordà*, *Terra Alta* and *Montsant*) were initially considered. Samples were analyzed as previously described in Section 2.4, and an extract of the recorded signals has already been shown in Fig. 2.

Once confirmed the cross-response features of the ET, we should look now for (dis)similarities along the recorded signals that might indicate whether or not analyzed samples might be distinguished by means of the ET. Hence, looking more deeply in the voltammetric responses, we can observe some distinguished features that seem to originate depending on the DO; e.g. some anodic peaks that can

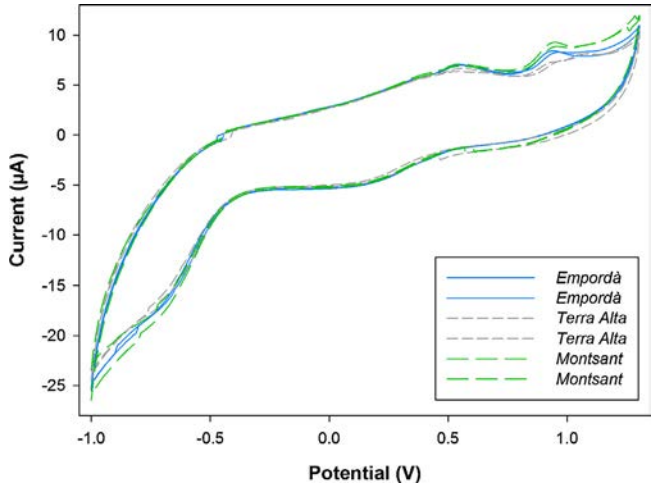


**Fig. 4.** Example of the different voltammograms obtained with graphite–epoxy sensor for some samples of the same grape variety (*Garnatxa Blanca*). Signals provided correspond to: (solid line) *Empordà*, (short dashed line) *Terra Alta* and (long dashed line) *Montsant* DOs.

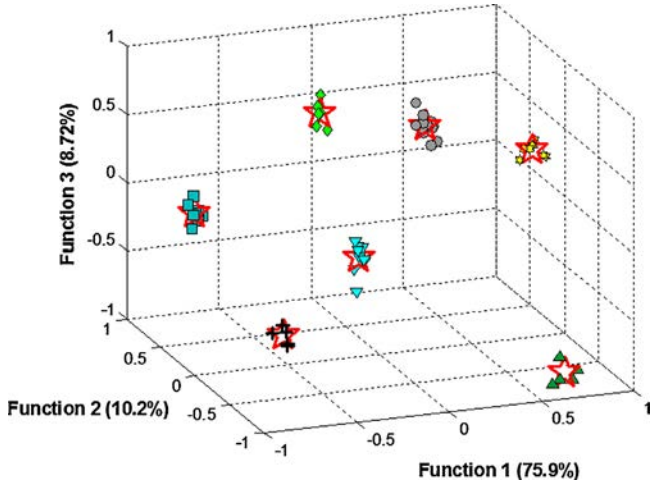


**Fig. 6.** Score plot of the first three functions obtained after LDA analysis of the wine samples, according to their DO: (■) Empordà, (▼) Penedès, (♦) Costers del Segre, (●) Terra Alta, (+) Priorat, (▲) Montsant and (☆) Catalunya; also the centroid of each class is plotted (⋆).

be observed around +1.0 V for graphite–epoxy sensor (Fig. 4), but also at the anodic wave in the region from −0.5 to −1.0 V.

To confirm this differentiated behaviour, voltammetric responses were compressed employing FFT, and obtained coefficients were analyzed employing PCA (Fig. 5); an unsupervised method which provides a better representation of samples (dis)similarities, but not performing its classification. As could be expected from the voltammograms, the PCA plot shows how some samples seem to group in clusters, thus indicating some similarities between those samples and suggesting that the ET should be capable of distinguishing such factor (i.e. the effect of the different DOs in the final wine). Moreover, it should be also noticed that with only the first two PCs, the accumulated explained variance was ca. 79.8%; a large value which means that most of the variance contained in the original information is now represented by only these two new coordinates.

### 3.2. Discrimination of different DOs

Due to the satisfactory trend already observed in the previous analysis, the whole set of samples were analyzed with the ET

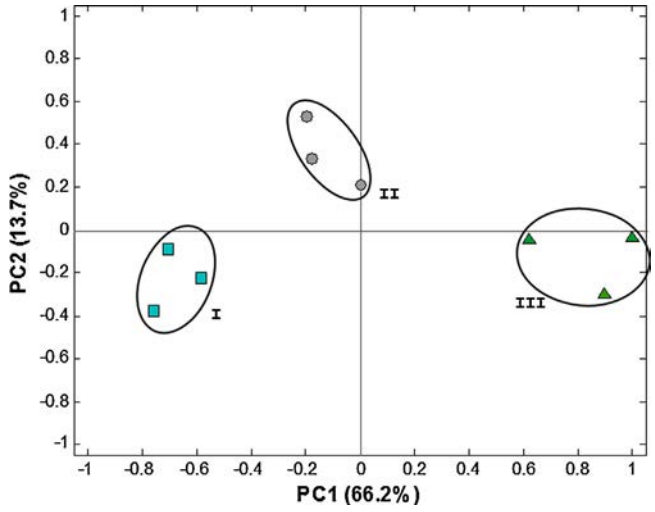


**Fig. 5.** Score plot of the first two components obtained after PCA analysis of *Garnatxa Blanca* wine samples: (■), I, *Empordà*, (●), II, *Terra Alta* and (▲), III, *Montsant*.

array and recorded signals compressed employing FFT as previously done, but this time LDA was chosen for pattern recognition of the different DOs. This alternative was chosen given that, unlike PCA which only provides a visualization tool of the variability of the data, LDA is a supervised method that allows to actually build a classification model [27]. That is, LDA explicitly attempts to model the difference between the classes of data, while PCA does not.

Therefore, the whole set of 71 samples was categorized according its DO as follows (number of samples): *Empordà* (10), *Penedès* (11), *Costers del Segre* (8) *Terra Alta* (16), *Priorat* (7), *Montsant* (7), *Catalunya* (10) and *Tarragona* (2). Unfortunately, compared to the other classes, very few samples from DO *Tarragona* were available, and hence it would result problematic to build a proper classification model without overfitting it if those were included. Accordingly, those samples were not considered for further calculations.

Lastly, as LDA is a supervised method, some samples from the set must be left out when building the model so that they can be used to assess its performance. In our case, the model was trained with 80% of the data (training subset), using the remaining 20% of the data (testing subset) to characterize the accuracy of the classification model and obtain unbiased data (Tables S3 and S4, supplementary data).

Fig. 6 displays the distribution of the wine samples along the first three new coordinates, showing an accumulated variance of 94.8%; a high value indicating that nearly all the variance contained in the original information is represented now by only these three new functions. As can be observed, discrimination of the different wines according to its DOs can be achieved with this simple analysis of the new coordinates. Nevertheless, it should be taken into account that the actual LDA model is composed by 6 functions (number of groups − 1) and that all of them are used to perform the classification task; although not being possible to visualize it.

Despite the good clustering observed in the built pattern recognition model (Fig. 6), its actual performance should be assessed employing the samples from the testing subset, and not only the ones from the training subset. To this aim, the generated model was used to predict the expected DO for the 14 samples that were left out (not being used at all) during the modelling stage and predicted classes were compared to the expected ones. The corresponding confusion matrix was then built (Table 1), allowing to calculate the performance of the model by means of three different indicators: classification rate, sensitivity and specificity.

**Table 1**
Confusion matrix built according to the DO category obtained using the LDA model for the testing subset samples.

| | Emp[b] | Pen[b] | CdS[b] | TA[b] | Pri[b] | Mon[b] | Cat[b] |
|---|---|---|---|---|---|---|---|
| Emp[a] | 1 | 0 | 0 | 0 | 1 | 0 | 0 |
| Pen[a] | 0 | 2 | 0 | 0 | 0 | 0 | 0 |
| CdS[a] | 0 | 0 | 2 | 0 | 0 | 0 | 0 |
| TA[a] | 0 | 0 | 0 | 2 | 0 | 0 | 0 |
| Pri[a] | 0 | 0 | 0 | 0 | 2 | 0 | 0 |
| Mon[a] | 0 | 0 | 0 | 0 | 0 | 2 | 0 |
| Cat[a] | 0 | 0 | 0 | 0 | 0 | 0 | 2 |

Emp: Empordà; Pen: Penedès; CdS: Costers del Segre; TA: Terra Alta; Pri: Priorat; Mon: Montsant; Cat: Catalunya.
[a] Expected.
[b] Found.

The former corresponds to the ratio between the number of samples correctly classified and the total number of samples. While the latter two, are related to the number of false positives or false negatives. Sensitivity is calculated as the percentage of objects of each class identified by the classifier model, and specificity as the percentage of objects from different classes correctly rejected by the classifier model; averaging those for the classes. In this case, values reached 92.9%, 92.9% and 98.8% for the classification rate, sensitivity and specificity, respectively.

Similarly, in order to evaluate if the only miss-classified sample could be an outlier, model performance was also evaluated employing the leave-one-out strategy, regardless the fact this has been sometimes criticized as overoptimistic [8]. The idea here is that the use of a larger number of samples in the training subset might improve the model generalization ability. In this manner, LDA model was rebuilt, and as it could be expected given that wines are already subjected to strict DO controls, none of the samples were now miss-classified, achieving a classification rate of 100% in terms of accuracy, sensitivity and specificity.

### 3.3. Prediction of global scores of the sensory panel

To further assess the ability of the ET as a tool for wine tasting, the correlation between the ET measurements and the global scores assigned by the sensory panel was also attempted. That is, the average scores assigned to each wine by the sensory panel were modelled from the set of voltammetric responses, previously compressed with FFT, by means of an ANN model.

Unlike the previous cases, where qualitative information was extracted, a quantitative model was built this time. For this, ANN was selected as the modelling tool due to its superior performance compared to linear methods; i.e. more flexible modelling methodologies, since both linear and non-linear functions can be used (or combined) in the processing units [31]. Thus, ANNs are specially suitable to be used with non-linear sensor responses and allow for more complex relationships between a high-dimensional descriptor space and the given retention data; all this leads to a better predictive power of the resulting ANN model compared with other linear methods [25], although if linearity exists, a proper behaviour may be obtained also with the latter.

As before, the set of samples were split into two subsets: the training subset (49 samples, 71%) used to build the model and the testing subset (20 samples, 29%) used to assess its performance. Again, this division was randomly performed, taking as only precaution to avoid that extreme values are used in the testing subset; that is, to avoid extrapolation from the model.

After a systematic study to optimize the topology of the neural network (i.e. training algorithm, number of hidden layers, number of neurons, transfer functions, etc.), the final architecture of the ANN model had 80 neurons (corresponding to the selected FFT coeffs. after CI analysis) in the input layer, 6 neurons and *logsig* transfer function in the hidden layer and one neuron and *tansig* transfer function in the output layer, viz. the score assigned by the sensory panel.

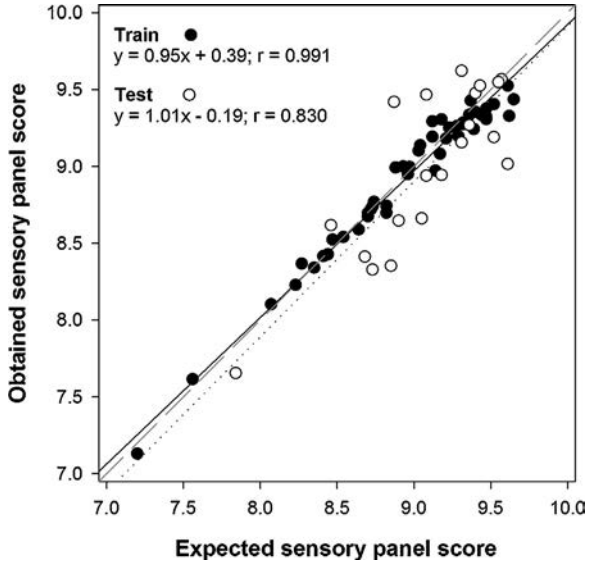


**Fig. 7.** Modelling ability of the optimized FFT-ANN for the prediction of wines global scores assigned by the sensory panel. Set adjustments of obtained vs. expected values, both for training (●, solid line) and testing subsets (○, dotted line). The dashed line corresponds to theoretical diagonal line.

Subsequently, comparison graphs of predicted vs. expected scores, both for the training and testing subsets, were built and the linear fitted regression parameters were calculated to easily check the performance of the ANN model (Fig. 7). As it can be observed, a satisfactory trend was obtained for both subsets, with regression lines close to the theoretical ones; i.e. values of slope and intercept close to 1 and 0, respectively.

To numerically assess the predictive ability of the ET three different parameters were calculated: standard error of prediction (SEP), ratio of standard error of performance to standard deviation (RPD) and range error ratio (RER) [32]; with obtained values of 0.30, 1.48 and 5.93, respectively.

However, despite the good trend observed, it is true that the observed dispersion, especially for the testing subset, is larger than desirable for a quantitative application; but still good enough to be considered at least as a semi-quantitative approach. It should be highlighted anyhow that still correlation and the followed trend are highly significant. Moreover, considering the subjective nature of the scores, which are provided by the sensory panel.

As an additional verification of the proposed approach, a Student's paired samples *t* test for the testing subset was performed. Obtained experimental *t* value was 1.42, while the critical tabulated *t* value with 95% confidence level and 19 degrees of freedom is 2.09. Therefore, confirming the agreement observed between the ET response and the scores assigned by the sensory panel.

And last but not least, it should be taken into account the complexity of the approach and the promising capabilities that this represents; i.e. achieving to artificially reproduce the tasting perception of a sensory panel.

## 4. Conclusions

Electronic tongues have proved to be a useful tool for wine tasting, either for qualitative or quantitative analysis, especially suitable for screening purposes, with interesting advantages as might be its simplicity and low cost. Concretely, in this case we reported its application towards the qualitative discrimination

of different wine DOs and the quantification of the global score assigned by a sensory panel; the latter corresponding to the first attempt to correlate such parameter in wines, to the best of author's knowledge.

Moreover, the use of both bulk-modified electrodes and metallic electrodes has also been demonstrated to be a feasible way to obtain sensors with differentiated and cross-selectivity response towards desired samples; which if required, can be easily miniaturized and mass-produced through the use of screen-printed technologies.

Finally, future efforts with this approach may involve its further validation (e.g. extending it to the analysis of wines from other regions) and the miniaturization of the system. Beyond, further work is still required to improve the biomimetic capabilities of the ET array to artificially assess the tasting score of the wines. In this direction, this might be improved through the incorporation of new voltammetric electrodes in the array or through the combination of the ET response with sensors from other nature such as would be an electronic nose or an electronic eye. That is, to better reproduce the overall perceptions perceived by the sensory panel or the sommelier when tasting a wine (i.e. taste, odour and colour) in what might be considered as an electronic panel.

## Acknowledgments

Financial support for this work was provided by the Spanish Ministry of Science and Innovation, MCINN (Madrid) through project CTQ2010-17099. Manel del Valle thanks the support from *Generalitat de Catalunya* and from the program ICREA Academia. Andreu González thanks *Universtitat Autònoma de Barcelona* for the PIF fellowship.

## Appendix A. Supplementary data

Supplementary data associated with this article can be found, in the online version, at http://dx.doi.org/10.1016/j.snb.2014.09.081.

## References

[1] W. Yang, K.R. Ratinac, S.P. Ringer, P. Thordarson, J.J. Gooding, F. Braet, Carbon nanomaterials in biosensors: should you use nanotubes or graphene? Angew. Chem. Int. Ed. 49 (2010) 2114–2138.
[2] Y. Shao, J. Wang, H. Wu, J. Liu, I.A. Aksay, Y. Lin, Graphene based electrochemical sensors and biosensors: a review, Electroanalysis 22 (2010) 1027–1036.
[3] Y. Vlasov, A. Legin, A. Rudnitskaya, C. Di Natale, A. D'Amico, Nonspecific sensor arrays ("electronic tongue") for chemical analysis of liquids (IUPAC technical report), Pure Appl. Chem. 77 (2005) 1965–1983.
[4] R. Bro, Review on multiway analysis in chemistry – 2000–2005, Crit. Rev. Anal. Chem. 36 (2006) 279–293.
[5] K. Toko, A taste sensor, Meas. Sci. Technol. 9 (1998) 1919.
[6] A. Rudnitskaya, H. Nieuwoudt, N. Muller, A. Legin, M. du Toit, F. Bauer, Instrumental measurement of bitter taste in red wine using an electronic tongue, Anal. Bioanal. Chem. 397 (2010) 3051–3060.
[7] A. Rudnitskaya, E. Polshin, D. Kirsanov, J. Lammertyn, B. Nicolai, D. Saison, F.R. Delvaux, F. Delvaux, A. Legin, Instrumental measurement of beer taste attributes using an electronic tongue, Anal. Chim. Acta 646 (2009) 111–118.
[8] D. Kirsanov, O. Mednova, V. Vietoris, P.A. Kilmartin, A. Legin, Towards reliable estimation of an electronic tongue predictive ability from PLS regression models in wine analysis, Talanta 90 (2012) 109–116.
[9] A. Riul Jr., C.A.R. Dantas, C.M. Miyazaki, O.N. Oliveira Jr., Recent advances in electronic tongues, Analyst 135 (2010) 2481–2495.
[10] L. Escuder-Gilabert, M. Peris, Review highlights in recent applications of electronic tongues in food analysis, Anal. Chim. Acta 665 (2010) 15–25.
[11] J. Zeravik, A. Hlavacek, K. Lacina, P. Skladal, State of the art in the field of electronic and bioelectronic tongues – towards the analysis of wines, Electroanalysis 21 (2009) 2509–2520.
[12] P. Ciosek, W. Wroblewski, Sensor arrays for liquid sensing – electronic tongue systems, Analyst 132 (2007) 963–978.
[13] Commission Regulation (EEC), Quality schemes for agricultural products and foodstuffs, in: Official Journal L 343, Publication Office of the European Union, 14 December 2012, pp. 1–29.
[14] Commission Regulation (EEC), Protection of geographical indications and designations of origin for agricultural products and foodstuffs, in: Official Journal L 369, Publication Office of the European Union, 14 December 2006, pp. 1–19.
[15] J. Alcover, S. Naranjo, Guia de vins de Catalunya 2014, Editorial Pòrtic, Barcelona, 2013.
[16] INCAVI, 2014, Available from http://incavi.gencat.cat/ca/dar_denominacions_origen_protegides/ (retrieved 9.07.14).
[17] Commission Regulation (EEC), Community methods for the analysis of wines, in: Official Journal L 272, Publication Office of the European Union, 17 September 1990, pp. 0001–0192.
[18] R.S. Jackson, Wine Tasting: a Professional Handbook, Academic Press, London, 2002.
[19] A. Gutés, F. Cespedes, M. del Valle, D. Louthander, C. Krantz-Rülcker, F. Winquist, A flow injection voltammetric electronic tongue applied to paper mill industrial waters, Sens. Actuators B 115 (2006) 390–395.
[20] S. Alegret, J. Alonso, J. Bartroli, F. Céspedes, E. Martinez-Fábregas, M. del Valle, Amperometric biosensors based on bulk-modified epoxy graphite biocomposites, Sens. Mater. 8 (1996) 147–253.
[21] M.L. Rodríguez-Méndez, V. Parra, C. Apetrei, S. Villanueva, M. Gay, N. Prieto, J. Martinez, J.A. de Saja, Electronic tongue based on voltammetric electrodes modified with materials showing complementary electroactive properties, Appl. Microchim. Acta 163 (2008) 23–31.
[22] J.M. Gutiérrez, L. Moreno-Barón, M.I. Pividori, S. Alegret, M. del Valle, A voltammetric electronic tongue made of modified epoxy–graphite electrodes for the qualitative analysis of wine, Microchim. Acta 169 (2010) 261–268.
[23] F. Winquist, Voltammetric electronic tongues – basic principles and applications, Microchim. Acta 163 (2008) 3–10.
[24] X. Cetó, J.M. Gutiérrez, L. Moreno-Barón, S. Alegret, M. del Valle, Voltammetric electronic tongue in the analysis of cava wines, Electroanalysis 23 (2011) 72–78.
[25] X. Cetó, F. Céspedes, M. del Valle, Comparison of methods for the processing of voltammetric electronic tongues data, Microchim. Acta 180 (2013) 319–330.
[26] X. Cetó, F. Céspedes, M. del Valle, BioElectronic tongue for the quantification of total polyphenol content in wine, Talanta 99 (2012) 544–551.
[27] R.A. Johnson, D.W. Wichein, Applied Multivariate Statistical Analysis, Pearson Education, Harlow, GB, 2007.
[28] Z. Boger, Selection of quasi-optimal inputs in chemometrics modeling by artificial neural network analysis, Anal. Chim. Acta 490 (2003) 31–40.
[29] J.R.M. Smits, W.J. Melssen, L.M.C. Buydens, G. Kateman, Using artificial neural networks for solving chemical problems: Part I. Multi-layer feed-forward networks, Chemom. Intell. Lab. Syst. 22 (1994) 165–189.
[30] L. Moreno-Barón, R. Cartas, A. Merkoçi, S. Alegret, M. del Valle, L. Leija, P.R. Hernandez, R. Muñoz, Application of the wavelet transform coupled with artificial neural networks for quantification purposes in a voltammetric electronic tongue, Sens. Actuators B 113 (2006) 487–499.
[31] F. Despagne, D.L. Massart, Neural networks in multivariate calibration, Analyst 123 (1998) 157R–178R.
[32] T. Fearn, Assessing calibrations: SEP, RPD, RER and R2, NIR News 13 (2002) 12–14.

## Biographies

**Xavier Cetó** completed his M.Sc. degree in chemistry in 2009 at the *Universitat Autònoma de Barcelona*, and received his Ph.D. in Analytical Chemistry in 2013 from the same university. At present, he is a postdoctoral researcher at Mawson Institute. His main research topics deal with the development of new voltammetric (bio)sensors and the application of electronic tongues and chemometric tools for data analysis, mainly employing voltammetric (bio)sensors, albeit also potentiometric ones.

**Andreu Gonzàlez** received his M.Sc. degree in Chemistry in 2013 from the *Universtitat Autònoma de Barcelona*, where he is at the moment completing his Ph.D. in Analytical Chemistry. His main research topics deal with the application of Electronic Tongues as a tool for security and food safety analysis.

**Josefina Capdevila** received a degree in Chemistry from the *Universtitat Autònoma de Barcelona* in 1997, where she later finished her M.Sc. in Food Science with the research study titled "Study of phenolic composition applied to the characterization of wines from Penedès D.O.". Since 1999 she is working as a researcher at INCAVI and her scientific interests are chemical analysis of wine.

**Anna Puig** received his degree in Biology from the *Universitat de Barcelona* in 1992, and her PhD in Biology (Microbiology) in 1998 from the same University. She also completed the degree in Oenology in 2001 from the *Universitat Rovira i Virgili*, where she received a final special award in Oenology studies. Since 1998 she is working as a researcher at INCAVI, and in 2003 she became a member of the research staff of IRTA. At present, she is responsible of the biotechnology laboratory of INCAVI.

**Manel del Valle** received his Ph.D. in Chemistry in 1992 from the *Universtitat Autònoma de Barcelona*, where he got a position of associate professor in Analytical Chemistry. He is a member of the Sensors & Biosensors Group where he is a specialist for instrumentation and electrochemical sensors. He has initiated there the research lines of sensor arrays and electronic tongues. Other interests of his work are the use of impedance measurements for sensor development, biosensors and the design of automated flow systems.

# Article 5:

**Electronic tongues to assess wine sensory descriptors**

Xavier Cetó, Andreu González-Calabuig, Nora Crespo, Sandra Pérez, Josefina Capdevila, Anna Puig-Pujol and Manel del Valle

*Talanta* 162 (2017) 218–224

DOI: 10.1016/j.talanta.2016.09.055

Talanta 162 (2017) 218–224

Contents lists available at ScienceDirect

Talanta

journal homepage: www.elsevier.com/locate/talanta

# Electronic tongues to assess wine sensory descriptors

Xavier Cetó[a], Andreu González-Calabuig[b], Nora Crespo[b], Sandra Pérez[a,b], Josefina Capdevila[c], Anna Puig-Pujol[c], M.del Valle[b,*]

[a] Future Industries Institute, University of South Australia, 5095 Adelaide, Australia
[b] Sensors and Biosensors Group, Department of Chemistry, Universitat Autònoma de Barcelona, Edifici Cn, 08193 Bellaterra, Barcelona, Spain
[c] Estació de Viticultura i Enologia, INCAVI-IRTA, 08720 Vilafranca del Penedès, Spain

ARTICLE INFO

*Keywords:*
Electronic tongue
Voltammetric sensors
Partial least squares regression
Wine
Sensory panel
Ageing

ABSTRACT

This work reports the application of an electronic tongue as a tool towards the analysis of wine in tasks such as its discrimination based on the maturing in barrels or the prediction of the global scores assigned by a sensory panel. To this aim, red wine samples were first analysed with the voltammetric sensor array, without performing any sample pretreatment. Afterwards, obtained responses were preprocessed employing fast Fourier transform (FFT) for the compression and reduction of signal complexity, and obtained coefficients were then used as inputs to build the qualitative and quantitative models employing either linear discriminant analysis (LDA) or partial least squares regression (PLS), respectively. Satisfactory results were obtained overall, with a classification rate of 100% in the discrimination of the type of barrel used during wine maturing, a normalized NRMSE of 0.077 in the estimation of ageing time (months) or 0.11 in the prediction of the scores (0–10) from a trained sensory panel (all for the external test subset).

## 1. Introduction

Wine is a specially regulated beverage, and its characterization receives much attention from different bodies and administrations [1–3]. However and despite the interest, wine quality control is still highly dependant on wine tasters; this is due to the difficulties to reproduce human perception using classical analytical techniques. That is, the challenge is to relate wine aroma or taste to specific compounds (and later to carry out its quantification), whereas it is known that perceived organoleptic properties originate on the contribution of the many compounds present and on their interactions.

Therefore, to get a system capable to artificially reproduce the wine tasting descriptors perceived by a skilled sensory panel, it should simultaneously detect a large spectrum of compounds and provide comprehensive information of the sample [4]. These two pre-requisites perfectly suit the concept of electronic tongues (ETs) and electronic noses [5], that thanks to their bioinspired nature, represent a straightforward solution when trying to analytically reproduce the sensory information perceived by subjects or tasters towards food or beverages.

ETs are based on the usage of an array of sensors with low-selectivity and/or cross-response features in order to obtain some added value in the generation of analytical information; the latter is further coupled with advanced chemometric tools that allow the interpretation and extraction of meaningful data from the complex readings [6]. Thus, instead of focusing on finding highly selective sensors, ETs are inspired and try to mimic the sensory ability of taste in mammals: in these, a few receptors can respond to a large variety of substances thanks to the combinatorial principles used, being the obtained information later processed by the brain [7].

On this account, ETs have started to be significant in foodstuff analysis over the last years, with application examples as the identification of different types/varieties/defects of samples or as the quantification of certain components present [8]. More specifically, ETs have already been successfully applied to the classification or identification of several beverage types: mineral water, wine, beer, spirits, milk, juice, tea or coffee, among others [9–11].

In the case of wine analysis [4], reported publications are aimed mainly to classification tasks (e.g. the discrimination of samples of different varieties/origins) [12–14] or to the prediction of certain chemical parameters or individual taste descriptors (e.g. total acidity, phenolic content or bitterness level) [12,15]. Moreover, there are also other interesting works focused on e.g. the detection of inappropriate handling practices or adulteration processes [16,17], the use of alternative ageing methods [12,18] or the monitoring of alcoholic fermentation [19]. However, to the best of authors' knowledge, very few attempts have been described in relation to the correlation between ET measurements and the global scores assigned to wines by a standardized sensory panel. A global score is a numerical mark, given

* Corresponding author.
*E-mail address:* manel.delvalle@uab.cat (M.d. Valle).

http://dx.doi.org/10.1016/j.talanta.2016.09.055
Received 26 July 2016; Received in revised form 20 September 2016; Accepted 23 September 2016
Available online 24 September 2016

mostly in wine marketing context in order to indicate the quality of a wine from the subjective point of view of an expert.

In this context, the work presented herein aims to demonstrate the capabilities of ET-based systems to mimic the human taste perception, and hence to provide an analytical tool for the evaluation of wine tasting descriptors. Among the different wine descriptors, wine maturing practices and wine tasting scores were the considered scenarios to evaluate the potential of ETs in this field. To this aim, a voltammetric sensor array based on metallic electrodes and bulk-modified graphite-epoxy composites was prepared and employed for the analysis of the wine samples.

## 2. Experimental

### 2.1. Reagents and chemicals

All reagents were analytical reagent grade and all solutions were prepared using deionised water from a Milli-Q system (Millipore, Billerica, MA, USA). Potassium chloride was purchased from Merck KGaA (Darmstadt, Germany). Cobalt (II) phtalocyanine, copper and platinum nanoparticles ( < 50 nm) which were used as electrode modifiers, were purchased from Sigma-Aldrich (St. Louis, MO, USA). The Au and Pt wires (diameter 1 mm) employed in the construction of the metallic electrodes were purchased from Goodfellow (Cambridge, UK).

Besides, graphite powder (particle size 50 μm; BDH Laboratory Supplies, Poole, UK) and Epotek H77 resin and its corresponding hardener (Epoxy Technology, Billerica, MA, USA) were also used for the construction of the graphite-epoxy electrodes.

### 2.2. Samples under study

To illustrate the capabilities of ETs as a tool for wine tasting, two different scenarios were considered; viz. wine maturing practices (the effect of the barrel and ageing time in its maturing) and the overall tasting attributes. For each of them, a different set of samples was considered and measured with the sensor array, building afterwards the chemometric model that correlates the ET response with the parameters of interest (class or score value).

All considered samples were red wines produced in Catalonia region, each from a different producer, selected according to the nature of the study case. Besides, other factors such as grape varieties, vintage, region, etc. were also taken into account in order to have a more representative set of samples. Overall, a total of 52 wines were obtained from different local wine shops and producers.

### 2.3. Wine tasting by the sensory panel

Taste attributes of the wines considered were assessed by a panel of 8 wine experts under usual established procedures [3]. The panellists were professional wine tasters from the tasting panel of the different DOs considered in this study. All of them were fully trained and with more than five years of experience in evaluating wines from the Catalan region. Briefly, the subjects were asked to rate the global sensory quality of the wines (sight, aroma and taste) by scoring them in the range from 0 to 10. To this end, wine samples were served randomized in clear glasses NF V09-110 (AFNOR 1995) marked with three digit random numbers and covered with Petri dishes. The blind evaluations were conducted at 20–22 °C, and water was provided to the panel for rinsing the palate during tasting. An average of the three features formed the score of one expert; the final global score was taken as the mean from the 8 panellists. Further information of considered samples can be found in *La guia de vins de Catalunya* (a 2014 guide of Catalan wines) [20].

### 2.4. Electronic tongue

The voltammetric ET was formed by an array of 2 metallic electrodes and 4 bulk-modified graphite composite electrodes acting as working electrodes, plus a reference double junction Ag/AgCl electrode (Thermo Orion 900200, Beverly, MA, USA) and a commercial platinum counter electrode (Model 52–67, Crison Instruments, Barcelona, Spain).

The metal electrodes were fabricated encasing the metal wire (Au and Pt) in epoxy resin and fixing an electrical connection in the other end, obtaining a final disk electrode of 1 mm diameter. Composite electrodes were prepared by mixing the resin, graphite powder and selected modifier in a ratio 83:15:2 (w/w) [21]. Afterwards, the mixture was allowed to harden at 80 °C for three days, and then polished with different sandpapers of decreasing grain size. In this way, cobalt (II) phtalocyanine, copper and platinum nanoparticles were incorporated as modifiers/catalysts for three of the composite electrodes, additionally one blank graphite-epoxy composite (which did not incorporate any modifier) was also prepared. The final sensor array was formed by one Pt and one Au metal electrodes, plus the four composite electrodes.

Analyses of the wine samples with the ET were carried out using a 6-channel potentiostat AUTOLAB PGSTAT20 (Ecochemie, Netherlands) controlled with GPES Multichannel 4.7 software package. To this aim, a complete voltammogram was recorded for each sample by cycling the potential between −1.0 V and +1.3 V vs. Ag/AgCl with a step potential of 9 mV and a scan rate of 100 mV $s^{-1}$.

Although wine analysis did not require any sample pretreatment, some precautions were taken to guarantee sensors response stability along the whole experiment. On one side, electrodes were first cycled in a saline solution (i.e. 10 mM KCl) in order to get stable voltammetric signals prior to proceed with wine samples measurements. On the other side, an electrochemical cleaning stage was performed between each measurement to prevent any cumulative effect of impurities on the working electrode surfaces, while not performing any physical surface regeneration of those. To this end, before analysing each sample, a conditioning potential of +1.5 V was applied during 40 s in a cell containing 25 ml of distilled water [22]. Lastly, a model wine control sample was analysed periodically to guarantee that no sensor drift was present during the experiment.

### 2.5. Data processing

Chemometric analysis were done in MATLAB 8.2 (MathWorks, Natick, MA, USA), by specific routines written by the authors, using its Statistics Toolbox. In particular, fast Fourier transform (FFT) was used for signal compression [23], genetic algorithms (GAs) were used as the feature selection tool [24], and linear discriminant analysis (LDA) and partial least squares regression (PLS) were used for the qualitative and quantitative modelling of the data [25,26], respectively. Besides, Sigmaplot (Systat Software Inc., San Jose, CA) was used for graphic representations of data and results.

The usage of FFT and GAs was aimed to the reduction of the large dimensionality and complexity of the recorded voltammetric signals, which allows to gain advantages in training time, to avoid redundancy in input data and to obtain a model with better generalization ability [27]. Hence, the idea is to extract maximum information of the waveforms themselves with a smaller number of variables, while at the same time, to identify and select the ones that most contribute to the prediction task, discarding the less significant ones.

Furthermore, to guarantee that performance of the generated models was not dependant on the specific subdivision of samples between the train and test subsets, its accuracy was evaluated employing the *repeated random sub-sampling validation method* (RRSS) [28]. Briefly, a model was first trained employing 75% of the data, and its performance evaluated towards the remaining 25% of the samples (which have not been used at all during the modelling). Next, random

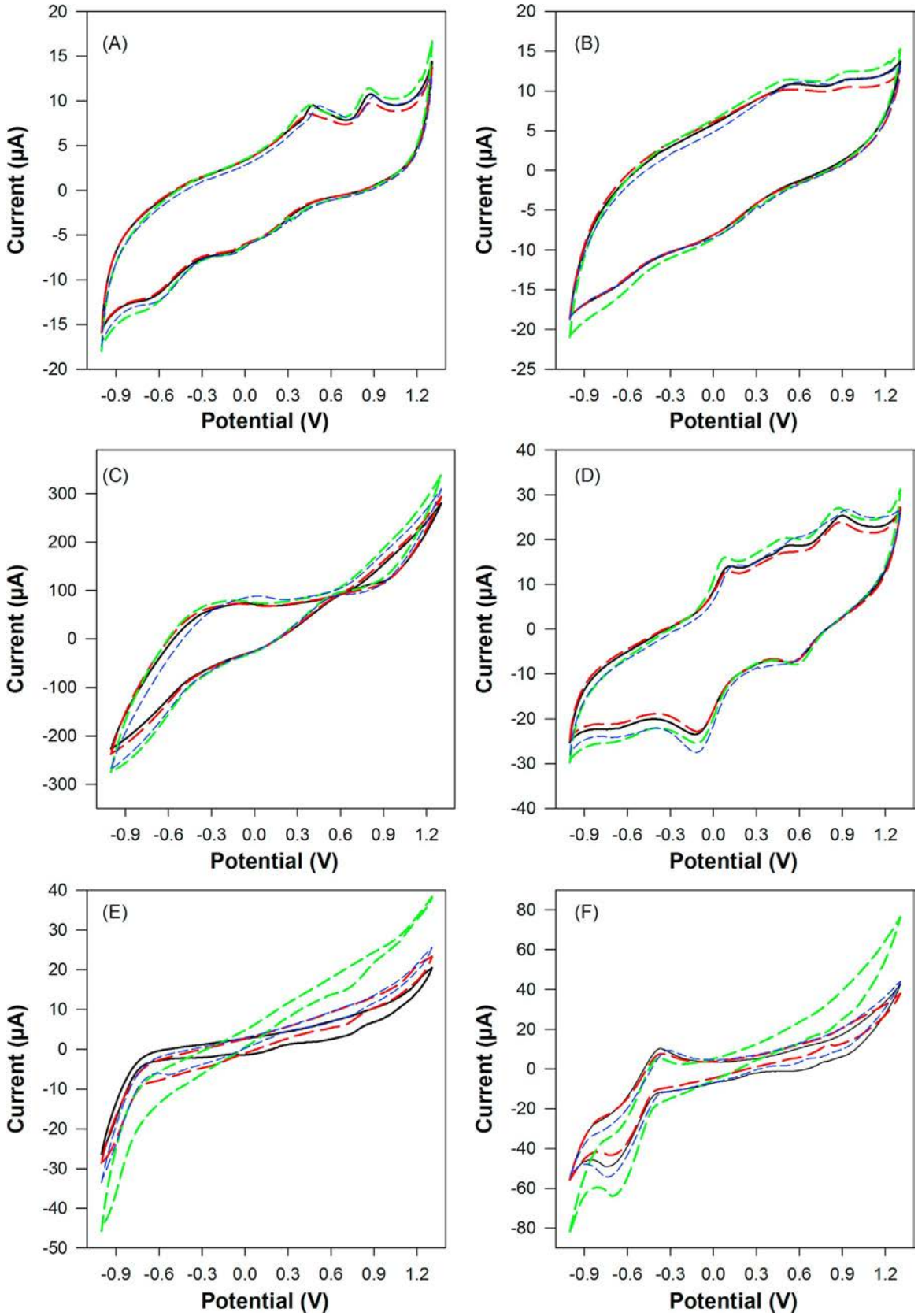


**Fig. 1.** Example of the different voltammograms obtained with the different sensors forming the ET array for four arbitrary red wine samples. Signals provided correspond to: (A) graphite–epoxy sensor, (B) Cu nanoparticles modified sensor, (C) Pt nanoparticles modified sensor, (D) Co phthalocyanine modified sensor, (E) Au metallic sensor and (F) Pt metallic sensor.

subdivision of the data between train and test subsets was repeated again, and a new model was built and its performance evaluated. This process was repeated $k$ times to guarantee that there was not any dependence of the predictions related to the specific subdivision of data. Then, once all responses from all the constructed models were obtained, predicted values by each model were grouped depending on if they were used in the training process or in the testing subset. To finish, average values for each sample were calculated, allowing us to estimate model uncertainties and obtain unbiased data [28].

## 3. Results and discussion

To illustrate the capabilities of ETs as a tool for wine tasting, two different scenarios were considered: wine maturing practices (barrel effect and period) and prediction of the global scores from a wine tasting panel. Each of these scenarios represents a different application, as there is no correlation between them, and consequently, each of the features is predicted independently. This was checked in a preliminary inspection of the data, in which no significant correlation between ageing time and global scores was found. For each of the study cases, a different set of samples was considered and measured with the sensor array, building afterwards the chemometric model that correlates the ET response with the parameters of interest (class or index value). Maximum precautions were taken to separate the training process or building of the identification model, and the fine-tuning of the response model configuration, for which a cross-validation scheme was used. Afterwards, to actually assess the performance of the built model, RRSS method was used to rebuilt the model several times and used to predict the values for the external test samples that were left out (not being used at all) during the modelling stage and those compared to the expected ones, in this way avoiding any bias in performance.

The two commented scenarios perfectly fit in the biomimetic approach of ETs, and clearly illustrate the particularities of those over conventional analytical methods. That is, the fact that the wines' taste and flavour perceived by the skilled sensory panel is not related to a specific compound, but to a joint effect of different ones or groups of them. Besides, those compounds have sometimes not been perfectly identified, what in turn hinders the use of classical methods as those would require its targeting. In contrast, ETs combine obtained chemical information from the array of sensors to generate a model like the human brain would do; in this way, not focusing on which specific compounds are responsible for those flavours or tastes, but still being able to identify or quantify specific compounds if the proper knowledge (from the expert personnel) can be isolated and the proper correspondence can be established.

Obviously, the sensors used are not measuring directly the ageing time or the global score of the samples; they in practice are measuring compounds with electroactive properties. Thus, the idea behind our approach is to use an appropriate array of sensors to obtain information about the different compounds present in the sample (e.g. polyphenols, saccharides, organic acids, etc.), and then use some chemometric tools to build a proper model that indirectly relates the former with the sought information, either ageing time or knowledge aspects of the skilled sensory panel, so as to reproduce its operation intelligently. In this way, the end goal would be obtaining an automated method that would allow significant reduction of wine tasting by the panel; it must be remarked that the final aim is not replacing the human expertise, but replicating it and allowing an increase of the number or frequency of samples that may be analysed.

### 3.1. Voltammetric sensor array

Based on the aforementioned, and according to the IUPAC definition of ET [6], we first need an array of low-selective sensors with cross-response features allowing us to extract rich-enough data from the sample. These data must be somehow directly or indirectly related with the analytical information finally sought, if not, the building of the response model will not be feasible; if all information obtained from the wine samples is their physical characteristics, deduction of properties related to the chemical nature will be very difficult. This means the sensors to be used in a given case must not be any, but with certain connection to the information sought; as second condition these must provide non-specific measurements, this viewpoint related to the cross-response requirement.

In the present work we have combined metallic electrodes with catalyst-modified carbon electrodes; the goal is to accomplish better complementary and more varied voltammograms with the wines considered; in this sense, example of the voltammetric responses obtained for the selected sensor array are shown in Fig. 1. As can be seen, differentiated response is achieved thanks to the use of the different modifiers for the epoxy graphite electrodes and the different metallic electrodes; even in the case of Pt, the responses of the electrode modified with Pt nanoparticles and the Pt metal electrode still display some differences, useful for obtaining complementary information from the voltammograms. In this case, differences are probably due to catalytic phenomena attributable to large surface to volume ratio when metal nanoparticles are used.

Besides, not only the cross-response features need to be checked, but also whether or not sensors responses are related to the phenomena under study. However, this is not straightforward, as the proper evaluation needs to be done by its modelling with the different chemometric tools (as from the IUPAC definition of ET [6]). Hence, on the next sections we are going to evaluate the richness of the generated data and suitability of the ET approach.

Additionally in our case, and due to the large dimensionality of the generated signals, a preprocessing stage based on the usage of FFT was also performed prior the modelling stage itself, aimed to improve model's robustness and performance [27]. In this manner, prior to the modelling, each voltammogram was compressed from the registered 512 current intensities down to 32 coefficients without any loss of significant information [23]; this allowed a compression of the original data up to 93.8%.

### 3.2. Effect of the barrel in wine maturing

In the first study case, we assessed whether there was or not some identifiable trend in the ET response that could be related to the type of barrel used during wine maturing; that is, the type of wood oak used for the construction of the barrel in which the wine will be aged. On this account, Fernández de Simón and colleagues demonstrated that there was a clear effect based on the type of oak used, as they found that wines with different characteristics were obtained from the same base wine after 21 months of ageing [29].

Among the different types of oak barrels, there are mainly two that are used among producers in Catalonia region; namely, French (*Quercus robur*, *Quercus petraea*) or American (*Quercus alba*) oak wood, although also their mixtures might be used. Hence, we will focus on the analysis of different wines aged on those.

As a first attempt to assess the capabilities of the ET to distinguish barrel effect in wine ageing, we initially focused only on wines aged in French and American barrels to asses if there is or not any pattern found. To this aim, a total subset of 16 samples, were initially considered. Samples were analysed as previously described by means of the sensor array. Next, obtained responses were compressed by means of FFT and obtained coefficients were analysed employing PCA (Fig. 2). This, as an unsupervised method, provides a better representation of samples (dis)similarities, but it does not perform its classification.

Interestingly, the PCA plot shows how French oak samples seem to group in the left side, whereas the American ones seem to group in the opposite one; thus indicating some effect due to the oak barrel

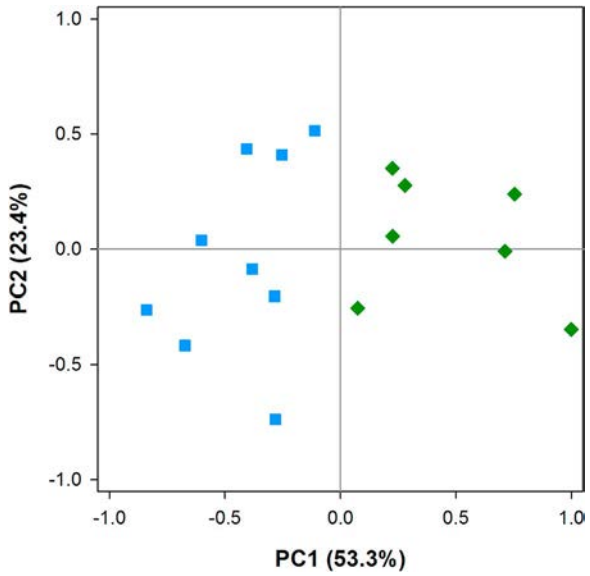


**Fig. 2.** Score plot of the first two components obtained after PCA analysis of the wine samples: (■) French and (◆) American.

employed and suggesting that the ET should be capable of distinguishing such factor.

To further confirm the observed trend, some additional samples aged in mixed oak barrels were analysed as described with our sensor array. Obtained responses were compressed by means of FFT as before, and the whole set modelled using LDA as the pattern recognition method (Fig. 3). This was chosen given that LDA is a supervised method that allows to actually build a classification model [25]. That is, LDA looks specifically for differences among the data classes, while unsupervised methods do not.

At first sight, it can be seen how the ET is able to distinguish the different types of barrels with this simple analysis of the projected coordinates; however, to numerically assess the performance of the model, cross validation was performed and three different indicators (namely, classification rate, sensitivity and specificity) were calculated [30]. To this aim, the generated model was used to predict the expected group for the test samples that were left out (28% not being used at all during the modelling stage) and predicted classes were compared to the expected ones. The corresponding confusion matrix was then built (Table 1), and the efficiency of the classification was evaluated for samples of the external test subset as 100% according to classification rate, sensitivity and specificity. With the goal of providing a further measure of the goodness of fit, a Pearson's chi-squared test was calculated for the contingency table (Table 1), obtaining a calculated statistic of $\chi^2$=14.0, larger than the tabulated value at the 95% confidence level (9.49). This parameter, plus the calculated coefficient of contingency (0.8165, a 100% of the maximum value for the number of classes considered) describes numerically the ability in the identification of ageing wood used.

### 3.3. Prediction of the wine maturing period

In the same direction, we also evaluated the capabilities of the ET not only to discriminate ageing in different types of oak barrels, but also to identify the number of months that wines were aged for; this application case is also of interest in the wine field, specially to prevent fraud, as it was already demonstrated for sparkling wines [31].

As before, another set of samples was analysed with the ET, and responses were modelled employing PLS instead of LDA to quantitatively predict their ageing time. Details of the PLS model, such as number of latent variables used (5) were derived from a leave-one-out cross-validated initial calculation. After model optimization, a more complete cross-validation stage (RRSS) with separate training and test subsets was done, whereas comparison graphs of predicted vs. expected ageing months were built to check its prediction ability (Fig. 4), and regression lines were fitted. To ensure the robustness of the approach, and that the results obtained were not dependant on the specific subdivision of the samples for the train and test subsets, a repeated resampling approach was used (n=24), which in turn allowed us to assign prediction uncertainties to the different samples and to obtain unbiased data, both for training and test subsets.

As can be seen in Table 2, a satisfactory trend was obtained for both subsets, with regression lines of the predicted vs. expected comparison plot almost indistinguishable from the theoretical ones; that is, with slope, intercept and correlation values close to 1, 0 and 1, respectively.

In addition, joint confidence intervals were calculated and plotted according to described methodology (Fig. 5) [32]. Its usage allows to simultaneously assess the goodness of slope and intercept, and therefore represents a rapid visualization tool to detect if there are or not differences between two compared methods. In this direction, uncertainties in both axes are used to calculate the estimated covariance matrix based on an F distribution, and to examine whether or not the theoretical (slope, intercept) comparison point (1,0) is included in the elliptical region of the 95% joint confidence intervals. Therefore, we can state that there are not significant differences between the actual ageing time and the values predicted by the ET, thus suggesting the ET as a promising approach for the obtaining of an analytical tool to assess the wine ageing process.

### 3.4. Prediction of global scores of the sensory panel

Lastly, the capabilities of the ET as a tool able to reproduce the global scores assigned by a trained human sensory panel were also evaluated. This represents a more complex approach compared to the previous ones, as those scores depend from the mouthfeel and flavours perceived when tasting the wine, and can be related to both the presence and absence of several compounds and classes of those. This is why the ET system represents an interesting straightforward approach for this scenario, as its biomimetic nature aligns with the biological scheme. Hence, the hypothesis if the ET can be trained employing the scores assigned by the sensory panel to reproduce the knowledge from the experts is thus assessed.

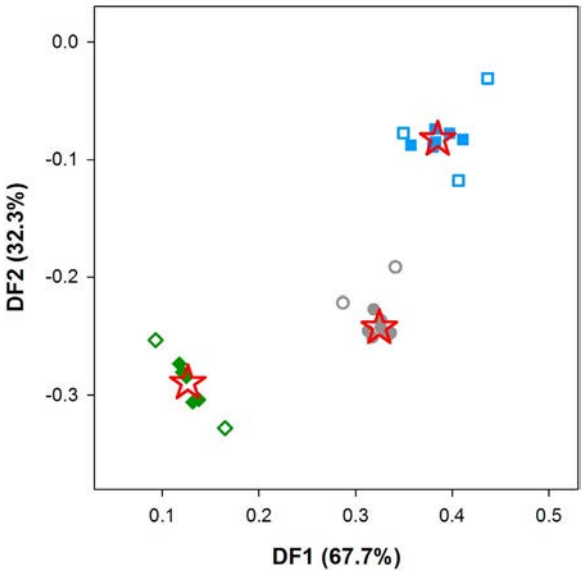


**Fig. 3.** Score plot of the first two functions obtained after LDA analysis of the wine samples, according to its maturing: (■) French, (•) French/American and (◆) American; with filled symbols for the training subset and empty ones for the testing subset. Additionally, the centroid for each class is plotted (★).

**Table 1**
Confusion matrix built according to the maturing category obtained using the LDA model for the testing subset. Results provided correspond to the average of the values obtained for each sample after 25 repeated calculations done with random division of samples for train/test subsets each time.

| | $F^b$ | $FA^b$ | $A^b$ |
|---|---|---|---|
| $F^a$ | 100% | 0 | 0 |
| $FA^a$ | 0 | 100% | 0 |
| $A^a$ | 0 | 0 | 100% |

F: French; FA: French/American; A: American.
[a] Expected.
[b] Found.

After analysing the wine samples with the sensor array, obtained responses were processed as previously described; a PLS model was constructed from the FFT coefficients available from each sample and optimized to correlate the ET responses with the average scores assigned to each wine by the sensory panel. Fine tuning of the PLS model, such as number of latent variables used (6) were derived from a separate leave-one-out cross-validated initial calculation. After model optimization, a more complete cross-validation (RRSS) stage with separate training and test subsets was done, whereas comparison graphs of predicted vs. expected scores assigned by the sensory panel were built to check its prediction ability (Fig. 6), and corresponding regression lines were fitted. Again, to ensure the robustness of the approach, and that the results obtained were not dependant on the specific subdivision of the samples for the train and test subsets, a repeated sampling and calculation (n=30) was performed, which in turn allowed us to assign prediction uncertainties to the different samples and to obtain unbiased data, both for training and test subsets.

As can be observed from Fig. 6, the obtained comparison results are close to the ideal values, with regression lines very close to the theoretical ones. This was further confirmed by numerically assessing the regression parameters (Table 2) and building the joint confidence intervals plot (Fig. 5); which intercepts were close to 0 and slopes and correlation coefficients close to 1, being these theoretical values included in the 95% confidence interval. Thus, meaning there is no significant model bias or differences between the values predicted by the ET and the ones assessed by the panel.

This satisfactory trend confirms the potential of such an approach (i.e. to artificially reproduce the tasting perception of a sensory panel), even more if considering the subjective nature of the scores originated from the human sensory panel.

**Table 2**
Parameters of the fitted regression lines for the comparison between obtained vs. expected values, both for the training and testing subsets of samples, and the two scenarios considered (intervals calculated at the 95% confidence level).

| | Correlation | Slope | Intercept | NRMSE |
|---|---|---|---|---|
| | ***Ageing time*** | | | |
| *Train* | 0.982 | 0.964 ± 0.025 | 0.45 ± 0.33 | 0.048 |
| *Test* | 0.969 | 1.011 ± 0.061 | 0.14 ± 0.84 | 0.077 |
| | ***Global scores (0–10) assigned by the sensory panel*** | | | |
| *Train* | 0.981 | 0.976 ± 0.023 | 0.22 ± 0.20 | 0.045 |
| *Test* | 0.917 | 0.973 ± 0.087 | 0.29 ± 0.74 | 0.11 |

NRMSE: Normalized Root Mean Square Error; Intercept values are expressed in months and arb. unit (0–10), respectively.

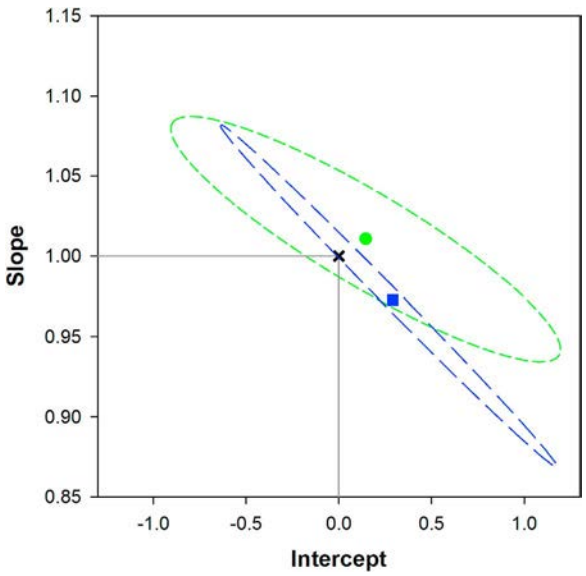


**Fig. 5.** Joint confidence intervals for the testing subsets: (●, short-dashed line) the ageing time and (■, long-dashed line) the global scores assigned by the sensory panel. Also the ideal point (1,0) is plotted (x); intervals calculated at the 95% confidence level.

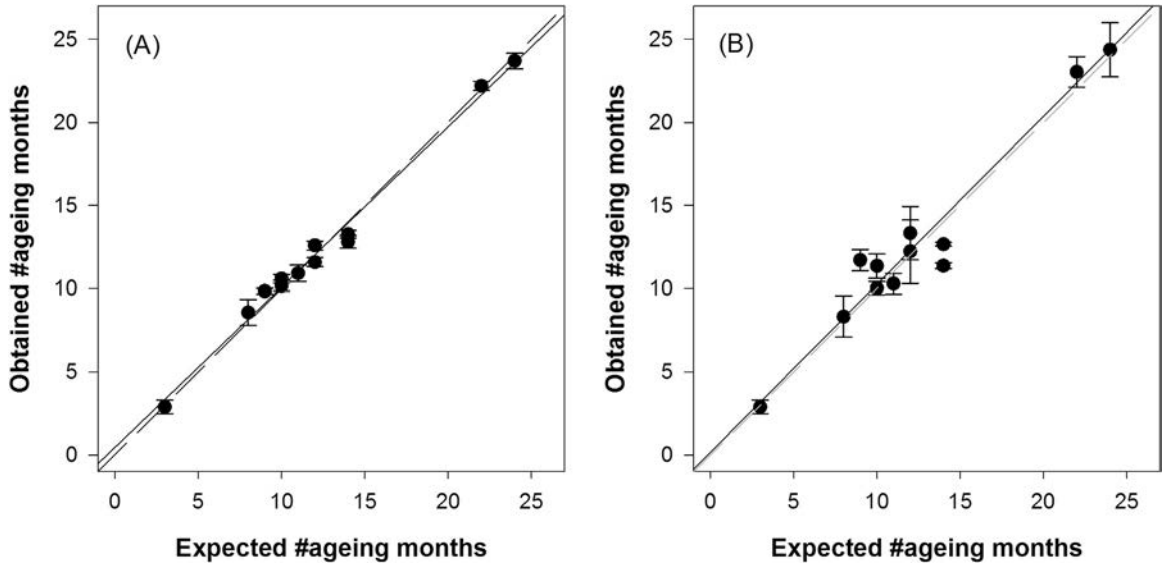


**Fig. 4.** Performance of the optimized FFT-PLS model for the prediction of wines ageing time. Set adjustments of obtained vs. expected values, both for (A) training and (B) testing subsets. The dashed line corresponds to theoretical diagonal line. Results provided correspond to the average of the values obtained for each sample after 24 repeated calculations done with random division of samples for train/test subsets each time. Uncertainties calculated at the 95% confidence level.

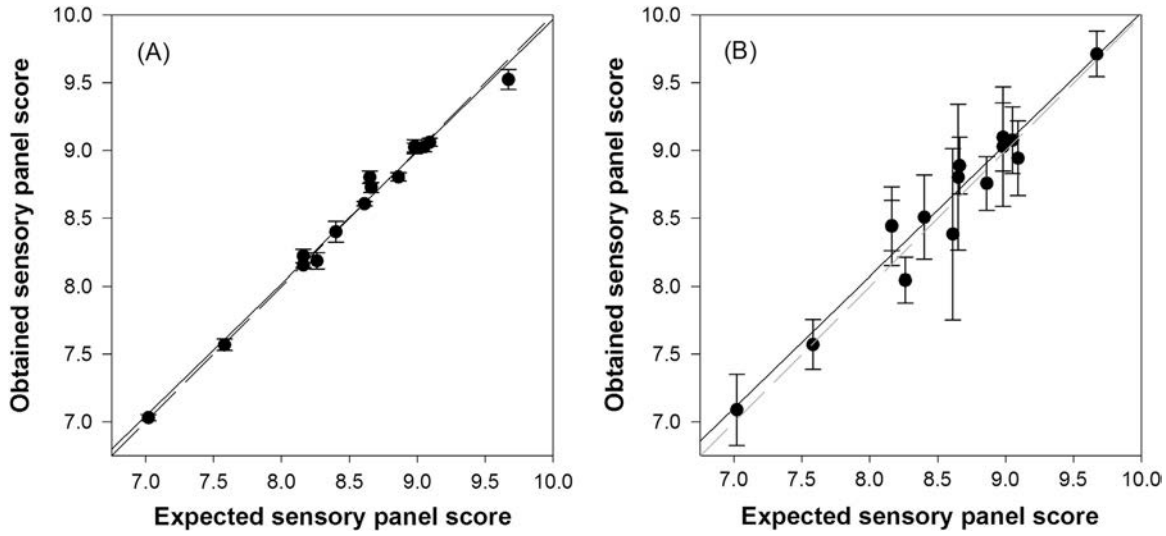


**Fig. 6.** Performance of the optimized FFT-PLS model for the prediction of wines global scores assigned by the sensory panel. Set adjustments of obtained vs. expected values, both for (A) training and (B) testing subsets. The dashed line corresponds to theoretical diagonal line. Results provided correspond to the average of the values obtained for each sample after 30 repeated calculations done with random division of samples for train/test subsets each time. Uncertainties calculated at the 95% confidence level.

## 4. Conclusions

In this report, we have illustrated the interesting capabilities of ETs as analytical tool applicable in the tasting and sensory analysis of wine. More specifically, the proposed ET has been successfully applied in the discrimination of wine samples based on its maturing in barrels or the prediction of the global scores assigned by a sensory panel.

To this end, wine samples were analysed with the voltammetric sensor array, and obtained responses were preprocessed employing FFT and GAs for the compression and reduction of signal complexity, followed by its modelling employing LDA for the qualitative and PLS for the quantitative approaches, respectively.

Overall, ETs represent an interesting alternative to more conventional methods due to its biomimetic behaviour, which provides them with the most straightforward approach to overcome the lack of knowledge of the compounds responsible for certain wine sensations. That is, their ability to reproduce the knowledge from the experts, although not replacing them, but being highly suitable as a screening tool which would allow an increase of the number or frequency of samples that can be analysed.

## Acknowledgments

Financial support for this work was provided by the Spanish Ministry of Economy and Innovation, MINECO (Madrid) through project CTQ2013-41577-P. Xavier Cetó thanks the financial support from the Premier's Research and Industry Fund through the Catalyst Research Grants scheme CRG69. Andreu González-Calabuig thanks Universitat Autònoma de Barcelona for the PIF fellowship. Manel del Valle thanks the support from program ICREA Academia.

## References

[1] Commission Regulation (EEC), in: Off. J. L 272, Publication Office of the European Union, 17 September 1990, pp. 1–192.
[2] Office International de la Vigne et du Vin (OIV), Recueil des méthodes internationales d'analyse des vins et des moûts, 2005 ed., OIV, Paris, 2005.
[3] R.S. Jackson, Wine Tasting: A Professional Handbook, Academic Press, London, 2002.
[4] J. Zeravik, A. Hlavacek, K. Lacina, P. Skladal, Electroanalysis 21 (2009) 2509–2520.
[5] K. Toko, Meas. Sci. Technol. 9 (1998) 1919–1936.
[6] Y. Vlasov, A. Legin, A. Rudnitskaya, C. Di Natale, A. D'Amico, Pure Appl. Chem. 77 (2005) 1965–1983.
[7] M. del Valle, Sensors 11 (2011) 10180.
[8] M. Śliwińska, P. Wiśniewska, T. Dymerski, J. Namieśnik, W. Wardencki, J. Agr. Food Chem. 62 (2014) 1423–1448.
[9] P. Ciosek, W. Wroblewski, Analyst 132 (2007) 963–978.
[10] L. Escuder-Gilabert, M. Peris, Anal. Chim. Acta 665 (2010) 15–25.
[11] A. Riul Jr, C.A.R. Dantas, C.M. Miyazaki, O.N. Oliveira Jr, Analyst 135 (2010) 2481–2495.
[12] M. Gay, C. Apetrei, I. Nevares, M. del Alamo, J. Zurro, N. Prieto, J.A. De Saja, M.L. Rodriguez-Mendez, Electrochim. Acta 55 (2010) 6782–6788.
[13] M. Gutiérrez, A. Llobera, J. Vila-Planas, F. Capdevila, S. Demming, S. Buttgenbach, S. Mínguez, C. Jiménez-Jorquera, Analyst 135 (2010) 1718–1725.
[14] A. Riul Jr, H.C. de Sousa, R.R. Malmegrim, D.S. dos Santos Jr, A.C.P.L.F. Carvalho, F.J. Fonseca, O.N. Oliveira Jr, L.H.C. Mattoso, Sens. Actuators B: Chem. 98 (2004) 77–82.
[15] A. Legin, A. Rudnitskaya, L. Lvova, Y. Vlasov, C. Di Natale, A. D'Amico, Anal. Chim. Acta 484 (2003) 33–44.
[16] J.M. Gutiérrez, L. Moreno-Barón, M.I. Pividori, S. Alegret, M. del Valle, Microchim. Acta 169 (2010) 261–268.
[17] V. Parra, Á.A. Arrieta, J.-A. Fernández-Escudero, M.L. Rodríguez-Méndez, J.A. De Saja, Sens. Actuators B: Chem. 118 (2006) 448–453.
[18] X. Cetó, M. Llobet, J. Marco, M. del Valle, Anal. Methods 5 (2013) 1120–1129.
[19] S. Buratti, D. Ballabio, G. Giovanelli, C.M.Z. Dominguez, A. Moles, S. Benedetti, N. Sinelli, Anal. Chim. Acta 697 (2011) 67–74.
[20] J. Alcover, S. Naranjo, Guia de Vins de Catalunya 2014, Editorial Pòrtic, Barcelona, 2013.
[21] F. Céspedes, E. Martínez-Fàbregas, S. Alegret, TrAC-Trend Anal. Chem. 15 (1996) 296–304.
[22] X. Cetó, J.M. Gutiérrez, L. Moreno-Barón, S. Alegret, M. del Valle, Electroanalysis 23 (2011) 72–78.
[23] X. Cetó, F. Céspedes, M. del Valle, Talanta 99 (2012) 544–551.
[24] E. Richards, C. Bessant, S. Saini, Chemom. Intell. Lab. 61 (2002) 35–49.
[25] R.A. Johnson, D.W. Wichein, Applied Multivariate Statistical Analysis, Pearson Education, Harlow, GB, 2007.
[26] V.E. Vinzi, W.W. Chin, J. Henseler, H. Wang, Handbook of Partial Least Squares: Concepts, Methods and Applications, Springer, Berlin, DE, 2010.
[27] X. Cetó, F. Céspedes, M. del Valle, Microchim. Acta 180 (2013) 319–330.
[28] A.M. Molinaro, R. Simon, R.M. Pfeiffer, Bioinformatics 21 (2005) 3301–3307.
[29] B. Fernández de Simón, E. Cadahía, J. Jalocha, J. Agric. Food Chem. 51 (2003) 7671–7678.
[30] D. Broadhurst, D. Kell, Metabolomics 2 (2006) 171–196.
[31] X. Cetó, J. Capdevila, A. Puig-Pujol, M. del Valle, Electroanalysis 26 (2014) 1504–1512.
[32] D.C. Montgomery, E.A. Peck, G.G. Vining, Introduction to Linear Regression Analysis, Wiley, Chichester, GB, 2012.

# Article 6:

**Voltammetric electronic tongue to identify Brett character in wines. On-site quantification of its ethylphenol metabolites**

Andreu González-Calabuig and Manel del Valle

*Talanta* 179 (2018) 70–74

DOI: 10.1016/j.talanta.2017.10.041

Talanta 179 (2018) 70–74

Contents lists available at ScienceDirect

Talanta

journal homepage: www.elsevier.com/locate/talanta

# Voltammetric electronic tongue to identify Brett character in wines. On-site quantification of its ethylphenol metabolites

Andreu González-Calabuig, Manel del Valle*

*Sensors and Biosensors Group, Department of Chemistry, Universitat Autònoma de Barcelona, Edifici Cn, Barcelona, 08193 Bellaterra, Spain*

ARTICLE INFO

*Keywords:*
Electronic tongue
Artificial neural networks
Phenolic defects
Brettanomyces defect
Wine

ABSTRACT

This work reports the applicability of a voltammetric sensor array able to evaluate the content of the metabolites of the Brett defect: 4-ethylphenol, 4-ethylguaiacol and 4-ethylcatechol in spiked wine samples using the electronic tongue (ET) principles. The ET used cyclic voltammetry signals, obtained from an array of six graphite epoxy modified composite electrodes; these were compressed using Discrete Wavelet transform while chemometric tools, among these artificial neural networks (ANNs), were employed to build the quantitative prediction model. In this manner, a set of standards based on a modified full factorial design and ranging from 0 to 25 mg $L^{-1}$ on each phenol, was prepared to build the model; afterwards, the model was validated with an external test set. The model successfully predicted the concentration of the three considered phenols with a normalized root mean square error of 0.02 and 0.05, for the training and test subsets respectively, and correlation coefficients better than 0.958.

## 1. Introduction

The wine sector is an important economic that still has some unsolved issues, such as the generation of undesired volatile phenols during the early stages of wine production, in parallel to the alcoholic fermentation. Volatile phenols such as phenol, guaiacol, cresol, ethylphenol, vinylphenol, eugenol and vainilline are contained in wine and are the main responsible for the wine aroma [1]. Depending on their concentration levels and their aromatic properties, some of them contribute positively to wine aroma, but others are responsible for undesired aromas and flavors. Among these compounds the 4-ethylphenols and vinylphenols are mainly the responsible for unpleasant aromas often described as “phenolic”, “leather” or “barnyard”, and are the origin of this defect in wine product [2].

Presence of 4-ethylphenols in wine is mainly due to the enzymatic side-processes during fermentation, especially when the *Brettanomyces* and *Dekkera* yeast families proliferate [3,4]. These yeasts are naturally occurring in the fruit skin so it is almost impossible to assure their absence when harvesting; the problem arises when the activity of these yeasts is very high, producing a wine with a concentration of 4-ethylphenols surpassing the human threshold, which has been reported to be approx. 0.5 mg $L^{-1}$ of 4-ethylphenols [2]. In the wine industry, there are two alternatives to detect the Brett defect: an early detection of proliferating *Brettanomyces* yeasts via cell culture [4] or the chromatography analysis of their metabolites [5]; it has to be remarked that both methods are time consuming, require trained personnel and cannot be used on-site.

In this context, electrochemical sensors offer an opportunity to detect the *Brettanomyces* metabolites on-site; this is, at the foot of the fermenter tank at the wine producer, with possibility of detecting the contamination event when it occurs, what it has been also named analytical measurement at-line. Electrochemical systems share known advantages that include high sensitivity and selectivity, a wide linear range, and low-cost instrumentation for this monitoring strategy. In addition, electrochemical measurement devices can be readily miniaturized and/or integrated to facilitate on-site testing. Unfortunately, there are some factors that hinder the applicability of such sensors in real samples, e.g. matrix effects, interferents, electrode fouling, etc. In this context a new sensor approach was proposed in the early 90s to overcome some of the limitations that a single sensory element could produce: the use of sensor arrays [6]. However, the highly complex data generated by the sensor array needs to be treated in order to extract the meaningful information; the data is processed employing advanced mathematical tools such as Principal Component analysis (PCA), partial least squares (PLS) or artificial neural networks (ANNs) [7]. The resulting approach is known as electronic tongue (ET) [8], due to its similarities to the biological sense of taste. ETs have been specifically employed in applications related to the wine field as the determination of the total polyphenolic content in wine, prediction of the sensory score or the detection of adulterations, among many others [9–12].

* Corresponding author.
*E-mail address:* manel.delvalle@uab.cat (M. del Valle).

http://dx.doi.org/10.1016/j.talanta.2017.10.041
Received 10 July 2017; Received in revised form 19 October 2017; Accepted 21 October 2017
Available online 22 October 2017

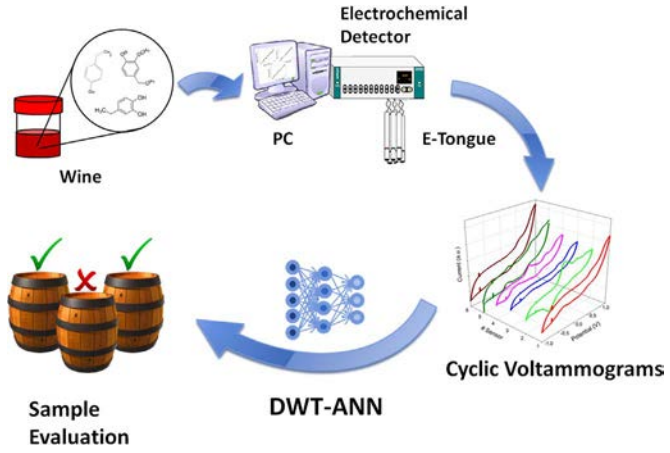


**Fig. 1.** Scheme of the experimental setup used for the early detection of volatile phenol defects in wine.

Hence, with this methodology, it is possible to achieve a simultaneous determination of a large number of different species, while diminishing any interference effect using these advanced mathematical tools [13].

The ET principles are reported here in an approach based on the coupling of cyclic voltammetry responses obtained from an array of modified epoxy graphite electrodes, compressed with Discrete Wavelet Transform [14], and processed with ANNs to build a predictive model able to quantify the content in 4-ethylphenol (4-EP), 4-ethylguayacol (4-EG) and 4-ethylcatechol (4-EC) in wine. This approach, as depicted in Fig. 1, attempts to obtain an on-site alert tool for detection of the Brett character in wine, it would be easily applicable in the vineyard and may be employed to improve wine quality and prevent the appearance of this defect.

## 2. Experimental

### 2.1. Reagents and chemicals

All reagents used in this work were analytical reagent grade. 4-ethylphenol, 4-ethylguaiacol, 4-ethylcatechol, Cu nanoparticles (particle size 50 nm), $WO_3$ nanoparticles (particle size < 100 nm), 2% $Bi_2O_3$ nanoparticles (particle size 90–210 nm), polypyrrole and Co phtalocyanine were purchased from Sigma-Aldrich (St. Louis, MO, USA).

Graphite powder (particle size 50 μm) was received from BDH (BDH Laboratory Supplies, Poole, UK). Epotek H77 resin was purchased from Epoxy Technology (Billerica MA, USA). *Don Simon* wine was purchased at the local supermarket.

### 2.2. Electronic tongue

The voltammetric ET was formed by an array of 6 sensors, plus a combined Pt auxiliary and a Ag/AgCl reference electrode (Crison 5261, Barcelona, Spain). Working electrodes were bulk modified graphite epoxy composites, which were prepared by mixing the resin, graphite powder and modifiers in the ratio 83:15:2 (w/w) [15]. Afterwards, resin was allowed to harden at 80 °C for 24 h; and electrode surfaces were next polished with different sandpapers of decreasing grain size.

In this manner, the array of 6 voltammetric electrodes was prepared, consisting in one blank electrode plus five composite electrodes modified with Cu nanoparticles, $WO_3$ nanoparticles, Co phtalocyanine, $Bi_2O_3$ nanoparticles and polypyrrole. This choice was intended as to maximize the differences in the obtained voltammograms for the different sensors used as is demonstrated in Section 3.1.

Electrochemical measurements were performed at room temperature (25 °C), using a 6-channel AUTOLAB PGSTAT20 (Ecochemie, Netherlands) controlled with GPES Multichannel 4.7 software package. A complete voltammogram was recorded for each sample by cycling the potential between −1.1 V and +1.2 V vs. Ag/AgCl with a step potential of 9 mV and a scan rate of 100 mV $s^{-1}$.

In order to get stable voltammetric responses and ensure reproducible signals from the array during the experiment, the electrodes were cycled in buffer solution after the sample measurements and an electrochemical cleaning step was performed between samples at +1.4 V during 40 s in a cell containing 20 ml of 100 mM saline solution at pH 10 [16].

### 2.3. Data pre-processing

The main objective of the pre-processing is to reduce the complexity of the input signal (6 sensors × 490 current values at different potential) while preserving the relevant information, this step allows a gain in training time, avoids redundancy in the input data and a obtained model with better generalization ability [7].

The compression of the voltammetric data was achieved by means of Discrete Wavelet Transform [14]: each voltamogram was compressed using *Daubechies* 3 and a 4th decomposition level. In this manner, the 2940 inputs per sample were reduced down to 132 coefficients, achieving a compression ratio of 93.5%.

The statistical treatment and analysis was performed using routines written by the authors through MATLAB 2016b (MathWorks, Natick, MA) programming environment and its Neural Network Toolbox; the graphical representation and analysis of the results was performed with Sigmaplot (Systat Software Inc., San Jose, CA).

## 3. Results and discussion

### 3.1. Voltammetric array response

The voltammetric responses for each of the electrodes towards the individual compounds were first evaluated, to assure that the generated signals was different enough and the obtained data were rich enough to be the departure point for a multivariate calibration model.

Therefore, under the described conditions in Section 2.2, individual stock solutions of 25 mg $L^{-1}$ of 4-EP, 4-EG and 4-EC in a wine matrix were analyzed (Fig. 2). No further optimization of the media composition or pH was done, as the simplest procedure possible was desired. Even pH was not regulated, although in this case, being wine a natural fermented product, pH value is within narrow values for a given variety. As a general trend, and as it is already reported in the literature [17], two processes are observed for all the sensors corresponding to the oxidation of the corresponding phenol to its quinone form, and the reduction of the quinone to the phenolic form.

Moreover, it can also be seen that the copper nanoparticle modified electrode displayed higher currents, a fact somehow explained by the fact that the main natural phenolic-degrading enzymes, like *tyrosinase* or *laccase*, are copper containing redox enzymes [18,19]. Besides, slightly differentiated curves were obtained for each of the compounds, a necessary condition for any ET study.

However, if it is not enough to asses visually that each sensor in the array responded in a different manner towards 4-ethylphenol, 4-ethylguaiacol and 4-ethylcatechol a chemometric assay was further done. In order to assess mathematically the complementarities between the voltammetric responses of Fig. 2, a principal component analysis (PCA) was performed [20]. In Fig. 3A are plotted the scores of samples corresponding to the two first principal components for the array response towards the 3 ethylphenols; in there, it can be seen that each compound sample is differentiated and clearly clustered. Fig. 3B also plots the scores of the two first principal components but taking into account each sensor, as it can be seen each sensor provides a distinct signal for each analyte. Moreover, the different sensors appear in different coordinates in the scores plot meaning that they have different

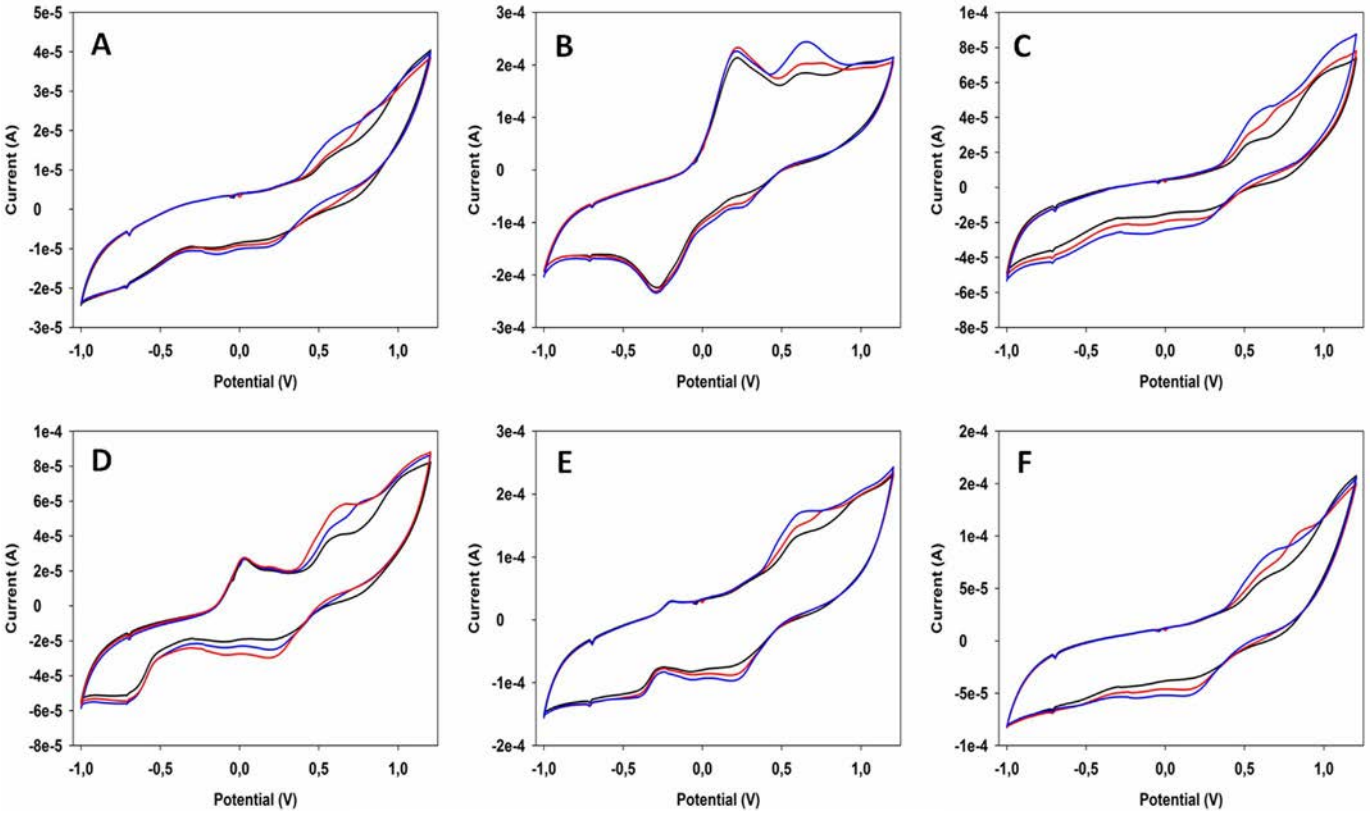


**Fig. 2.** Example of the different voltammograms obtained for 25 ppm of 4-EP (black), 4-EG (red) and 4-EC (blue) in a wine matrix for a **(A)** Bare epoxy-graphite electrode, and electrodes modified with **(B)** Cu nanoparticles, **(C)** $WO_3$ nanoparticles, **(D)** $Bi_2O_3$ nanoparticles, **(E)** Polypyrrole and **(F)** Co(II) phthalocyanine. (For interpretation of the references to color in this figure legend, the reader is referred to the web version of this article.)

responses that complement each other. Perhaps the two electrodes showing the closest response were these of Co (II) phthalocyanine and $WO_3$ that were kept given the very different nature of the catalysts involved.

The array response towards the compounds of interest, once confirmed the different behaviour of the employed electrodes, allowed the differentiation of the different ethylphenol compounds considered; the next step was to proceed with the design of the architecture of the ANN model capable to quantify these compounds in the wine matrix considered here.

### 3.2. Building of the ANN model

The first step in the construction of the artificial neural network model is the definition of the training and test subsets. In this case the chosen experimental design for the train subset was a modified (tilted) $3^3$ factorial design (27 samples) [21]; while the validation of the constructed model was done with the test set (10 samples), these were randomly distributed along the experimental domain (0–25 ppm for each phenolic compound). These values are in consistence with typical concentrations of the Brett defect, and also determined by the threshold

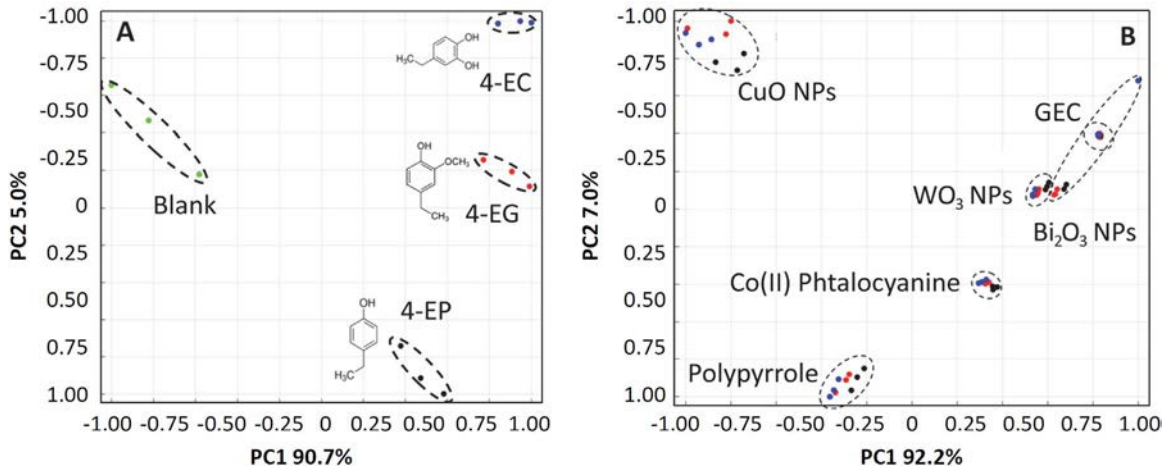


**Fig. 3. (A)** Score plot of the first two components obtained after PCA analysis. A total of 12 samples were analyzed corresponding to triplicate determinations of: 4-EP (black), 4-EG (red), 4-EC (blue) and wine matrix (green). **(B)** The scores plot of graphite-epoxy electrode (GEC), CuO NPs electrode, $WO_3$ NPs electrode, $Bi_2O_3$ NPs electrode, polypyrrole electrode and Co(II) phthalocyanine electrode for 25 ppm of 4-EP (black), 25 ppm of 4-EG (red) and 25 ppm of 4-EC (blue). (For interpretation of the references to color in this figure legend, the reader is referred to the web version of this article.)

detected by a trained wine taster, which is around 1 ppm. All standards were prepared on a *Don Simon* commercial wine matrix as background.

Once the data of the samples in the different subsets was collected the voltammograms were compressed by use of DWT, as result the obtained dataset is suited to be feed to the different ANN models. The next step is to optimize the appropriate ANN architecture, this is usually done by trial-and-error procedure due to the difficulties to predict the best configuration as there are several parameters involved (compression pretreatment, number of neurons in the hidden layer, transfer functions, etc.) [22].

As previously commented, the samples from the training subset were used to build the ANN model and the performance of the model was evaluated with the prediction of the analyte concentrations in the test subset samples. As mentioned, the test subset is an external set that has not been used in the modeling procedure; the goodness of fit for this subset is a good parameter to evaluate the modeling performance.

After the evaluation of different topologies, the final ANN architecture had 132 neurons (6 sensors × 22 DWT coeffs.) in the input layer, 3 neurons and *satlins* transfer function in the hidden layer and 3 neurons and *purelin* transfer function in the output layer, providing simultaneously the concentration of the three compounds considered.

Comparison graphs of predicted vs. expected concentrations for training and testing subsets, for each of the compounds, were built to evaluate the prediction ability of the ANN model (Fig. 4). A satisfactory trend is obtained for both subsets, with regression lines values very close to the theoretical ones, slope and intercept equal to 1 and 0 respectively. Nevertheless, the training subset showed better correlation coefficients ($r \geq 0.99$) than the test subset ($r \geq 0.95$) but this is expected to be as the train subset is used to optimize the architecture, therefore the model is tailored to fit this data, while the test subset is not used at all during the modeling. The detailed results, described in Table 1, showed promising results for the test subset as the NRSME (normalized root mean square error) for the three compounds was 0.05, a remarkably low value. From the statistics of comparative graphs (external test subset), an estimation on the reproducibility associated with each determination was 4.6%, 6.5% and 13.0%RSD for 4-EP, 4-EG and 4-EC, respectively. The detection limits obtained for the different ethylphenols were 1.8 ppm, 5.5 ppm and 3.0 ppm for 4-EP, 4-EG and 4-EC, respectively, not far away from the thresholds detected by a human expert. To complement and contrast these results, a PLS treatment was employed to compare the ANN model with the usual chemometric methods, such as partial least squares model. The NRMSE obtained for the test subset with the PLS model was 0.159, clearly worse than the chosen variant. Curiously, the PLS models achieved comparable NRMSE values in quantification of 4-EG, probably this is the electroactive species with best linearity; with PLS, the individual NRMSE errors were 0.059, 0.062 and 0.135 for 4-EP, 4-EG and 4EC, respectively. The results of the PLS model are detailed in the Supporting information.

**Table 1**
Results of the fitted regression lines for the comparison between obtained vs. expected values, both for the training and testing subsets of samples and the three considered species (intervals calculated at the 95% confidence level).

| | | *r* | *Slope* | *Intercept* (mg $L^{-1}$) | *NRMSE* | *Total NRMSE* |
|---|---|---|---|---|---|---|
| ***Train*** | *4-EP* | *0.998* | *0.990 ± 0.049* | *0.13 ± 0.72* | *0.019* | *0.022* |
| | *4-EG* | *0.998* | *0.981 ± 0.049* | *0.21 ± 0.67* | *0.018* | |
| | *4-EC* | *0.995* | *0.974 ± 0.082* | *0.28 ± 1.10* | *0.029* | |
| ***Test*** | *4-EP* | *0.997* | *1.089 ± 0.133* | *−1.24 ± 1.80* | *0.037* | *0.050* |
| | *4-EG* | *0.958* | *0.969 ± 0.474* | *0.7 ± 6.4* | *0.069* | |
| | *4-EC* | *0.988* | *0.886 ± 0.227* | *1.5 ± 3.1* | *0.043* | |

NRMSE: Normalized Root Mean Square Error.

Additionally, to visualize the goodness of the fit joint confidence intervals (JCI) were calculated and plotted according to advanced linear regression methodology [23]. The use of JCI plots has been previously employed as a rapid visualization tool to detect if two methods have significant differences [24], allowing simultaneous evaluation of the slope and intercept. The plotting of the JCI takes into account the uncertainties from both axes to calculate the estimated covariance matrix based on a F distribution. In this manner the plots were constructed, for the pooled data of the plots shown in Fig. 4, and the theoretical comparison point (0,1) was included for comparison purposes. As can be observed in Fig. 5, the theoretical point is included within the confidence intervals for both for the training and testing subsets; confirming that statistically there are no significant differences for the ET predicted values and the expected ones.

Again, it can be seen that the test subset gives a bigger joint confidence ellipse, this fact can be easily explained; firstly, the test subset is not employed at all during the construction of the model. Moreover, the number of samples in the testing subset is much lower that the train subset, and consequently, the tabulated values of t and F are higher, resulting in higher dispersion and larger confidence intervals.

## 4. Conclusions

The approach reported here combines an array of six voltammetric sensors with artificial neural networks to simultaneously quantify the concentrations of 4-ethylphenol, 4-ethylguaiachol and 4-ethylcatechol, as important defect episode in wine samples.

The ET strategy allowed the resolution of signal overlapping and therefore the quantification of the individual species considered. This

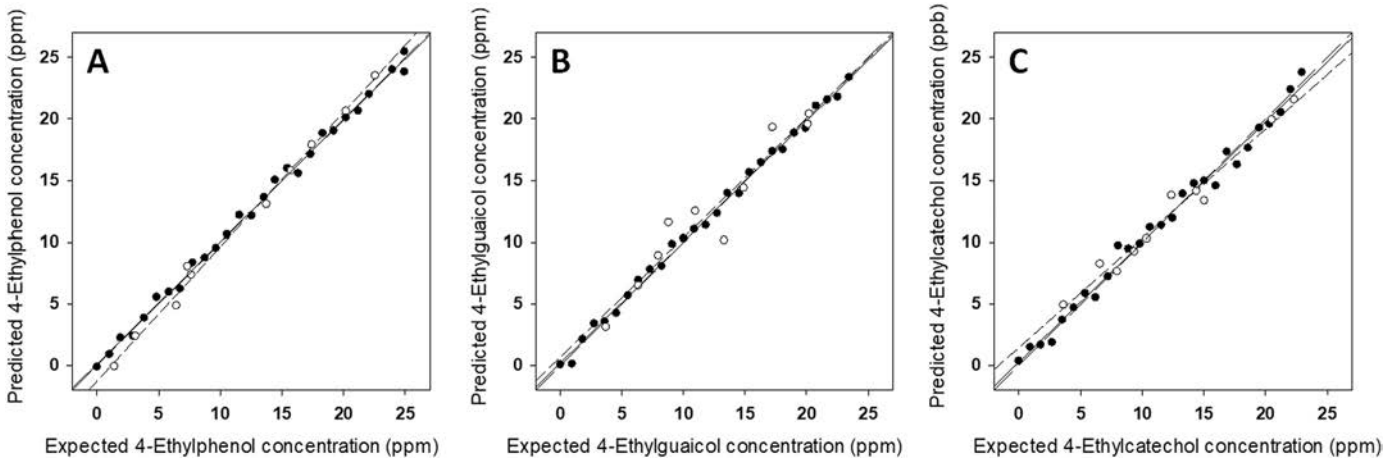


**Fig. 4.** Modeling ability of the developed DWT-ANN. Adjustments of expected vs. predicted concentrations for **(A)** 4-EP, **(B)** 4-EG and **(C)** 4-EC, both for training (•, solid line) and testing subsets (○, dashed line). Dotted line corresponds to theoretical diagonal line.

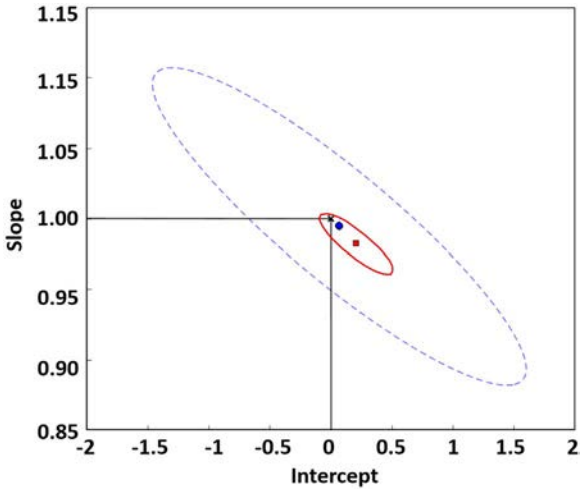


**Fig. 5.** Joint confidence intervals for the train subset: (red square, solid line) and the test subset (blue circle, dashed line). Also ideal point (1,0) is plotted (x); intervals calculated at the 95% confidence level. (For interpretation of the references to color in this figure legend, the reader is referred to the web version of this article.)

fact combined with the advantages of electrochemical sensors for on-site analysis results in a promising tool that substituted the classical expensive and time consuming methods to help winemakers in the early detection of the Brett defect.

## Acknowledgments

Financial support for this work was provided by the Spanish Ministry of Economy and Innovation, MINECO (Madrid) through project CTQ2013-41577-P. Andreu González-Calabuig thanks Universitat Autònoma de Barcelona for the PIF fellowship. Manel del Valle thanks the support from program ICREA Academia.

## Appendix A. Supporting information

Supplementary data associated with this article can be found in the online version at http://dx.doi.org/10.1016/j.talanta.2017.10.041.

## References

[1] H. Maarse, Volatile Compounds in Foods and Beverages, CRC Press, Boca Ratón, 1991.
[2] P. Chatonnet, D. Dubourdie, Jn Boidron, M. Pons, The origin of ethylphenols in wines, J. Sci. Food Agric. 60 (1992) 165–178.
[3] R. Suárez, J. Suárez-Lepe, A. Morata, F. Calderón, The production of ethylphenols in wine by yeasts of the genera Brettanomyces and Dekkera: a review, Food Chem. 102 (2007) 10–21.
[4] V. Loureiro, M. Malfeito-Ferreira, Spoilage yeasts in the wine industry, Int. J. Food Microbiol. 86 (2003) 23–50.
[5] A.P. Pollnitz, K.H. Pardon, M.A. Sefton, Quantitative analysis of 4-ethylphenol and 4-ethylguaiacol in red wine, J. Chromatogr. A 874 (2000) 101–109.
[6] Y. Vlasov, A. Legin, A. Rudnitskaya, C. Di Natale, A. D'amico, Nonspecific sensor arrays ("electronic tongue") for chemical analysis of liquids (IUPAC Technical Report), Pure Appl. Chem. 77 (2005) 1965–1983.
[7] L. Moreno-Barón, R. Cartas, A. Merkoçi, S. Alegret, J.M. Gutiérrez, L. Leija, P.R. Hernandez, R. Muñoz, M. del Valle, Data compression for a voltammetric electronic tongue modelled with artificial neural networks, Anal. Lett. 38 (2005) 2189–2206.
[8] M. del Valle, Sensor arrays and electronic tongue systems, Int. J. Electrochem. 2012 (2012).
[9] Y. Ni, S. Kokot, Does chemometrics enhance the performance of electroanalysis? Anal. Chim. Acta 626 (2008) 130–146.
[10] X. Cetó, J.M. Gutiérrez, M. Gutiérrez, F. Céspedes, J. Capdevila, S. Mínguez, C. Jiménez-Jorquera, M. del Valle, Determination of total polyphenol index in wines employing a voltammetric electronic tongue, Anal. Chim. Acta 732 (2012) 172–179.
[11] V. Parra, Á.A. Arrieta, J.-A. Fernández-Escudero, M.L. Rodríguez-Méndez, J.A. De Saja, Electronic tongue based on chemically modified electrodes and voltammetry for the detection of adulterations in wines, Sens. Actuators B: Chem. 118 (2006) 448–453.
[12] X. Cetó, A. González-Calabuig, J. Capdevila, A. Puig-Pujol, M. del Valle, Instrumental measurement of wine sensory descriptors using a voltammetric electronic tongue, Sens. Actuators B: Chem. 207 (2015) 1053–1059.
[13] J. Zeravik, A. Hlavacek, K. Lacina, P. Skládal, State of the art in the field of electronic and bioelectronic tongues–towards the analysis of wines, Electroanalysis 21 (2009) 2509–2520.
[14] S.G. Mallat, A theory for multiresolution signal decomposition: the wavelet representation, IEEE Trans. Pattern Anal. Mach. Intell. 11 (1989) 674–693.
[15] J. Alonso, E. Martínez, M. del Valle, Amperometric biosensors based on bulk-modified epoxy graphite biocomposites, Sens. Mater. 8 (1996) 147–153.
[16] X. Cetó, J.M. Gutiérrez, L. Moreno-Barón, S. Alegret, M. del Valle, Voltammetric electronic tongue in the analysis of Cava wines, Electroanalysis 23 (2011) 72–78.
[17] T.A. Enache, A.M. Oliveira-Brett, Phenol and para-substituted phenols electrochemical oxidation pathways, J. Electroanal. Chem. 655 (2011) 9–16.
[18] K. Lerch, Neurospora tyrosinase: structural, spectroscopic and catalytic properties, Mol. Cell. Biochem. 52 (1983) 125–138.
[19] A. Yaropolov, O. Skorobogat'Ko, S. Vartanov, S. Varfolomeyev, Appl. Biochem. Biotechnol. 49 (1994) 257–280.
[20] J.A. Giacometti, F.M. Shimizu, O. Carr, O.N. Oliveira, A guiding method to select and reduce the number of sensing units in electronic tongues, Sensors, IEEE, 2016, pp. 1–3.
[21] X. Cetó, F. Céspedes, M.I. Pividori, J.M. Gutiérrez, M. del Valle, Resolution of phenolic antioxidant mixtures employing a voltammetric bio-electronic tongue, Analyst 137 (2012) 349–356.
[22] F. Despagne, D.L. Massart, Neural networks in multivariate calibration, Analyst 123 (1998) 157R–178R.
[23] J. Mandel, F. Linning, Study of accuracy in chemical analysis using linear calibration curves, Anal. Chem. 29 (1957) 743–749.
[24] X. Cetó, A. González-Calabuig, M. del Valle, Use of a bioelectronic tongue for the monitoring of the photodegradation of phenolic compounds, Electroanalysis 27 (2015) 225–233.

# Article 7:

**Electronic tongue for nitro and peroxide explosive sensing**

Andreu González-Calabuig, Xavier Cetó and Manel del Valle

*Talanta* 153 (2016) 340–346

DOI: 10.1016/j.talanta.2016.03.009

Talanta 153 (2016) 340–346

Contents lists available at ScienceDirect

Talanta

journal homepage: www.elsevier.com/locate/talanta

# Electronic tongue for nitro and peroxide explosive sensing

Andreu González-Calabuig, Xavier Cetó, Manel del Valle*

*Sensors and Biosensors Group, Department of Chemistry, Universitat Autònoma de Barcelona, Edifici Cn, 08193 Bellaterra, Barcelona, Spain*

ARTICLE INFO

*Article history:*
Received 9 November 2015
Received in revised form
29 February 2016
Accepted 2 March 2016
Available online 3 March 2016

*Keywords:*
Electronic tongue
Artificial neural network
Voltammetric sensor
Explosives
TNT
TATP

ABSTRACT

This work reports the application of a voltammetric electronic tongue (ET) towards the simultaneous determination of both nitro-containing and peroxide-based explosive compounds, two families that represent the vast majority of compounds employed either in commercial mixtures or in improvised explosive devices. The multielectrode array was formed by graphite, gold and platinum electrodes, which exhibited marked mix-responses towards the compounds examined; namely, 1,3,5-trinitroperhydro-1,3,5-triazine (RDX), octahydro-1,3,5,7-tetranitro-1,3,5,7-tetrazocine (HMX), pentaerythritol tetranitrate (PETN), 2,4,6-trinitrotoluene (TNT), *N*-methyl-*N*,2,4,6-tetranitroaniline (Tetryl) and triacetone triperoxide (TATP). Departure information was the set of voltammograms, which were first analyzed by means of principal component analysis (PCA) allowing the discrimination of the different individual compounds, while artificial neural networks (ANNs) were used for the resolution and individual quantification of some of their mixtures (total normalized root mean square error for the external test set of 0.108 and correlation of the obtained vs. expected concentrations comparison graphs $r > 0.929$).



## 1. Introduction

The increased terrorism activities have brought the world's attention on explosive compounds, and have given rise to increased research into explosive early detection as well as further developments in existing analytical techniques to enable faster, more sensitive, less expensive and simpler determinations to facilitate the trace identification of these energetic materials [1]. Specifically, the analyses of explosive compounds are demanded by the environmental monitoring and protection agencies, crime scene investigations and homeland securities.

Explosive chemicals are useful and widely used in warfare, mining industries and civil constructions; unfortunately also in terrorist attacks. These compounds are categorized in four major classes: nitroaromatics, nitroamines, nitrate esters and peroxides according to their chemical structures [2]. Among them, special attention must be paid to peroxide explosives since those compounds contain neither nitro groups nor aromatic functionalities, what makes them difficult to detect with the analytical methods used to determine more established explosives [3], e.g. 2,4,6-trinitrotoluene (TNT) or 1,3,5-trinitroperhydro-1,3,5-triazine (RDX). That is, the challenge being that many current chemical identification techniques are based on the nitrogen and carbon content of a substance for its identification, and this practice is not suitable for peroxide explosive. Furthermore, the peroxide explosives are not suitable for spectroscopic detection [4] because of their lack of chromophores and their instability under illumination of UV light – all necessary parameters upon which traditional detection techniques are based [5].

These characteristics, as well as their large explosive power [6], have led to the increasing use of those by terrorists and criminals over the last few decades [3]. Concretely, triacetone triperoxide (TATP) became a well known explosive after its use by the thwarted “shoe bomber” in 2001 [7].

In this context, electrochemical sensors offer an opportunity to detect peroxide-based explosives that would otherwise prove problematic [8,9]. The inherent redox activity of nitrogen-based commercial explosives [10,11], such as nitroaromatic or nitroamine compounds, namely the presence of easily-reducible nitro groups, makes them ideal candidates for electrochemical (voltammetric) monitoring. Besides, the advantages of electrochemical systems for on-site measurements include high sensitivity and selectivity, a wide linear range, minimal space and power requirements, and low-cost instrumentation. In addition, both the sensor and the controlled instrumentation can be readily miniaturized to yield compact and user-friendly hand-held meters for on-site (indoor and outdoor) testing [12]. Therefore, electrochemical devices represent a promising solution for on-site explosive detection.

Nevertheless, the presence of the reducible nitro groups on the aromatic ring, which differ only in their number and position,

* Correspondence to: Sensors and Biosensors Group, Universitat Autonoma de Barcelona, Campus UAB, Edifici Cn, 08193 Bellaterra, Spain.
*E-mail address:* manel.delvalle@uab.es (M. del Valle).

http://dx.doi.org/10.1016/j.talanta.2016.03.009
0039-9140/

results in overlapping voltammetric signals and makes the simultaneous discrimination of mixtures of nitro-containing explosives problematic [10].

On that account, over the last years, a new concept in the field of sensors has appeared to tackle these problems: Electronic Tongues (ETs) [13]. These biomimetic systems, in opposition to conventional approaches, are directed towards the combination of low selectivity sensors array response (or with cross response features) in order to obtain some added value in the generation of analytical information; and afterwards they are coupled with complex data treatment tools, which allows to identify or to quantify the substances under scrutiny. In this sense, the use of chemometric tools such as principal component analysis (PCA) or artificial neural networks (ANNs) can help to overcome limitations in data interpretation [14,15], by identifying and processing the electrochemical fingerprint produced by the explosive mixture.

Initial attempts with such an approach have been directed to the discrimination of different nitroaromatic explosives [16–18]. Similarly, electronic noses (ENs) and colorimetric devices in conjunction with some chemometric methods have also been applied to the qualitative identification of some explosive compounds [19–22]. However, most of the works focus only on nitroaromatic or peroxide explosives separately, with almost none of them attempting its simultaneous quantification.

Herein, we propose the use of the electronic tongue approach for the detection of different nitro- and peroxo- types of explosives, utilizing voltammetric data acquired from a multielectrode array. The proposed approach is based on the coupling of cyclic voltammetric responses obtained from an array of graphite, gold and platinum electrodes with chemometric tools such as PCA for visualization of sample (dis)similarities and ANNs for building the quantitative prediction models. In this sense, the combination of fast voltammetric detection and chemometrics could possibly simplify measurements in security premises and lead to a new generation of on-site field deployable explosive detectors.

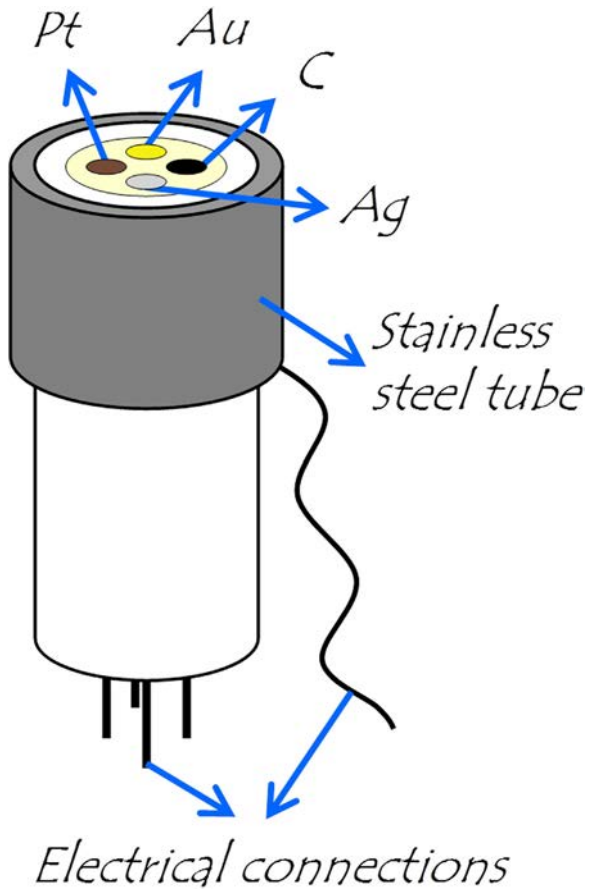


**Fig. 1.** Design of the multielectrode array: silver, gold, platinum and graphite wires were introduced into a PVC tube and casted into a resin, which additionally was stuck to a stainless steel tube. Silver was used as pseudoreference electrode and stainless steel tube as the counter electrode, while the others ones acted as working electrodes.

## 2. Experimental

### 2.1. Reagents and solutions

All reagents used were analytical reagent grade and all solutions were prepared using deionised water from a Milli-Q system (Millipore, Billerica, MA, USA). Reference standard solutions (1000 μg $mL^{-1}$ in acetonitrile) of 1,3,5-trinitroperhydro-1,3,5-triazine (RDX), octahydro-1,3,5,7-tetranitro-1,3,5,7-tetrazocine (HMX), pentaerythritol tetranitrate (PETN), 2,4,6-trinitrotoluene (TNT) and *N*-methyl-*N*,2,4,6-tetranitroaniline (Tetryl) were purchased from LGC standards (Teddington, Middlesex, UK). Acetone and Acetonitrile (ACN) were purchased from Scharlab (Barcelona, Spain). Potassium dihydrogenphosphate, potassium monohydrogenphosphate and $H_2O_2$ were purchased from Sigma-Aldrich (St. Louis, MO, USA). Sulfuric acid and Potassium chloride were purchased from Merck KGaA (Darmstadt, Germany).

### 2.2. TATP synthesis

The synthesis of triacetone triperoxide (TATP) was done following previously reported procedures [23,24]. The peroxide can be easily synthesized by the acid catalyzed reaction between $H_2O_2$ and acetone at low temperatures (see supplementary, Fig S1). However, special care must be taken when synthesizing and handling TATP due to it is a primary explosive, but also to avoid the formation of the diacetone diperoxide (DADP). Thus, reaction was optimized, considering safety principles, to produce less than 1 g of final product.

Synthesis was carried out according to the following procedure: a 0.68 mL aliquot of chilled 30% $H_2O_2$ and 0.95 mL of chilled acetone were placed in a 10 mL beaker within an ice bath. The mixture was gently stirred and 20 μL of chilled, concentrated $H_2SO_4$ (98% w/w) were added every 4 min during 48 min to give a total volume of 240 μL of $H_2SO_4$ added. Special care was taken to add $H_2SO_4$, as adding it too quickly might cause a violent reaction or even an explosion. The mixture was kept during 24 h without stirring or cooling to complete the precipitation of TATP.

### 2.3. Voltammetric measurements

#### 2.3.1. Multielectrode array and measurement cell

The ET array consists in four discs of silver, gold, platinum and graphite-epoxy composite of 1 mm diameter, plus a stainless steel tube of 8 mm inner diameter. The four wire electrodes were cast in epoxy resin (Epotek H77, Epoxy Technologies) in a 8 mm outer diameter PVC tube used as body [25], which was afterwards stuck in the stainless steel tube (Fig. 1). Platinum, gold and epoxy-graphite discs were used as working electrodes, whereas silver was used as pseudo-reference electrode (after proper chloridization) and the stainless steel tube as the auxiliary electrode.

Whereas graphite has already been demonstrated as an attractive material to achieve the detection of nitro-containing explosives [10,16,17]; platinum and gold were selected as it was found that metals such as gold, silver or platinum represent interesting electrodes that might provide a distinguished and characteristic fingerprint for each of the explosive compounds,

including peroxide-based ones (see supplementary info, Fig. S2) [9].

Besides, the usage of such a compact array of electrodes with integrated reference and auxiliary electrodes, makes the system suitable to perform drop measurements as it would be done with a screen printed electrode. But with advantages over those such as its better reproducibility over long periods of usage, thanks to the higher robustness of the materials, or the possibility of regenerating by polishing and new electrolysis.

#### 2.3.2. Measurement procedure

Cyclic Voltammetry measurements were carried out at room temperature (25 °C), in a multichannel configuration, using a 6-channel AUTOLAB PGSTAT20 (Ecochemie, Netherlands) controlled with GPES Multichannel 4.7 software package.

Firstly, prior to sample measurements, electrodes were cycled in saline solution in order to get stable voltammetric responses. For the measurements, potential was cycled between −1.0 V and +0.9 V vs Ag/AgCl pseudo reference electrode, with a scan rate of 100 mV $s^{-1}$ and a step potential of 9 mV. All experiments were carried out without performing any physical surface regeneration of the working electrodes. Thus, in order to prevent the accumulative effect of impurities on the working electrode surfaces, an electrochemical cleaning stage was done between each measurement applying a conditioning potential of +1.2 V for 40 s after each experiment, in a cell containing 150 μL of 50 mM KCl at pH=10 [25].

### 2.4. Samples under study

Firstly, the voltammetric response of the sensor array towards the different explosive compounds was characterized. For this purpose, stock solutions of each of the available compounds were analyzed. To confirm that the discrimination between the different compounds is due to its differentiated electrochemical fingerprint and grouping is not a consequence of any other factor, all samples were prepared in triplicate and randomly measured, considering each replicate as a new sample to ensure the robustness of the approach. In the same direction, to ensure that the discrimination was not due to the different sensitivity of the sensors towards each compound, the same concentration stock solutions were initially used.

Afterwards, in order to prove the capabilities of the ET to achieve the simultaneous discrimination and quantification of different explosive compounds mixtures at different concentrations, the quantitative resolution of TNT, tetryl and TATP mixtures was attempted. To this aim, a total set of 37 samples were manually prepared with a concentration range of 0 to 165 μg $mL^{-1}$ for TNT ant tetryl, and 0 to 300 μg $mL^{-1}$ for TATP. The set of samples was divided into two data subsets: a training subset formed by 27 samples (73%) which were distributed based on a factorial design ($3^3$) and used to build the response model, plus 10 additional samples (27%) for the testing subset, distributed randomly along the experimental domain and used to evaluate the model predictive ability.

In all cases, given the solutions of the explosive compounds were all supplied as an ACN solution, and to ensure that the variation of its proportion does not affect sensor's response, its volume was kept constant throughout all the measurements. For this, the right amount of each compound was mixed, adding the remaining volume of ACN up to 75 μL. Then, this was mixed with 75 μL of phosphate buffer pH 6.5 and 50 mM KCl to stabilize the pH and to ensure enough conductivity of the media.

### 2.5. Data processing

Chemometric processing of the data was performed by specific routines in MATLAB 7.1 (MathWorks, Natick, MA) written by the authors using its Neural Network toolbox; except, Simplified Fuzzy ARTMAP Neural Network which was already implemented by other authors (http://www.mathworks.com/, file ID: #11721) [26]. In this fashion, PCA was used for qualitative analysis of the results, while quantitative analysis was achieved by means of ANN response model. Additionally, Sigmaplot (Systat Software Inc., San José, CA, USA) was used for graphic representations of data and results.

A known problem when voltammetric sensors are used within electronic tongues is the large dimensionality of the generated data (samples × sensors × polarization potentials) which hinders their treatment; especially if ANNs are to be used, in which case departure information needs to be preprocessed. In this fashion, prior to building the quantification model, removal of less significant coefficients that barely contribute to the network was carried out by means of Causal Index (CI) pruning of the inputs [27–29].

Briefly, this method is based on the usage of ANNs as feature selection tools, and aimed to the selection of an optimal set of inputs that can successfully classify or predict the desired outputs. To this end, a first ANN model (which configuration is defined from previous experience) is built employing the whole set of input variables, followed by the determination of the contribution and relevance of each of the network inputs to the variance in the output layer. This can be achieved with the sensitivity analysis of its input connection weights, which allows to easily identifying the most important inputs since inputs that make relatively small contributions indicate that the output does not change significantly; and therefore, can be discarded, viz. pruned. Afterwards, selection of the most relevant inputs can proceed until a near-optimal, small, set of inputs is identified by repeating the training process of the ANN model with the reduced input set and selecting the most relevant ones each time. Finally, once the reduced set of inputs is identified, a final re-optimization of the ANN architecture can proceed as usual [30].

It has to be reckoned that some of the resulting minimal sets will not be unique, and might depend on the exact ANN architecture initially selected to initiate the process. However, the accuracy of the resulting pruned ANN models is usually better, and more robust, than that of the large initial ANN one.

## 3. Results and discussion

### 3.1. TATP synthesis

Although the conditions are optimized to produce the trimer, the reaction described previously can give the DADP and the TATP mixture. Consequently, a $^1$H NMR spectrum (250 MHz, $CDCl_3$) was acquired to ensure that the product resulting from the reaction was the trimer (see supplementary info, Fig. S1). The resulting peaks in the $^1$H NMR spectra were compared with the ones reported in previous works [31]. The NMR shows a very intense peak corresponding to TATP ($\delta$=1.48 (s)) and various peaks corresponding to the $CDCl_3$ ($\delta$=7.28), $H_2O$ ($\delta$=1.55), HDO ($\delta$=1.37); meanwhile, no peaks corresponding to decomposition products were observed ($\delta$=2.03, $\delta$=1.82, $\delta$=1.80, $\delta$=1.31). Therefore, confirming that TATP was the product obtained.

### 3.2. Voltammetric responses

Following the described procedure, the set of samples was measured employing the multielectrode array, obtaining a whole cyclic voltammogram for each of the sensors from the array.

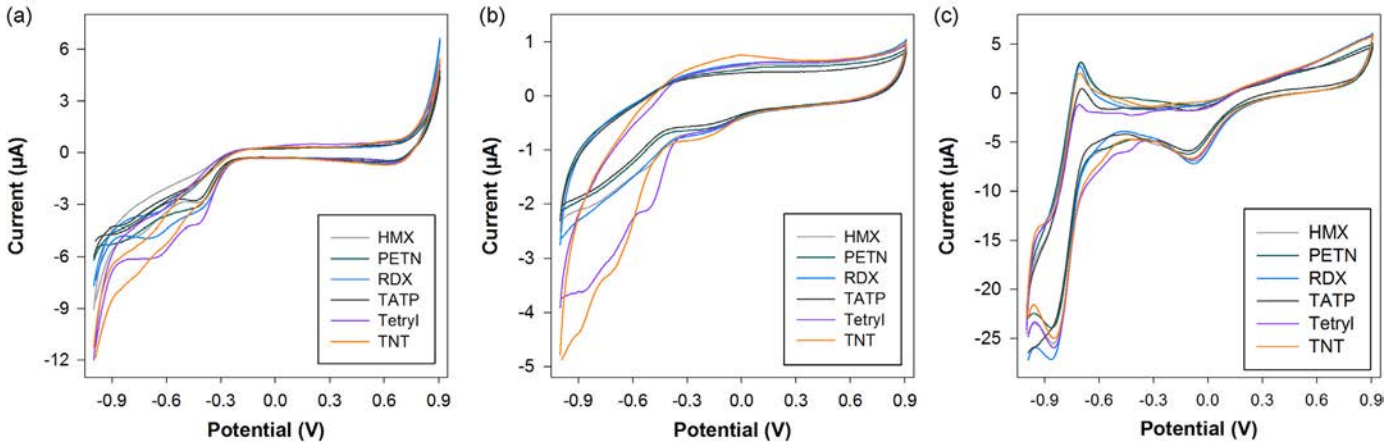


**Fig. 2.** Example of different voltammograms obtained for (a) epoxy graphite electrode, (b) Au electrode and (c) Pt electrode measuring 100 μg $mL^{-1}$ standard solutions of each of the explosive pure compounds under study (grey for HMX, green for PETN, blue for RDX, black for TATP, purple for Tetryl and orange for TNT). (For interpretation of the references to color in this figure legend,the reader is referred to the web version of this article.)

An extract of those results is shown in Fig. 2. As can be seen, complex and highly overlapped signals are obtained along the whole voltammogram, with differentiated signals obtained for the different kinds of sensors.

Although at first sight might seem difficult to attribute any peak to a specific compound, characteristic features from the different compounds are still observed. For example, a clear peak corresponding to tetryl can be observed around −0.5 V and a second one at around −0.85 V at the graphite-epoxy electrode, whereas in the case of the gold electrode similar peak might be seen at around −0.4 V and −0.65 V. More significant differences can be found for RDX, where not such clear peaks can be found for the graphite-epoxy electrode, but a clearer peak is observed at around −0.8 V for the gold electrode. This same behavior is observed for the other species such as HMX or TATP for example. Lastly, platinum electrode seems to provide more distinguished features for TATP which oppositely to the other nitro-compounds does not present a reduction peak at around −0.85 V, plus clear response is obtained at the oxidative scan at around −0.70 V. Overall, a situation highly desirable for building an ET application, i.e. when the different sensors display marked distinct features for the different samples.

### 3.3. Qualitative analysis of explosives

In a first approach, discrimination of different explosive compounds by means of the ET was attempted. That is, to asses if the system presented herein was able to carry out the identification of the most common explosive compounds.

To this aim, voltammetric responses obtained for the stock solutions of each of the pure compounds were analyzed by means of PCA and grouped using cluster analysis tools.

Upon completion of the PCA analysis (Fig. 3), the accumulated explained variance was calculated with the three first PCs as 99.85%. This large value shows that nearly all the variance contained in the original data can be explained by just using the first new coordinates. In addition, patterns in the figure evidence that samples are clearly grouped based on each explosive compound, with replicas for the same class close one to each other.

After the initial representation of data, a fuzzy ARTMAP ANN model with binary outputs (1/0) was used as classifier, which allowed quantification of the classification performance of the system in contrast to PCA analysis which just provides a visualization of the grouping regions.

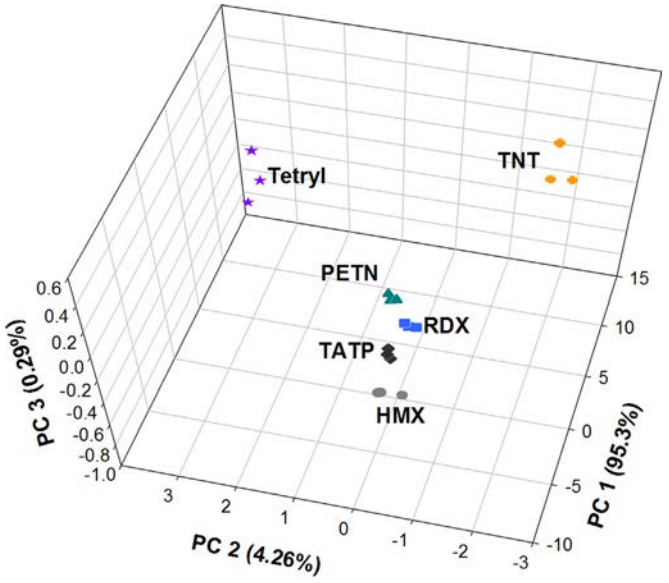


**Fig. 3.** Score plot of the first three components obtained after PCA analysis. A total of 18 samples were analyzed corresponding to triplicate determinations of: (1) RDX, (2) HMX, (3) PETN, (4) TNT, (5) Tetryl and (6) TATP.

The PCA–ANN model was trained with 67% of the data (12 samples) and evaluated using the information of the testing set (remaining 33% of the data; 6 samples) in order to characterize the accuracy of the identification model and obtain unbiased data. From the classification results, the corresponding confusion matrix was built. Correct classification for all the classes was obtained (i.e., a classification rate of 100% for each of the groups), as indicated from the direct visualization of the PCA analysis. The efficiency of the classification obtained was also evaluated according to its sensitivity, i.e., the percentage of objects of each class identified by the classifier model, and to its specificity, the percentage of objects from different classes correctly rejected by the classifier model. The value of sensitivity, averaged for the classes considered, was 100%, and that of specificity was 100%.

With the goal of providing a measure of performance for the identification, a Pearson's chi-squared test was calculated for the contingency table containing the test set samples alone; this calculation provided, for the six compounds considered, a calculated statistic of $\chi^2 = 90.0$, significantly larger than the tabulated value at

the 95% confidence level (37.7). This statistic also allowed calculation of the contingency coefficient (0.913), equal to the maximum achievable value for the number of samples and classes considered and that describes numerically the power of identification

In view of the good results obtained in the qualitative approach, and to further assess the capabilities of the ET to perform its individual quantitative determination, even in the presence of other explosive compounds, the next step was the resolution of ternary mixtures of TNT, tetryl and TATP as the illustrative case. Thus in this way, also demonstrating how the ET would be able to correctly identify each compound regardless of its concentration.

### 3.4. Feature selection

As stated, when dealing with voltammetric sensor arrays, the main problem is the huge dimensionality of the recorded data (the set of voltammograms) which hinders the modeling step, especially if ANNs are to be used. Therefore, requiring a compression step, which in addition allows to gain advantages in training time, to avoid redundancy in input data and to obtain a model with better generalization ability [28]. In our case this was accomplished by the use of the causal index analysis (CI).

Main advantage of this method is the fact that allows the identification of the most relevant features, that is, not only the identification of which sensors most contribute to the discrimination and the quantification of the compounds under scrutiny, but also which points from the voltammograms (i.e. the currents associated to the applied potentials). However, its main drawbacks are the amount of time required for the feature extraction process, the fact that the reduced sets are not unique and the arrival to an optimal set depends on the architecture of the ANN used.

As said, to carry out the selection of the most significant inputs by means of an ANN, first of all, the number of neurons in the hidden layer and the transfer functions (both in the hidden and output layers) are selected in advance to represent the intrinsic dimensionality of the dataset. In this case, and based on previous calculus (see supplementary info, Fig. S3), the selected ANN architecture to carry out the pruning of the inputs was formed by 5 neurons and *logsig* transfer function in the hidden layer, and 3 neurons and *purelin* transfer function in the output layer. Upon assignation of the weights by the ANN model, the most relevant features were identified, allowing the reduction of the number of inputs by repetitive pruning of the less significant inputs, without any loss of relevant information and an improvement in model robustness as can be seen in Fig. 4.

After this, the final input set was formed by 48 inputs, which meant that a reduction of ca. 96.2% in the size of data to feed the ANN model was achieved. In addition to the large compression ratio, the usage of a pruning strategy of the raw data instead of a compression method such as fast Fourier transform or discrete wavelet transform, offers further advantages as the obtaining of a simpler and more robust model due to non-significant inputs are not included into the model. Even more, allows to identify which sensors mostly contribute to the model (see supplementary info, Fig. S4). In this direction, the analysis of the selected inputs confirmed the complimentary and cross-response features provided by the chosen sensor array, as all the sensors contributed significantly to the final model. Namely, 12:23:13 were the number of features selected from the responses of the graphite-epoxy, gold and platinum electrodes, respectively.

Hence, once the predictors data matrix was defined, the next step was the optimization of the neural network architecture with the reduced input information by an iterative process varying its configuration (number of neurons in the hidden layer plus transfer functions in the hidden and output layers) in order to generate the best response model.

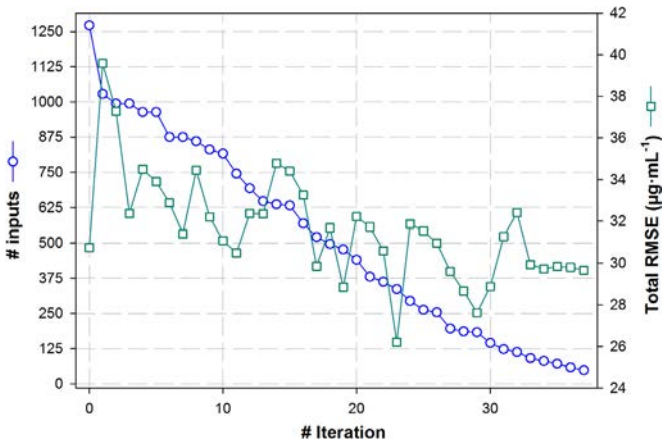


**Fig. 4.** Feature selection and reduction of the number of inputs by means of CI–ANN method. In each iteration a model is fitted, its RMSE for testing subset is calculated and inputs to which the model has assigned lower weights are discarded. This process is repeated until an increase in the RMSE is obtained for several successive iterations or the desired reduction in the number of inputs is achieved.

### 3.5. Quantitative analysis of explosive mixtures

Upon completion of an extensive study varying its configurations (see supplementary info, Fig. S5), the final architecture of the ANN model had 48 neurons (the ones corresponding to the currents previously selected during feature extraction stage) in the input layer, 8 neurons and *logsig* transfer function in the hidden layer and three neurons and *purelin* transfer function in the output layer, providing the concentrations of the three species considered.

The accuracy of the generated model was then evaluated towards samples of the external test subset by using the built model to predict the concentrations of the explosives of those samples. Since the external test subset data is not employed at all for the modeling, its goodness of fit is a measure of the accomplished modeling performance. To easily check the prediction ability of the obtained ANN model, comparison graphs of predicted vs. expected concentration for the three compounds were built, both for training subset and testing subsets.

As can be observed in Fig. 5, a satisfactory trend is obtained for the three compounds, with regression lines close to the theoretical ones. Additionally, regression parameters were calculated (Table 1), and as expected from the graphs, a good linear trend is attained for all the cases, but, as usual, with improved behavior for the training subsets due to this subset is the one used to build the model. Despite this, the results obtained for both subsets are close to the ideal values, with intercepts close to 0, and slopes and correlation coefficients close to 1.

Although not initially considered in this case, individual ANN models may also be developed to separately predict the concentrations of the three species; what would lead to better prediction of the individual concentrations of the three species (see supplementary info, e.g. Fig. S6 and Table S1). However, this configuration was neglected as it does not represent the true nature of the approach and complicates its final application as three models would be used rather than a single one. Nevertheless, this option may represent an easy way to improve the performance of the final ET approach if required.

Lastly, it has to be point out that using the same experimental setup, the approach proposed herein can be also applied to the identification and quantification of analogous or different explosive mixtures (even quaternary or more complex mixtures), by making use of a proper training set of samples. This would be

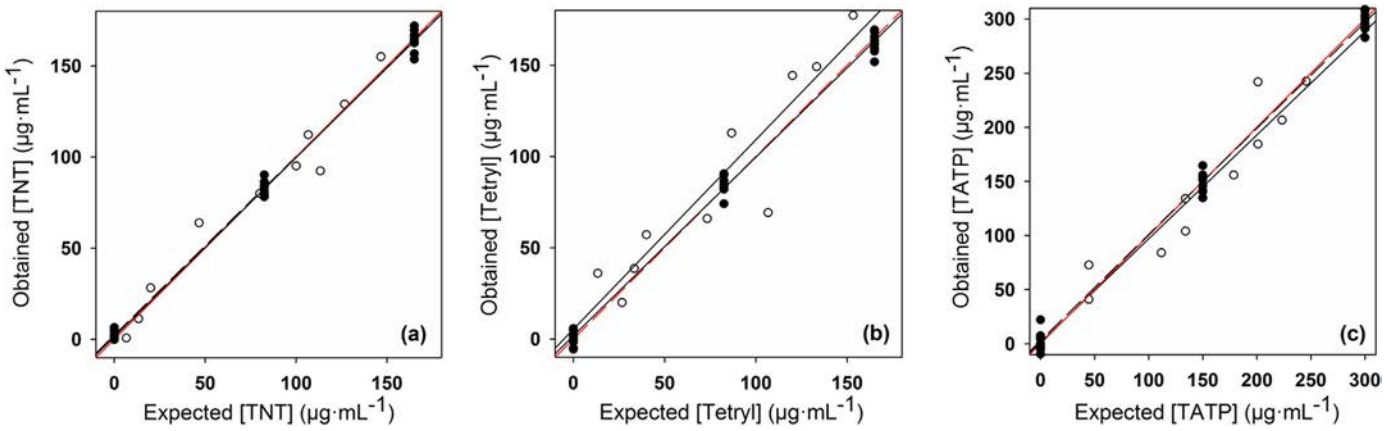


**Fig. 5.** Modeling ability of the optimized ANN. Sets adjustments of obtained vs. expected concentrations for (a) TNT, (b) Tetryl and (c) TATP, both for training (•, dashed line) and testing subsets (○, solid line). Red dashed line corresponds to theoretical diagonal line.

**Table 1**
Results of the fitted regression lines for the comparison between obtained vs. expected concentration values, both for the training and testing subsets of samples and the three considered explosive compounds (intervals calculated at the 95% confidence level).

| *Explosive* | *Correlation* | *Slope* | *Intercept* ($\mu g\ mL^{-1}$) | *NRMSE* | *Total NRMSE* |
|---|---|---|---|---|---|
| ***Training subset*** | | | | | |
| TNT | 0.997 | $0.984 \pm 0.030$ | $1.4 \pm 3.2$ | 0.027 | |
| Tetryl | 0.997 | $0.980 \pm 0.030$ | $1.7 \pm 3.2$ | 0.030 | 0.028 |
| TATP | 0.998 | $0.981 \pm 0.028$ | $2.8 \pm 5.6$ | 0.027 | |
| ***Testing subset*** | | | | | |
| TNT | 0.979 | $0.981 \pm 0.166$ | $2.2 \pm 14.9$ | 0.064 | |
| Tetryl | 0.929 | $1.038 \pm 0.337$ | $5.4 \pm 30.8$ | 0.134 | 0.108 |
| TATP | 0.945 | $0.959 \pm 0.269$ | $1.2 \pm 44.7$ | 0.113 | |

NRMSE: Normalized Root Mean Square Error.

required as the model might not be able to extrapolate the presence of a specific compound if this has not been included in the set of samples used to build the model. However, even in such an scenario where a compound has not been initially considered, the usage of multi-way processing methods could permit the correction of the presence of an interfering species thanks to the "second order advantage" [32,33].

## 4. Conclusions

Proposed approach presented herein has demonstrated to be a useful tool for the detection and quantification of different explosive compounds, both nitro-containing and peroxide-based ones, representing the two main families of compounds employed either in commercial mixtures or in improvised explosive devices (IEDs). In this way, the approach overcomes the lack of response towards peroxide-based explosives of many of the methods reported in the literature.

Developed ET is based on a small multi-electrode array formed by simple metallic electrodes plus a graphite one, which have exhibited marked mix-responses towards the compounds examined. Analysis of samples was based on the combination of cyclic voltammetry for the extraction of the fingerprints of the individual components and mixtures of these species, coupled with chemometric tools that allowed the resolution of signal overlapping and identification of the different compounds. Specifically, PCA analysis showed the capability of the ET to discriminate most common explosive compounds, while in a further approach, resolution and quantification of ternary mixtures was achieved employing an artificial neural network model.

The usage of the small compact electrode is an interesting alternative to the usage of screen printed electrodes, which while still offering advantages of those such as the small volume of sample required, offers further advantages over those as its higher robustness or the possibility of obtaining a "fresh electrode" by simply polishing the surface of the array.

These results suggested that voltammetric electronic tongues could be useful for the detection of explosive compounds and pointed towards the possibility that this, or similar ET-based systems, could be of application for their detection in real explosive formulation samples and a good candidate for homeland security applications; leading to a new generation of on-site field deployable explosive detectors.

## Acknowledgments

Financial support for this work was provided by the Spanish Ministry of Science and Innovation, MCINN (Madrid) trough project CTQ2013-41577-P. Manel del Valle thanks the support from the program 2010. A. González thanks Universitat Autònoma de Barcelona (UAB) for the award of PIF studentship. The authors thank Jonathan De Tovar for his help in $^{1}$H NMR measurements.

## Appendix A. Supporting information

Supplementary data associated with this article can be found in the online version at http://dx.doi.org/10.1016/j.talanta.2016.03.009.

## References

[1] J.S. Caygill, F. Davis, S.P.J. Higson, Talanta 88 (2012) 14–29.
[2] W. Miao, C. Ge, S. Parajuli, J. Shi, X. Jing, Trace detection of high explosives with nanomaterials, in: D.T. Pierce, J.X. Zhao (Eds.), Trace Analysis With Nanomaterials, Wiley-VCH Verlag GmbH, Weinheim, DE, 2010.
[3] R. Schulte-Ladbeck, M. Vogel, U. Karst, Anal. Bioanal. Chem. 386 (2006) 559–565.
[4] T. Lu, Y. Yuan, X. He, M. Li, X. Pu, T. Xu, Z. Wen, RSC Adv. (2015).
[5] J. Wang, Electroanalysis 19 (2007) 415–423.
[6] R. Meyer, J. Kohler, A. Homburg, Explosives, Wiley-VCH Verlag GmbH, Weinheim, DE, 2007.
[7] J. Jordan, Stud. Confl. Terror. 35 (2012) 382–404.
[8] R.A.A. Munoz, D. Lu, A. Cagan, J. Wang, Analyst 132 (2007) 560–565.
[9] S.K. Mamo, J. Gonzalez-Rodriguez, SPIE Security+ Defence, Int. Soc. Opt. Photonics 9253 (2014) 925315.

[10] M. Galik, A.M. O'Mahony, J. Wang, Electroanalysis 23 (2011) 1193–1204.
[11] Ş. Sağlam, A. Üzer, Y. Tekdemir, E. Erçağ, R. Apak, Talanta 139 (2015) 181–188.
[12] J. Wang, TrAC-Trends Anal. Chem. 21 (2002) 226–232.
[13] M. del Valle, Electroanalysis 22 (2010) 1539–1555.
[14] M. Esteban, C. Ariño, J.M. Díaz-Cruz, TrAC-Trends Anal. Chem. 25 (2006) 86–92.
[15] Y. Ni, S. Kokot, Anal. Chim. Acta 626 (2008) 130–146.
[16] R. Polsky, C.L. Stork, D.R. Wheeler, W.A. Steen, J.C. Harper, C.M. Washburn, S. M. Brozik, Electroanalysis 21 (2009) 550–556.
[17] X. Cetó, A.M. O'Mahony, J. Wang, M. del Valle, Talanta 107 (2013) 270–276.
[18] A. Lichtenstein, E. Havivi, R. Shacham, E. Hahamy, R. Leibovich, A. Pevzner, V. Krivitsky, G. Davivi, I. Presman, R. Elnathan, Y. Engel, E. Flaxer, F. Patolsky, Nat. Commun. 5 (2014) 4195.
[19] Z. Li, W.P. Bassett, J.R. Askim, K.S. Suslick, Chem. Commun. 51 (2015) 15312–15315.
[20] J.R. Askim, Z. Li, M.K. LaGasse, J.M. Rankin, K.S. Suslick, Chem. Sci. 7 (2016) 199–206.
[21] M.O. Salles, G.N. Meloni, W.R. de Araujo, T.R.L.C. Paixao, Anal. Methods 6 (2014) 2047–2052.
[22] W.J. Peveler, A. Roldan, N. Hollingsworth, M.J. Porter, I.P. Parkin, ACS Nano 10 (2016) 1139–1146.
[23] D.F. Laine, C.W. Roske, I.F. Cheng, Anal. Chim. Acta 608 (2008) 56–60.
[24] J. Pachman, R. Matyáš, Forensic Sci. Int. 207 (2011) 212–214.
[25] X. Cetó, J.M. Gutiérrez, L. Moreno-Barón, S. Alegret, M. del Valle, Electroanalysis 23 (2011) 72–78.
[26] T. Kasuba, AI Expert 8 (1993) 18–25.
[27] Z. Boger, Anal. Chim. Acta 490 (2003) 31–40.
[28] X. Cetó, F. Céspedes, M. del Valle, Microchim. Acta 180 (2013) 319–330.
[29] Z. Xiaobo, Z. Jiewen, M.J.W. Povey, M. Holmes, M. Hanpin, Anal. Chim. Acta 667 (2010) 14–32.
[30] M. del Valle, Chapter 30 potentiometric electronic tongues applied in ion multi-determination, in: S. Alegret, A. Merkoçi (Eds.), Comprehensive Analytical Chemistry, Elsevier, 2007, pp. 721–753.
[31] J.C. Oxley, J.L. Smith, H. Chen, Propellants Explos. Pyrotech. 27 (2002) 209–216.
[32] G.M. Escandar, H.C. Goicoechea, A. Muñoz de la Peña, A.C. Olivieri, Anal. Chim. Acta 806 (2014) 8–26.
[33] A. Mimendia, J.M. Gutiérrez, L.J. Opalski, P. Ciosek, W. Wróblewski, M. del Valle, Talanta 82 (2010) 931–938.